SYNTHESIS AND CHARACTERIZATION OF LUMINESCENT CONJUGATED ORGANOBORON OLIGOMERS AND MACROCYCLES

by

PANGKUAN CHEN

A Dissertation submitted to the

Graduate School – Newark

Rutgers, The State University of New Jersey

in partial fulfillment of requirements

for the degree of

Doctor of Philosophy

Graduate Program in Chemistry

written under the direction of

Professor Frieder Jäkle

and approved by

____

____

____

____

Newark, New Jersey

October, 2012

ABSTRACT OF THE THESIS

SYNTHESIS AND CHARACTERIZATION OF LUMINESCENT CONJUGATED ORGANOBORON OLIGOMERS AND MACROCYCLES

By Pangkuan Chen

Thesis Director: Professor Frieder Jäkle

Conjugated molecules have been explored as an important class of organic materials that are of paramount interest in organic electronics, such as organic light emitting diodes (OLEDs), organic field-effect transistors (OFETs) and organic solar cells. Although current studies frequently concentrate on conjugated polymers, small molecules are attractive in that they allow for facile fine-tuning of the HOMO and LUMO energy levels, which is crucial for enhancement of the overall performance of organic devices. Functionalization of conjugated organic systems with main group elements represents an active research area of current interest in the chemistry and matarial science community. One of the most often employed elements is the electron-deficient boron that features an empty p orbital that opens up a pathway to overlap with π orbitals of attached aryl groups. This interaction leads to unusual optical and electronic properties for organoborane compounds. The focus of this thesis is on the investigation of well-defined organoborane oligomers and macrocycles.

Chapter 1. Luminescent Conjugated Fluoreneborane Oligomers

A series of monodisperse conjugated organoborane oligomers **O-B*n*** (n = 1–6) were synthesized via a newly developed iterative method that takes advantage of the differential selectivity of arylsilane *vs* arylstannane functionalities and allows us to easily control the extension of π conjugation. These oligomers are highly emissive and their photophysical properties show a red shift as the chain length increases. An effective conjugation length that spans five borons (n_{ecl} = 5) was derived, addressing a fundamental question regarding the extension of conjugation through p-π overlap in organoboranes.

Chapter 2. Luminescent Donor-*π*-Acceptor Type Oligomeric Organoboranes

Following a similar approach, we synthesized a series of ambipolar oligomers **O-B*n*N*m*** and **O-BNB** in which alternating N donor and B acceptor are separated by phenylene bridges. The effective conjugation length was predicted to be n_{ecl} = 4. Moreover, a bathochromic effect was observed in the emission, but not in the absorption, indicating more polar structures in the excited state due to pronounced intramolecular N→B charge transfer (ICT). These oligomers are potentially useful as ambipolar semiconducting materials.

Chapter 3. Luminescent Electron-Deficient Organoborane Macrocycles

The first electron-deficient organoborane macrocycle **MC-B6** was achieved by reaction of the higher linear oligomer **O-B4-BBr2** with 2,7-bis-(trimethylstannyl)-9,9-

dimethylfluorene (**FlSn2**) under pseudo high dilution conditions. The electronic structure of **MC-B6** was found to be significantly distinct from that of its linear counterpart **O-B6**. This cycle shows blue fluorescence in solution, which can be quenched upon complexation with nucleophiles such as F^{-} and CN^{-}, leading to the formation of an electron-rich macrocycle. Six reversible redox waves were detected in the electrochemical measurements, corresponding to sequential reduction of each of the borons. The lowest energy transition ($S_1 \leftarrow S_0$) is forbidden due to the dipole moment cancellation as confirmed by TD-DFT calculations.

Chapter 4. Conjugated Ambipolar B-π-N Macrocycles

Several B-N containing macrocycles have been prepared under pseudo high dilution conditions. The first ambipolar macrocycle **MC-B3N3** resembles a π-expanded borazine in which the alternating N donors are separated from B acceptors by phenylene bridges as confirmed by X-ray structure analysis. In contrast, another macrocycle **MC-B4N2** is composed of a hybrid π system (carbazole and fluorene). In both cycles, a pronounced ICT is apparent from the strong solvatochromic effect on the emission, but only a small effect on the absorption is observed. Also, due to the D–π–A type arrangement in the cycles, interactions between B and N are evidenced by electrochemical measurements, and these cycles can potentially serve as a p- and n-type semiconducting material. A cooperative binding effect was derived from anion binding studies in macrocycle **MC-B4N2**, but not in **MC-B3N3**.

These organoborane oligomers and macrocycles were all fully characterized via multinuclear NMR spectroscopy, high resolution mass spectrometry, GPC, and their photophysical, electrochemical and anion binding properties were studied. To support of our experimental findings, extensive DFT and TD-DFT computations were also carried out.

Acknowledgments

I wish to take this opportunity to express my greatest gratitude to my supervisor, Prof. Frieder Jäkle, for his generous support and guidance throughout my Ph.D. study, and for providing an environment in which I could develop toward a chemical professional. Most of all, I am impressed by Dr. Jäkle's passion as a scientist in chemistry and by his persistent pursuit of new discoveries even though he has already made numerous exciting findings. These attributes are of particular significance to build our professional career. Fortunately, I was able to work with Dr. Jäkle who perfectly set an example of how to conduct a research team.

I would like to acknowledge my committee members, Prof. Elena Galoppini, Prof. Ralf M. Peetz (City University of New York) and Prof. Phillip Huskey, for spending their time reading and correcting my thesis, and for their helpful advice and encouragement.

I would also like to thank all the Rutgers University-Newark chemistry faculty and staff for their kind help over the past five years. My thanks also goes to the former and current members in the Jäkle group, and especially I would like to thank Dr. Chengzhong Cui who helped me out during my time and Dr. Haiyan Li who gave me so much training on my projects. I appreciate extensive discussions with Dr. Xiaodong Yin and Fei Cheng, which are quite important as well.

I am indebted to my parents and my family for understanding both my education and

my choice. They have fully supported and taught me so much about life, love and science. I will forever be grateful for their presence in my life and hold them so very close to my heart.

Table of Contents

List of Chart and Schemes

List of Figures

List of Tables

MC-*b*-B3N3, **MC-*b*-B2N4** and **MC-*b*-BN5**

General Introduction

1. π-Conjugated Systems

Studies on π-conjugated systems were refueled since the Nobel Prize for Chemistry in 2000 was awarded to Professors Heeger, Shirakawa, and MacDiarmid for their discovery of "doped" polyacetylene as a highly conducting polymer in 1977.[1,2] Conjugated molecules including polymers and small molecules are a class of hydrocarbons that feature some degree of electron delocalization in the molecular skeleton. This unique electronic structure is expected to afford interesting optical and optoelectronic properties, which drive fast development of their applications in the areas of optics and sensors (photosensing devices, vapor sensors, biological and chemical sensors) as well as next generation of organic electronics, such as light-emitting devices (OLEDs), field-effect transistors (OFETs) and solar cells.[3-15]

1.1 Polyacetylene (PA)

PA was remarkable not only because it was first discovered to be highly conductive, it also has a low band gap and shows large nonlinear optical susceptibilities.[16] Band diagrams of PA can be described by simple Hückel molecular orbital theory in which π-orbitals are viewed as an infinite conjugated system. In the smallest monomer, individual bonding and nonbonding orbitals are illustrated in the traditional fashion (**Figure 1**). As the π system is extended, each discrete molecular orbital (MO) from the monomer splits into two MOs for the dimer (an in-phase and out-of-phase MO, respectively). This trend continues as the size of the conjugated polymer increases from dimer to an infinite length. As a consequence, each of the initial monomer MOs comprises an infinite number of MOs in the infinite polymer, which leads to the formation of energy bands due to their linear combinations.

However, application of PAs is largely limited in that they usually show poor solubility and oxidative instability. These challenges have partially been overcome through the incorporation of electronically stabilizing cyano groups into the oligoene chain as well as bulky aryl groups for the protection of reactive terminal olefins, such as α,ω-diaryl-μ,ν-dicyano-oligoenes (DPDC) that were recently synthesized by Nuckolls and coworkers (**Figure 2**).[17]

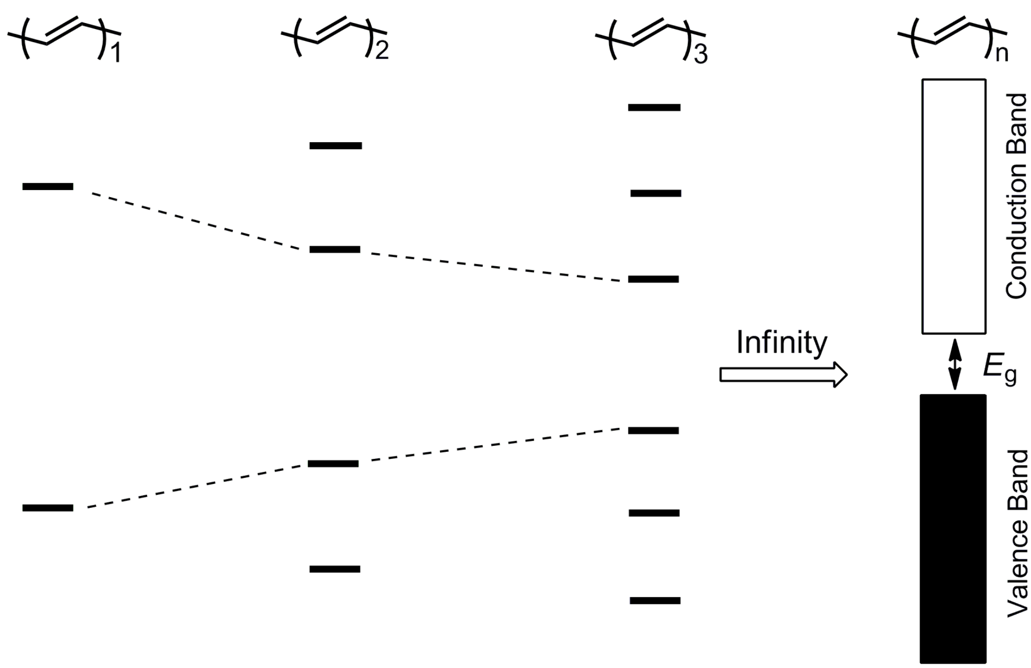

Figure 1. Band diagram developed by linear combination of MOs in polyacetylene.

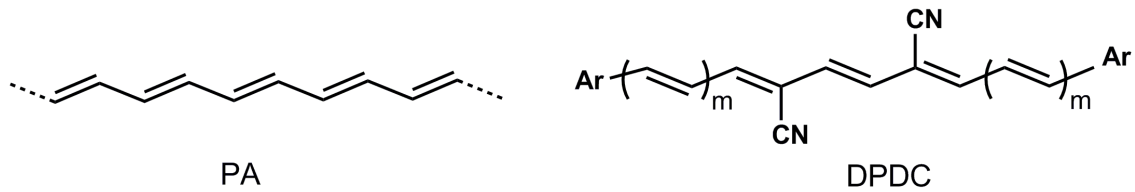

Figure 2. Chemical structures of polyacetylene (PA) and functionalized oligoenes (DPDC).

1.2 Aromatic Conjugated Systems

Alternatively, aromatic conjugated molecules and their derivatives are frequently investigated in the community of chemistry and materials science. Some early examples are poly(*p*-phenylene) (PPP), poly(phenylenevinylene) (PPV), polythiophene (PT), polyfluorene (PF) and polycarbazole (**Figure 3**).[15] Towards applications of conjugated molecules as semiconducting materials, a number of properties have to be taken into account. Specifically for photovoltaics, broad absorption bands (ca. 1.7 eV) and high absorption coefficients for effective sunlight harvesting, favorable HOMO and LUMO energy levels, HOMO-LUMO energy gaps (ideal value of 1.5 eV) for efficient charge transfer, device morphology depending on the self-assembly ability for efficient charge transport.[15] To address these issues, numerous molecular engineering strategies have been explored for fine-tuning the optoelectronic properties of the π-conjugated systems. The methodologies applied so far mainly include the increase of conjugation chain length, cross-conjugation, stabilization of the quinoidal resonance structure, enhancement of rigidity, planarization of building blocks, incorporation of main group elements (e.g. N, P, S, Si), and the use of donor-acceptor (D–A) alternating copolymerization.[18-21] In general, the HOMO-LUMO energy gaps can be narrowed by increasing the chain conjugation;[22] however, this method may not always take effect when the effective conjugation length is saturated.[23]

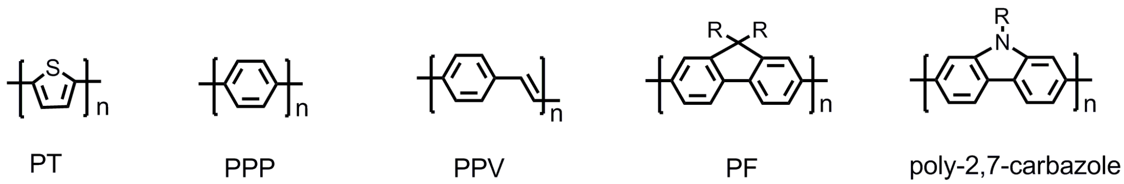

Figure 3. Chemical structures of early examples of aromatic conjugated polymers.

A prominent structural modification to polyphenylene compounds is to go to ladder-type polyphenylene, which is composed of linear fused fluorenes or heteroatom bridged phenylenes (**Figure 4**).[15,24] These compounds have proven to be advantageous in that the rigid structures favor electron delocalization which can further enhance the optical and electronic properties.[25-28] Another interesting class of polyphenylene derivatives are spiro compounds (**Figure 4**), which lead to excellent processability as a result of their improved solubility and high stability. They exist in the amorphous glassy state which is particularly desirable in active layer materials for various organic electronics.[29]

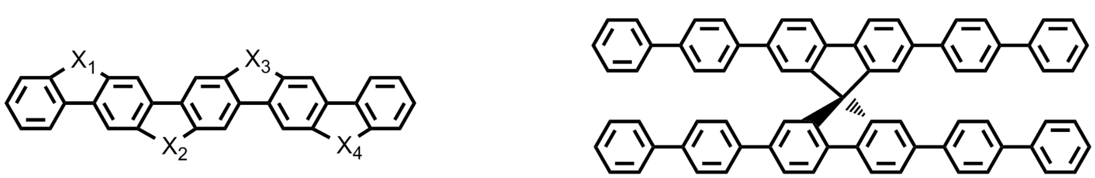

Figure 4. Representations of ladder-type (left) and spiro polyphenylene (right).

Another representative class of rigid π-conjugated systems are polycyclic aromatic hydrocarbons (PAHs) and their derivatives. These linearly fused aromatics have been demonstrated to exhibit considerable charge transfer ability resulting from their high HOMO levels, and thus serve as p-type semiconductors.[7] Although lots of studies have predicted intriguing electronic structures for larger PAHs, the synthesis and detailed studies of these materials suffer primarily from their poor solubility and low stability in the presence of light and oxygen.[30] To resolve this challenge, molecular modifications have been pursued that can modify the energy gaps by imposition of steric or electronic effects on the acene backbone. One efficient way of kinetic stabilization is the introduction of fluorinated moieties that potentially prevent the diffusion of water and oxygen into the active layers.[31] Studies showed that fluorinated acenes tend to give positively shifted redox potentials relative to the non-fluorinated derivatives and they adopt a face-to-face π-stacked structure, which benefits efficient charge mobility.[7] For example, pentacene shows a HOMO-LUMO gap of 2.07 eV, and a lower energy gap (1.95 eV) was obtained for perfluoropentacene (**Figure 5**).[32]

E_{re} = -1.87 V, E_{ox} = 0.22 V

E_g = 2.07 eV

E_{re} = -1.13 V, E_{ox} = 0.79 V

E_g = 1.95 eV

Figure 5. Structures and electrochemical data for pentacene and perfluoropentacene.[32]

Moreover, addition of bulky functional groups at certain positions of the acene molecules is desired to modify molecular ordering and improve π-orbital overlap. As shown in **Figure 6A,** the bulky TIPS group (TIPS = triisopropylsilyl) can also significantly improve the solubility of substituted pentacene.[33] Very similarly, an electron transport material of N-functionalized acene (**Figure 6B**) was recently synthesized, in which the HOMO-LUMO gap is lowered due to the stabilization of LUMO level by the electronegative nitrogens.[34] The combination of fluorination and bulky functional groups afforded a larger acene derivative (**Figure 6C**); larger structures tend to be notoriously difficult to stabilize and characterize.[35]

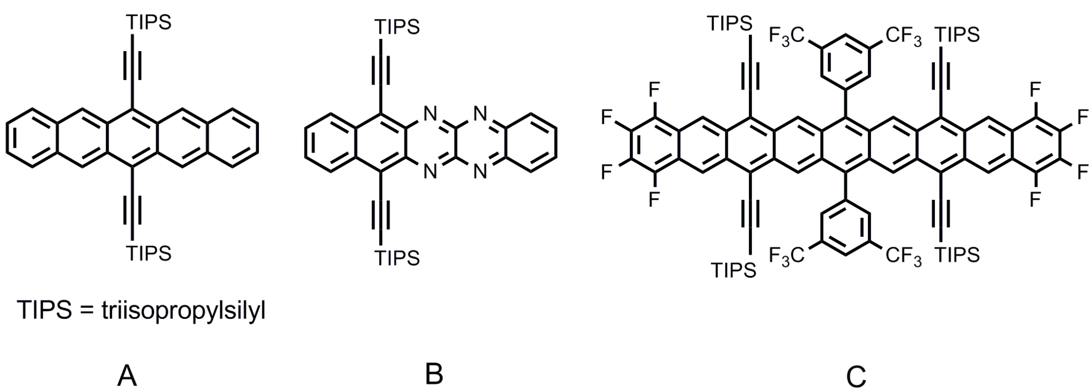

Figure 6. Stabilization of planar PAHs by imposition of steric and electronic effects.[33-35]

Another approach commonly used to tune the HOMO and LUMO energy levels is to incorporate electron rich donor (D) and electron deficient acceptor (A) units in the same ambipolar conjugated systems.[15] Hybridization of the donor and acceptor molecular orbitals results in a lowered HOMO-LUMO gap in that the donor tends to increase the HOMO level and the acceptor tends to decrease the LUMO level (**Figure 7**). The degree of the reduction of band gaps thus depends on the electron donating capability of the donor and electron accepting capability of the acceptor. Of the various electron donors known so far, the most often studied are thiophene-based compounds.[36, 37]

More recently, Bazan, Heeger and coworkers took advantage of this concept in combination with the addition of main group elements to develop an improved small molecule for optoelectronic application (**Figure 8**).[38] In this case, the $DTS(PTTh_2)_2$ structure is based on a core acceptor/donor/acceptor (A/D/A) framework with bithiophene donor end-capping units. Compared with the commonly used acceptor such as 2,1,3-benzothiadiazole (BTZ), the heterocycle [1,2,5]thiadiazolo[3,4-c]pyridine (PT) shows a higher electron affinity due to substitution of carbon with nitrogen. In the meantime, incorporation of the tetracoordinate Si atom in the dithieno(3,2-b;2'3'-d)silole (DTS) unit leads to a stronger donor relative to parent dithiophene.

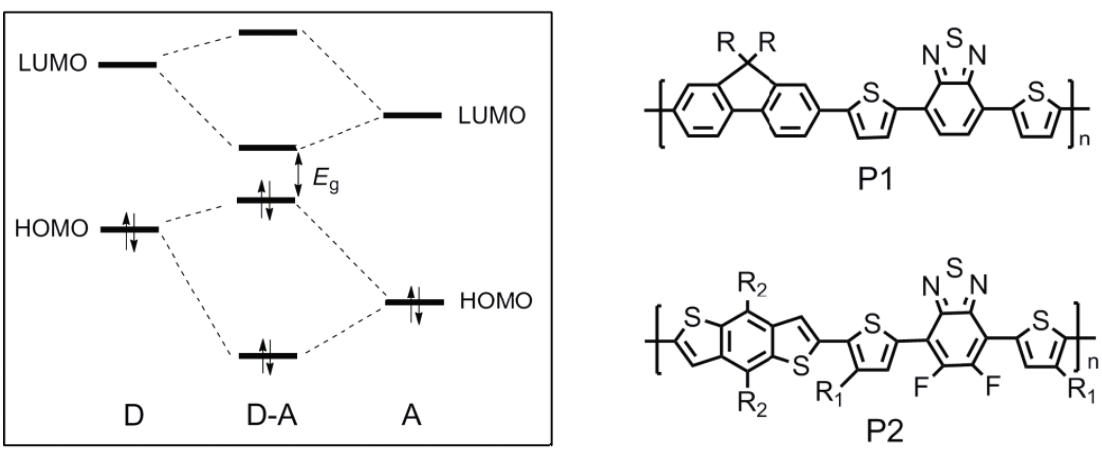

Figure 7. MO interactions (left) and typical examples (right) of D-π-A type conjugated systems.

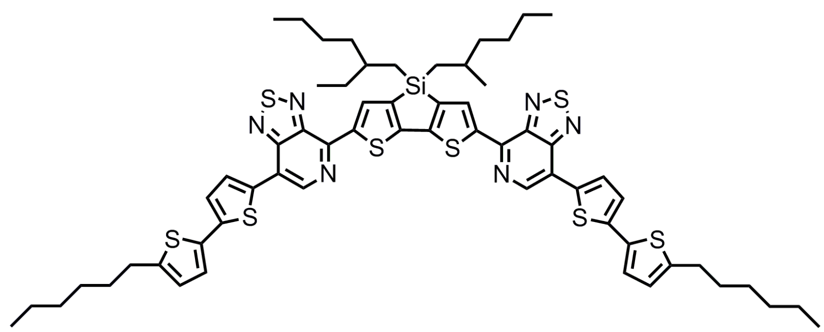

DTS(PTTh$_2$)$_2$

Figure 8. Molecular structure of D-π-A molecule with incorporation of main group elements.[38]

2. Conjugated Macrocycles

Research into macrocycles is of interest not only for their distinctly unique structures that feature an infinite chain length without any end groups, but also because they show potential for use in the area of host-guest chemistry and catalysis as a result of their unusual recognition and binding properties that are not found in the linear counterparts.[39,40]

Of particular significance in the advance of macrocycles is the preparation of conjugated cyclics. Full electron delocalization is expected as a consequence of their rigid and typically planar conformation, leading to a new strategy to π-conjugated electronics and semiconducting materials.[41] Another important aspect is the formation of tubular supramolecular nanostructures and of highly ordered self-assemblies at the solution/HOPG interface.[42]

Several approaches have been proposed to synthesize macrocycles of interest, including the traditional slow addition of bifunctional building blocks, templation,[43,44] and the recent strategy of phase separation.[45,46] But the efficient macrocyclization remains a big challenge in that competition reactions such as linear oligomerization and polymerization are always involved in the macrocyclization process, and these undesired reactions are more favorable in most cases. The reason for this problem is predominantly due to the presence of ring strain that prevents the success of macrocyclization.

Nevertheless, synthetic chemists have found some effective routes to prepare rigid aromatic macrocycles with reasonably high yield.

2.1 Post-aromatization

Interest in [*n*]-cyclo(*para*-phenylene)s ([*n*]CPPs; where [n] refers to the number of phenylene rings extended) was refueled by their structural relation to the single-walled carbon nanotubes (SWNTs). These carbon-based aromatic cycles can serve as finite models of armchair (n,n)-SWNTs (**Figure 9**).[47, 48] Since the pioneer work by Bertozzi, in 2008, a series of [6]-[18]CPPs have been prepared and isolated by three different methods.[47] The key idea is to perform post aromatization after macrocyclization.

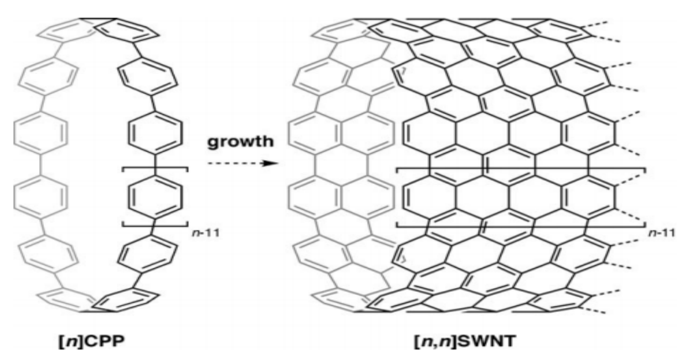

Figure 9. Structure of CPPs and their relationship to (n,n)-SWNTs (left).[48]

As shown in **Scheme 1** for the first method developed by Bertozzi and co-workers,[49] a cyclohexadiene unit plays a crucial role in formation of the non-aromatic cycle, adopting a bent boat-shaped conformation that exhibits much less ring strain and favors the macrocyclization. Using this building block, they generated the cyclic precursor by Suzuki coupling reaction, which was then reduced with lithium naphthalenide to produce the resulting aromatic cycles. Very similarly, another less strained building block containing chair-like cyclohexane was first used by Itami and coworkers (**Scheme 2**).[50] The third synthesis of [*n*]CPPs works slightly different, which was carried out by Yamago et al. **Scheme 3** illustrates the general procedures: reactions of distannylated species with [Pt(cod)Cl_2] generate the macrocyclic Pt-containing intermediates, which upon reductive elimination of platinum give rise to CPPs with different ring size depending on the combination of distannylated precursors.[51]

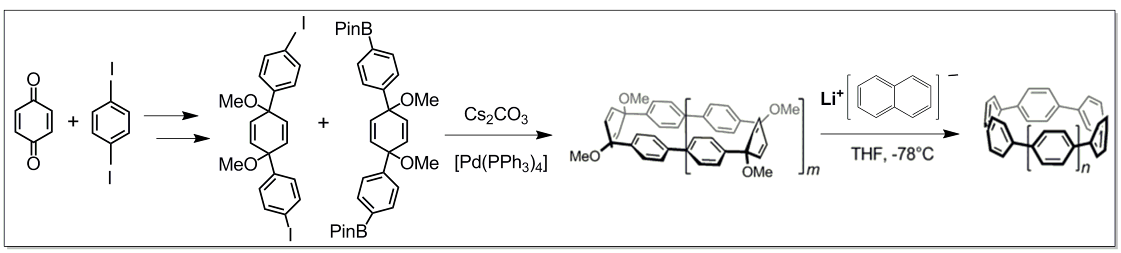

Scheme 1. Post-aromatization strategy for [*n*]CPPs by Bertozzi and co-workers.[49]

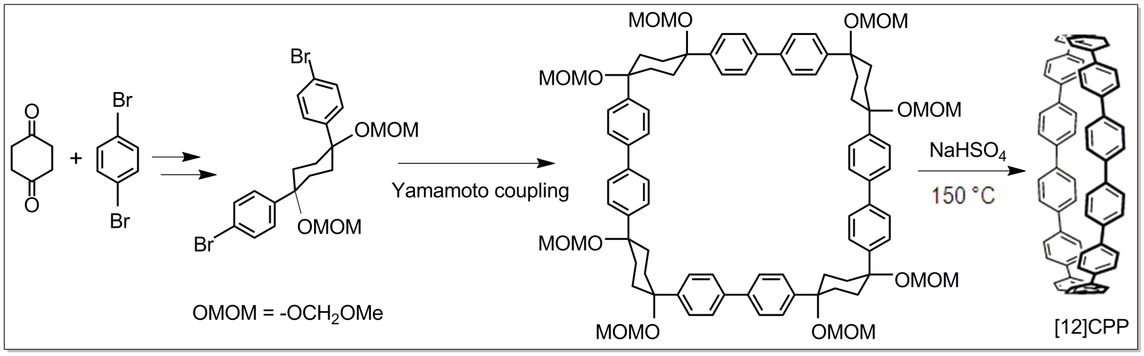

Scheme 2. Post-aromatization strategy for [12]CPP by Itami and co-workers.[50]

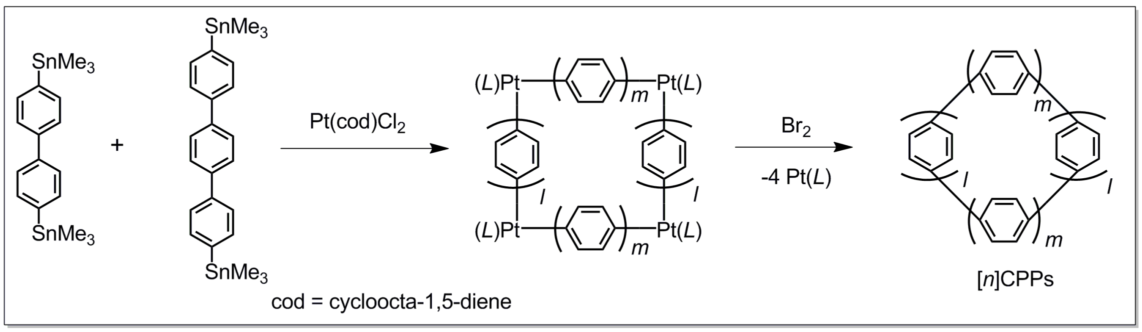

Scheme 3. Post-aromatization by reductive elimination for [*n*]CPPs by Yamago and co-workers.[51]

The synthesis of CPPs with different, but exactly known ring size allows people to capture their electronic and photophysical properties. For instance, the UV absorption does not show any size dependence. In contrast, the emission wavelengths are red shifted as the CPP size decreases. The HOMO energy levels increase gradually due to a decreased aromaticity when the cycles get smaller (i.e. the cycle tends to show polyene character), which was supported by an upfield shift of ^{1}H NMR signal. The oxidation potentials are lowered for the small ring size, in agreement with the increasing ring strain energies predicted by DFT calculations.[51]

2.2 Template-induction

Apart from the post-aromatization, use of templates can reduce the entropic and enthalpic barrier to cyclization. With this respect, excellent contributions have been made by Anderson and co-workers. As shown in **Scheme 4**, Glaser-Hay coupling of the linear Zn porphyrin complex bearing terminal acetylene functionalities in the presence of hyperbranched pyridine ligands (T6 or T8) as templates gives rise to conjugated porphyrin-based macrocycles. The key to success of macrocyclization arises from coordination of pyridine to the Zn centers. This dynamic supramolecular interaction facilitates equilibration shift to Vernier assembly. The coordination to templates can also ensure efficient overlap of the π orbitals in the final nanorings by preventing rotation of the individual porphyrin moieties. The ring size can be precisely controlled by selection of the pyridine templates.[52-54]

2.3 Depolymerization

A new strategy of depolymerization macrocyclization was first developed by Moore and co-workers to prepare carbazole-based conjugated macrocycles.[55] As described in **Scheme 5**, the standard Sonogashira coupling reaction of a terminal alkyne-functionalized carbazole monomer with an aryl halide readily generates a carbazolylethynylene homopolymer. In the next key step, this polymer is depolymerized to form a macrocycle using a highly active molybdenum alkylidyne catalyst. Such transformation of polymer to macrocycle is entropically favorable. The current method is ideally utilized to pursue functionalized macrocycles, such as amphiphilic cycles through simple modifications of the substituents on the carbazole moieties.[56]

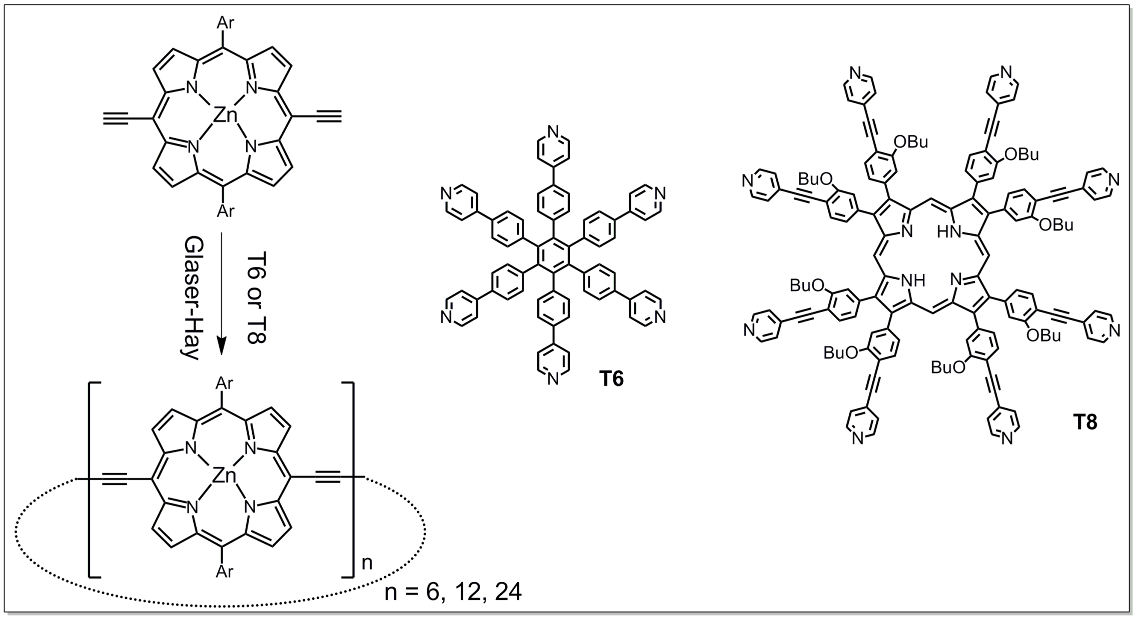

Scheme 4. Template macrocyclization of porphyrin-based macrocycles by Anderson et al.[52-54]

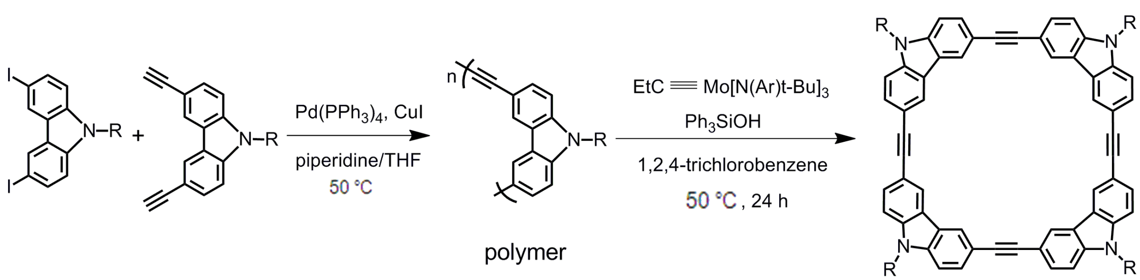

Scheme 5. Depolymerization for conjugated macrocycles by Moore and co-workers.[55]

2.4 Heteroatom Containing Conjugated Macrocycles

In addition to the carbon rich [*n*]CPPs, porphyrin-based and ethynylene-containing macrocycles discussed in early section, heteroatom doped macrocycles of other types have also been investigated, such as cyclic oligothiophenes, cyclopyridines, and cyclocarbazoles.[41]

The first synthesis of fully conjugated cyclic oligothiophenes was achieved by Bäuerle and co-workers in 2000.[57] The Cu(I)/Cu(II) catalyzed Glaser-Hay coupling reaction of terminal thiophenediynes was performed to yield a cyclic intermediate, oligo(thienylbutadiyne), which was then treated with Na_2S, leading to formation of the resulting macrocyclic oligothiophenes (**Scheme 6**).

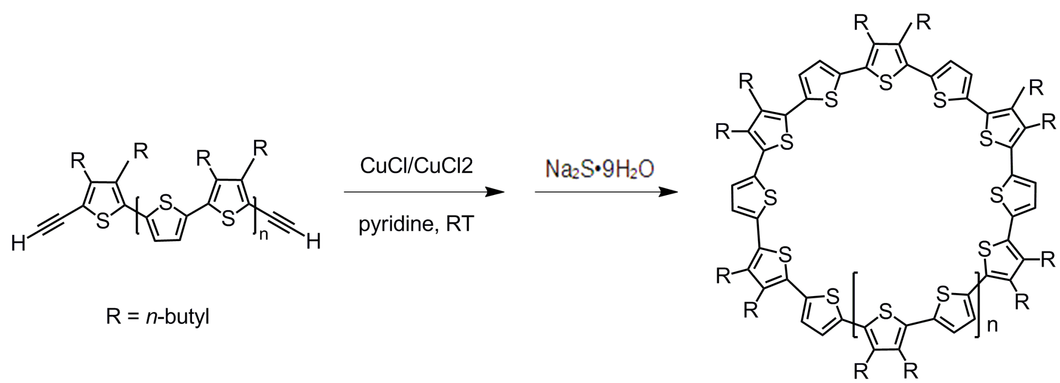

Scheme 6. Synthesis of the fully conjugated cyclic oligothiophenes.[57]

Since cyclosexipyridine was first reported by Newkome and Lee in 1980s,[58] various pyridine-containing macrocycles have been obtained through structural modifications of the building blocks, including terpyridine, pyridine-acetylene and pyridine-butadiyne units (**Figure 10**).[59] This class of pyridine-functionalized cycles provides multiple coordination sites that can form metallocycles for new applications.

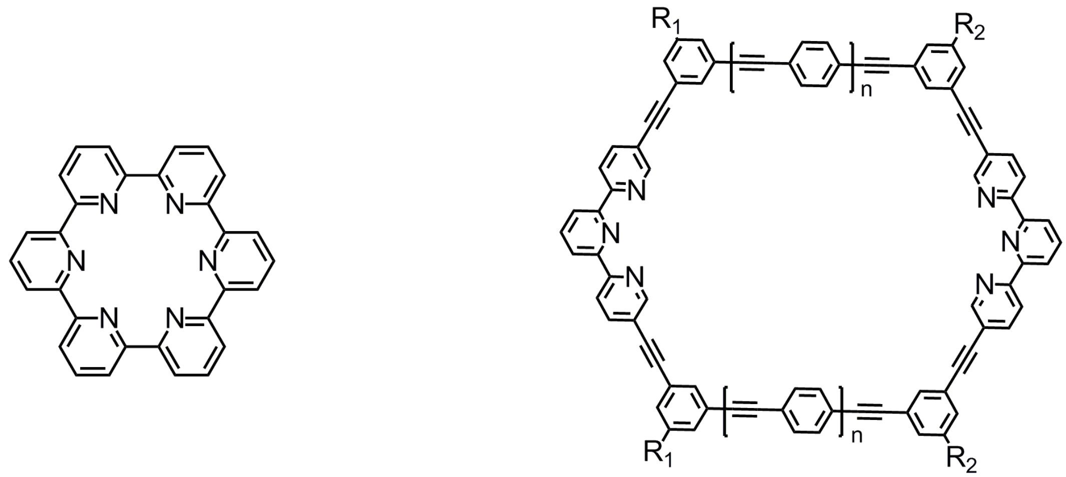

Figure 10. Examples of pyridine-containing conjugated macrocycles.[58,59]

Fully conjugated cyclododeca-2,7-carbazole and its fluorene analogue were synthesized by Müllen and co-workers with the use of meso-tetra(4-carboxyphenyl) porphyrin as a template.[60,61] The cyclization was conducted through a nickel-mediated Yamamoto coupling reaction of halogen-terminated trimer units under highly dilute conditions. Treated with a base (e.g. KOH), the porphyrin templates were removed from the cyclic intermediates to generate the target macrocycles (**Figure 11**).

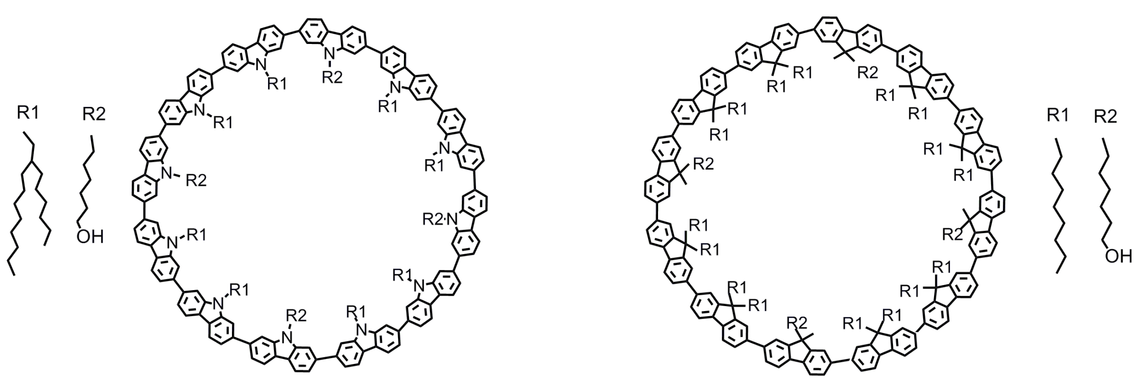

Figure 11. Cyclododeca-2,7-carbazole and cyclododeca-2,7-fluorene by Müllen et al.[60,61]

3. Main Chain Conjugated Organoboranes

Of the π-conjugated systems with incorporation of main group elements, tricoordinate boron containing compounds are unique. Electron deficient boron provides a vacant p orbital and thus functions as a strong π-electron acceptor capable of significant delocalization (**Figure 12**).[62] Overlap of the empty p orbital on the boron with the LUMO of organic scaffolds leads to a decrease of the HOMO-LUMO gap. This phenomenon brings about interesting optical and electronic properties that are desirable for applications in functional materials. Such compounds have been demonstrated to show nonlinear optical activity and large two-photon absorption cross-sections. They can also be employed as electron-transporting layers in organic electronics.[63-65]

On the other hand, three-coordinate boron exhibits Lewis acidic nature, and thereby the nucleophilic attack by electron donors can significantly change the electronic structure of boron. The original trigonal planar three-coordinate boron is converted to a tetracoordinate species in which the p-π overlap is turned off. As a result, three-coordinate organoboranes have been extensively explored as colorimetric and luminescent sensors for anions such as fluoride and cyanide.[66] Noteworthy is that stabilization of tricoordinate boron is important. Steric protection is generally required to prevent decomposition in air and moisture using bulky groups such as 2,4,6-trimethylphenyl (Mes), 2,4,6-triisopropylphenyl (Tip) and the most bulky 2,4,6-tritertbutylphenyl (Mes*) (**Figure 13**).[67]

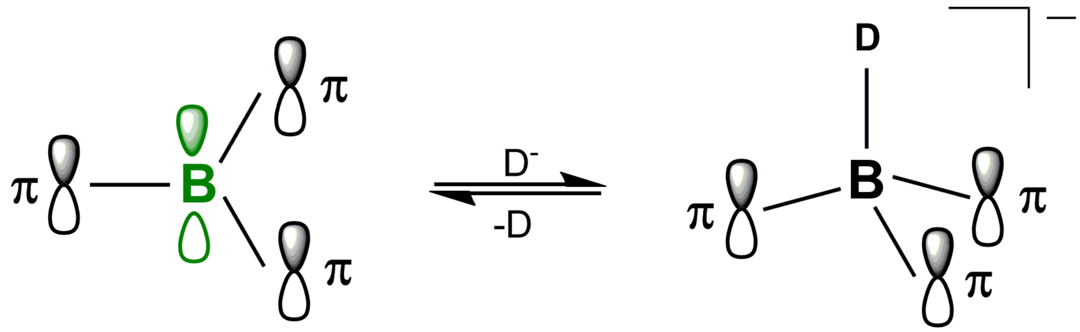

Figure 12. Illustration of MO interactions of boron with π substituents and nucleophiles.

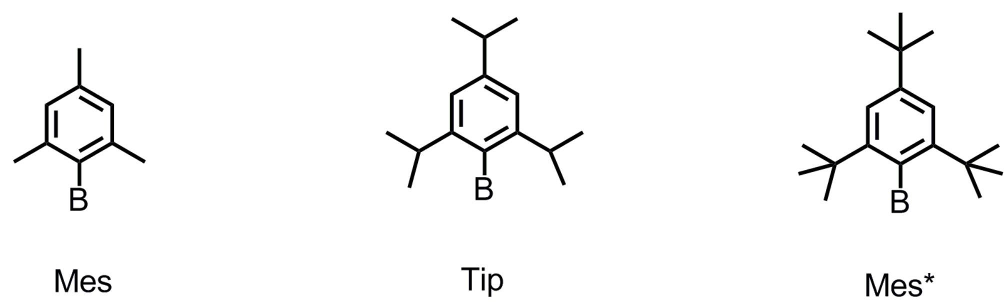

Figure 13. Bulky groups usually used to protect boron species.

To date, several routes for the incorporation of boron in the π-conjugated systems have been introduced. Hydroboration,[68-72] and metathesis reactions[73,74] are now well-established to form main chain boron-containing compounds (**Figure 14**). Hydroboration polymerization was first proposed by the Chujo group in 1998 for the extension of π-conjugation using mesitylborane moieties.[68] However, these polymers proved to be not thermally very stable in part owing to the retro-hydroboration at high temperature above 100 °C. Given this drawback, the same research group developed another approach of metathesis. Polycondensation between aryldimethoxyborane and di-Grignard reagents afford π-conjugated polymers. For such kind of polymerization, the key issue of success is the use of bulky aryl substituent on the alkoxyborane.

Our group found a facile method of Sn/B exchange to access boron containing polymers under very mild conditions.[75,76] In addition to the formation of side-chain functionalized organoboron polymers, the incorporation of boron in the main chain is also quite facile (**Figure 14**).[77]

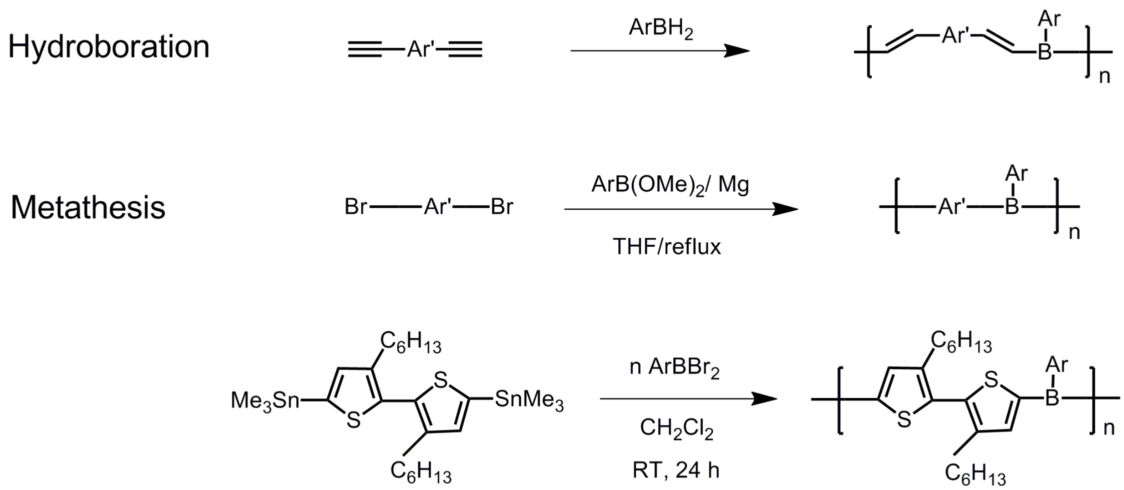

Figure 14. General strategies for main-chain organoborane π conjugated systems.

One of the most prominent boron-based substituents is the dimesitylboryl ($BMes_2$) moiety, in which the unsaturated boron is stabilized by *ortho*-methyl groups. Mes_2BF is an ideal boron source for side-chain boron-containing polymers through reaction with Grignard or organolithium reagents (**Figure 15**).[65,78,79] The $BMes_2$ groups serve as π acceptors comparable to the commonly used electron-withdrawing nitro and cyano functionalities.[80,81]

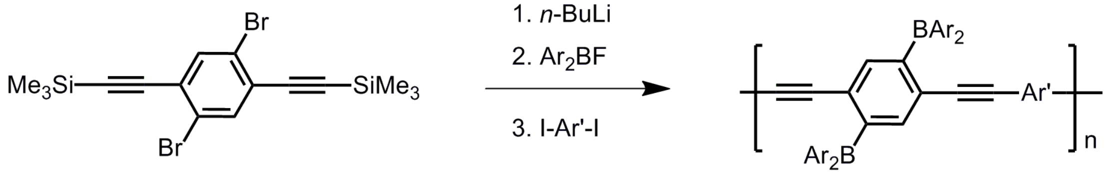

Figure 15. Borylation reaction for side-chain boron containing conjugated polymers.[79]

The reactions discussed above all constitute step-growth polymerizations, leading to the formation of polymers with a relatively large polydispersity and no control over molecular weight and polymer end groups. In order for the molecular structures to be exactly controlled, research has been pursued for this thesis that will focus on the synthesis of monodisperse conjugated organoborane oligomers and of macrocycles with all boron or B-N containing ambipolar moieties in the conjugated backbones. They have been characterized by photophysical and electrochemical measurements in combination with computational studies .

4. References

(1) Chiang, C. K.; Fincher, C. R.; Park, Y. W.; Heeger, A. J.; Shirakawa, H.; Louis, E. J.; Gau, S. C.; MacDiarmid, A. G. *Phys. Rev. Lett.* **1977**, *39*, 1098.

(2) Wang, C.; Dong, H.; Hu, W.; Liu, Y.; Zhu, D. *Chem. Rev.* **2012**, *112*, 2208.

(3) McQuade, D. T.; Pullen, A. E.; Swager, T. M. *Chem. Rev.* **2000**, *100*, 2537.

(4) Dimitrakopoulos, C. D.; Malenfant, P. R. L. *Adv. Mater.* **2002**, *14*, 99.

(5) Martínez-Máñez, R.; Sancenón, F. *Chem. Rev.* **2003**, *103*, 4419.

(6) Shirota, Y.; Kagayama, H. *Chem. Rev.* **2007**, *107*, 953.

(7) Murphy, A. R.; Fréchet, J. M. J. *Chem. Rev.* **2007**, *107*, 1066.

(8) Walzer, K.; Maennig, B.; Pfeiffer, M.; Leo, K. *Chem. Rev.* **2007**, *107*, 1233.

(9) Zaumseil, J.; Sirringhaus, H. *Chem. Rev.* **2007**, *107*, 1296.

(10) Günes, S.; Neugebauer, H.; Sariciftci, N. S. *Chem. Rev.* **2007**, *107*, 1324.

(11) Thomas III, S. W.; Joly, G. D.; Swager, T. M. *Chem. Rev.* **2007**, *107*. 1339.

(12) Grimsdale, A. C.; Chan, K. L.; Martin, R. E.; Jokisz, P. G.; Holmes, A. B. *Chem. Rev.***2009**, *109*. 897.

(13) Wen, Y.; Liu, Y. *Adv. Mater.* **2010**, *22*, 1.

(14) Duan, X.; Liu, L.; Feng, F.; Wang, S. *Acc. Chem. Res.* **2010**, *43*, 260.

(15) Li, C.; Liu, M.; Pschirer, N. G.; Baumgarten, M.; Müllen, K. *Chem. Rev.* **2010**, *110*. 6817.

(16) Fann, W. S.; Benson, S.; Madey, J. M. J.; Etemad, S.; Baker, G. L.; Kajzar, F. *Phys. Rev. Lett.* **1989**, *62*, 1492.

(17) Meisner, J. S.; Sedbrook, D. F.; Krikorian, M.; Chen, J.; Sattler, A.; Carnes, M. E.; Murray, C. B.; Steigerwald, M.; Nuckolls, C. *Chem. Sci.* **2012**, *3*, 1007.

(18) Bruch, A.; Fukazawa, A.; Yamaguchi, E.; Yamaguchi, S.; Studer, A. *Angew. Chem. Int. Ed.* **2011**, *50*, 12094.

(19) Ren, Y.; Kan, W. H.; Henderson, M. A.; Bomben, P. G.; Berlinguette, C. P.; Thangadurai,V.; Baumgartner, T. *J. Am. Chem. Soc.* **2011**, *133*, 17014.

(20) Ren, Y.; Kan, W. H.; Thangadurai, V.; Baumgartner, T. *Angew. Chem. Int. Ed.* **2012**, *51*, 3964.

(21) Zalar, P.; Henson, Z. B.; Welch, G. C.; Bazan, G. C.; Nguyen, T. *Angew. Chem. Int. Ed.* **2012**, *51*, 7495.

(22) Tour, J. M. *Chem. Rev.* **1996**, *96*, 537.

(23) Roncali, J. *Chem. Rev.* **1997**, *97*, 173.

(24) Fan, H. H.; Guo, L.; Li, K. F.; Wong, M. S.; Cheah, K. W. *J. Am. Chem. Soc.* **2012**, *134*, 7297.

(25) Becker, K.; Lupton, J. M. *J. Am. Chem. Soc.* **2006**, *128*, 6468.

(26) Becker, K.; Lupton, J. M.; Feldmann, J.; Setayesh, S.; Grimsdale, A. C.; Müllen, K. *J. Am. Chem. Soc.* **2006**, *128*, 680.

(27) Usta, H.; Facchetti, A.; Marks, T. J. *J. Am. Chem. Soc.* **2008**, *130*, 8580.

(28) Usta, H.; Risko, C.; Wang, Z.; Huang, H.; Deliomeroglu, M. K.; Zhukhovitskiy, A.; Facchetti, A.; Marks, T. J. *J. Am. Chem. Soc.* **2009**, *131*, 5586.

(29) Saragi, T. P. I.; Spehr, T.; Siebert, A.; Fuhrmann-Lieker, T.; Salbeck, J. *Chem. Rev.* **2007**, *107*, 1011.

(30) Tönshoff, C.; Bettinger, H. F. *Angew. Chem. Int. Ed.* **2010**, *49*, 4125.

(31) Winkler, M.; Houk, K. N. *J. Am. Chem. Soc.* **2007**, *129*, 1805.

(32) Sakamoto, Y.; Suzuki, T.; Kobayashi, M.; Gao, Y.; Fukai, Y.; Inoue, Y.; Sato, F.; Tokito, S. *J. Am. Chem. Soc.* **2004**, *126*, 8138.

(33) Sheraw, C. D.; Jackson, T. N.; Eaton, D. L.; Anthony, J. E. *Adv. Mater.* **2003**, *15*, 2009.

(34) Lindner, B. D.; Engelhart, J. U.; Tverskoy, O.; Appleton, A. L.; Rominger, F.; Peters, A.; Himmel, H.; Bunz, U. H. F. *Angew. Chem. Int. Ed.* **2011**, *50*, 8588.

(35) Purushothaman, B.; Bruzek, M.; Parkin, S. R.; Miller, A.; Anthony, J. E. *Angew.*

Chem. Int. Ed. **2011**, *50*, 7013.

(36) Svensson, M.; Zhang, F.; Veenstra, S. C.; Verhees, W. J. H.; Hummelen, J. C.; Kroon, J. M.; Inganaes, O.; Andersson, M. R. *Adv. Mater.* **2003**, *15*, 988.

(37) Zhou, H.; Yang, L.; Stuart, A. C.; Price, S. C.; Liu, S.; You, W. *Angew. Chem. Int. Ed.* **2011**, *50*, 2995.

(38) Sun, Y.; Welch, G. C.; Leong, W. L.; Takacs, C. J.; Bazan, G. C.; Heeger, A. J. *Nat Mater.* **2012**, *11*, 44.

(39) Wessjohann, L. A.; Rivera, D. G.; Vercillo, O. E. *Chem. Rev.* **2009**, *109*, 796.

(40) Gessner, V. H.; Tannaci, J. F.; Miller, A. D.; Tilley, A. T. D. *Acc. Chem. Res.* **2011**, *44*, 435.

(41) Iyoda, M.; Yamakawa, J.; Rahman, M. J. *Angew. Chem. Int. Ed.* **2011**, *50*, 10522.

(42) Zang, L.; Che, Y.; Moore, J. S. *Acc. Chem. Res.* **2008**, *41*, 1596.

(43) Boyd, P. D. W. *Acc. Chem. Res.* **2005**, *38*, 235.

(44) Mulholland, A. R.; Woodward, C. P.; Langford, S. J. *Chem. Commun.* **2011**, *47*, 1494.

(45) Bédard, A.; Collins, S. K. *J. Am. Chem. Soc.* **2011**, *133*, 19976.

(46) Bédard, A.; Collins, S. K. *Chem. Common.* **2012**, *48*, 6420.

(47) Bunz, U. H. F.; Menning, S.; Martín, N. *Angew. Chem. Int. Ed.* **2012**, *51*, 7094.

(48) Omachi, H.; Matsuura, S.; Segawa, Y.; Itami, K. *Angew. Chem. Int. Ed.* **2010**, *49*, 10202.

(49) Jasti, R.; Bhattacharjee, J.; Neaton, J. B.; Bertozzi, C. R. *J. Am. Chem. Soc.* **2008**, *130*, 17646.

(50) Takaba, H.; Omachi, H.; Yamamoto, Y.; Bouffard, J.; Itami, K. *Angew. Chem. Int. Ed.* **2009**, *48*, 6112.

(51) Iwamoto, T.; Watanabe, Y.; Sakamoto, Y.; Suzuki, T.; Yamago, S. *J. Am. Chem. Soc.* **2011**, *133*, 8354.

(52) Kleij, A. W. *Angew. Chem. Int. Ed.* **2011**, *50*, 10770.

(53) Sprafke, J. K.; Kondratuk, D. V.; Wykes, M.; Thompson, A. L.; Anderson, H. L.; et al. *J. Am. Chem. Soc.* **2011**, *133*, 17262.

(54) Kondratuk, D. V.; Perdigao, L. M. A.; O'Sullivan, M. C.; Svatek, S.; Smith, G.; O'Shea, J. N.;Beton, P. H.; Anderson, H. L. *Angew. Chem. Int. Ed.* **2012**, *51*, 6696.

(55) Gross, D. E.; Moore, J. S. *Macromolecules* **2011**, *44*, 3685.

(56) Gross, D. E.; Discekici, E.; Moore, J. S. *Chem. Commun.* **2012**, *48*, 4426.

(57) Krömer, J.; Rios-Carreras, I.; Fuhrmann, G.; Musch, G.; Wunderlin, M.; Debaerdemaeker, T.; Mena-Osteritz, E.; Bäuerle, P. *Angew. Chem. Int. Ed.* **2000**, *39*, 3481.

(58) Newkome, G. R.; Lee, H. W. *J. Am. Chem. Soc.* **1983**, *105*, 5956.

(59) Grave, C.; Lentz, D.; Schäfer, A.; Samori, P.; Rabe, J. P.; Franke, P.; Schlüter, A. D. *J. Am. Chem. Soc.* **2003**, *125*, 6907.

(60) Jung, S.; Pisula, W.; Rouhanipour, A.; Räder, H. J.; Jacob, J.; Müllen, K. *Angew. Chem. Int. Ed.* **2006**, *45*, 4685.

(61) Simon, S. C.; Schmaltz, B.; Rouhanipour, A.; Räder, H. J.; Müllen, K. *Adv. Mater*. **2009**, *21*, 83

(62) Entwistle, C. D.; Marder, T. B. *Angew. Chem. Int. Ed.* **2002***, 41,* 2927.

(63) Jäkle, F. *Coord. Chem. Rev*. **2006**, *250*, 1107.

(64) Jäkle, F. *Chem. Rev*. **2010**, *110*, 3985.

(65) Matsumi, N.; Chujo, Y. *Polym. J.* **2008**, *40*, 77.

(66) Wade, C. R.; Broomsgrove, A. E. J.; Aldridge, S.; Gabbaï, F. P. *Chem. Rev.* **2010**, *110*, 3958.

(67) Wakamiya, A.; Mishima, K.; Ekawa, K.; Yamaguchi, S. *Chem. Commun*. **2008**, 579.

(68) Matsumi, N.; Naka, K.; Chujo, Y. *J. Am. Chem. Soc.* **1998**, *120*, 5112.

(69) Matsumi, N.; Miyata, M.; Chujo, Y. *Macromoleculars* **1999**, *32*, 4467.

(70) Matsumi, N.; Chujo, Y.; Lavastre, O.; Dixneuf, P. H. *Organometallics* **2001**, *20*, 2425.

(71) Matsumoto, F.; Matsumi, N.; Chujo, Y. *Polym. Bull.* **2001**, *46*, 257.

(72) Matsumoto, F.; Chujo, Y. *Pure Appl. Chem*. **2009**, *81*, 433.

(73) Matsumi, N.; Umeyama, T.; Chujo, Y. *Polym. Bull.* **2000**, *44*, 431.

(74) Matsumi, N.; Naka, K.; Chujo, Y. *J. Am. Chem. Soc*. **1998**, *120*, 10776.

(75) Qin, Y.; Cheng, G.; Sundararaman, A.; Jäkle, F. *J. Am. Chem. Soc*. **2002**, *124*, 12672.

(76) Parab, K.; Venkatasubbaiah, K.; Jäkle, F. *J. Am. Chem. Soc*. **2006**, *128*, 12879.

(77) Sundararaman, A.; Victor, M.; Varughese, R.; Jäkle, F. *J. Am. Chem. Soc*. **2005**, *127*, 13748.

(78) Zhao, C.; Sakuda, E.; Wakamiya, A.; Yamaguchi, S. *Chem. Eur. J.* **2009**, *15*, 10603.

(79) Zhao, C.; Wakamiya, A.; Yamaguchi, S. *Macromolecules* **2007**, *40*, 3898.

(80) Glogowski, M. E.; Williams, J. L. R. *J. Organomet. Chem*. **1981**, *218*, 137.

(81) Schulz, A.; Kaim, W. *Chem. Ber* **1989**, *122*, 1863.

Chapter 1 Luminescent Conjugated Fluoreneborane Oligomers[a]

Conjugated polymers are recognized as an important category of functional materials used for organic semiconductor applications in part due to the facile preparation and good solution processability.[1] However, conjugated small molecules can have specific benefits in certain applications. They can, for example, show improved hole mobility in comparison to polymers, which is attributed to the crystallinity and high level of ordering structures as well as the fabrication reproducibility.[2,3]

Monodisperse conjugated oligomers are intermediate between polymers and small molecules in terms of their size. One key advantage of using so-called oligomer approach to conjugated materials originates from the defined structures. The uniform structures and exactly known molecular weight allow for the correlation of physical properties with the chain conjugation. The combination of attributes from molecular and polymeric materials offer oligomers the merit of molecule-like structural purity while retaining polymer-like features. They show precise HOMO/LUMO energy levels, desirable solubility characteristics, high thermal stability and good mechanical properties.[4,5]

An issue that commonly arises in the development of polymeric materials is that chain-length related properties can be remarkably difficult to characterize for statistically averaged polymers. In sharp contrast, characterization of well-defined oligomers provides important clues for the investigation of polymers. As a common example,

[a] This chapter is adapted from a journal publication (ref. 98).

oligomers are frequently explored as model systems, which are informative to estimate the electronic properties of polymers through extrapolation of oligomer properties to infinite chain length.[6]

Despite often tedious synthetic procedures that involve several iterative steps, a variety of well-defined conjugated oligomers have been prepared to date. Typical systems are oligothiophenes, oligoanilines, oligofluorenes and oligophenylenes, etc. Of these oligomers, oligothiophenes including linear systems and higher dimensional dendrimers have been studied for electronic materials and for the controlled bottom-up fabrication of electronic devices as a consequence of their hole transporting capability and ease of synthetic modifications as well as self-assembly process for highly stereoregualr structures.[7-11] N-functionalized linear oligoanilines were synthesized for applications of conductive and redox active materials.[12-14] In addition, oligofluorenes were prepared for detailed study of their structure-property relationships. These studies suggested that chain length of oligomers plays an important role in their optical and electronic properties as well as in solid morphology.[15-17]

Another recent example are oligomeric *o*-phenylenes, which are of interest in the area of molecular chirality that is of paramount importance for the separation of chiral compounds and for asymmetric catalysis.[18,19] Oligomeric *o*-phenylenes are optically active as they adopt a helical conformation. Fukushima, Aida and co-workers isolated oligophenylenes that are optically pure in the solid state, The optical activity was lost in solution, but can be stabilized by one-electron oxidation (**Figure 1-1**).[19] They also discovered that the helical conformation is dependent both on the solvent and on the terminal groups attached to the oligomer chains.[20]

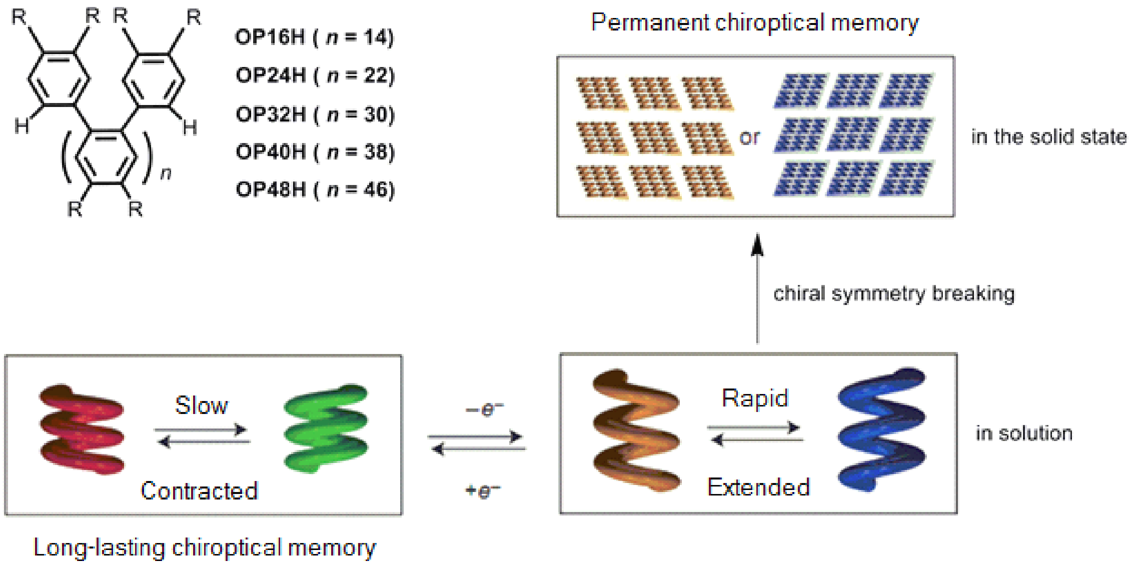

Figure 1-1. Molecular structures (top left) of chiral oligophenylenes and representations of the helical inversion dynamics in solution and in the solid state.[19]

1.1 Conjugated Organoborane π Systems

The functionalization of conjugated systems with main group heteroatomS has been an active area of research over the past several years.[21-32] While phosphorus-containing polymers[33-36] and their higher homologues, the arsenic and antimony derivatives,[37,38] feature electron-rich donor sites that can, for example, act as ligands for transition metal complexes, the respective organoborane-functionalized polymers[39-53] may be viewed as electron-deficient ("charge reverse") analogues with an empty *p*-orbital on boron as the characteristic feature.[54] Overlap of this empty *p*-orbital with conjugated organic *π*-systems is known to lead to unusual optical and electronic properties, and the ensuing *π*-acceptor effect is of interest for potential applications of organoboranes in optoelectronics (OLEDs, FETs, photovoltaics).[55-69] Lewis acidic organoborane molecules are also attractive as probes and sensors for anions and other nucleophiles, including toxic small molecules and chemical warfare agents.[49-53,70, 71]

A very fundamental question that is of great importance with respect to applications of organoborane polymers as conjugated materials is: how effective is the extended conjugation through the empty p_π orbital? Theoretical studies are consistent with gradual lowering of the HOMO-LUMO gap with increasing chain length and for some polymeric structures metallic properties have even been predicted.[72-80] Experimental verification has however proven difficult. On the other hand, an approach that has been very successful for a broad range of conjugated systems is to prepare well-defined oligomers of exact chain length and to compare their electronic structures and photophysical properties[9,12,81,82]

1.2 Synthesis and Structural Characterization of Oligofluoreneboranes

We present here the first experimental study on the extension of π-conjugation in organoborane polymers by incrementally increasing the oligomer chain length of fluoreneborane species **O-B*n*** all the way to a hexamer (n = 6).[83] Our new method takes advantage of the selective reactivity of arylsilane *vs* arylstannane functionalities in electrophilic substitution reactions with boron halides. In species $ArSiMe_3$, the aryl groups are typically cleaved with BBr_3 in CH_2Cl_2 at RT, but do not react with less reactive organoboron halides such as $PhBBr_2$ under these conditions.[84,85] The aryl groups in species $ArSnMe_3$ on the other hand react readily with organoboron halides $ArBBr_2$ to yield compounds Ar_2BBr without formation of any Ar_3B even in the presence of excess of the tin reagent when Ar = Ph. Based on this differential reactivity we have devised a stepwise assembly process that makes use of aromatic entities that contain one silyl and one stannyl moiety (**Scheme 1-1**). After every chain extension step the B-Br groups are capped with bulky aryl groups by reaction with triisopropylphenyl copper (TipCu) to give reasonably air-stable compounds with sterically protected borane functionalities and trimethylsilyl end groups. These oligomers can be isolated and purified by standard techniques, including column chromatography.

GPC analysis (**Figure 1-2**) confirmed the successful preparation of essentially monodisperse samples of oligomers with 1-6 boron centers. Even though the data were acquired vs. PS standards, the molecular weights are close to the calculated ones, which is an interesting coincidence that validates previously reported data[7] on related polymeric materials. High resolution MALDI-TOF mass spectra were acquired in negative mode with benzo[a]pyrene as the matrix and in all cases showed the molecular ion peaks $[M–H]^-$ with patterns that are in good agreement with simulated data (**Figure 1-3**). The data are summarized in **Table 1-1**.

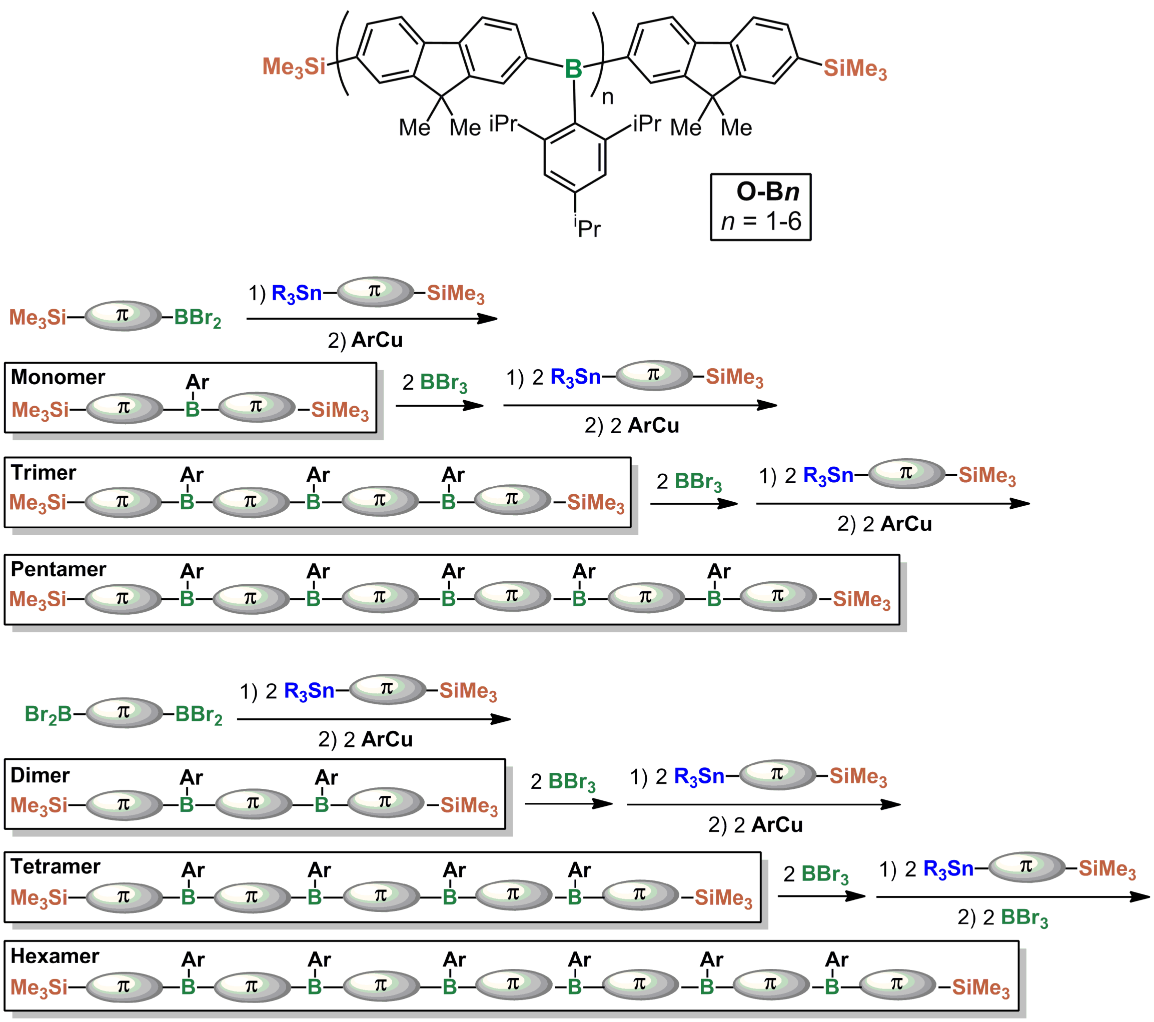

Scheme 1-1. Synthesis of conjugated organoborane oligomers **O-B*n***; Ar = Tip (2,4,6-triisopropyl-phenyl), π-system = 9,9-dimethylfluorene.

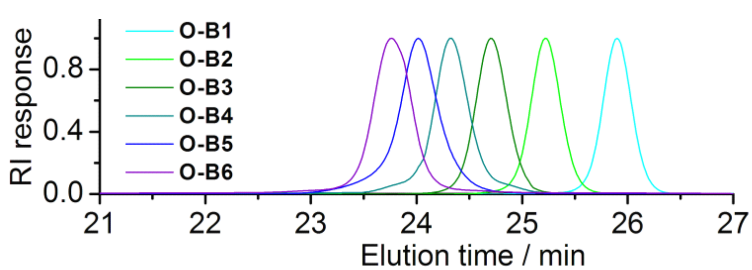

Figure 1-2. GPC-RI traces for oligomers **O-B*n*** (THF, vs PS standards).

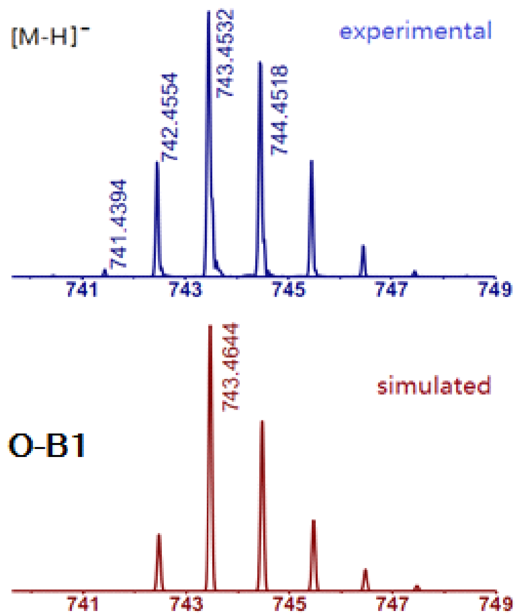
[M-H]⁻
experimental
741.4394
742.4554
743.4532
744.4518
741
743
745
747
749
simulated
743.4644
O-B1
741
743
745
747
749

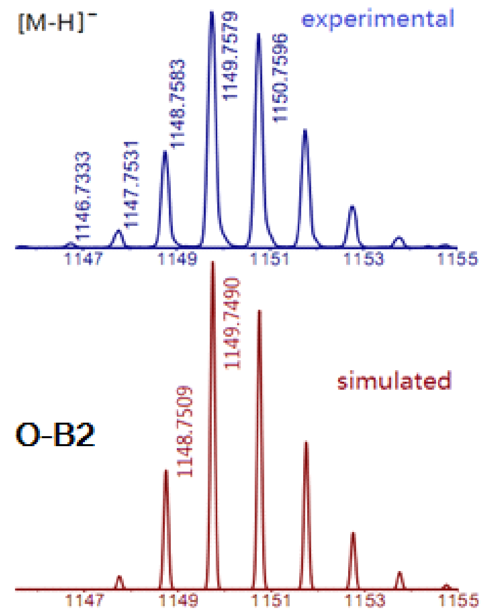
[M-H]⁻
experimental
1146.7333
1147.7531
1148.7583
1149.7579
1150.7596
1147
1149
1151
1153
1155
simulated
1148.7509
1149.7490
O-B2
1147
1149
1151
1153
1155

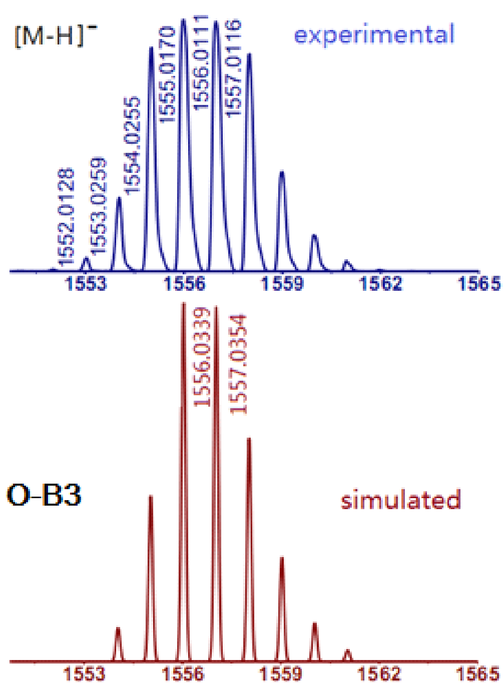
[M-H]⁻
experimental
1552.0128
1553.0259
1554.0255
1555.0170
1556.0111
1557.0116
1553
1556
1559
1562
1565
1556.0339
1557.0354
O-B3
simulated
1553
1556
1559
1562
1565

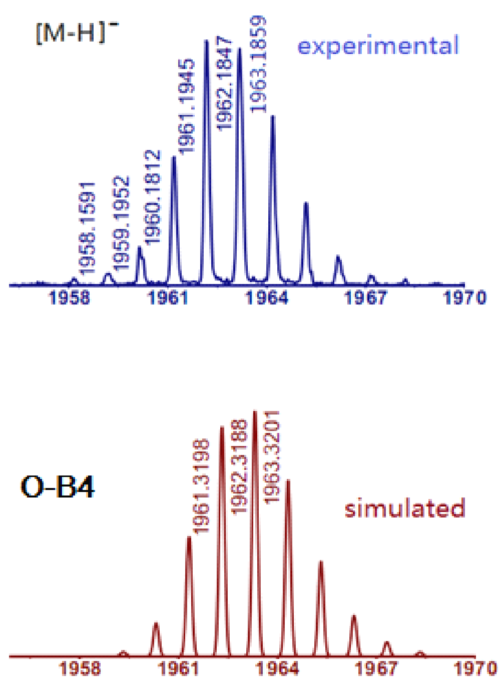
[M-H]⁻
experimental
1958.1591
1959.1952
1960.1812
1961.1945
1962.1847
1963.1859
1958
1961
1964
1967
1970
O-B4
1961.3198
1962.3188
1963.3201
simulated
1958
1961
1964
1967
1970

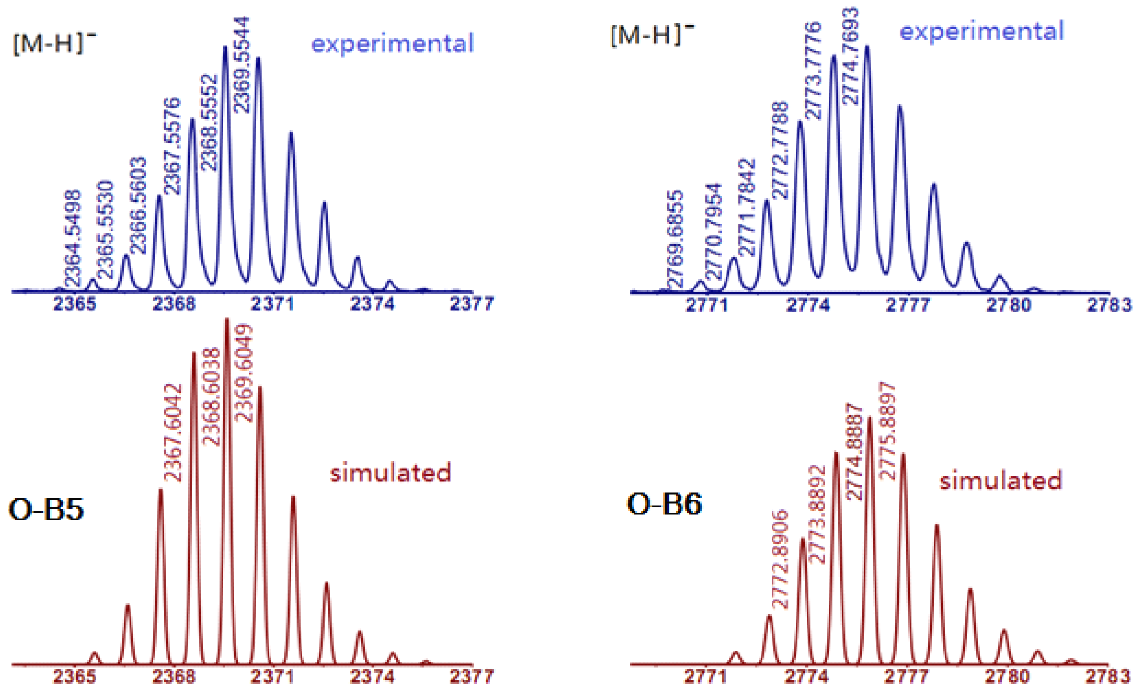

Figure 1-3. Molecular ion peaks for **O-B*n*** from MALDI-TOF mass spectra (neg. mode).

Table 1-1. GPC and MALDI-TOF MS Results for Oligomers **O-B*n***

	Fomula	M_{th} [a]	M_{MS} [b]	M_{n} [c]	M_{w} [c]	*PDI* [c]
O-B1	$C_{51}H_{65}BSi_2$	744.5	743.5	868	875	1.01
O-B2	$C_{81}H_{100}B_2Si_2$	1150.8	1149.8	1343	1354	1.01
O-B3	$C_{111}H_{135}B_3Si_2$	1557.0	1556.0	1875	1891	1.01
O-B4	$C_{141}H_{170}B_4Si_2$	1964.3	1963.2	2378	2402	1.02
O-B5	$C_{171}H_{205}B_5Si_2$	2370.6	2369.6	2920	2988	1.01
O-B6	$C_{201}H_{240}B_6Si_2$	2776.9	2775.8	3363	3402	1.01

[a] Calcd exact mass. [b] From (–) MALDI-TOF MS. [c] Relative to PS standards based on GPC-RI detection in THF at 35 °C; $PDI = M_{\mathrm{w}} / M_{\mathrm{n}}$

The oligomers were fully characterized by multinuclear NMR spectroscopy. The ^{1}H NMR data are useful to further confirm the oligomer chain length because the terminal silyl-substituted phenyl ring protons can easily be distinguished from the strongly downfield shifted protons attached to boron-bound phenyl groups (**Figure 1-4**). With increasing chain length, the intensity of the terminal fluorene signals remains the same, whereas that of the internal fluorenes and Tip groups gradually increases. Thus, integration of the signals at 7.5–7.7 ppm relative to those at ca. 7.03 ppm for the aromatic protons of the Tip groups clearly establishes the number of borane moieties that are embedded in the chain. Similar trends can be deduced from inspection of the ^{13}C NMR data (**Figure 1-5**). A single sharp signal at ca. –3.7 ppm in the ^{29}Si NMR corresponds to the terminal silyl groups, while a very broad signal at ca. 70 ppm in the ^{11}B NMR spectra results from overlap of resonances of both internal and terminal borane groups. A significant upfield shift with increasing chain length was not detected.

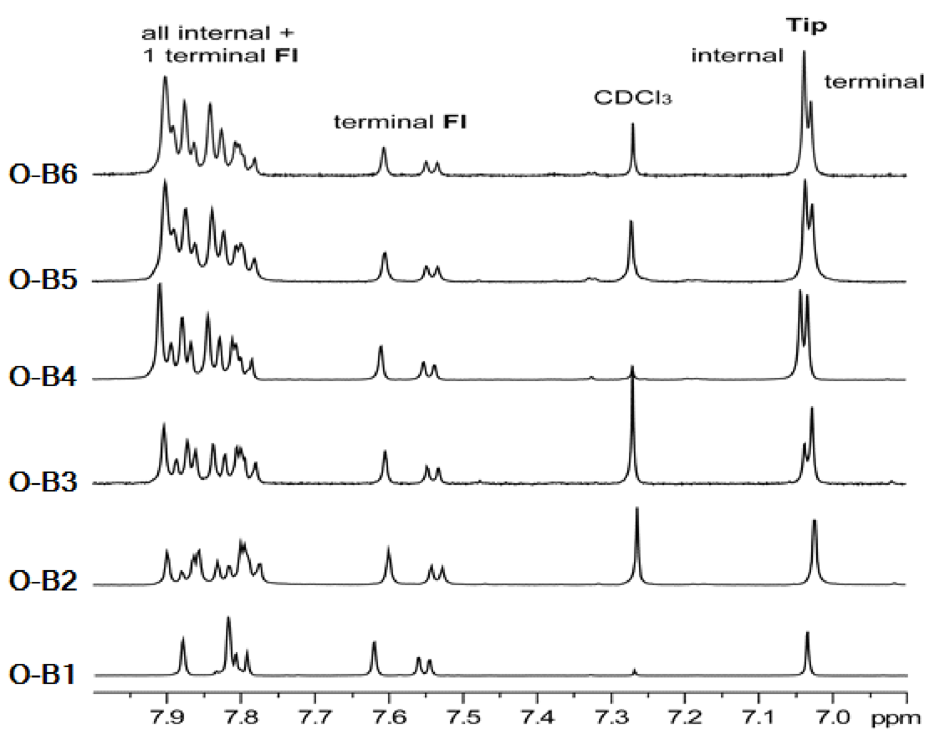

Figure 1-4. Partial ^{1}H NMR spectra of oligomers **O-B*n*** (aromatic region, $CDCl_3$, 25 °C).

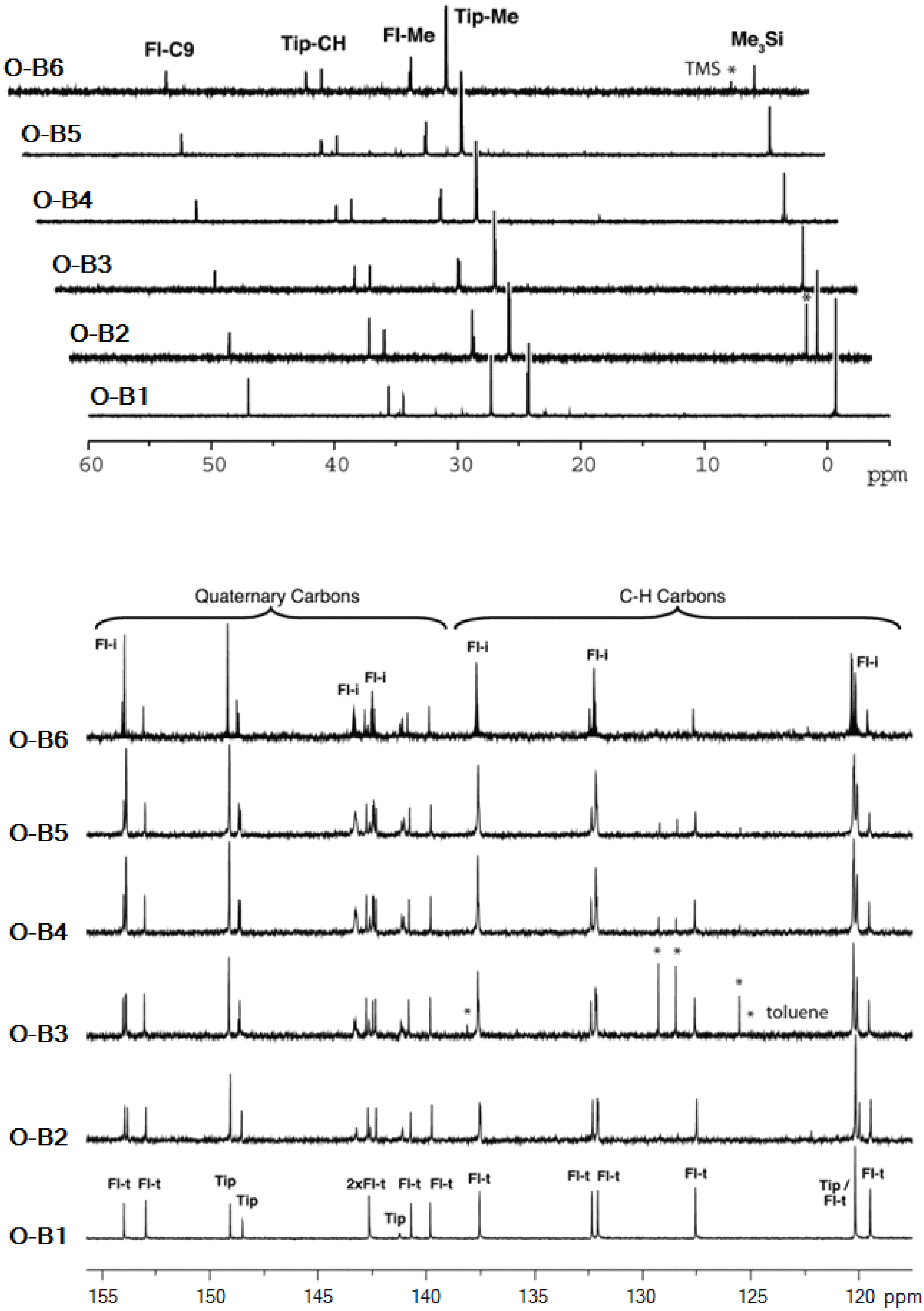

Figure 1-5. Aliphatic and aromatic regions of the [13]C NMR spectra of **O-B*n*** in $CDCl_3$ (Fl-t = fluorene carbon from the terminal Ph group; Fl-i = internal fluorene carbon).

We were not able to obtain single crystals of the oligomers **O-B*n***, but fortunately after Si/B exchange with BBr_3 the dimer **O-B2-BBr2** crystallized at –35 °C from hexanes. The structure shown in **Figure 1-6** reveals a zig-zag chain with two tricoordinate TipB groups inserted between three fluorene moieties. The bond lengths and angles at boron are in the expected range for triarylboranes. With respect to possible extended conjugation that involves the empty *p*-orbital on boron, two parameters are of interest: The interplanar angle between adjacent fluorene moieties amounts to 48.7 and 49.7°, indicating a significant twist in the conjugated main chain. Maybe even more important is the orientation of the fluorene π-system relative to the position of the empty p-orbital on boron. Interestingly, the interplanar angles between the internal fluorene moiety and the best planes through B_i and the 3 adjacent C atoms of 35.1 and 41.5° are considerably larger than the angles measured for the terminal fluorenes with respect to the same borane moieties (17.0, 18.7°). Although these relatively small angles suggest the possibility for good p_B-π overlap, the presence of the bulky Tip groups, which stand orthogonal to the fluoreneborane main chain, might somewhat limit the effective conjugation that can ultimately be achieved.[86]

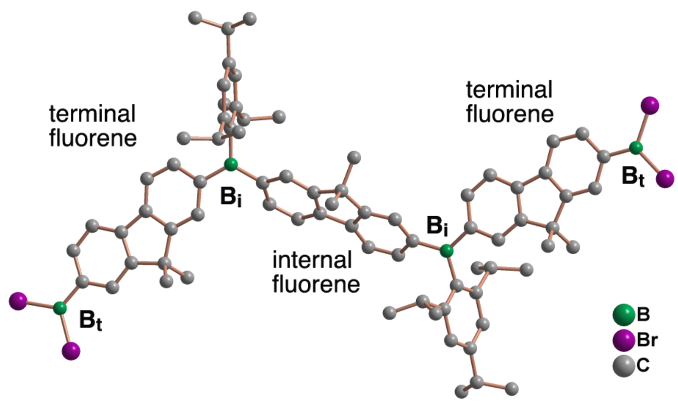

Figure 1-6. X-ray structure of **O-B2-BBr2**. Hydrogen atoms are omitted for clarity.

1.3 Photophysical, Electrochemical Properties and Computational Studies of Oligomers **O-B*n***

Having the spectroscopically pure and monodisperse oligomers in hand we studied the effect of chain extension on the optical properties and electrochemical characteristics. We acquired both differential pulse voltammetry (DPV) (**Figure 1-7**) and cyclic voltammetry (CV) (**Figure 1-8**) data in THF/0.1M Bu_4NPF_6 as the electrolyte. Reversible reductions were observed for all the oligomers; the number of redox steps corresponds directly to the number of boron centers present in the individual oligomers, suggesting that the LUMO levels are boron centered, in agreement with prior studies on arylborane compounds.[70,87,88] The relatively large splitting between the redox waves suggests that coulombic interactions and likely also some degree of through bond interactions lead to communication between the individual borane groups. This results in a gradual decrease in the onset of the first reduction with increasing number of organoborane groups and therefore lowering of the LUMO energy level.

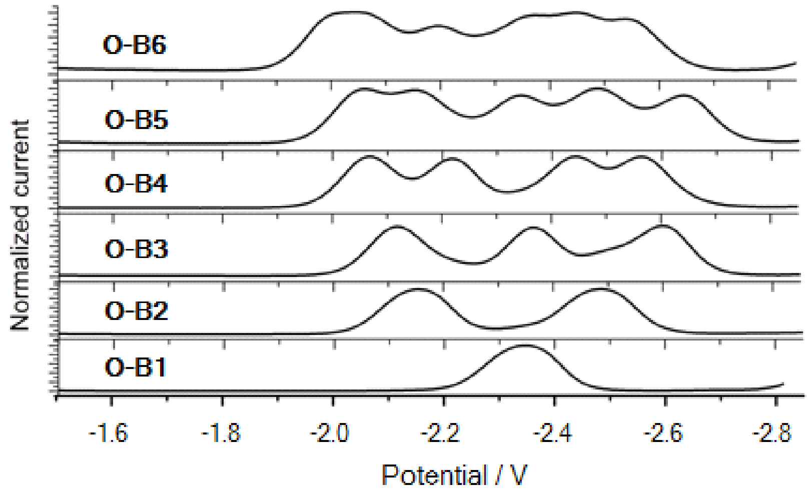

Figure 1-7. Differential pulse voltammetry plots of **O-B*n*** in THF/0.1M Bu_4NPF_6 vs. Fc/Fc^+.

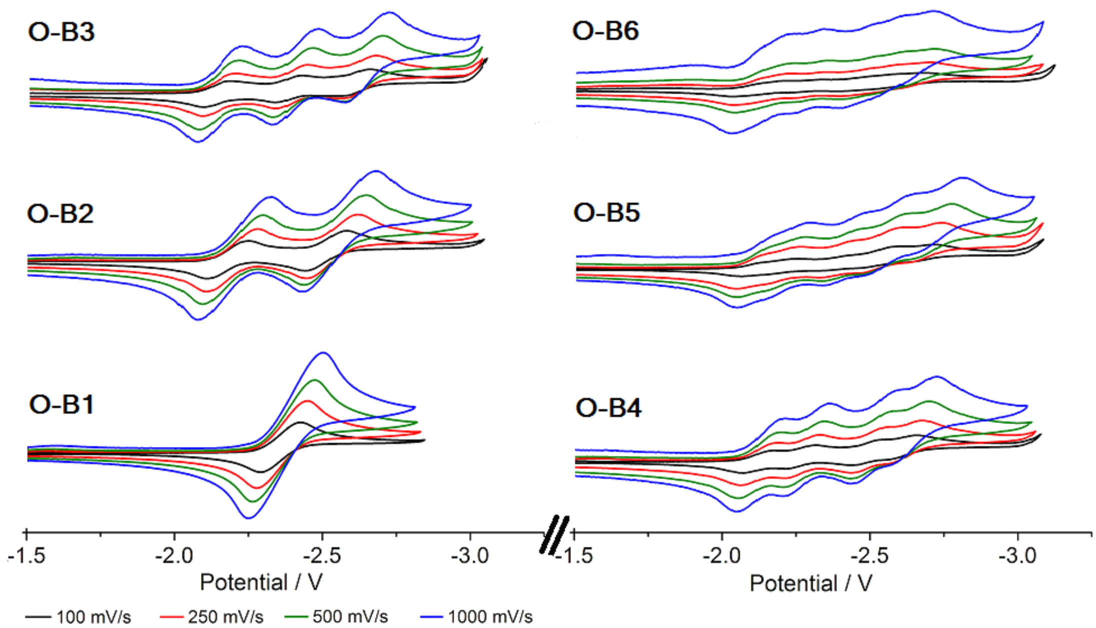

Figure 1-8. Cyclic voltammetry plots of **O-B*n*** in THF/0.1M Bu_4NPF_6 vs. Fc/Fc^+.

A decrease in the LUMO energy levels with increasing chain length was reproduced by DFT calculations (B3LYP, 6-31G(d))[89] on molecules **O-Bn-calc**, in which the methyl groups on fluorene and isopropyl groups of the pendent Tip groups were replaced with hydrogens (**Table 1-2**). According to these calculations, the HOMO levels are essentially unaffected by chain extension, resulting in an overall gradual decrease in the HOMO-LUMO gap. The stronger effect on the LUMO levels arises from the fact that the boron *p*-orbital does not contribute to the HOMO level, but shows a strong contribution in the LUMO, opening up an extended conjugation pathway that involves up to 6 boron centers and 4 fluorene moieties (**Figure 1-9**). It is important to note, however, that the terminal fluorene moieties have very little or no contributions to the LUMO orbitals of the larger oligomers. Worth noting is also that in all cases an all-trans geometry was used as a the starting point in the calculations, which converged to a “U-shaped” geometry. Nonetheless other conformations should be possible, especially in solution. They are likely to result in slightly different orbital localizations, orbital energies, and electronic transitions. A more extensive study in this respect has not been performed due to large computer time required for the larger oligomers.

Table 1-2. Calculated Orbital Energies for ***O-Bn*-calc**[a] (DFT, B3LYP, 6-31G(d))

Compound	HOMO (eV)	LUMO (eV)	HOMO-LUMO gap (eV)
O-B1-calc	–5.66	–1.80	3.86
O-B2-calc	–5.66	–1.99	3.67
O-B3-calc	–5.66	–2.07	3.59
O-B4-calc	–5.66	–2.10	3.56
O-B5-calc	–5.66	–2.12	3.54
O-B6-calc	–5.66	–2.15	3.51

[a] For **OFn-calc** the Me groups on fluorene and ^{i}Pr on Tip are replaced with H

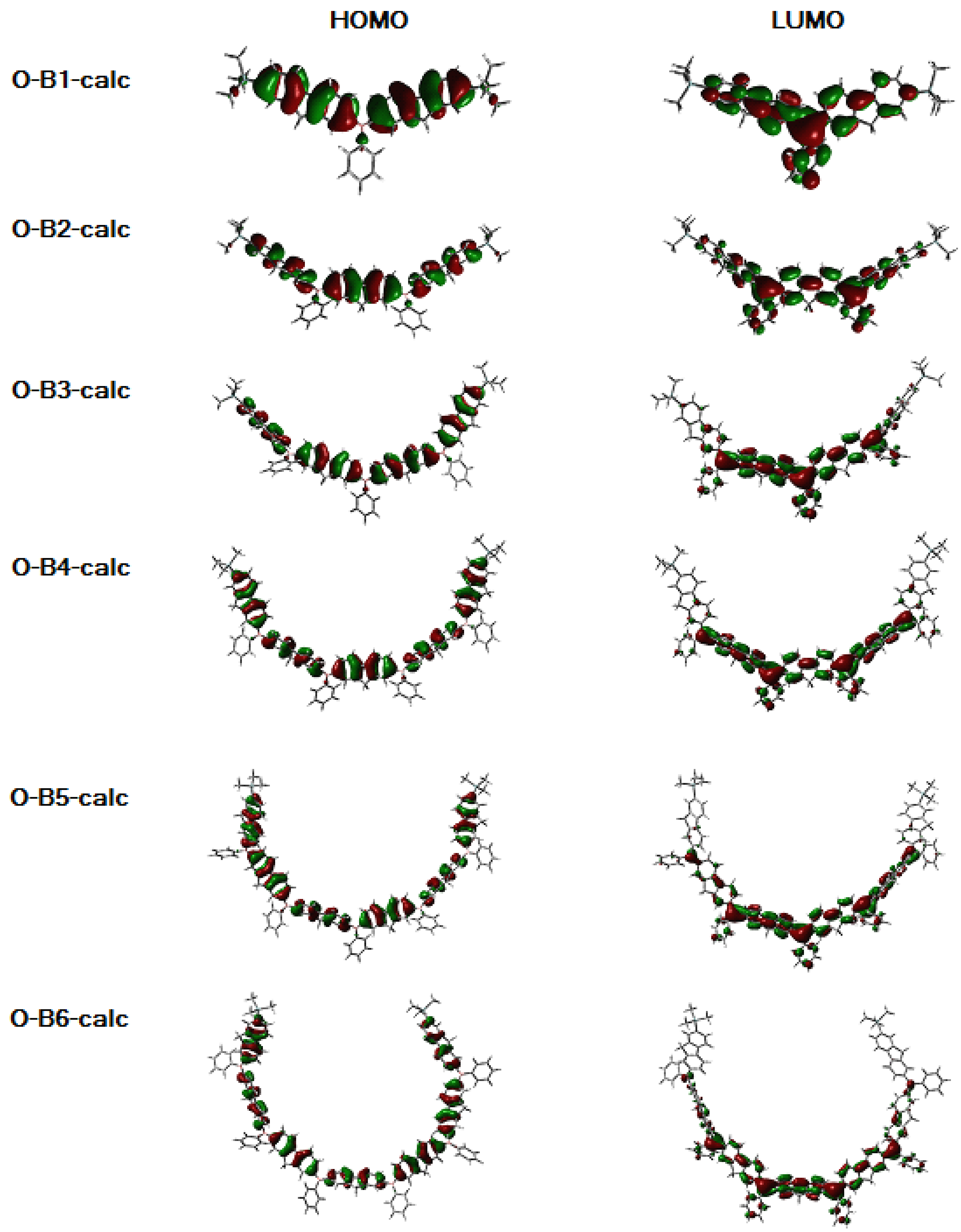

Figure 1-9. The HOMO (left) and LUMO (right) orbitals for **O-B*n*-calc** (B3LTY, 6-31G*) in the gas phase. The Me groups on fluorene and ^{i}Pr on Tip are replaced with H.

A gradual decrease in the band gap is also evident in the absorption and emission spectra (**Figure 1-10**). The lowest energy absorption band moves from 358 nm for **O-B1** to 390 nm for **O-B6**. A concurring bathochromic shift (**Figure 1-11**) in the emission maximum is accompanied by an increase in the quantum yield to 95%.[90] Hence, the higher organoborane oligomers are highly fluorescent with emission maxima in the blue region of the spectrum. TD-DFT calculations on the oligomers **O-B*n*-calc** give results that are in good agreement with the experimental absorption data (**Table 1-3**) and suggest that the lowest energy absorptions are primarily due to contributions from HOMO and LUMO, although especially for the higher oligomers other orbitals also contribute to a lesser extent (**Table 1-4**).

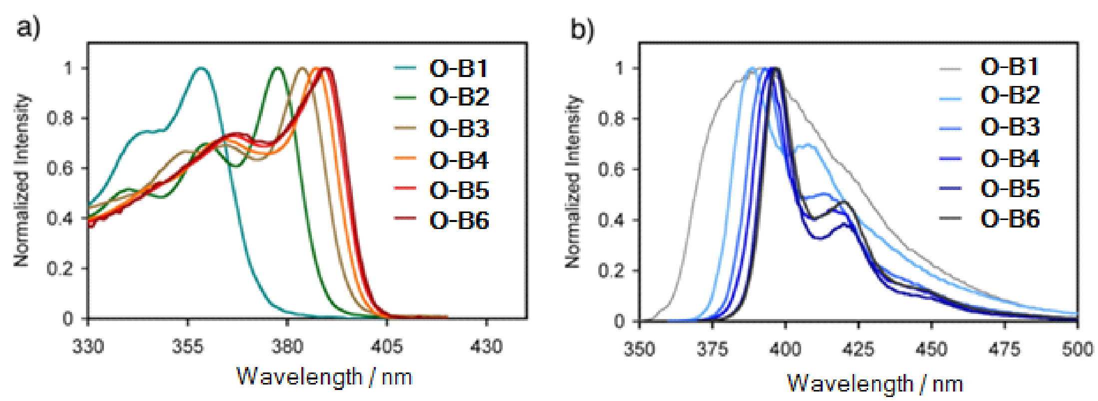

Figure 1-10. a) UV-vis and b) fluorescence spectra of oligomers **O-B*n*** in CH_2Cl_2.

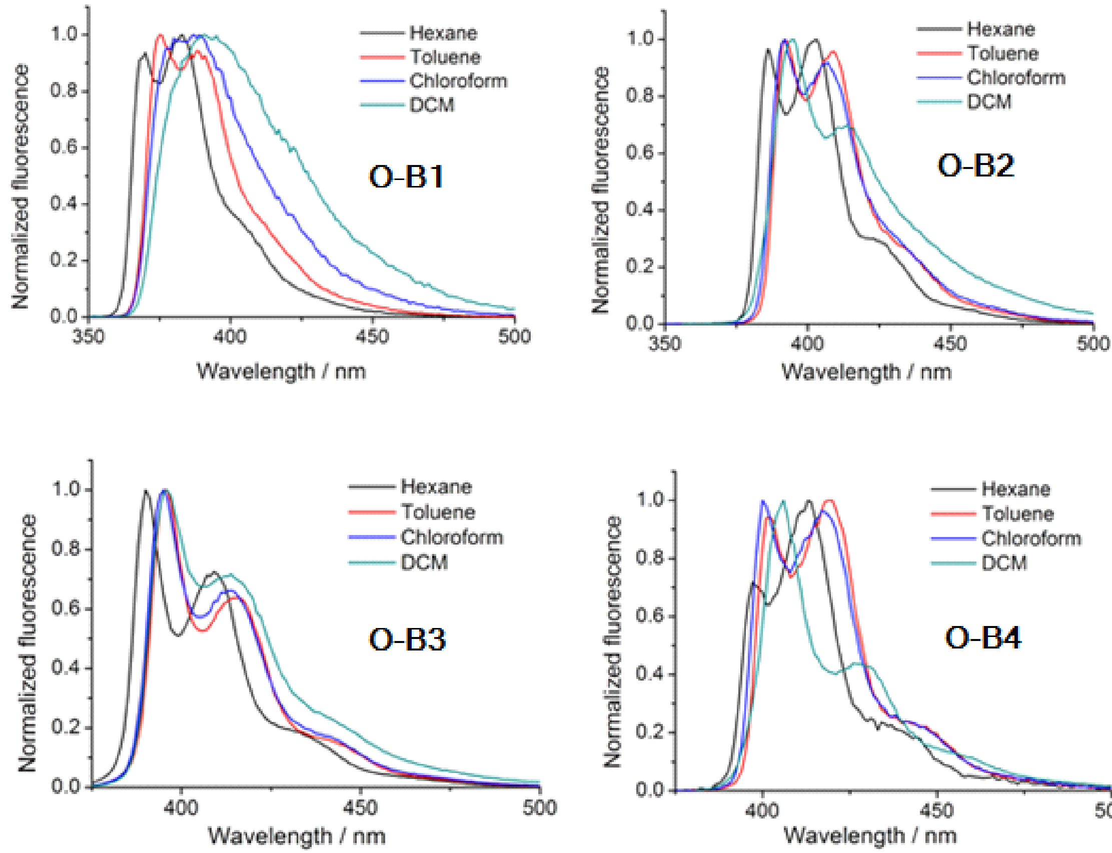

Figure 1-11. Solvent dependence of emission spectra (excited at λ_{max} in CH_2Cl_2).

Table 1-3. Optical Properties and Electrochemical Data of Oligomers **O-B*n*** and Comparison with Data from DFT Calculations (Gaussian03, B3LYP, 6-31G(d))

	Experimental Data (**O-B*n***)					DFT Results (**O-B*n*-calc**)	
	λ_{max}[a] [nm]	ε_{max}[a]	λ_{em}[a] [nm]	ϕ[a]	λ_{edge}[b] [nm]	$E_{gap,DFT}$[c] [nm]	$\lambda_{abs,TD\text{-}DFT}$[d] [nm]
O-B1	358	60,000	392	0.73	373	321	365
O-B2	378	85,800	389	0.89	388	337	386
O-B3	384	100,000	393	0.89	396	345	396
O-B4	387	94,500	395	0.91	398	348	400
O-B5	389	95,000	396	0.94	400	351	404
O-B6	390	120,000	397	0.95	401	353	406

[a] In CH_2Cl_2. [b] From absorption edge. [c] HOMO-LUMO gap based on DFT calculations , λ_{abs} based on TD-DFT results on **O-B*n*-calc** (Me and ^{i}Pr groups replaced with H).

Table 1-4. Comparison of TD-DFT Results for **O-B*n*-calc**[a] with Experimental Data

compound		TD-DFT calculation results
O-B1-calc	λ / nm; f	365; 1.0911
	Transition	151←150 (LUMO←HOMO), 0.679
O-B2-calc	λ / nm; f	386; 1.6767
	Transition	217←216 (LUMO←HOMO), 0.664 218←215 (LUMO+1←HOMO-1), –0.133
O-B3-calc	λ / nm; f	396; 2.0269
	Transition	283←282 (LUMO←HOMO), 0.636 283←280 (LUMO←HOMO-2), –0.156 284←281 (LUMO+1←HOMO-1), –0.192
O-B4-calc	λ / nm; f	400; 2.2383
	Transition	349←348 (LUMO←HOMO), 0.602 349←346 (LUMO←HOMO-2), –0.191 351←346 (LUMO+2←HOMO-2), 0.103 350←347 (LUMO+1←HOMO-1), –0.234
O-B5-calc	λ / nm; f	404; 2.1988
	Transition	415←414 (LUMO←HOMO), 0.562 416←413 (LUMO+1←HOMO-1), 0.261 417←412 (LUMO+2←HOMO-2), –0.133 415←412 (LUMO←HOMO-2), –0.227 416←411 (LUMO+1←HOMO-3), –0.122
O-B6-calc	λ / nm; f	406 ; 1.8665
	Transition	481←480 (LUMO←HOMO), 0.523 482←479 (LUMO+1←HOMO-1), 0.276 483←478 (LUMO+2←HOMO-2), 0.155 481←478 (LUMO←HOMO-2), –0.251 482←477 (LUMO+1←HOMO-3), –0.144

[a] For **O-B*n*-calc** the Me groups on fluorene and ^{i}Pr on Tip are replaced with H.

The absorption data can be plotted against $1/n_B$, where n_B is the number of boron centers that also corresponds to the number of repeat units in the oligomer chains (**Figure 1-12a**). This linear fit of the data gives an excellent correlation (R^2 = 0.9993) and extrapolation to $n \rightarrow \infty$ predicts an absorption maximum at ν = 2510 cm^{-1} (λ_∞ = 398 nm) for an infinite polymer chain. The experimental absorption maximum at ν = 2540 cm^{-1} (λ_{max} = 394 nm) for a polymer with an average of n = 17 [53] almost perfectly fits the linear extrapolation (2530 cm^{-1}).

Meier proposed that an exponential fit of the absorption data of conjugated oligomers to Eq (1) is more appropriate as it takes into account a non-linear behavior typically observed when reaching relative large numbers of repeating units n.[91,92] **Figure 1-12b** shows a fit of our data to Eq (1). A reasonably good correlation (R^2 = 0.997) is obtained. A limiting wavelength of λ_∞ = 390±1 nm is derived, $\Delta\lambda = \lambda_\infty - \lambda_1$ amounts to 31.5±1 nm, and the parameter b comes to 0.93±0.08, which reflects a fast rate of convergence. An effective conjugation length of n_{ecl} = 5 can be derived from Eq (2) using the criterion of $\Delta\lambda \leq 1$ for convergence. This further suggests that saturation is reached relatively quickly.

$$\lambda_{\max}(n) = \lambda_\infty - (\lambda_\infty - \lambda_1)e^{-b(n-1)} \qquad (1)$$

$$n_{ecl} = \frac{\ln(\lambda_\infty - \lambda_1)}{b} + 1 \qquad (2)$$

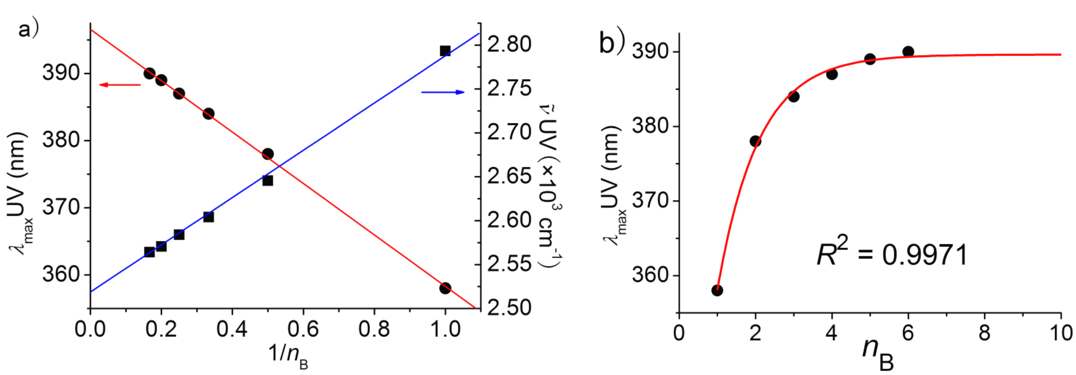

Figure 1-12. a) linear and b) exponential fits of absorption data for oligomers **O-B*n***.

A comparison with data for monodisperse all-organic oligofluorenes is also interesting. Applying Meier's fit to absorption data of oligofluorenes reported in the literature[15,16,93] gives values of n_{ecl} in the range from 8 to 11, depending on the substitution pattern at the C9 position, which is only slightly higher than what we find for the boron-modified conjugated oligomers.

1.4 Anion Binding Studies

Electron deficient tricoordinate organoborane species can be attacked by nucleophiles such as fluoride and cyanide. As shown in **Figure 1-13**, stepwise addition of a tetra-n-butylammonium fluoride (TBAF) solution as fluoride source to a solution of **O-B2** in THF gradually decreases the major absorption band at *ca.* 380 nm. As the titration proceeded, a new charge transfer band developed after 1.0 eq. of fluoride was added. The formed tetracoordinate boron center becomes an electron-rich donor, whereas the other tricoordinate boron remains electron deficient (**Scheme 1-2**). TD-DFT (B3LYP/6-31G*) calculations further suggest charge transfer from the tetracoordinate boron moiety to the tricoordinate boron moiety (HOMO-1→LUMO, f = 0.2391; HOMO-2→LUMO, f = 0.2391). Interesting to know is that the emission of **O-B2** can be almost completely quenched by addition of 1.0 eq. of fluoride, and the intermediate in the CT state is much less emissive. The same phenomenon is also observed for higher oligomers up to **O-B6** (**Figures 1-15, 1-16, 1-17, 1-18)**.

Table 1-5. Summary of Results from Anion Binding Analysis for **O-B*n***

compound	lgβ_{11}	lgβ_{12}	lgβ_{13}	lgβ_{14}	lgβ_{15}	lgβ_{16}	f
O-B1	7.6						1.1
O-B2	8.0	13.7					1.7
O-B3	8.0	14.5	20.1				2.0
O-B4	8.0	15.3	20.0	24.8			2.2
O-B5	7.7	15.0	20.5	26.5	30.0		2.2
O-B6	8.0	15.3	22.0	28.6	34.7	40.2	1.9

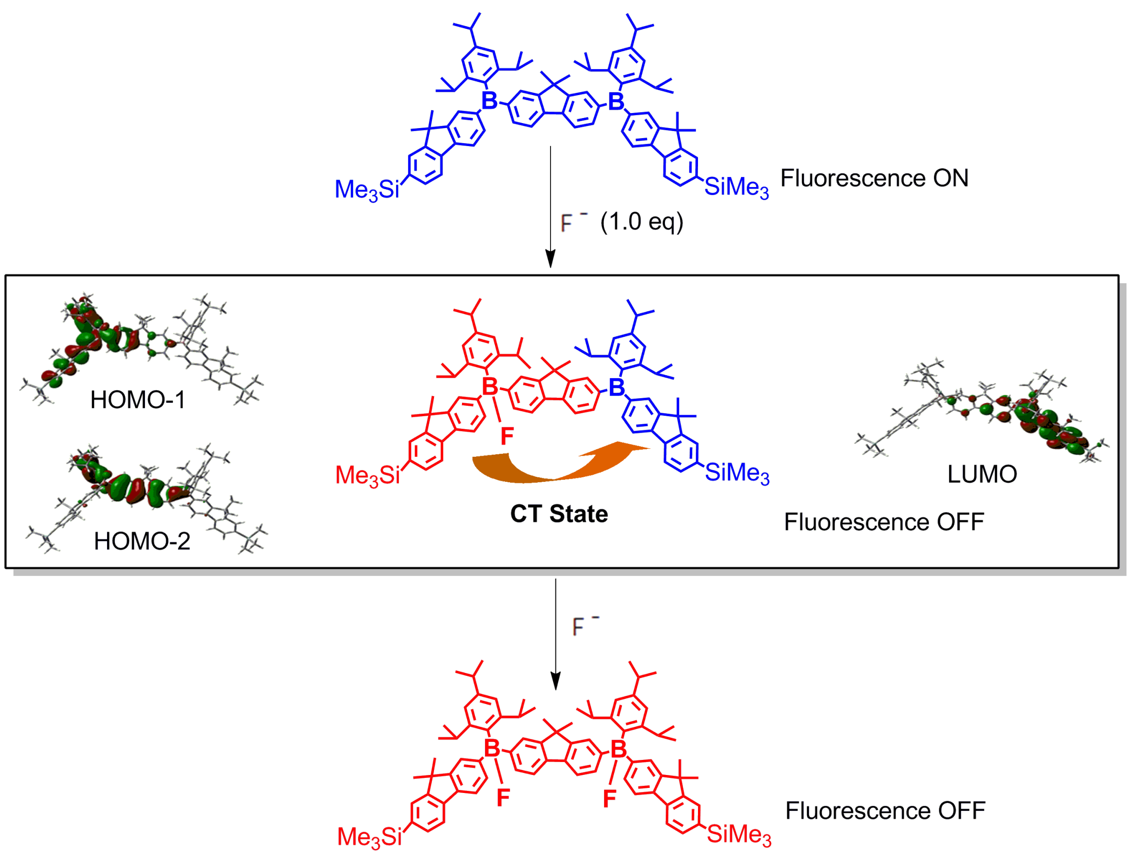

Scheme 1-2. Schematic binding mechanism of **O-B2** with fluoride. DFT calculations (B3LYP/ 6-31 G*) are in support of the proposed charge transfer (CT) state.

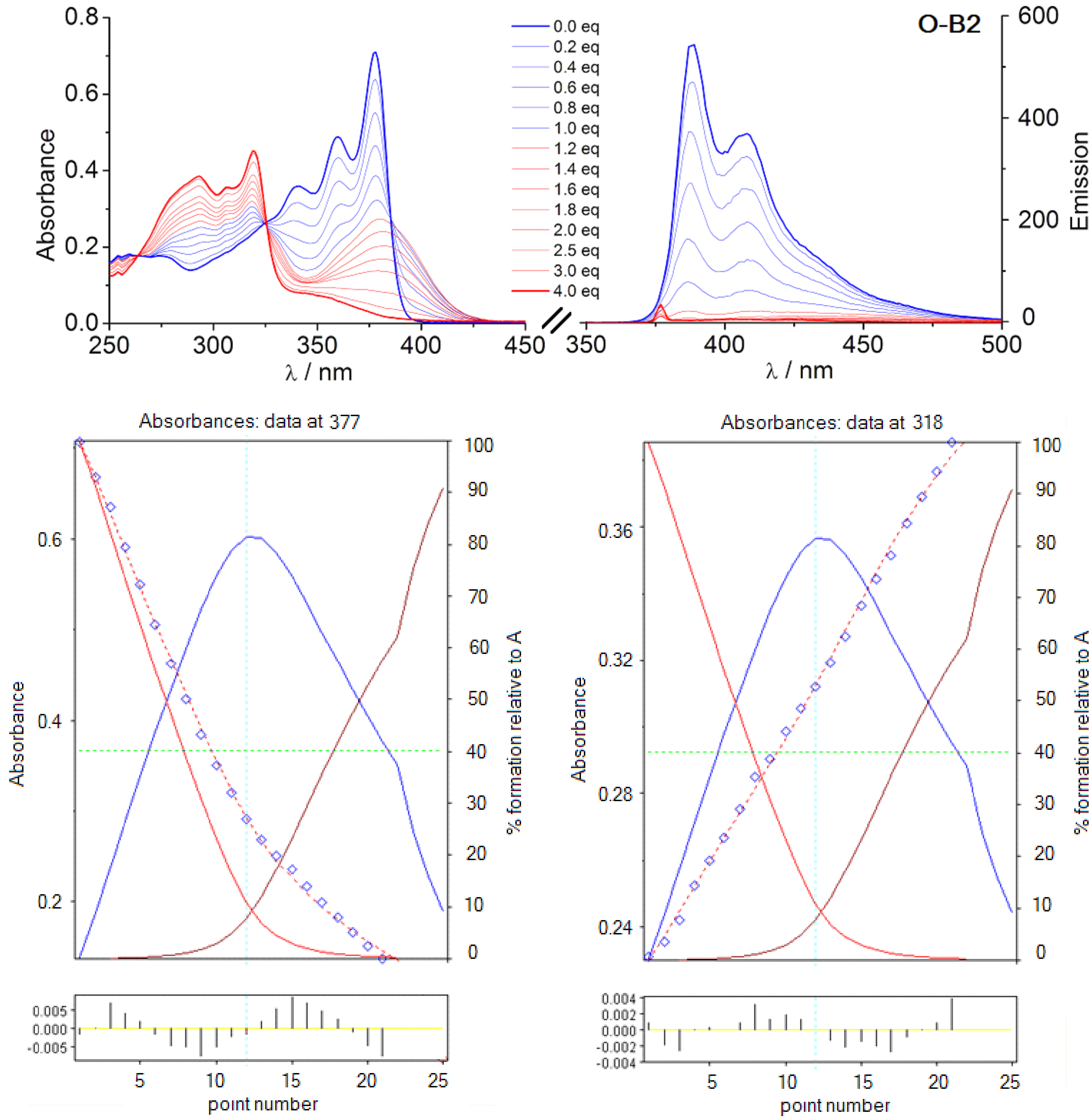

Figure 1-13. Complexation of **O-B2** with F^- anions (2.68×10^{-4} M) in THF, monitored by UV-vis and fluorescence spectroscopy. [**O-B2**] = 8.29×10^{-6} M; λ_{exc} = 378 nm. Bottom: Fit of absorption data (Hyperquad™) at λ = 377 and 318 nm.

Table 1-6. Relative concentrations of individual complexes after addition of varying amounts of F^- to a solution of **O-B2** in THF based on the binding constants in Table 1-5.

F^- (eq.)	[**O-B2**] (%)	[**O-B2**]F (%)	[**O-B2**]F_2 (%)
1	11.6	85.2	3.1
2	0.2	45.4	54.4
3	0.0	21.0	79.0
4	0.0	12.8	87.2

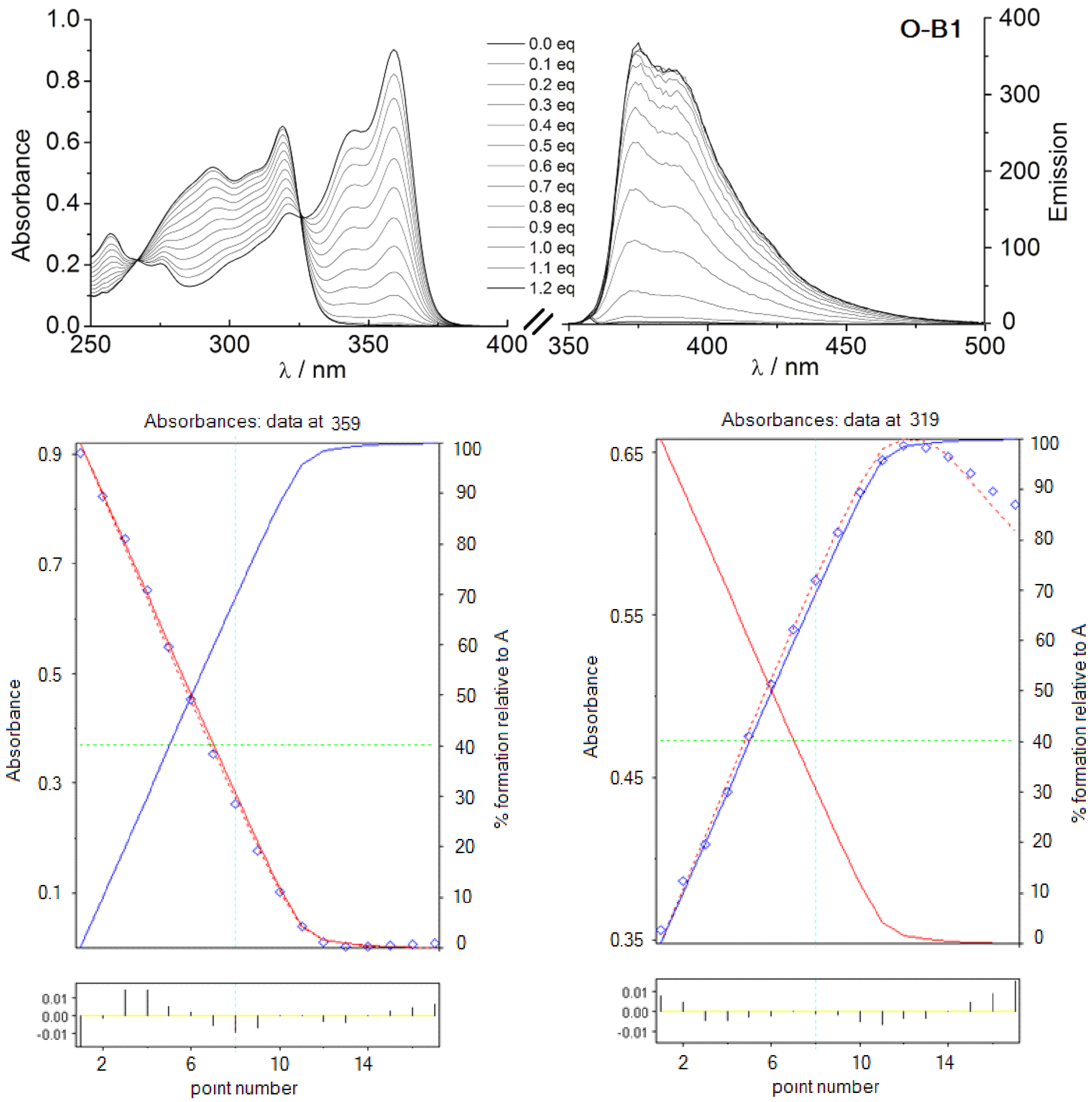

Figure 1-14. Complexation of **O-B1** with F^- anions (2.68×10^{-4} M) in THF, monitored by UV-vis and fluorescence spectroscopy. [**O-B1**] = 1.54×10^{-5} M; λ_{exc} = 358 nm. Bottom: Fit of absorption data (Hyperquad™) at λ = 359 and 319 nm.

Table 1-7. Relative concentrations of individual complexes after addition of varying amounts of F^- to a solution of **O-B1** in THF based on the binding constants in Table 1-5.

F^- (eq.)	[**O-B1**] (%)	[**O-B1**]F (%)
1	4.4	95.6
1.2	1.0	99.0

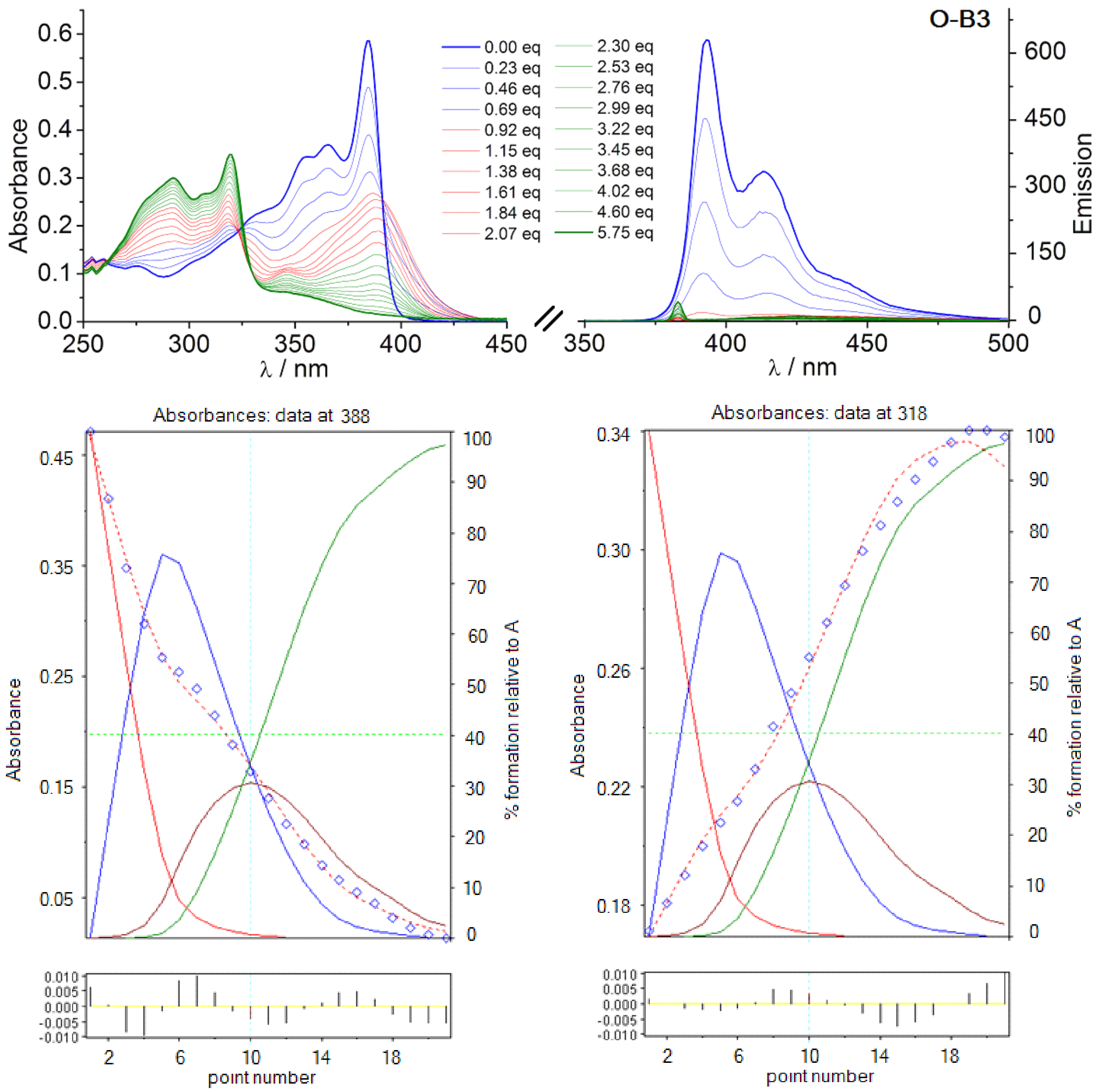

Figure 1-15. Complexation of **O-B3** with F¯ anions (3.50×10^{-4} M) in THF, monitored by UV-vis and fluorescence spectroscopy. [**O-B3**] = 5.70×10^{-6} M; λ_{exc} = 384 nm. Bottom: Fit of absorption data (Hyperquad™) at λ = 388 and 318 nm.

Table 1-8. Relative concentrations of individual complexes after addition of varying amounts of F¯ to a solution of **O-B3** in THF based on the binding constants in Table 1-5.

F¯ (eq.)	[**O-B3**] (%)	[**O-B3**]F (%)	**[O-B3]**F_2 (%)	**[O-B3]**F_3 (%)
0.92	9.8	72.7	17.0	0.5
2.07	0.2	19.6	58.3	21.9
2.99	0.0	3.1	38.0	58.9
4.02	0.0	0.8	22.7	76.5
5.75	0.0	0.2	11.9	87.9

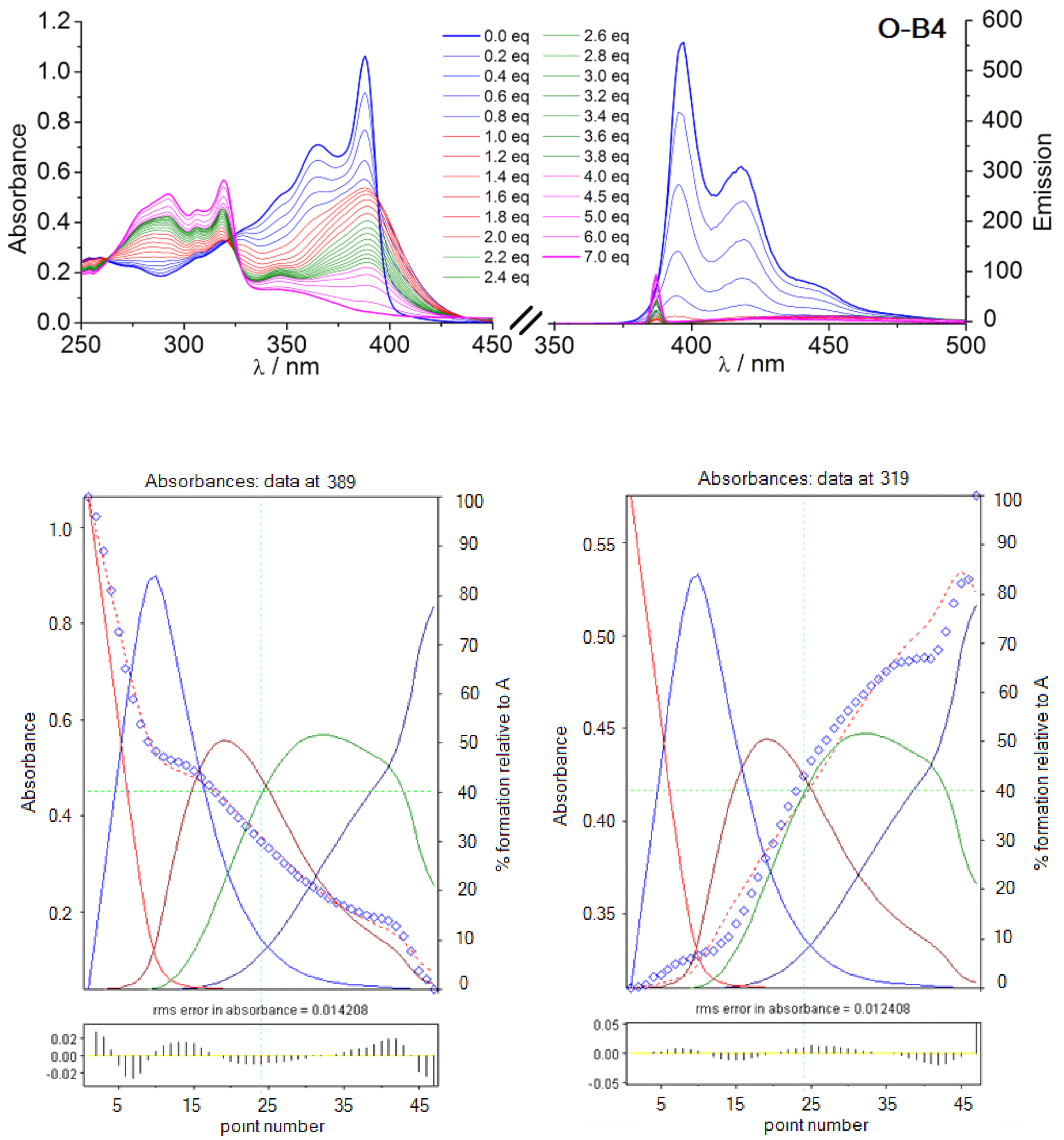

Figure 1-16. Complexation of **O-B4** with F^{-} anions (3.50×10^{-4} M) in THF, monitored by UV-vis and fluorescence spectroscopy. [**O-B4**] = 1.150×10^{-5} M; λ_{exc} = 387 nm. Bottom: Fit of absorption data (Hyperquad™) at $\lambda = 389$ and 319 nm.

Table 1-9. Relative concentrations of individual complexes after addition of varying amounts of F^{-} to a solution of **O-B4** in THF based on the binding constants in Table 1-5.

F^{-} (eq.)	[**O-B4**] (%)	[**O-B4**]F (%)	[**O-B4**F_2 (%)	[**O-B4]**F_3 (%)	[**O-B4**]F_4 (%)
1	11.1	47.7	41.1	0.1	0
2	0.0	1.0	79.0	16.0	4.0
3	0.0	0.2	48.4	29.2	22.2
4	0.0	0.1	29.3	30.6	40.0
5	0.0	0.0	18.6	28.1	53.3
6	0.0	0.0	12.6	25.0	62.4
7	0.0	0.0	6.8	20.0	73.2

Table 1-10. Relative concentrations of individual complexes after addition of varying amounts of F^{-} to a solution of **O-B5** in THF based on the binding constants in Table 1-5.

F^{-} (eq.)	[**O-B5**] (%)	[**O-B5**]F (%)	[**O-B5**]F_2 (%)	[**O-B5]**F_3 (%)	[**O-B5**]F_4 (%)	[**O-B5**]F_5 (%)
1	44.7	40.6	14.7	0.0	0.0	0.0
2	9.4	35.6	53.6	1.3	0.1	0.0
3	0.5	9.4	76.3	9.8	4.0	0.0
4	0.0	2.0	51.2	20.6	26.1	0.1
5	0.0	0.4	24.6	20.5	54.0	0.5
6	0.0	0.1	7.6	13.7	77.3	1.3
7	0.0	0.0	2.2	7.8	86.9	3.1
8	0.0	0.0	1.0	5.1	89.0	4.9
9	0.0	0.0	0.5	3.8	89.1	6.6

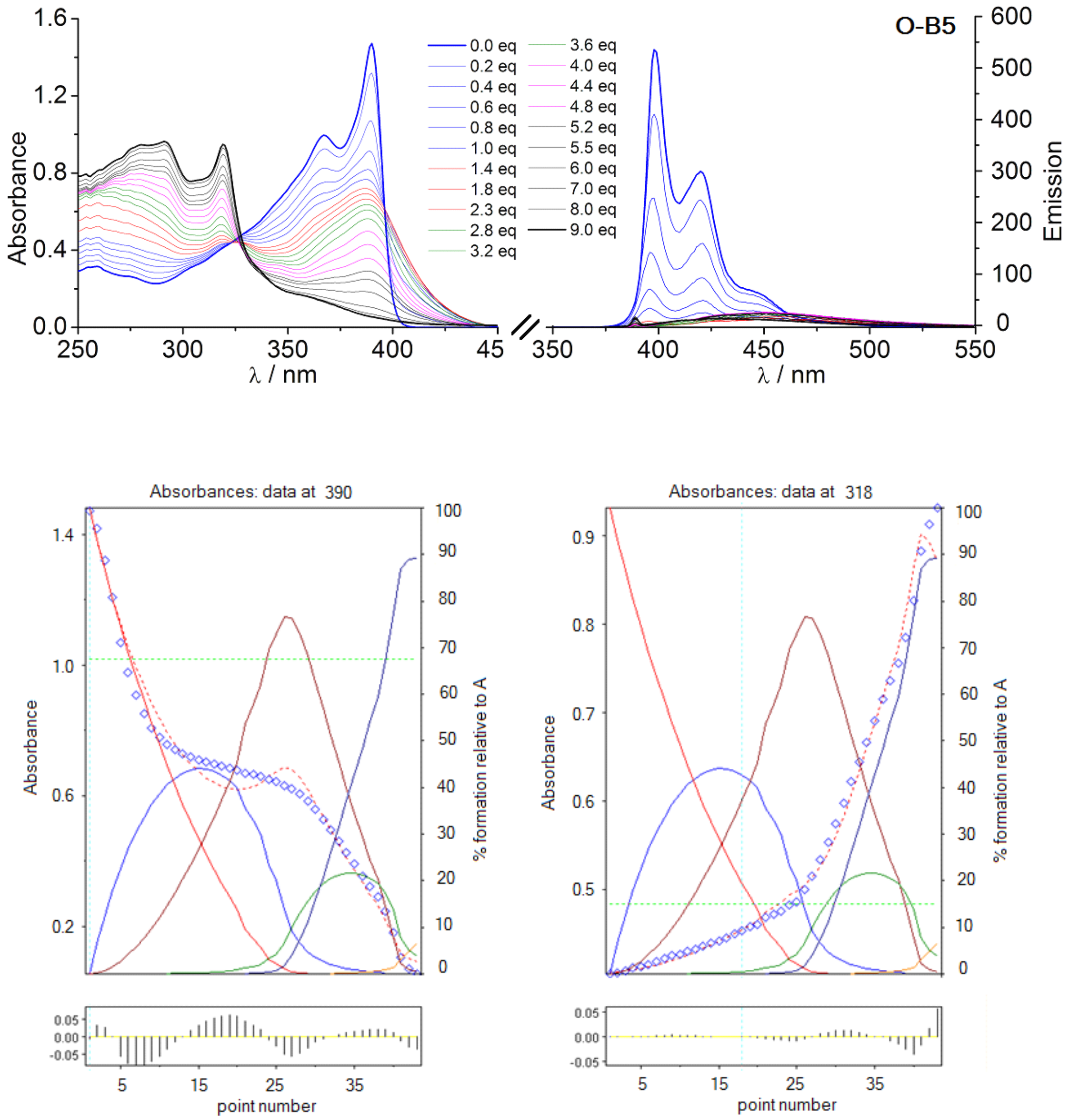

Figure 1-17. Complexation of **O-B5** with F^- anions (1.90×10^{-4} M) in THF, monitored by UV-vis and fluorescence spectroscopy. [**O-B5**] = 1.546×10^{-5} M; λ_{exc} = 389 nm. Bottom: Fit of absorption data (Hyperquad^{TM}) at λ = 390 and 318 nm.

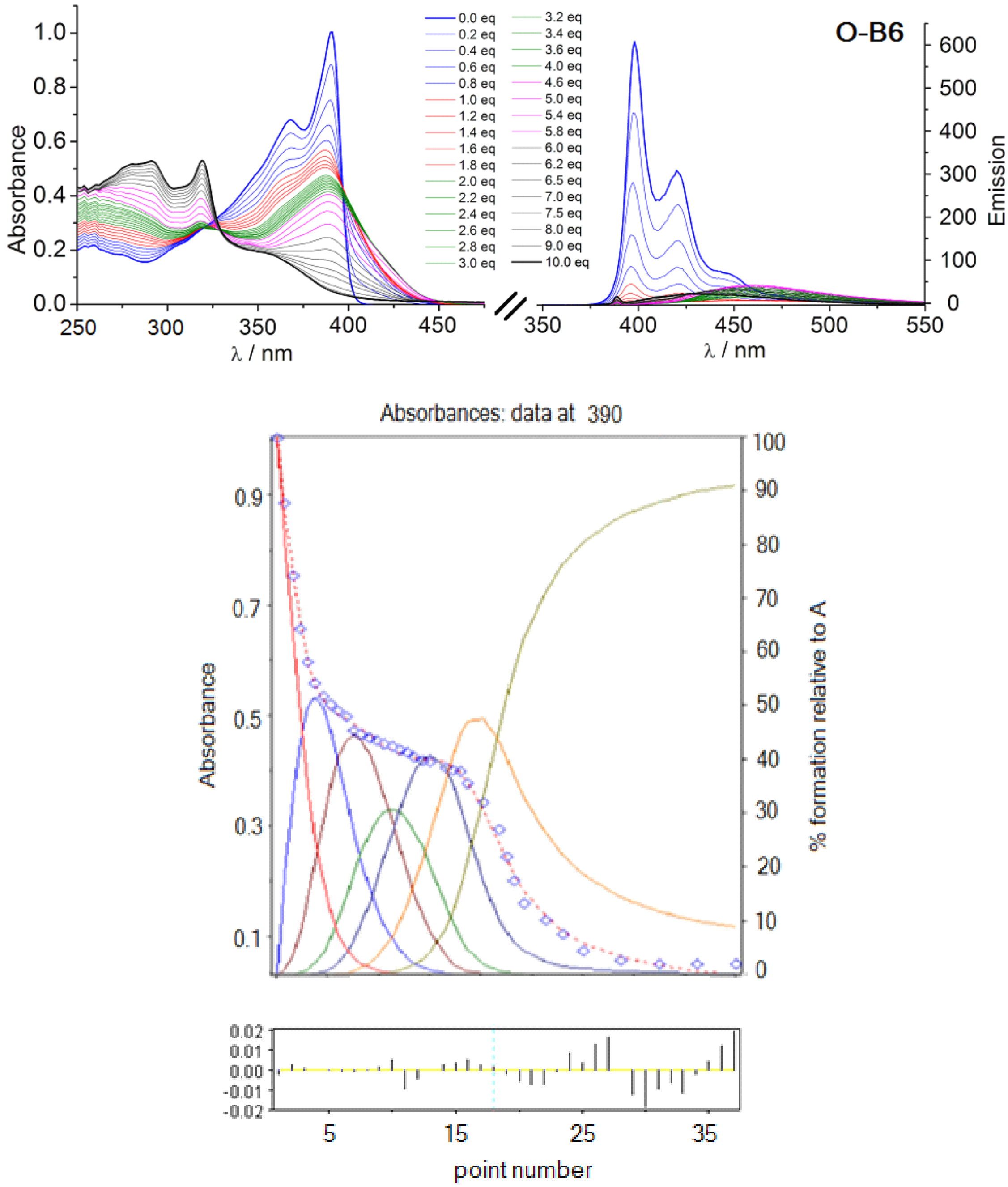

Figure 1-18. Complexation of **O-B6** with F^- anions (1.79×10^{-4} M) in THF, monitored by UV-vis and fluorescence spectroscopy. [**O-B6**] = 8.327×10^{-6} M; λ_{exc} = 390 nm. Bottom: Fit of absorption data (Hyperquad™) at λ = 390 nm.

Table 1-11. Relative concentrations of individual complexes after addition of varying amounts of F^{-} to a solution of **O-B6** in THF based on the binding constants in Table 1-5.

F^{-} (eq.)	[**O-B6**] (%)	[**O-B6**]F (%)	[**O-B6**]F_2 (%)	[**O-B6**]F_3 (%)	[**O-B6**]F_4 (%)	[**O-B6**]F_5 (%)	[**O-B6**]F_6 (%)
1	25.2	51.5	21.0	2.1	0.2	0.0	0.0
2	3.1	26.5	44.5	18.8	6.3	0.7	0.0
3	0.3	6.6	28.4	30.7	26.4	7.2	0.5
4	0.0	0.8	7.9	20.1	40.8	26.2	4.2
5	0.0	0.0	0.7	4.7	26.4	47.1	21.1
6	0.0	0.0	0.0	0.5	7.8	40.1	51.5
7	0.0	0.0	0.0	0.1	2.4	26.2	71.3
8	0.0	0.0	0.0	0.0	1.1	18.5	80.4
9	0.0	0.0	0.0	0.0	0.6	14.2	85.2
10	0.0	0.0	0.0	0.0	0.4	11.7	87.9

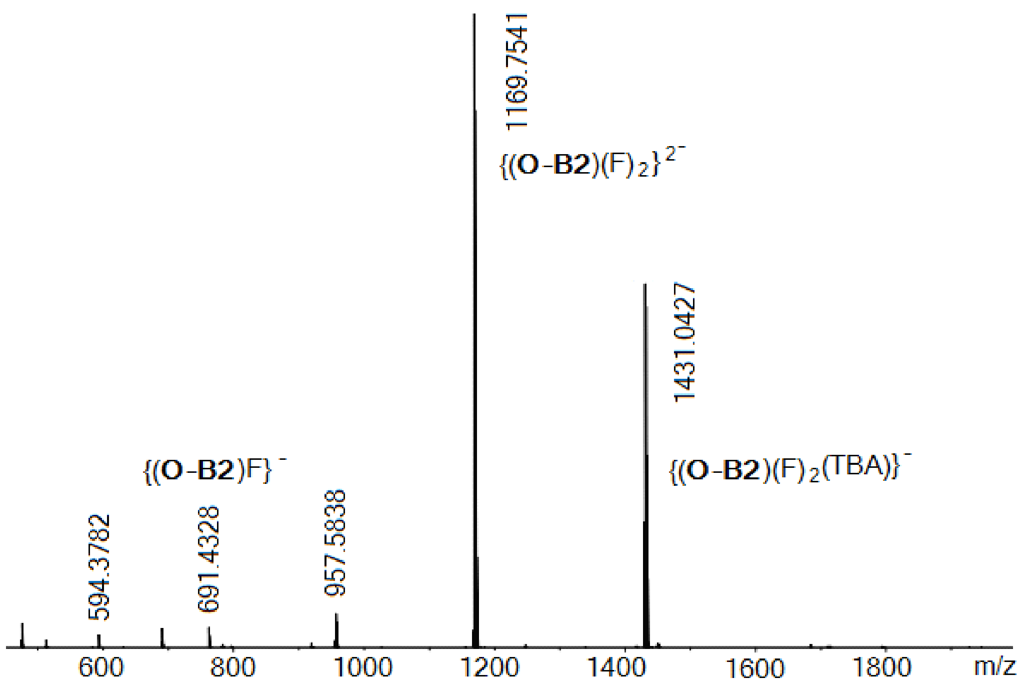

Figure 1-19. Fluoride (TBAF = tetra-n-butylammonium fluoride) complexes of **O-B2** in THF confirmed by high resolution ESI-MS (neg. mode). [**O-B2**] = 1.738 × 10^{-4} M, V_{THF} = 5 mL, n(F^{-}) = 1.737 × 10^{-3} mmol.

In contrast to the neutral oligomers **O-B*n***, the introduction of negative charge upon complexation with anions leads to easier ionization for MS measurements. For instance, the electrospray ionization mass spectra (ESI-MS) for the fluoride complex of **O-B2** are readily assigned to fully coordinated species as well as a small amount of partially coordinated species (**Figure 1-19**).

1.5 Conclusions

A series of highly luminescent monodisperse fluoreneborane oligomers (n = 1–6) were prepared using a new iterative synthetic procedure that takes advantage of the highly selective and differential reactivity of bromoboranes with arylsilanes and arylstannanes. Electrochemical, UV-vis and fluorescence studies, as well as DFT calculations, provide important insights into the effect of chain extension of conjugated organic π-systems via tricoordinate boron moieties. Our results are of direct relevance to potential applications of conjugated organoborane oligomers and polymers in optoelectronic devices. Moreover, the preparation of well-defined conjugated organoborane oligomers allowed us to shed some light on the origin of signal amplification effects reported for the fluorescent sensing of anions such as fluoride and cyanide with conjugated organoborane polymers.

1.6 Experimental Section

n-BuLi (1.6 M in hexanes), BBr_3 and tetrabutylammonium fluoride (TBAF: 1.0 M in

THF) were purchased from Aldrich, Me_3SiCl (TMSCl) and 1,3,5-triisopropylbenzene from Acros, Me_3SnCl from Strem chemicals, and benzo[a]pyrene from TCI chemicals. BBr_3 and Me_3SiCl were distilled under vacuum and all other commercially available chemicals were used as received without further purification. 9,9-Dimethylfluorene, 2,7-dibromo-9,9-dimethylfluorene,[94] 2-bromo-7-trimethylsilyl-9,9-dimethylfluorene,[95] and 2,4,6-triisopropylphenylcopper[96] (TipCu) were prepared according to the previously published procedures. Ether solvents (diethyl ether and THF here) were distilled from Na/benzophenone prior to use. Hexanes and toluene were purified using a solvent purification system (Innovative Technologies; alumina/copper columns for hydrocarbon solvents). Dichloromethane (DCM) and $CDCl_3$ were distilled from CaH_2 and degassed via several freeze-pump-thaw cycles for air-sensitive compounds. All reactions and manipulations were carried out under an atmosphere of prepurified nitrogen using either Schlenk techniques or an inert-atmosphere glove box.

All 499.893 (or 600) MHz ^{1}H, 125.7 MHz ^{13}C, 160.4 MHz ^{11}B NMR, 99.25 MHz ^{29}Si NMR, and 186.455 MHz ^{119}Sn NMR spectra were recorded on a Varian INOVA spectrometer equipped with a boron-free 5 mm dual broadband gradient probe (Nalorac, Varian Inc., Martinez, CA). ^{11}B NMR spectra were acquired with boron-free quartz NMR tubes and the spectra were referenced externally to $BF_3 \cdot Et_2O$ ($\delta = 0$). ^{29}Si NMR spectra were referenced to $SiMe_4$ ($\delta = 0$). All NMR spectra were obtained at ambient temperature.

GC-MS spectra were acquired on a Hewlett Packard HP 6890 Series GC system equipped with a series 5973 mass selective detector and a series 7683 injector. A temperature profile with a heating rate of 20 °C/min from 70 to 300 °C was used. MALDI-TOF measurements were performed on an Applied Biosystems 4800 Proteomics Analyzer as specified either in linear or in reflection (-) mode with delayed extraction. Benzo[a]pyrene (10 mg/mL) used as the matrix was mixed with the samples (10 mg/mL in toluene) in a 10:1 ratio, and then spotted on the wells of a target plate inside a glove box.

GPC analyses were performed in THF (1 mL/min) using a Waters Breeze system equipped with a 717 plus autosampler, a 1525 binary HPLC pump, a 2998 photodiode array detector, and a 2414 refractive index detector. For separation the samples were passed through a series of styragel columns (Polymer Laboratories; two columns 5 μm / Mixed-C), which were kept in a column heater at 35 °C. The columns were calibrated with polystyrene standards (Polymer Laboratories).

UV-visible absorption data were acquired on a Varian Cary 500 UV-Vis/NIR spectrophotometer. The fluorescence data and quantum yields were measured on a Varian Cary Eclipse fluorescence spectrophotometer with the same solutions as those used in the UV-visible measurements. The quantum yields (Φ) in DCM were calculated using 9, 10-diphenylanthracene as a standard, which is reported to be Φ = 0.92 in dichloromethane.[97] Sample solutions were prepared using a microbalance (± 0.1 mg) and volumetric flasks. For titration experiments, fluoride ion solutions were prepared by dilution of desired amount of TBAF solution (1.0 M) in dry THF; stock solutions of the samples were prepared in THF in the glove box. Fluoride was added to the sample solution through a microsyringe (± 0.1 μL), minimizing exposure to air. Binding constants β_{1n} are given in units of M^{-n}. In the case of lower oligomers **O-B1** and **O-B2**, all the constants are automatically generated from the Hyperquad™. However, in higher oligomers, the binding constant $\lg\beta_{11}$ had to be manually fixed to allow for a stable refinement. Electrospray ionization mass spectra (ESI-MS) experiments were recorded on an Apex-ultra 7T Hybrid FT-MS (Bruker Daltonics). Solutions in THF were prepared in the glovebox.

Cyclic voltammetry (CV) and square wave voltammetry experiments were carried out on a CV-50W analyzer from BAS. The three-electrode system consisted of an Au disk as working electrode, a Pt wire as secondary electrode and a Ag wire as the reference electrode. The voltammograms were recorded with ca. 10^{-3} to 10^{-4} M solution in THF and $Bu_4N[PF_6]$ (0.1 M) was used as the supporting electrolyte. The scans were referenced after the addition of a small amount of ferrocene as internal standard. The potentials are reported relative to ferrocene/ferrocenium couple.

Single crystal X-ray diffraction data were collected on a Smart Apex CCD diffractometer at 100 K using Cu Kα (1.54178 Å) radiation. The structure was solved by direct methods and refined by full-matrix least squares based on F^2 with all reflections (SHELXTL V5.10; G. Sheldrick, Siemens XRD, Madison, WI). Non-hydrogen atoms were refined with anisotropic displacement coefficients, and hydrogen atoms were treated as idealized contribution. SADABS (Sheldrick, G.M. SADABS 2.01), Bruker/Siemens Area Detector Absorption Correction Program; Bruker AXS: Madison, WI, 1998) absorption correction was applied. Crystallographic data for the structure have been deposited with the Cambridge Crystallographic Data Center as supplementary publication CCDC-823516. Copies of the data can be obtained free of charge on application on CCDC, 12 Union Road, Cambridge CB2 1EZ, UK(fax: (+44) 1223-336-033; email: deposit@ccdc.cam.ac.uk).

DFT calculations (gas phase) have been performed with the Gaussian03 program. Geometries and electronic properties are calculated by means of hybrid density functional B3LYP with the basis set of 6-31G(d). The input files and orbital representations were generated with Gaussview 3.07 (scaling radii of 75%, isovalue of 0.02). Excitation data were calculated using TD-DFT (B3LYP, 6-31G(d)).

Synthesis of 2,7-bis-(trimethylsilyl)-9,9-dimethylfluorene (FlSi2). 2,7-Dibromo-9,9-dimethylfluorene (10.0 g, 28.4 mmol) was dissolved in 550 mL of dry ether and TMEDA (12 mL, 68.2 mmol) was added. The solution was cooled to -78 °C and *n*-BuLi (27.3 mL, 2.5 M, 68.2 mmol) was added through an addition funnel under N_2. At this temperature the reaction mixture was stirred for one more hour followed by stirring at R.T. for 2 h. The reaction mixture was cooled back to -78 °C, and then dry TMSCl (9.4 mL, 73.5 mmol) was added via syringe. The reaction mixture was kept stirring at R.T. overnight. After standard workup the crude material was purified by recrystallization from ethanol to give colorless crystals (6.43 g, 67%). ^{1}H NMR (499.893 MHz, $CDCl_3$): δ 0.33 (s, 18H), 1.52 (s, 6H), 7.50 (d, J = 7.5 Hz, 2H), 7.57 (s, 2H), 7.72 (d, 7.5 Hz, 2H). ^{29}Si NMR

(99.25 MHz, $CDCl_3$): δ -3.47. GC-MS: *m*/*z* 338 (50%) [M^+], 323 (100%) [M^+–Me].

Synthesis of 2-trimethylsilyl-7-trimethylstannyl-9,9-dimethylfluorene (FlSiSn). 2-Bromo-7-trimethylsilyl-9,9-dimethylfluorene (7.40 g, 21.5 mmol) was dissolved in 300 mL of dry ether and TMEDA (3.6 mL, 23.7 mmol) was added. *n*-BuLi (9.5 mL, 2.5 M, 23.7 mmol) was added dropwise at -78 °C over 1 h and the reaction solution was stirred for one more hour followed by stirring at R.T. for 2 h. The reaction mixture was cooled down to -78 °C, and 4.72 g (23.7 mmol) of Me_3SnCl were added. The reaction mixture was allowed to warm up to room temperature and kept stirring overnight. After standard workup the crude material was purified by recrystallization from ethanol to give colorless crystals (6.1 g, 66%). ^1H NMR (499.893 MHz, $CDCl_3$): δ 0.33 (s, 9H), 0.34 (s/d, $J(^{117/119}Sn, H)$ = 54 Hz, 9H), 1.53 (s, 6H), 7.47 (d, J(H, H) = 7.5 Hz, $J(^{117/119}Sn, H)$ = 44 Hz, 1H), 7.51 (d, J = 7.5 Hz, 1H), 7.56 (s/d, $J(^{117/119}Sn, H)$ = 44 Hz, 1H), 7.58 (s, 1H), 7.72 (d, J = 7.5 Hz, 2H). ^{29}Si NMR (99.25 MHz, $CDCl_3$): δ -3.73. ^{119}Sn NMR (186.455 MHz, $CDCl_3$): δ -24.26. GC-MS: *m*/*z* 430 (10%) [M^+], 415 (100%) [M^+ – Me].

Synthesis of 2,7-bis-(trimethylstannyl)-9,9-dimethylfluorene (FlSn2). 2,7-Dibromo-9,9-dimethylfluorene (6.50 g, 18.5 mmol) was dissolved in 200 mL of dry ether and TMEDA (6.8 mL, 44.3 mmol) was added. To this solution *n*-BuLi (27.7 mL, 1.6 M, 44.3 mmol) was added at -78 °C over 1 h. The reaction mixture was stirred at -78 °C for 1 h and then at R. T. for 2 h and finally cooled back to -78 °C. Me_3SnCl (9.56 g, 47.8 mmol) was added via syringe, the reaction mixture was allowed to warm up to R.T. and kept stirring overnight. After standard workup the crude material was purified by recrystallization from ethanol to give colorless crystals (7.0 g, 73%). ^{1}H NMR (499.893 MHz, $CDCl_3$): δ 0.35 (s, J($^{117/119}$Sn, H) = 54 Hz, 18H), 1.53 (s, 6H), 7.47 (d, J(H, H) = 7.5 Hz, J(Sn, H) = 44 Hz, 2H), 7.56 (s, J($^{117/119}$Sn, H) = 44 Hz, 2H), 7.71 (d, J = 7.5 Hz, 2H). ^{119}Sn NMR (186.455 MHz, $CDCl_3$): δ -24.32. GC-MS: m/z 520 (8%) [M^+], 505 (100%) [M^+ – Me].

Synthesis of Br_2B-Fl-BBr_2 (FlB2). To BBr_3 (2.63 g, 10.50 mmol) in 5 mL of CH_2Cl_2 was added a solution of **FlSi2** (1.50 g, 4.44 mmol) in 15 mL CH_2Cl_2 with stirring. The reaction mixture was kept stirring overnight, and then all volatile components were removed under high vacuum. The crude product was purified by recrystallization from toluene at -35 °C to give **FlB2** as colorless crystals (1.68 g, 71%). ^{1}H NMR (499.893MHz, $CDCl_3$): δ 1.62 (s, 6H), 7.91 (d, J = 8.0 Hz, 2H), 8.31 (m, 4H). ^{11}B NMR (160.4 MHz, $CDCl_3$): δ 56 ($w_{1/2}$ = 3,200 Hz). ^{13}C NMR (125.7 MHz, $CDCl_3$): 27.04, 47.44, 121.16, 132.15, 137.87, 144.79, 154.83, C_B not observed.

Synthesis of TMS-Fl-BBr_2 (FlSiB). To a solution of **FlSi2** (1.00 g, 2.96 mmol) in15 mL of CH_2Cl_2 was added a solution of BBr_3 (0.74 g, 2.96 mmol) in 15 mL of CH_2Cl_2 at 0 °C with stirring. The reaction mixture was kept stirring overnight, and then all volatile components were removed under high vacuum. The crude product was purified by recrystallization from hexanes at -35 °C to give **FlSiB** as a white solid (0.97 g, 75%). ^{1}H NMR (499.893 MHz, $CDCl_3$): δ 0.34 (s, 9H), 1.57 (s, 6H), 7.57 (d, J = 8.0 Hz, 1H), 7.63 (s, 1H), 7.81 (d, J = 8.0 Hz, 1H), 7.82 (d, J = 8.0 Hz, 1H), 8.27 (d, J = 8.0 Hz, 1H), 8.28 (s, 1H). ^{11}B NMR (160.4 MHz, $CDCl_3$): δ 56 ($w_{1/2}$ = 1,300 Hz). ^{13}C NMR (125.7 MHz,

$CDCl_3$): -0.73, 27.23, 47.18, 119.89, 120.92, 127.76, 132.02, 132.63, 138.01, 138.58, 142.61, 146.73, 153.48, 154.63 C_B not observed. ^{29}Si NMR (99.25 MHz, $CDCl_3$): δ -3.54.

Synthesis of Dimer O-B2. To solution of **FlB2** (1.00 g, 1.87 mmol) in 10 mL of CH_2Cl_2 was added a solution of **FlSiSn** (1.61 g, 3.74 mmol) in 25 mL of CH_2Cl_2 with stirring. The reaction mixture was kept stirring overnight, followed by the removal of all volatile components under high vacuum. **O-B2-BBr** was obtained as a colorless solid (1.54 g, 91%). ^{1}H NMR (499.893 MHz, $CDCl_3$): δ 0.35 (s, 18H), 1.58 (s, 12H), 1.62 (s, 6H), 7.57 (d, J = 7.5 Hz, 2H), 7.64 (s, 2H), 7.83 (d, J = 7.5 Hz, 2H), 7.87 (d, J = 8.0 Hz, 2H), 7.96 (d, J = 8.0 Hz, 2H), 8.10 (m, 8H). ^{11}B NMR (160.4 MHz, $CDCl_3$): δ 64 (two overlapping B signals: $w_{1/2}$ = 4,400 Hz). ^{13}C NMR (125.7 MHz, $CDCl_3$): -0.66, 27.20, 27.34, 47.20, 47.35, 119.76, 120.51, 120.57, 127.68, 131.98, 132.20, 132.54, 137.25, 137.61, 139.16, 139.32 (B-C), 140.80 (B-C), 141.70, 143.15, 144.53, 153.24, 154.12, 154.23. ^{29}Si NMR (99.25 MHz, $CDCl_3$): δ -3.48. The crude product (1.00 g, 1.11 mmol) was dissolved in 20 mL of toluene and then treated with “TipCu” (0.59 g, 2.21 mmol) in 20 mL of toluene. The reaction mixture was refluxed at 115 °C under N_2 for 2 d. A solid precipitate (CuBr) was removed by filtration through a fritted glass disk. All volatile components were removed under high vacuum. The crude product was purified by column chromatography on silica gel using hexanes/toluene (10:1) as the eluent and then precipitated from hexanes at -35 °C to give **O-B2** as a white powder (1.04 g, 82%). ^{1}H NMR (499.893 MHz, $CDCl_3$): δ 0.34 (s, 18H), 0.99 (m, 24H), 1.36 (d, J = 7.0 Hz, 12H), 1.51 (s, 6H), 1.52 (s, 12H), 2.51 (septet, J = 7.0 Hz, 4H), 2.98 (septet, J = 7.0 Hz, 2H), 7.03 (s, 4H), 7.54 (d, J = 7.0 Hz, 2H) 7.61 (s, 2H), 7.79–7.91 (m, 14H). ^{11}B NMR (160.4 MHz, $CDCl_3$): δ 68 ($w_{1/2}$ = 7,900 Hz). ^{13}C NMR (125.7 MHz, $CDCl_3$): -0.64 ($SiMe_3$), 24.32 (CH*Me*$_2$), 24.34 (CH*Me*$_2$), 24.39 (CH*Me*$_2$), 27.22 (Fl-Me), 27.34 (Fl-Me), 34.49 (*C*HMe_2), 35.70 (*C*HMe_2), 47.05 (Fl-C9), 47.09 (Fl-C9), 119.53, 120.06, 120.24, 127.58, 132.14, 132.18, 132.39, 137.58, 137.63, 139.82, 140.80, 141.18 (B-C) , 142.39, 142.68, 142.78, 143.30 (B-C), 148.62, 149.14, 153.04, 153.90, 154.02. ^{29}Si NMR (99.25 MHz, $CDCl_3$): δ -3.66. MALDI-TOF (neg.) m/z: calcd. for $C_{81}H_{99}B_2Si_2$ [M–H$^+$] 1149.7490, found 1149.7579.

Synthesis of Tetramer O-B4. To a solution of BBr_3 (0.30 g, 1.20 mmol) in 5 mL of CH_2Cl_2 was added a solution of **O-B2** (0.58 g, 0.50 mmol) in 15 mL of CH_2Cl_2 with stirring. The reaction mixture was kept stirring overnight, and then all volatile components were removed under high vacuum. The crude product was purified by precipitation from hexanes/toluene mixture at -35 °C to give **O-B2-BBr2** as a white solid (0.51 g, 76%). ^{1}H NMR (499.893 MHz, $CDCl_3$): δ 0.99 (m, 24H), 1.35 (d, J = 7.0 Hz, 12H), 1.52 (s, 6H), 1.56 (s, 12H), 2.49 (septet, J = 7.0 Hz, 4H), 2.99 (septet, J = 7.0 Hz, 2H), 7.04 (two overlapping s, 4H), 7.84–7.93 (m, 14H), 8.29–8.31 (m, 4H). ^{11}B NMR (160.4 MHz, $CDCl_3$): δ 62 (two overlapping B signals: $w_{1/2}$ = 3,200 Hz). ^{13}C NMR (125.7 MHz, $CDCl_3$): 24.35, 24.37, 27.11, 27.20, 34.50, 35.82, 47.12, 47.26, 120.21, 120.36, 120.45, 120.82, 132.08, 132.13, 132.26, 137.50, 137.72, 138.10, 140.75 (B-C), 141.03, 142.60, 143.11 (B-C), 146.35, 148.90, 149.13, 153.99, 154.26, 154.55. To a solution of **O-B2-BBr2** (0.33 g, 0.24 mmol) in 5 mL of CH_2Cl_2 was added a solution of **FlSiSn** (0.21 g, 0.48 mmol) in 15 mL of CH_2Cl_2 with stirring. The reaction mixture was stirred overnight and all volatile components were removed under high vacuum. The crude product was precipitated from hexanes/toluene mixture at -35 °C to give **O-B4-BBr** as a light yellow powder (0.36 g, 86%). ^{1}H NMR (499.893 MHz, $CDCl_3$): δ 0.35 (s, 18H), 1.00 (m, 24H), 1.36 (d, J = 7.0 Hz, 12H), 1.54, 1.56 (m, 30H), 2.52 (septet, J = 7.0 Hz, 4H), 2.99 (septet, J = 7.0 Hz, 2H), 7.05 (s, 4H), 7.57 (d, J = 7.5 Hz, 2H), 7.63 (s, 2H), 7.82–7.92 (m, 18H), 8.10 (m, 8H). ^{11}B NMR (160.4 MHz, $CDCl_3$): δ 61 (two overlapping B signals: $w_{1/2}$ = 7,600 Hz). ^{29}Si NMR (99.25 MHz, $CDCl_3$): δ -3.43. Compound **O-B4-BBr** (0.1755 g, 0.10 mmol) was dissolved in 10 mL of toluene and then treated with "TipCu" (0.0545 g, 0.20 mmol) in 10 mL of toluene. The reaction mixture was refluxed at 115 °C under N_2 for 2 d. A solid precipitate (CuBr) was removed by filtration through a fritted glass disk. All volatile components were removed under high vacuum. The crude mixture was purified by column chromatography on silica gel using hexanes/toluene (10:1) as the eluent, and then precipitated from hexanes/toluene mixture at -35 °C to give **O-B4** as a white solid (0.15 g, 75%). ^{1}H NMR (499.893 MHz, $CDCl_3$): δ 0.34 (s, 18H), 0.99 (m, 48H), 1.35 (m, 24H), 1.52 (m, 30H), 2.52 (m, 8H), 3.00 (m, 4H), 7.03 (s, 4H), 7.04 (s, 4H), 7.54 (d, J = 7.0 Hz, 2H), 7.61 (s, 2H), 7.78–7.92 (m, 26H). ^{11}B NMR (160.4 MHz, $CDCl_3$): δ 68 (two overlapping B signals: $w_{1/2}$ = 8,700 Hz). ^{13}C NMR (125.7 MHz, $CDCl_3$): -0.65, 24.30, 24.34, 24.38, 27.20, 27.32, 34.46, 35.69, 35.73, 47.03, 47.07, 119.53, 120.08, 120.22, 120.26, 127.57, 132.11, 132.16, 132.38, 137.58, 137.62, 139.79, 140.78, 141.02 (B-C), 141.13 (B-C), 142.31, 142.41, 142.47, 142.61, 142.77, 143.20 (B-C), 143.25 (B-C), 143.28 (B-C), 148.59, 148.65, 149.09, 153.00, 153.87, 153.98. ^{29}Si NMR (99.25 MHz, $CDCl_3$): δ -3.54. MALDI-TOF (neg.) *m/z*: calcd. for $C_{141}H_{169}B_4Si_2$ [M–H$^+$] 1963.3201, found 1963.1859.

Synthesis of Hexamer O-B6. The procedure is similar to that for compound **O-B4** except that tetramer **O-B4** (0.6442 g, 0.3279 mmol) is taken instead of **O-B2** as the precursor. Precipitation from hexanes/toluene mixture at -35 °C gave **O-B4-BBr2** as a white solid (0.58 g, 82%). ^{1}H NMR (600 MHz, $CDCl_3$): δ 1.00 (m, 48H), 1.35-1.37 (m, 24H), 1.51, 1.56 (m, 30H), 2.50 (m, 8H), 2.98 (m, 4H), 7.04 (overlapped singlets, 8H), 7.83–7.92 (m, 26H), 8.30 (m, 4H). ^{11}B NMR (160.4 MHz, $CDCl_3$): δ 57 (three overlapping B signals: $w_{1/2}$ = 8,200 Hz). To a solution of **O-B4-BBr2** (0.20 g, 0.0926 mmol) in 5 mL of CH_2Cl_2 was added dropwise a solution of **FlSiSn** (0.0796 g, 0.1852 mmol) in 5 mL of CH_2Cl_2 and the mixture was kept stirring overnight. All volatile components were removed under high vacuum, leaving behind a yellowish solid. Without further purification the crude product was dissolved in toluene (10 mL)and then treated with “TipCu” (0.0494 g, 0.1852 mmol) in 10 mL of toluene. The reaction mixture was refluxed at 115 °C under N_2 for 2 d. A solid precipitate (CuBr) was removed by filtration through a fritted glass disk. All volatile components were removed under high vacuum. The crude product was purified by column chromatography on silica gel using hexanes/toluene (10:1) as the eluent, and then precipitated from hexanes/toluene mixture at -35 °C to give **O-B6** as a white solid (0.18 g, 70%). ^{1}H NMR (499.893 MHz, $CDCl_3$):

δ 0.34 (s, 18H), 0.99 (m, 72H), 1.35 (m, 36H), 1.51 (m, 42H), 2.52 (m, 12H), 2.98 (m, 6H), 7.03 (m, 12H), 7.54 (d, J = 7.5 Hz, 2H), 7.61 (s, 2H), 7.80–7.90 (m, 38H). ^{11}B NMR (160.4 MHz, $CDCl_3$): δ 68.4 (three overlapping B signals: $w_{1/2}$ = 7,400 Hz). ^{13}C NMR (125.7 MHz, $CDCl_3$): -0.64, 24.33, 24.35, 24.38, 27.21, 27.28, 27.33, 34.48, 35.70, 35.74, 47.05, 47.09, 119.53, 120.10, 120.24, 120.27, 127.58, 132.13, 132.19, 132.39, 137.62, 139.81, 140.80, 141.05 (B-C), 141.09 (B-C), 141.13 (B-C), 141.16 (B-C), 142.33, 142.44, 142.49, 142.65, 142.79, 143.23 (B-C), 143.28 (B-C), 148.62, 148.69, 149.13, 153.03, 153.90, 154.01. ^{29}Si NMR (99.25 MHz, $CDCl_3$): δ -3.61. MALDI-TOF (neg.) m/z: calcd. for $C_{201}H_{239}B_6Si_2$ [M–H$^+$] 2775.8897 found 2775.7704.

Synthesis of Monomer O-B1. To a solution of compound **FlSiB** (0.60 g, 1.38 mmol) in 10 mL of CH_2Cl_2 was added a solution of **FlSiSn** (0.59 g, 1.38 mmol) in 15 mL of CH_2Cl_2 and the mixture was kept stirring overnight. All volatile components were removed under vacuum, leaving behind a yellowish solid. Without further purification the crude product was dissolved in toluene (20 mL) and then treated with “TipCu” (0.37 g, 1.38 mmol) in 10 mL of toluene. The reaction mixture was refluxed at 115 °C under N_2 for 2 d. A solid precipitate (CuBr) was removed by filtration through a fritted glass disk. All volatile components were removed under high vacuum. The crude product was purified by column chromatography on silica gel using hexanes/toluene (10:1) as the eluent, and then precipitated from hexanes/toluene mixture at -35 °C to give **O-B1** as a white solid (0.86 g, 84%). ^{1}H NMR (499.893 MHz, $CDCl_3$): δ 0.35 (s, 18H), 0.99 (d, J = 7.5 Hz, 12H), 1.36 (d, J = 7.0 Hz, 6H), 1.53 (s, 12H), 2.51 (septet, J = 7.0 Hz, 2H), 2.99

(septet, J = 7.0 Hz, 1H), 7.04 (s, 2H), 7.55 (d, J = 8.0 Hz, 2H), 7.62 (s, 2H), 7.81 (m, 6H), 7.88 (s, 2H). ^{11}B NMR (160.4 MHz, $CDCl_3$): δ 69 ($w_{1/2}$ = 3,900 Hz). ^{13}C NMR (125.7 MHz, $CDCl_3$): δ -0.62, 24.31, 24.41, 27.35, 34.48, 35.68, 47.06, 119.53, 120.22 (2C), 127.59, 132.12, 132.39, 137.59, 139.86, 140.73, 141.28 (B-C), 142.69 (2C), 148.53, 149.10, 153.00, 154.01. ^{29}Si NMR (99.25 MHz, $CDCl_3$): δ -3.69. MALDI-TOF (neg.) *m/z*: calcd. for $C_{51}H_{64}BSi_2$ [M–H$^+$] 743.4644 found 743.4532.

Synthesis of Trimer O-B3. The procedure is similar to that for **O-B4** except that monomer **O-B1** (0.600 g, 0.805 mmol) was used here instead of the dimer **O-B2**. After reaction overnight, all volatile components were removed under high vacuum and the crude product was precipitated from hexanes/toluene mixture at -35 °C to give **O-B1-BBr2** as a white solid (0.72 g, 95%). ^{1}H NMR (600 MHz, $CDCl_3$): δ 1.00 (d, J = 6.5 Hz, 12H), 1.36 (d, J = 6.0 Hz, 6H), 1.57 (s, 12H), 2.48 (septet, J = 6.5 Hz, 2H), 2.99 (septet, J = 6.5 Hz, 1H), 7.05 (s, 2H), 7.84–7.93 (m, 8H), 8.31 (m, 4H). ^{11}B NMR (160.4 MHz, $CDCl_3$): δ 58 (two overlapping B signals: $w_{1/2}$ = 4,700 Hz). To a solution of compound **O-B1-BBr2** (0.70 g, 0.745 mmol) in 10 mL of CH_2Cl_2 was added a solution of **FlSiSn** (0.64 g, 1.489 mmol) in 15 mL of CH_2Cl_2 and the mixture was kept stirring overnight. All volatile components were removed under vacuum, leaving behind a yellowish solid. Without further purification the crude product was dissolved in toluene (15 mL) and then treated with "TipCu" (0.40 g, 1.4894 mmol) in 10 mL of toluene. The reaction mixture was refluxed at 115 °C under N_2 for 2 d. A solid precipitate (CuBr) was removed by filtration through a fritted glass disk. All volatile components were removed under high vacuum. The crude product was purified by column chromatography on silica gel using hexanes/toluene (10:1) as the eluent, and then precipitated from hexanes/toluene mixture at -35 °C to give **O-B3** as a white solid (0.77 g, 66%). ^{1}H NMR (499.893 MHz, $CDCl_3$): δ 0.33 (s, 18H), 0.98 (m, 36H), 1.35 (m, 18H), 1.52 (m, 24H), 2.50 (m, 6H), 2.98 (m, 3H), 7.03 (s, 4H), 7.04 (s, 2H), 7.53 (d, J = 8.0 Hz, 2H), 7.61 (s, 2H), 7.78–7.90 (m, 20H). ^{11}B NMR (160.4 MHz, $CDCl_3$): δ 69 (two overlapping B signals: $w_{1/2}$ = 6,900 Hz). ^{13}C NMR (125.7 MHz, $CDCl_3$): δ -0.64, 24.31, 24.34, 24.35, 24.38, 27.21, 27.33, 34.48, 35.70, 35.73, 47.04, 47.09, 119.53, 120.08, 120.23, 127.58, 132.12, 132.17, 132.38, 137.58, 137.62, 139.81, 140.80, 141.06 (B-C), 141.16 (B-C), 142.34, 142.47, 142.65, 142.78, 143.24 (B-C), 143.32 (B-C), 148.61, 148.68, 149.12, 153.02, 153.90, 154.01. ^{29}Si NMR (99.25 MHz, $CDCl_3$): δ -3.68. MALDI-TOF (neg.) *m/z*: calcd. for $C_{111}H_{134}B_3Si_2$ [M–H$^+$] 1557.0354 found 1557.0116.

Synthesis of O-B5. The procedure is similar to that for **O-B4** except that trimer **O-B3** (0.15 g, 0.096 mmol) was used instead of the dimer **O-B2**. After reaction overnight, all volatile components were removed under high vacuum and the crude product was precipitated from hexanes/toluene mixture at -35 °C to give **O-B3-BBr2** as a white solid (0.13 g, 77%). ^{1}H NMR (600 MHz, $CDCl_3$): δ 1.01 (m, 36H), 1.37 (m, 18H), 1.53 (s, 12H), 1.57 (s, 12H), 2.52 (m, 6H), 2.99 (m, 3H), 7.05 (two overlapped s, 6H), 7.84–7.93 (m, 20H), 8.31 (m, 4H). ^{11}B NMR (160.4 MHz, $CDCl_3$): δ 55 (three overlapping B signals: $w_{1/2}$ = 7,100 Hz). To a solution of compound **O-B3-BBr2** (0.12 g, 0.068 mmol) in 5 mL of CH_2Cl_2 was added the solution of **FlSiSn** (0.06 g, 0.137 mmol) in 10 mL of

CH_2Cl_2 and the mixture was kept stirring overnight. All volatile components were removed under high vacuum, leaving behind a yellowish solid. Without further purification the crude product was dissolved in toluene (10 mL) and then treated with "TipCu" (0.04 g, 0.137 mmol) in 5 mL of toluene. The reaction mixture was refluxed at 115 °C under N_2 for 2 d. A solid precipitate (CuBr) was removed by filtration through a fritted glass disk. All volatile components were removed under high vacuum. The crude product was purified by column chromatography on silica gel using hexanes/toluene (10:1) as the eluent, and then precipitated from hexanes/toluene mixture at -35 °C to give **O-B5** as a white solid (0.11 g, 65%). ^{1}H NMR (499.893 MHz, $CDCl_3$): δ 0.33 (s, 18H), 0.98 (m, 60H), 1.35 (m, 30H), 1.51 (m, 36H), 2.51 (m, 10H), 2.98 (m, 5H), 7.04 (m, 10H), 7.53 (d, J = 7.5 Hz, 2H), 7.61 (s, 2H), 7.78–7.90 (m, 32H). ^{11}B NMR (160.4 MHz, $CDCl_3$): δ 70 (three overlapping B signals: $w_{1/2}$ = 7,300 Hz). ^{13}C NMR (125.7 MHz, $CDCl_3$): δ -0.58, 24.38, 24.42, 24.45, 27.28, 27.40, 34.54, 35.76, 35.80, 47.10, 47.15, 119.60, 120.16, 120.30, 120.33, 127.63, 132.19, 132.24, 132.45, 137.69, 139.87, 140.85, 141.11 (B-C), 141.22 (B-C), 142.39, 142.51, 142.56, 142.70, 142.85, 143.30 (B-C), 143.35 (B-C), 148.67, 148.74, 149.18, 153.08, 153.96, 154.06. ^{29}Si NMR (99.25 MHz, $CDCl_3$): δ -3.60. MALDI-TOF (neg.) m/z: calcd. for $C_{171}H_{204}B_5Si_2$ [M–H$^+$] 2369.6049 found 2369.5544.

1.7 References

(1) Kanibolotsky, A. L.; Perepichka, I. F.; Skabara, P. J. *Chem. Soc. Rev.* **2010**, *39*,

2695.
(2) Braga, D.; Horowitz, G. *Adv. Mater*. **2009**, *21*, 1473.
(3) Arias, A. C.; MacKenzie, J . D.; McCulloch, I.; Rivnay, J.; Salleo, A. *Chem. Rev*. **2010**, *110*, 3.
(4) Huang, H.; Prabhakar, C.; Tang, K.; Chou, P.; Huang, G.; Yang, J. *J. Am. Chem. Soc*. **2011***, 133,* 8028.
(5) Bunz, U. H. F. *Angew. Chem. Int. Ed*. **2010**, *49*, 5037.
(6) Zade, S. S.; Zamoshchik, N.; Bendikov, M. *Acc. Chem. Res*. **2011**, *44*, 14.
(7) Ma, C.; Mena-Osteritz, E.; Debaerdemaeker, T.; Wienk, M. M.; Janssen, R. A. J.; Bäuerle, P. *Angew. Chem. Int. Ed*. **2007**, *46*, 1679.
(8) Allard, S.; Forster, M.; Souharce, B.; Thiem, H.; Scherf, U. *Angew. Chem. Int. Ed*. **2008**, *47*, 4070.
(9) Mishra, A.; Ma, C.; Bäuerle, P. *Chem. Rev*. **2009**, *109*, 1141.
(10) Mishra, A.; Bäuerle, P. *Angew. Chem. Int. Ed*. **2012**, *51*, 2020.
(11) Fitzner, R.; Mena-Osteritz, E.; Mishra, A.; Schulz, G.; Reinold, E.; Weil, M.; Körner, C.; Ziehlke, H.; Elschner, C.; Leo, K.; Riede, M.; Pfeiffer, M.; Uhrich, C.; Bäuerle, P. *J. Am. Chem. Soc*. **2012**, *134*, 11064.
(12) Sadighi, J. P.; Singer, R. A.; Buchwald, S. L. *J. Am. Chem. Soc*. **1998**, *120*, 4960.
(13) Wang, Y.; Tran, H. D.; Liao, L.; Duan, X.; Kaner, R. B. *J. Am. Chem. Soc*. **2010**, *132*, 10365.
(14) Wang, Y.; Liu, J.; Tran, H. D.; Mecklenburg, M.; Guan, X. N.; Stieg, A. Z.; Regan, B. C.; Martin, D. C.; Kaner, R. B. *J. Am. Chem. Soc*. **2012**, *134*, 9251.
(15) Geng, Y.; Trajkovska, A.; Katsis, D.; Ou, J. J.; Culligan, S. W.; Chen, S. H. *J. Am. Chem. Soc*. **2002**, *124*, 8337.
(16) Jo, J.; Chi, C.; Höger, S.; Wegner, G.; Yoon, D. Y. *Chem. -Eur. J.* **2004**, *10*, 2681.
(17) Wang, Q.; Qu, Y.; Tian, H.; Geng, Y.; Wang, F. *Macromolecules* **2011**, *44*, 1256.
(18) Reggelin, M.; Doerr, S.; Klussmann, M.; Schultz, M.; Holbach, M. *Proc. Natl Acad. Sci. USA* **2004**, *101*, 5461.
(19) Ohta, E.; Sato, H.; Ando, S.; Kosaka, A.; Fukushima, T.; Hashizume, D.; Yamasaki, M.; Hasegawa, K.; Muraoka, A.; Ushiyama, H.; Yamashita, K.; Aida, T. *Nature Chem*. **2011**, *3*, 68.
(20) Ando, S.; Ohta, E.; Kosaka, A.; Hashizume, D.; Koshino, H.; Fukushima, T.; Aida, T. *J. Am. Chem. Soc*. **2012**, *134*, 11084.
(21) Brook, M. A. *Silicon in organic, organometallic, and polymer chemistry*; Wiley-VCH: New York, **2000.**
(22) Baumgartner, T.; Réau, R. *Chem. Rev.* **2006**, *106*, 4681.
(23) Jäkle, F. *Coord. Chem. Rev.* **2006**, *250*, 1107.
(24) Matsumi, N.; Chujo, Y. *Polym. J.* **2008**, *40*, 77.
(25) Elbing, M.; Bazan, G. C. *Angew. Chem., Int. Ed.* **2008**, *47*, 834.

(26) Jäkle, F. *Chem. Rev.* **2010**, *110*, 3985.

(27) Sase, S.; Cho, Y.-S.; Kawachi, A.; Wakamiya, A.; Yamaguchi, S.; Tsuji, H.; Tamao, K. *Organometallics* **2008**, *27*, 5441.

(28) Barriére, F.; Fabre, B.; Hao, E. H.; LeJeune, Z. M.; Hwang, E.; Garno, J. C.; Nesterov, E. E.; Vicente, M. G. H. *Macromolecules* **2009**, *42*, 2981.

(29) Simon, Y. C.; Peterson, J. J.; Mangold, C.; Carter, K. R.; Coughlin, E. B. *Macromolecules* **2009**, *42*, 512.

(30) Dash, B. P.; Satapathy, R.; Gaillard, E. R.; Maguire, J. A.; Hosmane, N. S. *J. Am. Chem. Soc.* **2010**, *132*, 6578.

(31) Yang, J. A.; Aschemeyer, S.; Martinez, H. P.; Trogler, W. C. *Chem. Commun.* **2010**, *46*, 6804.

(32) Interrante, L. V.; Rathore, J. S. *Dalton Trans.* **2010**, *39*, 9193.

(33) Smith, R. C.; Protasiewicz, J. D. *J. Am. Chem. Soc.* **2004**, *126*, 2268.

(34) Jin, Z.; Lucht, B. L. *J. Am. Chem. Soc.* **2005**, *127*, 5586.

(35) Wright, V. A.; Patrick, B. O.; Schneider, C.; Gates, D. P. *J. Am. Chem. Soc.* **2006**, *128*, 8836.

(36) Romero-Nieto, C.; Merino, S.; Rodríguez-López, J.; Baumgartner, T. *Chem. Eur. J.* **2009**, *15*, 4135.

(37) Umeyama, T.; Naka, K.; Nakahashi, A.; Chujo, Y. *Macromolecules* **2004**, *37*, 1271.

(38) Naka, K.; Nakahashi, A.; Chujo, Y. *Macromolecules* **2007**, *40*, 1372.

(39) Matsumi, N.; Naka, K.; Chujo, Y. *J. Am. Chem. Soc.* **1998**, *120*, 5112.

(40) Matsumi, N.; Naka, K.; Chujo, Y. *J. Am. Chem. Soc.* **1998**, *120*, 10776.

(41) Matsumi, N.; Chujo, Y. *Polym. J.* **2001**, *33*, 383.

(42) Heilmann, J. B.; Scheibitz, M.; Qin, Y.; Sundararaman, A.; Jäkle, F.; Kretz, T.; Bolte, M.; Lerner, H.-W.; Holthausen, M. C.; Wagner, M. *Angew. Chem. Int. Ed.* **2006**, *45*, 920.

(43) Zhao, C.; Wakamiya, A.; Yamaguchi, S. *Macromolecules* **2007**, *40*, 3898.

(44) Yamaguchi, I.; Choi, B. J.; Koizumi, T. A.; Kubota, K.; Yamamoto, T. *Macromolecules* **2007**, *40*, 438.

(45) Li, H.; Sundararaman, A.; Venkatasubbaiah, K.; Jäkle, F. *J. Am. Chem. Soc.* **2007**, *129*, 5792.

(46) Scheibitz, M.; Li, H.; Schnorr, J.; Sánchez Perucha, A.; Bolte, M.; Lerner, H.-W.; Jäkle, F.; Wagner, M. *J. Am. Chem. Soc.* **2009**, *131*, 16319.

(47) Lorbach, A.; Bolte, M.; Li, H.; Lerner, H.-W.; Holthausen, M. C.; Jäkle, F.; Wagner, M. *Angew. Chem. Int. Ed.* **2009**, *48*, 4584.

(48) Li, H.; Sundararaman, A.; Pakkirisamy, T.; Venkatasubbaiah, K.; Schödel, F.; Jäkle, F. *Macromolecules* **2011**, *44*, 95.

(49) Miyata, M.; Chujo, Y. *Polym. J.* **2002**, *34*, 967.

(50) Sundararaman, A.; Victor, M.; Varughese, R.; Jäkle, F. *J. Am. Chem. Soc.* **2005**, *127*, 13748.

(51) Bonifácio, V. D. B.; Morgado, J.; Scherf, U. *J. Polym. Sci. Part A, Polym. Chem.* **2008**, *46*, 2878.
(52) Liu, W.; Pink, M.; Lee, D. *J. Am. Chem. Soc.* **2009**, *131*, 8703.
(53) Li, H.; Jäkle, F. *Angew. Chem. Int. Ed.* **2009**, *48*, 2313.
(54) Gabbaï, F. P. *Angew. Chem. Int. Ed.* **2003**, *42*, 2218.
(55) Entwistle, C. D.; Marder, T. B. *Angew. Chem. Int. Ed.* **2002**, *41*, 2927.
(56) Entwistle, C. D.; Marder, T. B. *Chem. Mater.* **2004**, *16*, 4574.
(57) Yamaguchi, S.; Wakamiya, A. *Pure Appl. Chem.* **2006**, *78*, 1413.
(58) Kobayashi, H.; Sato, N.; Ichikawa, Y.; Miyata, M.; Chujo, Y.; Matsuyama, T. *Synth. Met.* **2003**, *135-136*, 393.
(59) Hudson, Z. M.; Wang, S. *Acc. Chem. Res.* **2009**, *42*, 1584.
(60) Mercier, L. G.; Piers, W. E.; Parvez, M. *Angew. Chem. Int. Ed.* **2009**, *48*, 6108.
(61) Chai, J.; Wang, C.; Jia, L.; Pang, Y.; Graham, M.; Cheng, S. Z. D. *Synth. Met.* **2009**, *159*, 1443.
(62) Reitzenstein, D.; Lambert, C. *Macromolecules* **2009**, *42*, 773.
(63) Weber, L.; Werner, V.; Fox, M. A.; Marder, T. B.; Schwedler, S.; Brockhinke, A.; Stammler, H. G.; Neumann, B. *Dalton Transactions* **2009**, 1339.
(64) Zhao, C.; Sakuda, E.; Wakamiya, A.; Yamaguchi, S. *Chem. -Eur. J.* **2009**, *15*, 10603.
(65) Braunschweig, H.; Herbst, T.; Rais, D.; Ghosh, S.; Kupfer, T.; Radacki, K.; Crawford, A. G.; Ward, R. M.; Marder, T. B.; Fernández, I.; Frenking, G. *J. Am. Chem. Soc.* **2009**, *131*, 8989.
(66) Hoven, C. V.; Wang, H. P.; Elbing, M.; Garner, L.; Winkelhaus, D.; Bazan, G. C. *Nature Mater.* **2010**, *9*, 249.
(67) Cataldo, S.; Fabiano, S.; Ferrante, F.; Previti, F.; Patanè, S.; Pignataro, B. *Macromol. Rap. Comm.* **2010**, *31*, 1281.
(68) Proń, A.; Baumgarten, M.; Müllen, K. *Org. Lett.* **2010**, *12*, 4236.
(69) Caruso, A.; Siegler, M. A.; Tovar, J. D. *Angew. Chem. Int. Ed.* **2010**, *49*, 4213.
(70) Yamaguchi, S.; Akiyama, S.; Tamao, K. *J. Am. Chem. Soc.* **2000**, *122*, 6335.
(71) Wade, C. R.; Broomsgrove, A. E. J.; Aldridge, S.; Gabbaí, F. P. *Chem. Rev.* **2010**, *110*, 3958.
(72) Tanaka, K.; Ueda, K.; Koike, T.; Ando, M.; Yamabe, T. *Phys. Rev. B* **1985**, *32*, 4279.
(73) Tanaka, K.; Yamanaka, S.; Ueda, K.; Takeda, S.; Yamabe, T. *Synth. Met.* **1987**, *20*, 333.
(74) Yamanaka, S.; Inoue, T.; Aoyagi, T.; Komatsu, T. *Synth. Met.* **1992**, *46*, 221.
(75) Salzner, U.; Lagowski, J. B.; Pickup, P. G.; Poirier, R. A. *Synth. Met.* **1998**, *96*, 177.
(76) Brière, J.-F.; Côté, M. *J. Phys. Chem. B* **2004**, *108*, 3123.
(77) Narita, Y.; Hagiri, I.; Takahashi, N.; Takeda, K. *Jpn. J. Appl. Phys.* **2004**, *43*, 4248.

(78) Cao, H.; Ma, J.; Zhang, G.; Jiang, Y. *Macromolecules* **2005**, *38*, 1123.

(79) Zhang, Y.; Cai, X.; Bian, Y.; Li, X.; Jiang, J. *J. Phys. Chem. C.* **2008**, *112*, 5148.

(80) Nagai, A.; Murakami, T.; Nagata, Y.; Kokado, K.; Chujo, Y. *Macromolecules* **2009**, *42*, 7217.

(81) Tour, J. M. *Chem. Rev.* **1996**, *96*, 537.

(82) Ito, A.; Ino, H.; Tanaka, K.; Kanemoto, K.; Kato, T. *J. Org. Chem.* **2002**, *67*, 491.

(83) Niu, W.; Smith, M. D.; Lavigne, J. J. *J. Am. Chem. Soc.* **2006**, *128*, 16466.

(84) Qin, Y.; Cheng, G.; Sundararaman, A.; Jäkle, F. *J. Am. Chem. Soc.* **2002**, *124*, 12672.

(85) Qin, Y.; Cheng, G.; Achara, O.; Parab, K.; Jäkle, F. *Macromolecules* **2004**, *37*, 7123.

(86) Li, H.; Jäkle, F. *Polym. Chem.* **2011**, *2*, 897.

(87) Schulz, A.; Kaim, W. *Chem. Ber.* **1989**, *122*, 1863.

(88) Sundararaman, A.; Venkatasubbaiah, K.; Victor, M.; Zakharov, L. N.; Rheingold, A. L.; Jäkle, F. *J. Am. Chem. Soc.* **2006**, *128*, 16554.

(89) Frisch, M. J.; Gaussian 03, Revision C.02; Gaussian, Inc.: Wallingford, CT, **2004**.

(90) Broadened emission bands for the shorter oligomers are attributed to significant charge transfer (CT) character, as also evident from the orbital plots shown in **Figure 1-9**. Most likely, this is also the reason for the relatively large Stokes shifts especially for **OF1** and **OF2** and the resulting small difference in the emission maxima when going from **OF1** to **OF6**.

(91) Meier, H. *Angew. Chem. Int. Ed.* **2005**, *44*, 2482.

(92) Meier, H.; Stalmach, U.; Kolshorn, H. *Acta Polymerica* **1997**, *48*, 379.

(93) Dudek, S. P.; Pouderoijen, M.; Abbel, R.; Schenning, A. P. H. J.; Meijer, E. W. *J. Am. Chem. Soc.* **2005**, *127*, 11763.

(94) Hreha, R. D.; George, C. P.; Haldi, A.; Domercq, B.; Malagoli, M.; Barlow, S.; Brédas, J.; Kippelen, B.; Marder, S. R. *Adv. Funct. Mater*. **2003**, *13*, 967.

(95) Fukui, A.; Hattori, K.; Hu, Y. M.; Shiotsuki, M.; Sanda, F.; Masuda, T. *Polymer*, **2009**, *50*, 4159.

(96) Sasaki, S.; Sutoh, K.; Murakami, F.; Yoshifuji, M. *J. Am. Chem. Soc.* **2002**, *124*, 14830.

(97) Murov, S. L.; Carmichael, I.; Hug, G. L. *Handbook of Photochemistry*, 2nd ed., Marcel Dekker: New York, **1993**.

(98) Chen, P.; Lalancette, R. A.; Jäkle, F. *J. Am. Chem. Soc.* **2011**, *133*, 8802.

Appendix

Table 1. Crystal Data and Structure Refinement for **O-B2-BBr2**

empirical formula	$C_{87}H_{110}B_4Br4$
fw	1518.63
temp (K)	100(2)
λ (Å)	1.54178
cryst syst.	Triclinic
space group	P-1
a (Å)	12.6363(3)
b (Å)	16.8630(4)
c (Å)	21.4921(5)
α (°)	85.226(1)
β (°)	89.140(1)
γ (°)	68.436(1)
V (Å^3)	4243.75(17)
Z	2
F(000)	1584
cryst size (mm)	0.29 × 0.15 × 0.12
theta range (°)	2.8 – 67.4
index range	$-15<=h<=15$, $-19<=k<=19$, $0<=l<=25$
d_{calcd} (Mg/m^3)	1.188
abs coeff (CuKα,mm^{-1})	2.604
reflections collected/unique	14057/14057 [$R_{(int)}$ = 0.000]
data/restraints/parameters	14057 / 0 / 889
completeness	92.1%
absorption correction	numerical
max. and min. transmission	0.745 and 0.519
refinement method	full-matrix least-squares on F^2
GOF on F^2	1.07
final R indices ($I>2\sigma(I)$)^a	$R_1 = 0.043$, $wR_2 = 0.125$
R indices (all data)	$R_1 = 0.049$, $wR_2 = 0.129$
largest diff. peak and hole (e Å^{-3})	1.79, -0.49

^{a} $R_1 = \Sigma||F_o|-|F_c||/|F_o|$, $wR_2 = [\Sigma w(F_o^2-F_c^2)^2/\Sigma w(F_o^2)^2]^{1/2}$.

Table 2. Selected Interatomic Distances [Å], and Angles [°] for **O-B2-BBr2**

Bond	Distances (Å)			Interplanar	Angles (°)
B1-Br1	1.920(4)	Br1-B1-Br2	116.4(18)	Fl1 // Fl2	49.3
B1-Br2	1.914(4)	Br1-B1-C2	121.4(2)	Fl2 // Fl3	49.7
B1-C2	1.535(5)	Br2-B1-C2	122.3(3)		
B2-C2A	1.571(4)	C2A-B2-C7	122.6(3)	Fl2 // BC3 at B2 [a]	35.1
B2-C7	1.561(4)	C2A-B2-C12	117.6(3)	Fl2 // BC3 at B3 [b]	41.5
B2-C12	1.583(4)	C7-B2-C12	119.8(2)	Fl1/ / BC3 at B2 [a]	17.0
B3-C7A	1.573(4)	C7A-B3-C7B	120.1(3)	Fl3 // BC3 at B3 [b]	18.7
B3-C7B	1.567(4)	C7A-B3-C12A	119.6(3)		
B3-C12A	1.586(4)	C7B-B3-C12A	120.1(2)		
B4-Br3	1.923(3)	Br3-B4-Br4	115.2(17)		
B4-Br4	1.919(3)	Br3-B4-C2B	122.2(2)		
B4-C2B	1.526(4)	Br4-B4-C2B	122.6(2)		

[a] BC3 corresponds to best plane from B2, C2A, C7, C12. [b] BC3 corresponds to best plane formed by B3, C7A, C7B, C12A.

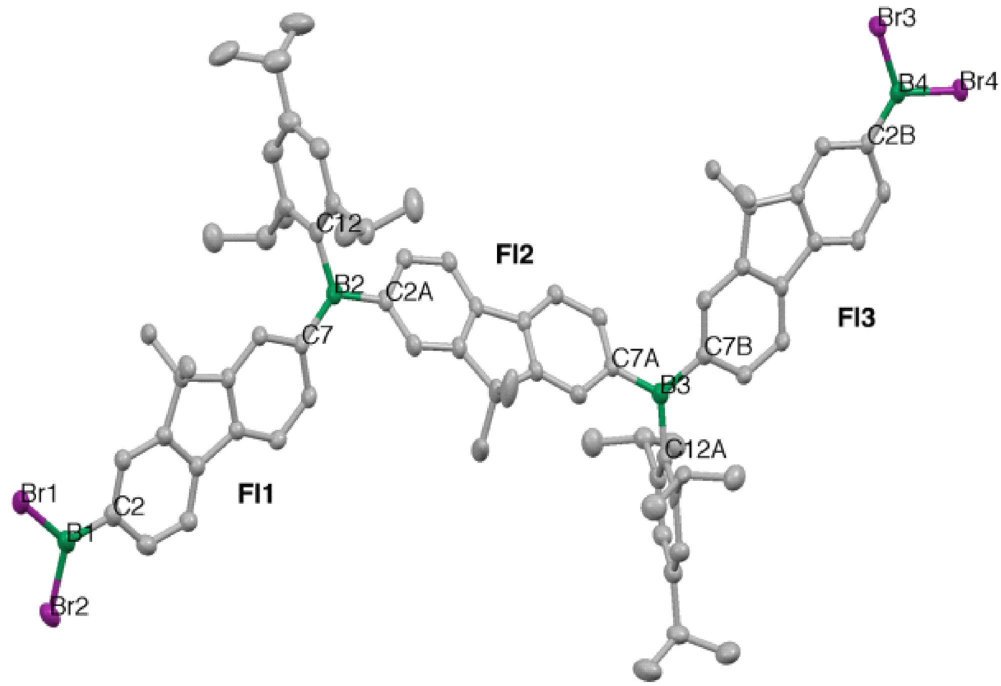

Table 3. Summary of Cyclic and Square Wave Voltammetry Data

		O-B1	O-B2	O-B3	O-B4	O-B5	O-B6
	Epc	-2.424	-2.262	-2.187	-2.183	-2.181	-2.209

E1	Epa	-2.288	-2.116	-2.090	-2.077	-2.069	-2.038
	ΔE	**0.136**	**0.146**	**0.097**	**0.106**	**0.112**	**0.171**
	$E^1_{1/2}$	**-2.356**	**-2.189**	**-2.138**	**-2.130**	**-2.125**	**-2.123**
	E^1_{sw}	**-2.348**	**-2.154**	**-2.116**	**-2.068**	**-2.060**	**-2.052**
E2	Epc		-2.593	-2.429	-2.320	-2.249	[a]
	Epa		-2.448	-2.339	-2.220	-2.114	[a]
	ΔE		**0.145**	**0.09**	**0.100**	**0.135**	[a]
	$E^2_{1/2}$		**-2.521**	**-2.384**	**-2.270**	**-2.182**	[a]
	E^2_{sw}		**-2.482**	**-2.364**	**-2.220**	**-2.150**	**-2.052 (nr)**
E3	Epc			-2.661	-2.558	-2.418	[a]
	Epa			-2.546	-2.442	-2.347	[a]
	ΔE			**0.115**	**0.116**	**0.071**	[a]
	$E^3_{1/2}$			**-2.603**	**-2.500**	**-2.383**	[a]
	E^3_{sw}			**-2.600**	**-2.444**	**-2.344**	**-2.196**
E4	Epc				-2.664	-2.587	[a]
	Epa				-2.573	-2.476	[a]
	ΔE				**0.091**	**0.111**	[a]
	$E^4_{1/2}$				**-2.618**	**-2.532**	[a]
	E^4_{sw}				**-2.564**	**-2.484**	**-2.376**
E5	Epc					-2.713	[a]
	Epa					-2.641	[a]
	ΔE					**0.072**	[a]
	$E^5_{1/2}$					**-2.677**	[a]
	E^5_{sw}					**-2.640**	**-2.446**
E6	Epc						[a]
	Epa						[a]
	ΔE						[a]
	$E^6_{1/2}$						[a]
	E^6_{sw}						**-2.540**

[a] Due to signal overlap, reliable data could only be obtained from square wave voltammetry.

Table 4. Coordinates (Å) for the Optimized Structure of **O-B1**

atom	x	y	z	atom	x	y	z
C	1.412594	-0.269750	0.802644	C	-7.331527	-0.260248	0.417623
C	1.352015	0.984077	0.147206	C	-7.076053	-2.345729	-0.775652
C	2.562590	1.508883	-0.367268	H	-5.090185	-2.838552	-1.463932
C	3.751045	0.804548	-0.243931	C	-7.915405	-1.435982	-0.101215
C	3.779541	-0.437678	0.425654	H	-7.947691	0.465643	0.947211
C	2.604520	-0.974038	0.959059	H	-7.497888	-3.260578	-1.184622
H	0.498228	-0.691038	1.210874	Si	9.769943	-1.755525	-0.117800
H	2.550794	2.469713	-0.876131	Si	-9.769965	-1.755474	0.117786
H	2.614202	-1.926595	1.483297	C	-10.226493	-3.446454	-0.601222
C	5.141819	1.160832	-0.733478	H	-9.682074	-4.260982	-0.109055
C	5.973360	-0.017122	-0.263598	H	-11.297774	-3.639898	-0.466645
C	7.331466	-0.260378	-0.417853	H	-10.017201	-3.505442	-1.675894
C	7.915366	-1.436048	0.101117	C	-10.754771	-0.405686	-0.777880
C	7.076043	-2.345685	0.775731	H	-11.833907	-0.546004	-0.637830
C	5.708778	-2.114876	0.938568	H	-10.500861	0.594127	-0.405926
C	5.155392	-0.945092	0.415666	H	-10.553525	-0.416771	-1.855551
H	7.947600	0.465446	-0.947568	C	-10.196691	-1.718084	1.964214
H	7.497892	-3.260478	1.184817	H	-11.271231	-1.871191	2.124179
H	5.090210	-2.838416	1.464174	H	-9.662325	-2.503731	2.511159
B	-0.000005	1.763060	-0.000026	H	-9.929721	-0.758316	2.422720
C	-1.352040	0.984099	-0.147265	C	10.196819	-1.717319	-1.964161
C	-1.412608	-0.269763	-0.802632	H	9.929921	-0.757280	-2.422151
C	-2.562627	1.508933	0.367157	H	11.271361	-1.870360	-2.124163
C	-2.604529	-0.974066	-0.959026	H	9.662447	-2.502629	-2.511575
H	-0.498237	-0.691067	-1.210831	C	10.226270	-3.446742	0.600789
C	-3.751085	0.804610	0.243803	H	11.297338	-3.640737	0.465321
H	-2.550839	2.469773	0.876000	H	10.017870	-3.505509	1.675649
C	-3.779564	-0.437669	-0.425687	H	9.681015	-4.261049	0.109185
H	-2.614198	-1.926660	-1.483197	C	10.754747	-0.406183	0.778546
C	-5.141879	1.160953	0.733247	H	10.553145	-0.417547	1.856149
C	-5.155417	-0.945085	-0.415691	H	11.833899	-0.546706	0.638817
C	-5.973410	-0.017028	0.263423	H	10.501177	0.593792	0.406800
C	-5.708780	-2.114942	-0.938457	C	0.000037	3.334733	0.000034
C	0.908565	4.073749	0.788861	H	0.000189	7.256913	0.000161

C	-0.908414	4.073870	-0.788776	H	-1.622909	3.541612	-1.411224
C	0.902146	5.468155	0.803244	H	1.623033	3.541389	1.411256
C	-0.901897	5.468277	-0.803053	H	5.497152	2.110786	-0.310225
C	0.000147	6.169646	0.000124	H	5.175294	1.278236	-1.825659
H	1.603026	6.008463	1.434873	H	-5.175411	1.278441	1.825418
H	-1.602730	6.008682	-1.434652	H	-5.497176	2.110879	0.309903

Table 5. Coordinates (Å) for the Optimized Structure of **O-B2**

atom	x	y	z	atom	x	y	z
C	2.959451	0.279805	0.566355	C	11.394740	-2.070719	0.284284
C	3.433566	1.609879	0.676153	C	9.603837	-2.414754	-1.857107
C	2.491413	2.653696	0.509603	C	11.751353	-2.925806	-0.780748
C	1.161462	2.372377	0.233043	H	12.078267	-1.927769	1.120654
C	0.718742	1.035022	0.141983	C	10.832473	-3.077662	-1.838885
C	1.621591	-0.017523	0.317223	H	8.918915	-2.554896	-2.689909
H	3.662456	-0.538240	0.695673	H	11.079468	-3.730023	-2.672896
H	2.823207	3.686112	0.588513	C	-6.065660	0.961324	-0.444493
H	1.291178	-1.051595	0.256534	C	-7.268880	0.769892	-1.166459
C	-0.000032	3.319323	0.000042	C	-5.921119	0.260700	0.777672
C	-1.161454	2.372342	-0.233180	C	-8.252337	-0.085638	-0.692943
C	-2.491426	2.653623	-0.509672	H	-7.411614	1.293306	-2.108728
C	-3.433507	1.609775	-0.676448	C	-6.913384	-0.579042	1.279084
C	-2.959282	0.279711	-0.566978	H	-5.009215	0.395004	1.352692
C	-1.621400	-0.017573	-0.317917	C	-9.591594	-0.451467	-1.303912
C	-0.718631	1.035000	-0.142429	C	-8.083159	-0.759149	0.535982
H	-2.823299	3.686032	-0.588334	H	-6.773403	-1.086648	2.230385
H	-3.662216	-0.538360	-0.696510	C	-10.176326	-1.405351	-0.280223
H	-1.290905	-1.051633	-0.257479	C	-9.274893	-1.574381	0.792407
B	-4.942101	1.915875	-0.975592	C	-11.394686	-2.070835	-0.284260
B	4.942134	1.916016	0.975367	C	-9.603830	-2.414658	1.857204
C	6.065714	0.961451	0.444336	C	-11.751320	-2.925822	0.780846
C	7.268946	0.770082	1.166301	H	-12.078195	-1.927967	-1.120658
C	5.921127	0.260671	-0.777732	C	-10.832462	-3.077574	1.839017
C	8.252395	-0.085489	0.692844	H	-8.918927	-2.554716	2.690036
H	7.411696	1.293574	2.108523	H	-11.079474	-3.729856	2.673085
C	6.913385	-0.579114	-1.279089	Si	-13.420335	-3.822107	0.761489

H	5.009190	0.394884	-1.352723	Si	13.420370	-3.822087	-0.761339
C	9.591666	-0.451258	1.303820	C	-13.587915	-4.926145	2.290003
C	8.083188	-0.759126	-0.536008	H	-13.544262	-4.349072	3.221203
H	6.773373	-1.086832	-2.230326	H	-14.551765	-5.449509	2.275054
C	10.176378	-1.405239	0.280210	H	-12.801788	-5.689296	2.331411
C	9.274921	-1.574375	-0.792384	C	-13.541872	-4.889771	-0.799969
H	-14.514854	-5.393327	-0.858061	H	-7.755730	5.604440	-2.036746
H	-13.426003	-4.290729	-1.711105	H	-4.214557	5.108636	-4.429523
H	-12.764462	-5.662698	-0.813283	C	5.328564	3.188644	1.812303
C	-14.819119	-2.542196	0.752552	C	6.509156	3.916594	1.547254
H	-15.800959	-3.029903	0.709388	C	4.510818	3.659004	2.862990
H	-14.794345	-1.920539	1.655266	C	6.847868	5.055856	2.276548
H	-14.746014	-1.870988	-0.111482	C	4.856632	4.780400	3.616212
C	13.541927	-4.889623	0.800205	C	6.024383	5.486694	3.319102
H	14.514919	-5.393158	0.858336	H	7.755269	5.604818	2.037063
H	13.426050	-4.290510	1.711293	H	4.214424	5.107874	4.430089
H	12.764530	-5.662562	0.813583	H	6.291201	6.368217	3.896923
C	13.587935	-4.926250	-2.289764	H	3.594136	3.125077	3.099212
H	13.544262	-4.349254	-3.221011	H	7.164098	3.587579	0.744784
H	14.551788	-5.449606	-2.274787	H	9.477632	-0.924996	2.288908
H	12.801812	-5.689411	-2.331098	H	10.229658	0.430207	1.457625
C	14.819152	-2.542172	-0.752523	H	0.173500	3.978800	-0.861699
H	15.800993	-3.029874	-0.709331	H	-0.173616	3.978583	0.861939
H	14.794366	-1.920590	-1.655287	H	-9.477537	-0.925298	-2.288952
H	14.746055	-1.870893	0.111457	H	-10.229584	0.429983	-1.457814
C	-5.328629	3.188641	-1.812270	H	-6.291595	6.368515	-3.896276
C	-6.509379	3.916320	-1.547188	H	-7.164359	3.586997	-0.744875
C	-4.510863	3.659365	-2.862780	H	-3.594073	3.125638	-3.099037
C	-6.848206	5.055692	-2.276256	C	-6.024686	5.486907	-3.318626
C	-4.856789	4.780874	-3.615781				

Table 6. Coordinates (Å) for the Optimized Structure of **O-B3**

atom	x	y	z	atom	x	y	z
C	6.903303	-0.273223	0.534584	C	-7.358624	-2.691396	-1.125226
C	7.713573	-1.300028	1.077816	C	-5.947508	-1.191770	0.795261
C	7.126431	-2.578775	1.236057	C	-8.044687	-1.692257	-0.393251

C	5.812155	-2.808537	0.856569	H	-7.901643	-3.276306	-1.863652
C	5.026842	-1.759590	0.331331	C	-7.299582	-0.954196	0.558418
C	5.573860	-0.482780	0.175273	H	-5.413105	-0.616708	1.547527
H	7.330020	0.717718	0.407793	H	-7.804931	-0.184964	1.135533
H	7.721609	-3.388778	1.650549	C	10.068018	0.017378	0.719193
H	4.977380	0.334654	-0.222424	C	11.074062	0.768048	1.375186
C	4.996184	-4.085224	0.919233	C	9.880302	0.250590	-0.664922
C	3.649367	-3.647651	0.376706	C	11.827073	1.703943	0.682126
C	2.489006	-4.384431	0.189501	H	11.244130	0.613827	2.437952
C	1.315499	-3.772352	-0.313732	C	10.648771	1.167493	-1.379066
C	1.384073	-2.394184	-0.632774	H	9.118421	-0.316939	-1.191896
C	2.550749	-1.649204	-0.477529	C	12.926952	2.620928	1.181730
C	3.687698	-2.277606	0.038638	C	11.623093	1.904286	-0.700096
H	2.469918	-5.441348	0.444025	H	10.486209	1.307202	-2.445010
H	0.497649	-1.903722	-1.024980	C	13.336388	3.366303	-0.073870
H	2.569742	-0.596247	-0.747838	C	12.558239	2.932341	-1.168446
B	-0.009064	-4.588792	-0.506357	C	14.307408	4.343220	-0.246793
B	9.200448	-1.029939	1.497373	C	12.760413	3.485402	-2.433943
C	-1.401423	-3.894247	-0.313117	C	14.531762	4.917817	-1.516402
C	-2.532370	-4.292001	-1.066583	H	14.898433	4.666625	0.609512
C	-1.578617	-2.850354	0.627489	C	13.740301	4.467352	-2.592240
C	-3.757464	-3.664985	-0.892641	H	12.167903	3.161010	-3.286070
H	-2.429869	-5.090797	-1.797097	H	13.890984	4.892758	-3.581358
C	-2.809768	-2.232024	0.833307	B	-9.572294	-1.420289	-0.622143
H	-0.726397	-2.530904	1.220691	C	-10.154626	0.024727	-0.454129
C	-5.078788	-3.911631	-1.594707	C	-9.380827	1.171083	-0.758135
C	-3.904255	-2.637238	0.064106	C	-11.478525	0.235326	0.002940
H	-2.911622	-1.446185	1.577747	C	-9.882313	2.465043	-0.634838
C	-6.005717	-2.919020	-0.919938	H	-8.363784	1.035549	-1.115113
C	-5.294997	-2.175877	0.047234	C	-11.980252	1.518909	0.158187
H	-12.099170	-0.623536	0.246535	C	11.732746	-2.899474	3.795058
C	-11.187389	2.640504	-0.166762	C	10.941163	-3.223991	4.899093
H	-9.263411	3.320489	-0.894409	H	8.975779	-3.095463	5.779068
C	-13.342061	1.971981	0.648947	H	12.779443	-3.192587	3.770628
C	-11.969597	3.855944	0.080723	Si	15.863414	6.247373	-1.736185
C	-13.242446	3.482787	0.562735	C	15.894216	6.849624	-3.531038
C	-11.650473	5.204897	-0.082271	H	16.661997	7.622719	-3.657627

C	-14.184611	4.452147	0.879082	H	16.128317	6.039330	-4.231629
C	-12.608160	6.168288	0.240129	H	14.935818	7.287728	-3.833928
H	-10.674000	5.506559	-0.453629	C	15.485521	7.707498	-0.588076
C	-13.886121	5.823119	0.724594	H	14.524796	8.171338	-0.840680
H	-15.162315	4.145917	1.249847	H	15.434068	7.394865	0.461754
H	-12.350577	7.216557	0.110060	H	16.260157	8.480704	-0.664070
C	-10.523041	-2.606171	-1.021074	C	17.556580	5.521438	-1.288789
C	-10.318532	-3.914257	-0.530086	H	17.576047	5.145593	-0.258818
C	-11.621274	-2.413976	-1.887679	H	17.816808	4.685885	-1.949148
C	-11.167366	-4.966924	-0.870356	H	18.346476	6.277479	-1.379383
C	-12.458176	-3.466885	-2.255745	Si	-15.178967	7.135437	1.167378
C	-12.236775	-4.746289	-1.741212	C	-14.499496	8.865366	0.806326
H	-10.993228	-5.959526	-0.462350	H	-15.248006	9.626718	1.057726
H	-13.285702	-3.290479	-2.938506	H	-13.600730	9.084109	1.394920
C	0.057898	-6.111041	-0.888664	H	-14.245945	8.992966	-0.252694
C	1.077837	-6.620570	-1.721782	C	-16.745319	6.846481	0.139839
C	-0.898847	-7.034312	-0.412803	H	-16.539967	6.940324	-0.932976
C	1.132854	-7.968918	-2.072963	H	-17.161222	5.846119	0.309391
C	-0.834538	-8.389316	-0.735556	H	-17.524612	7.575032	0.395918
C	0.179162	-8.858922	-1.573701	C	-15.607328	6.999252	3.009096
H	1.921029	-8.327795	-2.730247	H	-15.989331	6.003007	3.262208
H	-1.576431	-9.078346	-0.339469	H	-14.726693	7.182999	3.635747
C	9.821463	-1.813123	2.710172	H	-16.376373	7.729181	3.291071
C	9.045343	-2.169328	3.834771	H	-12.894115	-5.567057	-2.017608
C	11.181449	-2.192721	2.726844	H	-11.810942	-1.421887	-2.288723
C	9.595511	-2.850573	4.919978	H	-9.484781	-4.102452	0.141149
H	-14.157192	1.576559	0.026909	H	12.568930	3.302546	1.965973
H	-13.543204	1.630541	1.674008	H	11.370666	-3.765137	5.738628
H	-5.006954	-3.735358	-2.677098	H	11.811594	-1.938535	1.878626
H	-5.424189	-4.947780	-1.474007	H	7.994592	-1.893044	3.860701
H	5.442144	-4.888022	0.315611	H	0.225775	-9.912896	-1.836527
H	4.920138	-4.476242	1.943370	H	-1.698664	-6.681490	0.232836
H	13.764229	2.059807	1.619776	H	1.831960	-5.941010	-2.109911

Table 7. Coordinates (Å) for the Optimized Structure of **O-B4**

atom	x	y	z	atom	x	y	z

C	2.843651	-3.663935	0.997134	C	-11.249101	-1.347188	-1.916063
C	3.296271	-4.994157	1.174629	C	-9.762300	-0.972455	0.445963
C	2.388906	-6.037775	0.870593	C	-11.746929	-0.471077	-0.921608
C	1.114275	-5.755946	0.401403	H	-11.823489	-1.498066	-2.826836
C	0.689872	-4.418533	0.246513	C	-10.967725	-0.302598	0.248943
C	1.557146	-3.366199	0.553668	H	-9.200092	-0.832012	1.365976
H	3.519975	-2.846001	1.228986	H	-11.330774	0.362261	1.027650
H	2.705385	-7.070338	0.996414	C	5.934807	-4.348948	1.326664
H	1.239532	-2.332038	0.445256	C	7.023350	-4.160584	2.212824
C	-0.000061	-6.702892	0.000102	C	5.966559	-3.647103	0.096881
C	-1.114349	-5.756047	-0.401570	C	8.066665	-3.307367	1.884738
C	-2.389003	-6.037995	-0.870625	H	7.029816	-4.684146	3.165686
C	-3.296322	-4.994448	-1.175049	C	7.020620	-2.808000	-0.256935
C	-2.843638	-3.664181	-0.998064	H	5.145563	-3.779813	-0.601970
C	-2.843638	-3.664181	-0.998064	C	9.307937	-2.947142	2.677971
C	-0.689877	-4.418594	-0.247207	C	8.073506	-2.631610	0.645347
H	-2.705544	-7.070591	-0.996009	H	7.018131	-2.298443	-1.217372
H	-3.519944	-2.846306	-1.230178	C	10.034996	-1.996460	1.746634
H	-1.239447	-2.332149	-0.446721	C	9.290079	-1.819275	0.560722
B	-4.744555	-5.301813	-1.691890	C	11.249220	-1.347218	1.916162
B	4.744439	-5.301423	1.691713	C	9.762637	-0.972515	-0.446005
C	-5.934834	-4.349226	-1.326833	C	11.747176	-0.471178	0.921708
C	-7.023411	-4.160805	-2.212938	H	11.823513	-1.498070	2.826999
C	-5.966444	-3.647321	-0.097082	C	10.968077	-0.302707	-0.248913
C	-8.066646	-3.307504	-1.884814	H	9.200507	-0.832074	-1.366066
H	-7.029979	-4.684409	-3.165777	H	11.331212	0.362120	-1.027607
C	-7.020420	-2.808126	0.256769	B	-13.110737	0.280443	-1.108012
H	-5.145400	-3.780050	0.601710	B	13.110969	0.280347	1.108209
C	-9.307955	-2.947233	-2.677969	C	-13.313731	1.712074	-0.504863
C	-8.073355	-2.631699	-0.645448	C	-12.235805	2.624323	-0.398358
H	-7.017827	-2.298527	1.217183	C	-14.582721	2.147793	-0.051276
C	-10.034890	-1.996475	-1.746613	C	-12.393389	3.910231	0.114026
C	-9.289868	-1.819280	-0.560768	H	-11.253104	2.315284	-0.743301
C	-14.747079	3.414841	0.488277	Si	-16.480915	9.170737	3.069019
H	-15.431483	1.471453	-0.117759	Si	16.480720	9.170639	-3.069184
C	-13.655170	4.305905	0.565930	C	-17.174769	8.642688	4.752255
H	-11.545341	4.588965	0.163167	H	-17.766247	9.447871	5.205649

C	-15.993908	4.074087	1.046806	H	-17.825204	7.764209	4.664850
C	-14.118598	5.566429	1.154556	H	-16.368562	8.387208	5.449919
C	-15.495028	5.450095	1.443771	C	-17.912716	9.652118	1.924174
C	-13.441806	6.754124	1.436123	H	-18.505692	10.468291	2.355300
C	-16.185460	6.513949	2.008545	H	-17.543624	9.987065	0.947707
C	-14.149596	7.815434	2.003390	H	-18.591215	8.808829	1.748442
H	-12.381539	6.857491	1.218152	C	-15.333791	10.658905	3.303229
C	-15.524430	7.726337	2.301356	H	-14.498845	10.430208	3.976065
H	-17.247863	6.406714	2.225242	H	-14.912538	11.006293	2.352415
H	-13.614583	8.737178	2.218056	H	-15.886431	11.498452	3.742534
C	13.313935	1.711996	0.505092	C	17.912711	9.651984	-1.924563
C	12.236032	2.624299	0.398844	H	18.591227	8.808684	-1.748943
C	14.582851	2.147664	0.051245	H	18.505631	10.468153	-2.355773
C	12.393569	3.910217	-0.113530	H	17.543776	9.986928	-0.948036
H	11.253385	2.315287	0.743968	C	15.333585	10.658831	-3.303198
C	14.747157	3.414726	-0.488292	H	14.498525	10.430154	-3.975900
H	15.431591	1.471278	0.117517	H	14.912491	11.006221	-2.352314
C	13.655274	4.305845	-0.565684	H	15.886170	11.498370	-3.742587
H	11.545542	4.588991	-0.162475	C	17.174296	8.642595	-4.752536
C	15.993901	4.073935	-1.047054	H	16.367974	8.387136	-5.450075
C	14.118637	5.566365	-1.154370	H	17.765716	9.447773	-5.206016
C	15.495004	5.449981	-1.443866	H	17.824729	7.764104	-4.665243
C	13.441837	6.754095	-1.435769	C	-14.277160	-0.406335	-1.906043
C	16.185368	6.513826	-2.008738	C	-14.479964	-1.803209	-1.863645
C	14.149556	7.815391	-2.003149	C	-15.171726	0.344849	-2.699503
H	12.381617	6.857499	-1.217585	C	-15.522928	-2.414522	-2.558627
C	15.524330	7.726250	-2.301384	C	-16.199703	-0.261699	-3.420509
H	17.247724	6.406554	-2.225651	C	-16.382209	-1.644353	-3.345517
H	13.614538	8.737162	-2.217683	H	-15.663334	-3.490605	-2.492234
H	-16.861754	0.342292	-4.036101	H	15.663218	-3.490917	2.492513
C	-5.002671	-6.571632	-2.580092	H	16.862694	0.342047	4.035394
C	-4.038119	-7.037766	-3.500181	H	-17.189533	-2.119221	-3.897670
C	-6.210103	-7.299437	-2.497646	H	-15.047333	1.422764	-2.760244
C	-4.269168	-8.154393	-4.302779	H	-13.813453	-2.416396	-1.262856
C	-6.437664	-8.433858	-3.275846	H	-16.400874	3.521015	1.904903
C	-5.468797	-8.860172	-4.187025	H	-16.801296	4.126842	0.303150
H	-3.513407	-8.478238	-5.014102	H	-9.058556	-2.471387	-3.636682

H	-7.371005	-8.982610	-3.176932	H	-9.913356	-3.831368	-2.921507
C	5.002354	-6.570983	2.580345	H	-3.096434	-6.503641	-3.595167
C	4.037804	-7.036530	3.500729	H	-6.977066	-6.974461	-1.799563
C	6.209582	-7.299133	2.497991	H	-5.647589	-9.737696	-4.803529
C	4.268679	-8.152918	4.303711	H	0.298207	-7.362529	-0.826696
C	6.436957	-8.433329	3.276575	H	-0.298364	-7.362184	0.827163
C	5.468107	-8.859052	4.188049	H	3.096261	-6.502137	3.595630
H	3.512930	-8.476307	5.015255	H	6.976537	-6.974603	1.799689
H	7.370141	-8.982360	3.177732	H	5.646757	-9.736396	4.804850
C	14.277451	-0.406505	1.906091	H	9.913268	-3.831302	2.921590
C	14.480000	-1.803424	1.863898	H	9.058492	-2.471243	3.636646
C	15.172344	0.344660	2.699203	H	17.189997	-2.119551	3.897337
C	15.523018	-2.414797	2.558746	H	15.048155	1.422606	2.759788
C	16.200387	-0.261939	3.420071	H	13.813254	-2.416600	1.263361
C	16.382625	-1.644639	3.345290	H	16.801446	4.126624	-0.303563
H	16.400664	3.520876	-1.905256				

Table 8. Coordinates (Å) for the Optimized Structure of **O-B5**

atom	x	y	z	atom	x	y	z
C	1.227063	-6.040752	-0.437479	C	13.868985	0.683308	2.270008
C	1.149675	-7.445446	-0.274252	C	12.620746	0.021299	-0.165752
C	2.255798	-8.094163	0.326164	C	14.242360	1.378814	1.094570
C	3.359771	-7.368948	0.749826	H	14.352473	0.933229	3.211212
C	3.411213	-5.970884	0.560690	C	13.587792	1.022443	-0.109741
C	2.341590	-5.303845	-0.043421	H	12.152148	-0.236927	-1.112253
H	0.392517	-5.521549	-0.900186	H	13.860858	1.538873	-1.025611
H	2.227992	-9.172163	0.465246	C	-1.534690	-7.602403	-0.692794
H	2.372039	-4.228411	-0.200394	C	-2.528464	-7.939255	-1.643499
C	4.629047	-7.847110	1.427772	C	-1.880226	-6.659267	0.305808
C	5.416590	-6.563452	1.605407	C	-3.782998	-7.349177	-1.598293
C	6.663226	-6.362324	2.179636	H	-2.295200	-8.660447	-2.422918
C	7.238578	-5.069485	2.228322	C	-3.145266	-6.080733	0.380331
C	6.485914	-3.999724	1.685105	H	-1.136036	-6.388870	1.049589
C	5.220647	-4.182763	1.131806	C	-4.976345	-7.542897	-2.513605
C	4.685753	-5.473335	1.085458	C	-4.100238	-6.422639	-0.581477
H	7.215440	-7.205499	2.587402	H	-3.379758	-5.373417	1.172048

H	6.904808	-2.997777	1.714336	C	-6.020917	-6.632971	-1.897091
H	4.664985	-3.334368	0.739929	C	-5.484793	-5.979460	-0.766394
B	8.652228	-4.833118	2.864224	C	-7.332504	-6.401942	-2.285001
B	-0.109288	-8.253639	-0.743042	C	-6.268578	-5.080431	-0.037399
C	9.595268	-3.713377	2.303454	C	-8.147236	-5.486566	-1.575668
C	10.493107	-3.016745	3.148263	H	-7.741478	-6.917604	-3.150452
C	9.585706	-3.362368	0.931356	C	-7.574730	-4.836108	-0.455483
C	11.315121	-2.020157	2.643020	H	-5.869026	-4.574963	0.838356
H	10.524737	-3.261359	4.207206	H	-8.182088	-4.132255	0.106511
C	10.426137	-2.383934	0.405263	B	15.343285	2.495563	1.125475
H	8.908489	-3.886112	0.262632	B	-9.627905	-5.208625	-2.010377
C	12.324403	-1.143143	3.358619	C	15.260711	3.717615	0.148150
C	11.291176	-1.703958	1.267335	C	14.014474	4.242589	-0.272042
H	10.403022	-2.153896	-0.657144	C	16.430957	4.343129	-0.346890
C	12.887409	-0.296320	2.233847	C	13.915462	5.338317	-1.126808
C	12.263851	-0.637543	1.014270	H	13.102291	3.783200	0.098228
C	16.346525	5.415921	-1.221730	Si	16.930371	10.505102	-5.290083
H	17.404202	3.964455	-0.044096	C	17.958940	9.742460	-6.687769
C	15.088415	5.924243	-1.610502	H	18.383882	10.518702	-7.336338
H	12.940172	5.724275	-1.413282	H	18.792606	9.147041	-6.296676
C	17.454190	6.212843	-1.884002	H	17.348407	9.081429	-7.314087
C	15.299649	7.057227	-2.517243	C	18.026475	11.665292	-4.267776
C	16.687831	7.243441	-2.690551	H	18.459522	12.453818	-4.895775
C	14.393940	7.896897	-3.167456	H	17.452735	12.150899	-3.469680
C	17.162667	8.260606	-3.507365	H	18.856786	11.126883	-3.795369
C	14.886364	8.915487	-3.985517	C	15.493154	11.489946	-6.030872
H	13.321856	7.765256	-3.042254	H	14.836844	10.860901	-6.643804
C	16.267484	9.123079	-4.176242	H	14.876819	11.961414	-5.256219
H	18.237652	8.389831	-3.629620	H	15.875305	12.290003	-6.676627
H	14.173677	9.565067	-4.487754	C	16.535325	2.387042	2.143709
C	-10.263996	-3.791956	-1.794439	C	17.083925	1.138632	2.510567
C	-9.482976	-2.613597	-1.879107	C	17.105995	3.534288	2.737064
C	-11.643645	-3.641249	-1.513870	C	18.148923	1.039615	3.405194
C	-10.028861	-1.342742	-1.713151	C	18.152313	3.442430	3.654306
H	-8.422555	-2.704068	-2.097024	C	18.681527	2.193053	3.985430
C	-12.194215	-2.383653	-1.315635	H	18.560436	0.064732	3.654845
H	-12.271036	-4.526309	-1.441141	H	18.558983	4.343335	4.107137

C	-11.391429	-1.227324	-1.422988	C	9.125624	-5.724578	4.068037
H	-9.401255	-0.459555	-1.803835	C	8.216701	-6.199005	5.039128
C	-13.622062	-1.994574	-0.985452	C	10.480198	-6.089961	4.228982
C	-12.231165	-0.050080	-1.184853	C	8.635003	-6.979220	6.116457
C	-13.550822	-0.480932	-0.928550	C	10.902421	-6.893441	5.287493
C	-11.924180	1.313592	-1.179063	C	9.980149	-7.334571	6.239081
C	-14.555397	0.443137	-0.681487	H	7.913370	-7.315050	6.857046
C	-12.937330	2.228907	-0.902707	H	11.949795	-7.171787	5.374559
H	-10.913218	1.658544	-1.381858	C	0.057834	-9.725415	-1.266789
C	-14.273203	1.830354	-0.652933	C	1.199354	-10.125598	-1.995326
H	-15.570921	0.103265	-0.493633	C	-0.927389	-10.709496	-1.032270
H	-12.697443	3.288345	-0.892562	C	1.343626	-11.426410	-2.476503
C	-0.777407	-12.020025	-1.484321	H	-13.953919	-2.426143	-0.030810
C	0.357019	-12.379840	-2.215310	B	-15.398307	2.882493	-0.358614
H	2.226313	-11.699257	-3.049612	C	-15.061237	4.216686	0.390982
H	-1.545937	-12.759381	-1.272743	C	-15.773985	5.410450	0.120849
C	-10.478745	-6.354529	-2.666881	C	-14.037906	4.276741	1.368116
C	-10.316988	-7.705855	-2.290116	C	-15.461828	6.588946	0.781856
C	-11.440486	-6.080484	-3.663936	H	-16.565912	5.399335	-0.624076
C	-11.079281	-8.723313	-2.862924	C	-13.732812	5.447374	2.059362
C	-12.186640	-7.095122	-4.262347	H	-13.480505	3.372973	1.597635
C	-12.012083	-8.420296	-3.857299	C	-16.073311	7.969405	0.637344
H	-10.943325	-9.752324	-2.539368	C	-14.443881	6.612524	1.759378
H	-12.907399	-6.853806	-5.039715	H	-12.950974	5.450253	2.814998
H	19.504571	2.118654	4.691972	H	-15.962115	8.362866	-0.382775
H	16.709552	4.513595	2.482451	C	-15.294052	8.787383	1.648866
H	16.673190	0.232013	2.074109	H	-17.151294	7.967353	0.851105
H	18.089227	5.581488	-2.521157	C	-14.340736	7.973079	2.296932
H	18.123350	6.679852	-1.147937	C	-15.406724	10.131671	1.976580
H	11.853582	-0.528773	4.138740	C	-13.502615	8.516135	3.272023
H	13.103190	-1.734143	3.860324	C	-14.570564	10.705122	2.958655
H	7.165423	-5.937751	4.951598	H	-16.149238	10.745651	1.467925
H	11.210431	-5.747227	3.500726	C	-13.626438	9.870030	3.589717
H	10.307980	-7.952104	7.071721	H	-12.763835	7.899856	3.778721
H	4.421920	-8.340244	2.387743	H	-12.969628	10.285124	4.350140
H	5.171915	-8.580801	0.815683	C	-16.873726	2.594086	-0.816846
H	1.979466	-9.396697	-2.198481	C	-17.981165	3.023419	-0.053186

H	-1.819878	-10.441413	-0.473051	C	-17.154503	1.890226	-2.008346
H	0.471682	-13.397893	-2.579337	C	-19.291882	2.753433	-0.445257
H	-5.307379	-8.590218	-2.545687	H	-17.806759	3.566465	0.871883
H	-4.747544	-7.260590	-3.550790	C	-18.462503	1.641071	-2.422529
H	-12.599965	-9.212724	-4.313990	H	-16.329241	1.544240	-2.625184
H	-11.593204	-5.052815	-3.982687	C	-19.535814	2.066515	-1.636542
H	-9.588530	-7.957669	-1.523945	H	-20.123066	3.082392	0.173611
H	-14.332792	-2.346556	-1.746047	H	-18.646132	1.110850	-3.353777
H	-20.556746	1.863774	-1.950742	H	-16.700484	12.304024	4.939699
Si	-14.737619	12.541595	3.393578	C	-13.482698	13.012157	4.730789
C	-14.424616	13.585266	1.842607	H	-16.631103	13.939856	4.262686
H	-15.118752	13.327116	1.033896	H	-17.250042	12.601157	3.285657
H	-14.548553	14.654514	2.054952	H	-13.635813	12.444026	5.655997
H	-13.406941	13.435879	1.463130	H	-12.450483	12.843658	4.401608
C	-16.492062	12.877062	4.028591	H	-13.576321	14.075954	4.981272

Table 9. Coordinates (Å) for the Optimized Structure of **O-B6**

atom	x	y	z	atom	x	y	z
C	-4.581915	-7.502655	-0.086099	C	-15.034121	2.430066	-2.141991
C	-4.823927	-8.843964	-0.470632	C	-14.224244	1.094115	0.200718
C	-6.005491	-9.109391	-1.204166	C	-15.346080	2.998794	-0.883403
C	-6.874916	-8.083410	-1.544484	H	-15.349305	2.941115	-3.048380
C	-6.611348	-6.758594	-1.134538	C	-14.917142	2.300581	0.271756
C	-5.462184	-6.467725	-0.393745	H	-13.925813	0.578114	1.110010
H	-3.683460	-7.275393	0.480848	H	-15.150323	2.713986	1.248916
H	-6.220988	-10.129232	-1.513625	C	-2.283476	-9.709547	-0.029106
H	-5.251606	-5.452364	-0.066940	C	-1.445030	-10.419050	0.864905
C	-8.166768	-8.133430	-2.336918	C	-1.676004	-8.737503	-0.861158
C	-8.615664	-6.684930	-2.335254	C	-0.084779	-10.153387	0.924216
C	-9.731933	-6.103866	-2.918769	H	-1.880556	-11.171128	1.518184
C	-9.983353	-4.717468	-2.779133	C	-0.307631	-8.479276	-0.830941
C	-9.047149	-3.955947	-2.038055	H	-2.298479	-8.184108	-1.558498
C	-7.905533	-4.520704	-1.473770	C	0.985012	-10.771132	1.804031
C	-7.691645	-5.894487	-1.618076	C	0.491346	-9.187059	0.071488
H	-10.431875	-6.717109	-3.481157	H	0.126381	-7.737474	-1.496840
H	-9.217955	-2.889731	-1.918573	C	2.244386	-10.059851	1.347797

H	-7.199159	-3.900679	-0.927177	C	1.931505	-9.128040	0.334551
B	-11.244326	-4.048694	-3.427738	C	3.555078	-10.219306	1.773374
B	-3.823449	-9.993794	-0.102546	C	2.938527	-8.343825	-0.235217
C	-11.941880	-2.831617	-2.728020	C	4.595427	-9.430592	1.225123
C	-12.565636	-1.808484	-3.482329	H	3.790945	-10.947520	2.545578
C	-11.977820	-2.716169	-1.316965	C	4.245231	-8.492442	0.223641
C	-13.171457	-0.731316	-2.852389	H	2.710092	-7.626340	-1.019540
H	-12.554940	-1.866661	-4.568014	H	5.027305	-7.877670	-0.212854
C	-12.610248	-1.656421	-0.670744	B	-16.141616	4.346227	-0.776895
H	-11.508356	-3.490631	-0.716891	B	6.080476	-9.593434	1.700452
C	-13.869882	0.473057	-3.453526	C	-15.876777	5.334991	0.409567
C	-13.204973	-0.654628	-1.443133	C	-14.597043	5.449351	1.005178
H	-12.633791	-1.611147	0.415320	C	-16.909879	6.155439	0.925042
C	-14.321906	1.242870	-2.227859	C	-14.335005	6.334625	2.048662
C	-13.918506	0.565674	-1.056777	H	-13.786152	4.835106	0.623989
C	-16.669157	7.021216	1.981229	Si	-16.470224	11.399512	6.836977
H	-17.904742	6.091962	0.491061	C	-17.788456	10.717093	8.015668
C	-15.378779	7.120674	2.544551	H	-18.086603	11.471444	8.754418
H	-13.334715	6.406552	2.468759	H	-18.691871	10.408584	7.476102
C	-17.619162	7.965700	2.692446	H	-17.416966	9.842573	8.562634
C	-15.412421	8.115029	3.622005	C	-17.152810	12.933487	5.957127
C	-16.724176	8.625578	3.723367	H	-17.446040	13.705297	6.679627
C	-14.412386	8.580116	4.477525	H	-16.405278	13.371630	5.285440
C	-17.029182	9.593169	4.670945	H	-18.036913	12.693633	5.354343
C	-14.734452	9.552563	5.426245	C	-14.925652	11.872970	7.823976
H	-13.397328	8.195996	4.410374	H	-14.507893	11.016242	8.365803
C	-16.035997	10.080216	5.547820	H	-14.137135	12.278412	7.179044
H	-18.047014	9.976794	4.733563	H	-15.168702	12.642402	8.566957
H	-13.948636	9.908659	6.087934	C	-17.212217	4.706682	-1.869766
C	7.042626	-8.355604	1.721303	C	-18.008469	3.713914	-2.481570
C	6.561827	-7.055849	2.012787	C	-17.421825	6.039484	-2.286415
C	8.425641	-8.494757	1.452124	C	-18.968504	4.032000	-3.441609
C	7.398706	-5.943147	2.056897	C	-18.359383	6.362965	-3.266631
H	5.504245	-6.924858	2.224127	C	-19.141220	5.358839	-3.842057
C	9.264425	-7.389834	1.459067	H	-19.578027	3.246686	-3.881886
H	8.826180	-9.479321	1.223171	H	-18.485190	7.396895	-3.578457
C	8.756846	-6.110120	1.771536	C	-11.810187	-4.599829	-4.785444

H	6.996908	-4.963353	2.303184	C	-10.959348	-5.132380	-5.778831
C	10.751436	-7.301788	1.174464	C	-13.193279	-4.585073	-5.070291
C	9.857511	-5.144030	1.721839	C	-11.455827	-5.608898	-6.991585
C	11.042526	-5.826856	1.372356	C	-13.700737	-5.085632	-6.268702
C	9.883240	-3.765797	1.953696	C	-12.830766	-5.593080	-7.236405
C	12.242536	-5.139536	1.263622	H	-10.773311	-5.997155	-7.743550
C	11.090275	-3.084293	1.816382	H	-14.772418	-5.075826	-6.451557
H	8.979029	-3.230120	2.232253	C	-4.370074	-11.437406	0.188886
C	12.298078	-3.740310	1.474288	C	-5.616247	-11.639006	0.821833
H	13.152249	-5.673732	1.000653	C	-3.639987	-12.592542	-0.166974
H	11.108983	-2.012346	1.991092	C	-6.099336	-12.917125	1.100068
C	-4.129164	-13.874568	0.081132	H	10.993701	-7.635057	0.155653
C	-5.358464	-14.039575	0.723293	B	13.645146	-2.949999	1.332605
H	-7.054580	-13.039530	1.604588	C	13.642999	-1.463749	0.832880
H	-3.551245	-14.744786	-0.220168	C	14.610547	-0.535201	1.288059
C	6.608198	-11.001139	2.155667	C	12.676080	-0.997397	-0.090992
C	6.139969	-12.194511	1.563269	C	14.590301	0.781992	0.853404
C	7.573487	-11.131840	3.178182	H	15.367629	-0.861347	1.997011
C	6.615955	-13.444646	1.956855	C	12.660346	0.315307	-0.556512
C	8.034044	-12.379492	3.597130	H	11.927956	-1.693007	-0.460417
C	7.560455	-13.540184	2.981353	C	15.503095	1.936337	1.219929
H	6.248220	-14.344392	1.469771	C	13.617952	1.212491	-0.074993
H	8.765157	-12.447990	4.398880	H	11.911523	0.632891	-1.277984
H	-19.880986	5.608932	-4.598580	H	15.470614	2.159592	2.295497
H	-16.827002	6.832297	-1.840653	C	14.949216	3.077160	0.388142
H	-17.878562	2.675959	-2.186705	H	16.554459	1.723248	0.981652
H	-18.458053	7.430157	3.158600	C	13.838331	2.632563	-0.360823
H	-18.065032	8.697524	2.004435	C	15.382265	4.391349	0.287879
H	-13.193508	1.066462	-4.084529	C	13.153966	3.519192	-1.196984
H	-14.714362	0.184119	-4.094543	C	14.700401	5.317562	-0.537921
H	-9.887946	-5.158413	-5.598771	H	16.246207	4.723542	0.858423
H	-13.881456	-4.185445	-4.330192	C	13.580162	4.843694	-1.263312
H	-13.222287	-5.974122	-8.176427	H	12.300039	3.187131	-1.782414
H	-8.010133	-8.515956	-3.355120	H	13.042475	5.535486	-1.905559
H	-8.910671	-8.794544	-1.870828	C	15.004331	-3.651922	1.690933
H	-6.207733	-10.774576	1.111666	C	16.192049	-3.366800	0.982262
H	-2.677852	-12.479108	-0.659413	C	15.095305	-4.599049	2.734389

H	-5.737359	-15.037779	0.928586	C	17.397045	-3.999805	1.285155
H	1.052835	-11.859610	1.669557	H	16.162843	-2.645282	0.170095
H	0.784540	-10.604752	2.871700	C	16.302265	-5.215396	3.062645
H	7.925658	-14.514068	3.298030	H	14.203364	-4.844231	3.304923
H	7.957361	-10.236832	3.660542	C	17.456173	-4.921904	2.332472
H	5.399280	-12.136090	0.770151	H	18.290782	-3.771465	0.709707
H	11.340829	-7.933599	1.853426	H	16.343445	-5.927952	3.882770
H	18.396523	-5.409074	2.578466	Si	9.775429	15.327380	-3.145800
B	15.168259	6.810490	-0.648429	C	8.007348	15.600094	-2.525566
C	14.117900	7.952571	-0.867675	H	20.507507	8.036613	-0.244916
C	14.437217	9.115891	-1.609568	H	7.623744	16.562837	-2.884969
C	12.813460	7.864540	-0.323783	H	7.322254	14.822000	-2.882414
C	13.495638	10.116057	-1.801290	H	7.955575	15.615379	-1.430428
H	15.430004	9.214533	-2.041985	C	9.784101	15.327607	-5.041388
C	11.867908	8.875243	-0.483458	H	9.421586	16.284650	-5.436870
H	12.546040	6.983250	0.252395	H	10.792215	15.166021	-5.441550
C	13.612050	11.420630	-2.566483	C	10.884517	16.729816	-2.516205
C	12.208712	10.004890	-1.232136	H	9.140080	14.535593	-5.441265
H	10.881963	8.779988	-0.035063	H	10.875228	16.781778	-1.421121
H	14.421297	12.055363	-2.179259	H	11.926331	16.595269	-2.830765
C	12.247709	12.050786	-2.362626	H	10.547193	17.700870	-2.899579
H	13.833043	11.254066	-3.630116	C	16.695473	7.161408	-0.535284
C	11.437344	11.203281	-1.577250	C	17.693558	6.286344	-1.017282
C	11.754472	13.264564	-2.822003	C	17.134288	8.366482	0.055995
C	10.132243	11.580701	-1.257503	C	19.049320	6.600028	-0.928791
C	10.438164	13.669346	-2.512349	C	18.488968	8.675165	0.173861
H	12.393905	13.907453	-3.426114	H	19.793348	5.912973	-1.324320
C	9.650236	12.804084	-1.726516	H	18.795749	9.603401	0.649586
H	9.497540	10.937475	-0.652696	C	19.450701	7.794086	-0.325500
H	8.633033	13.091133	-1.471638	H	16.396762	9.065203	0.441714
H	17.396202	5.349794	-1.481519				

Chapter 2 Luminescent Donor-π-Acceptor Type Oligomeric Organoboranes

2.1 Donor-π-Acceptor Type Organoborane Oligomers

Considerable efforts have been devoted to developing ambipolar molecular systems with donor (D) and acceptor (A) moieties that are capable of transporting both holes and electrons.[1-4] These types of compounds are highly attractive primarily due to their established applications in the area of materials science, such as electronic devices (OLEDs, FETs and SCs),[5-11] as well as for use in bioimaging and photodynamic therapy (PDT).[12-14] Triarylamines have been extensively exploited as p-type semiconductor materials that enable hole transport thanks to their inherent electron-donating capability.[15-17] Among the wide range of acceptor materials studied, triarylboranes bearing empty p orbitals are of particular significance since p-π orbital interactions with attached π-conjugated organic groups favor extended chain conjugation, giving rise to unique photophysical and electronic properties. As discussed in Chapter 1, binding of anions, for example fluoride and cyanide, has been demonstrated to perturb this orbital overlap, allowing for use also as sensory materials.[18-25] Ambipolar molecules that are composed of organoboranes in combination with triarylamines are particularly attractive, because of the simultaneous n- and p-type behavior and the possibility for intramolecular charge transfer processes. These features have been exploited in OLEDs based on B/N compounds as the charge transport and emissive component, in non-linear optical materials, as well as in turn-on luminescent anion sensors.[26-38] In comparison, polymeric systems of this type are relatively less explored. Notable is work by Lambert et al., Müllen et al., Wenger et al., and Kawashima et al. who have prepared B-π-N dendrimer-like structures with varying D/A ratio.[33,39-42] A high molecular weight linear polymeric system, in which arylamine donors and arylborane acceptors alternate in the polymer main chain has recently been introduced by our group.[43] The successful synthesis of such a donor-π-acceptor polymer poses important questions in regard to electron delocalization and charge transport in this type of polymeric material.

Comparative investigations of structurally well-defined oligofluorenes (**O-F*n***),[44-48] oligothiophenes (**O-T*n***),[49-52] and oligoanilines (**O-A*n***)[53-55] in what since has been dubbed "the oligomer approach" have provided important information on the photophysical attributes and electronic structures of the corresponding conjugated polymers. Moreover, electrochemical studies on BODIPY-based oligomers, prepared by oxidative coupling,[56,57] led to *valuable insights* into the substantial interactions between the active building blocks. In Chapter 1 we have explored the effect of electron-deficient tricoordinate organoborane moieties (**O-B*n***), which are isolectronic to carbocation sites, on the electronic structure and properties of oligofluorenes.[58] Importantly, we found strong coupling between the individual fluoreneborane moieties and were able to deduce significant extension of conjugation up to 5 repeating units. These findings led us to consider the possibility of generating extended structures, in which electron-deficient organoborane moieties alternate with electron-rich arylamine moieties, corresponding to the isoelectronic carbanion and carbocation species. We were especially interested in evaluating whether chain extension results in extension of π-conjugation similar to our observations for the acceptor-doped oligomers **O-B*n*** (**Chart 2-1**) and what role intramolecular charge transfer (ICT) processes between N and B might play in oligomers **O-B*n*N*m***. It is to be noted that the Müllen group synthesized several para phenylene-bridged borylene-amine π-conjugated molecules that are structurally similar to **O-B1N2** but with different substituents. Their charge transfer behavior was investigated by means of optical studies and DFT calculations.[38]

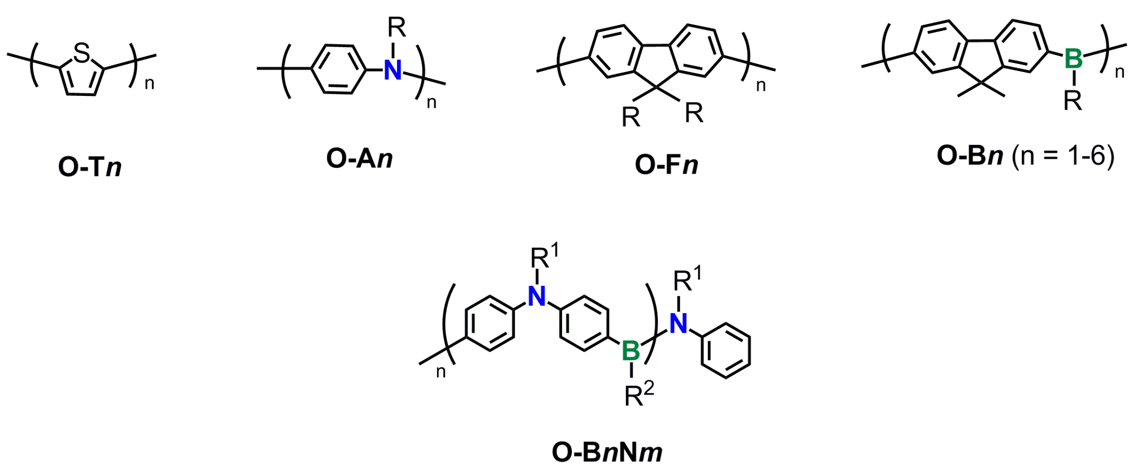

Chart 2-1. Examples of well-defined conjugated oligomers with electron donor and electron acceptor moieties and structure of the targeted ambipolar{B-π-N}$_n$ oligomers **O-B*n*N*m***.

2.2 Synthesis and Structural Characterization of {B-π-N}$_n$ Type Oligomers

Retrosynthetic analysis of the targeted ambipolar oligomers (**O-B*n*N*m***) suggests that chain extension to give larger oligomers should be readily achieved by activation of the trimethylsilyl end-capped triarylamine building block (**TPA-Si2**) with BBr_3 as a boron source in a Si/B exchange reaction, followed by selective Sn/B exchange using two equiv of the bifunctional reagent **TPA-SiSn** (**Scheme 2-1**). Subsequent stabilization of the boron center is accomplished by introducing bulky aryl groups using the copper reagent TipCu (Tip = 2,4,6-triisopropylphenyl) in refluxing toluene. For the preparation of **O-BNB**, the triarylamine donor was substituted with two fluorenylborane moieties. Gratifyingly, standard isolation of the crude samples followed by purification using preparative size-exclusion column chromatography on bio-beads™ afforded the analytically pure oligomers as pale-yellow powdery solids in good yields. The products are reasonably stable in air and moderately soluble in non-polar aliphatic hydrocarbons, but very soluble in chlorinated and aromatic solvents.

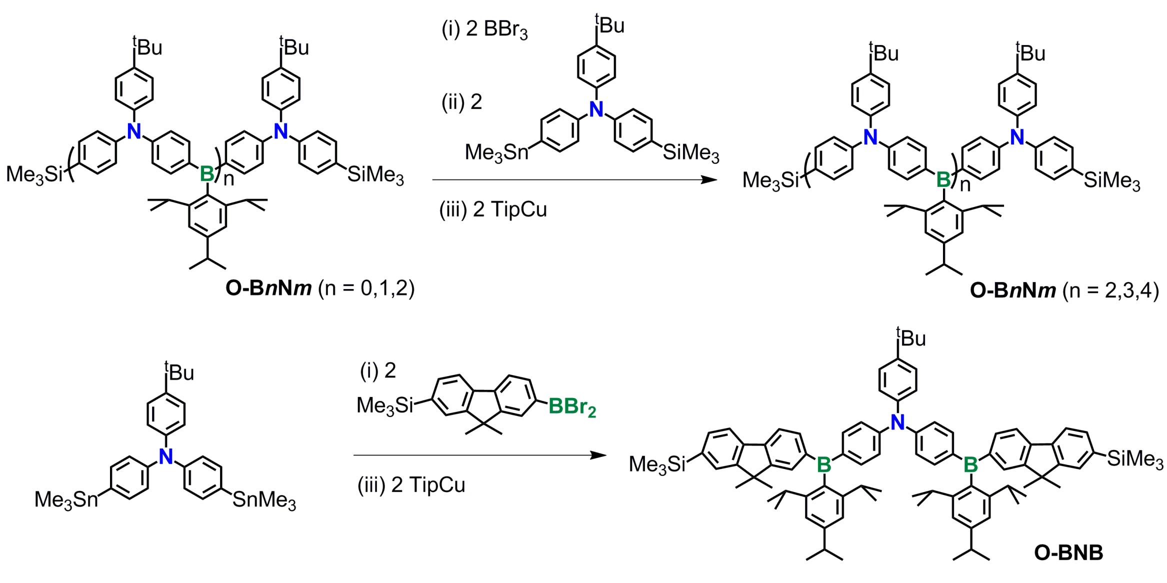

Scheme 2-1. Synthetic procedures for **O-B*n*N*m*** and **O-BNB**. Tip = 2,4,6-triisopropyl-phenyl.

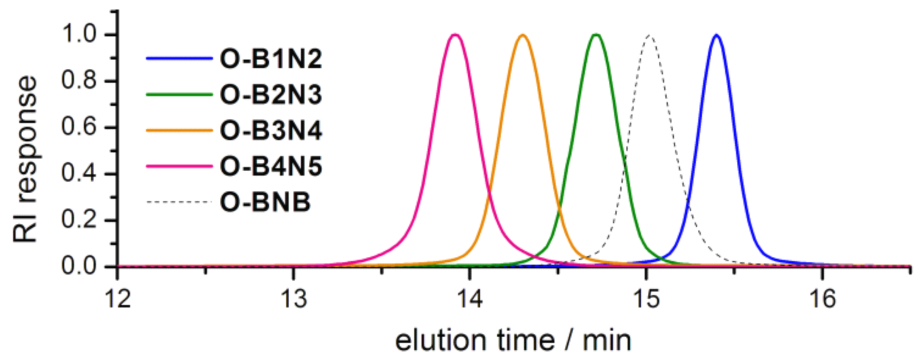

Figure 2-1. GPC traces for **O-B*n*N*m*** and **O-BNB** (THF, 1 mL/min).

The structure of the oligomer samples was verified by high-resolution MALDI-MS, which in all cases showed the molecular ion peaks (**Table 2-1**). Monodisperse GPC traces (PDI = 1.01) ascertained the high purity of the samples (**Figure 2-1**). The number average molecular weights (M_n) are in the range of 990 to 2800 Da; they match very well with the corresponding calculated values although measured relative to low molecular weight polystyrene standards.

Table 2-1. Summary of GPC and MALDI-MS Data for **O-B*n*N*m*** and **O-BNB**

	Formula	M_{th} [a]	M_{MS} [b]	M_n [c]	M_w [c]	PDI [c]
O-B1N2	$C_{65}H_{83}BN_2Si_2$	958.6	958.6	992	1003	1.01
O-B2N3	$C_{102}H_{127}B_2N_3Si_2$	1472.0	1472.0	1608	1622	1.01
O-B3N4	$C_{139}H_{171}B_3N_4Si_2$	1986.3	1986.3	2078	2109	1.01
O-B4N5	$C_{176}H_{215}B_4N_5Si_2$	2498.7	2498.7	2807	2838	1.01
O-BNB	$C_{88}H_{109}B_2NSi_2$	1257.8	1257.8	1278	1291	1.01

[a] Calcd exact mass. [b] From (+) MALDI MS. [c] Relative to low molecular PS standards based on GPC-RI detection in THF at 35 °C; $PDI = M_w/M_n$

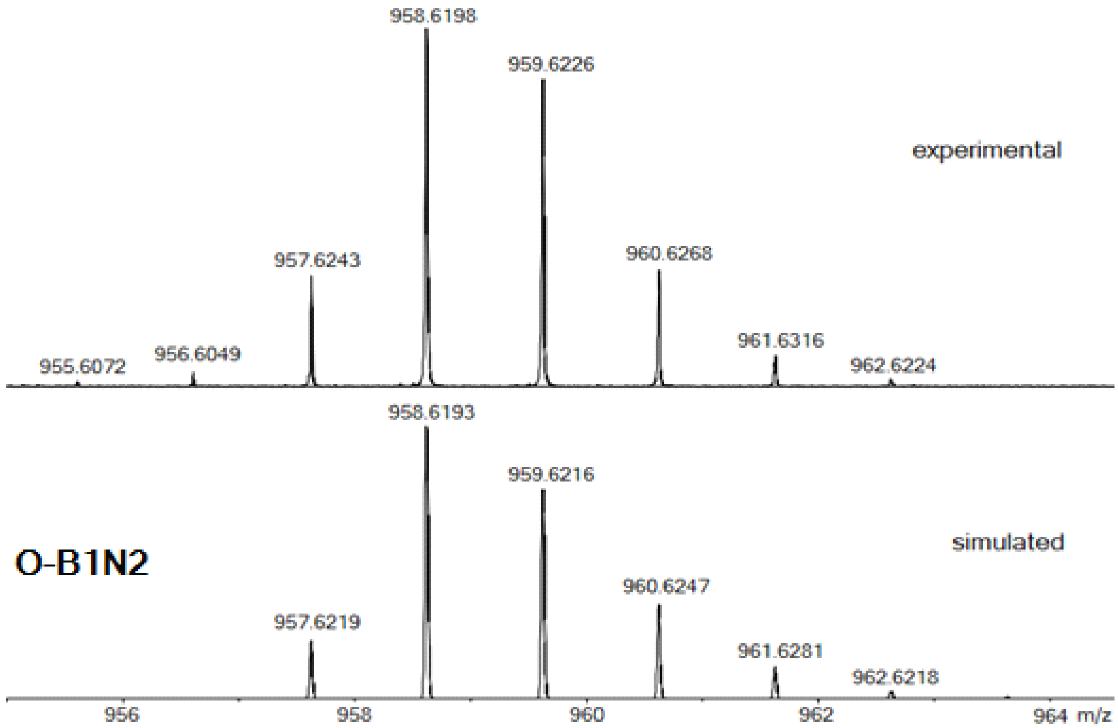
958.6198
959.6226
experimental
957.6243
960.6268
955.6072
956.6049
961.6316
962.6224
958.6193
959.6216
simulated
O-B1N2
960.6247
957.6219
961.6281
962.6218
956
958
960
962
964 m/z

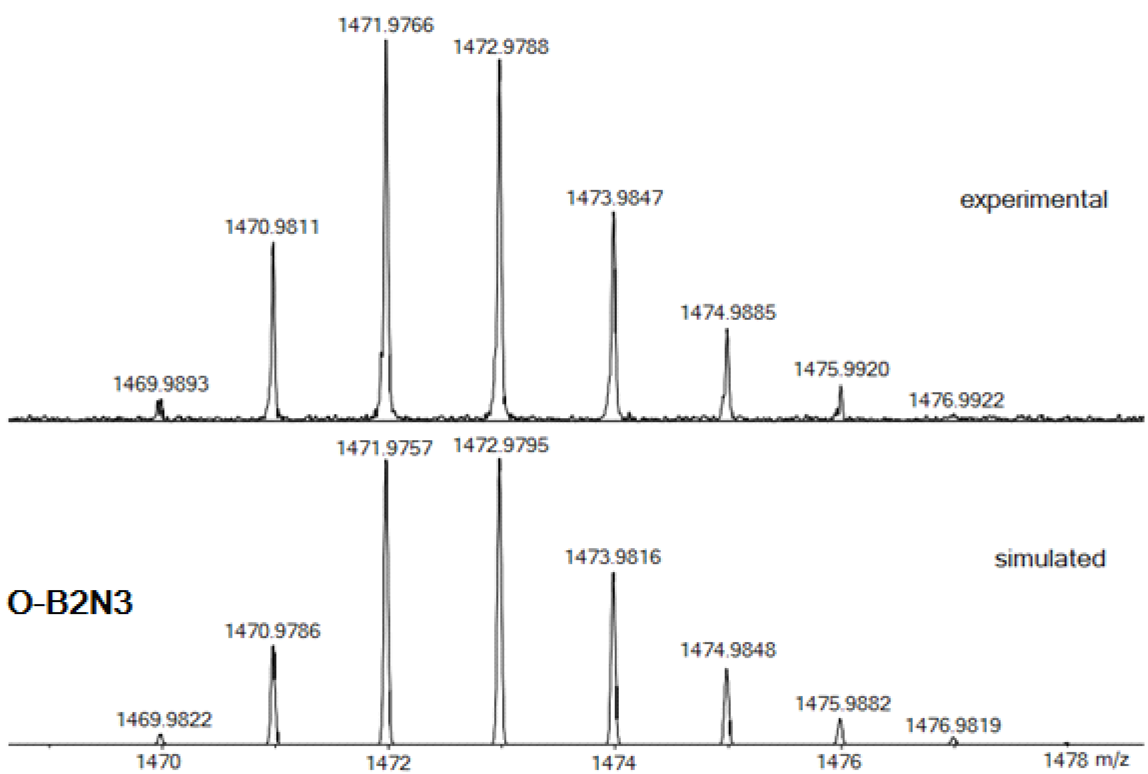
1471.9766
1472.9788
1473.9847
experimental
1470.9811
1474.9885
1469.9893
1475.9920
1476.9922
1471.9757
1472.9795
1473.9816
simulated
O-B2N3
1470.9786
1474.9848
1469.9822
1475.9882
1476.9819
1470
1472
1474
1476
1478 m/z

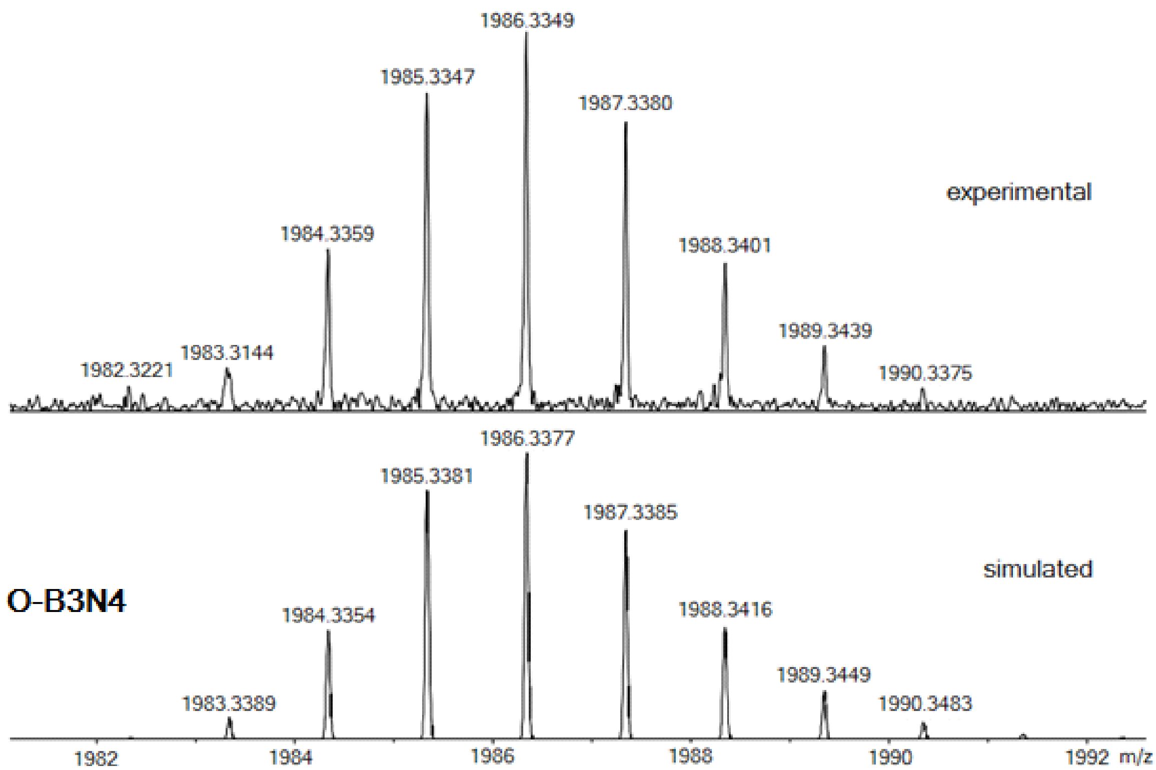
1986.3349
1985.3347
1987.3380
experimental
1984.3359
1988.3401
1989.3439
1983.3144
1982.3221
1990.3375
1986.3377
1985.3381
1987.3385
simulated
O-B3N4
1984.3354
1988.3416
1989.3449
1983.3389
1990.3483
1982
1984
1986
1988
1990
1992
m/z

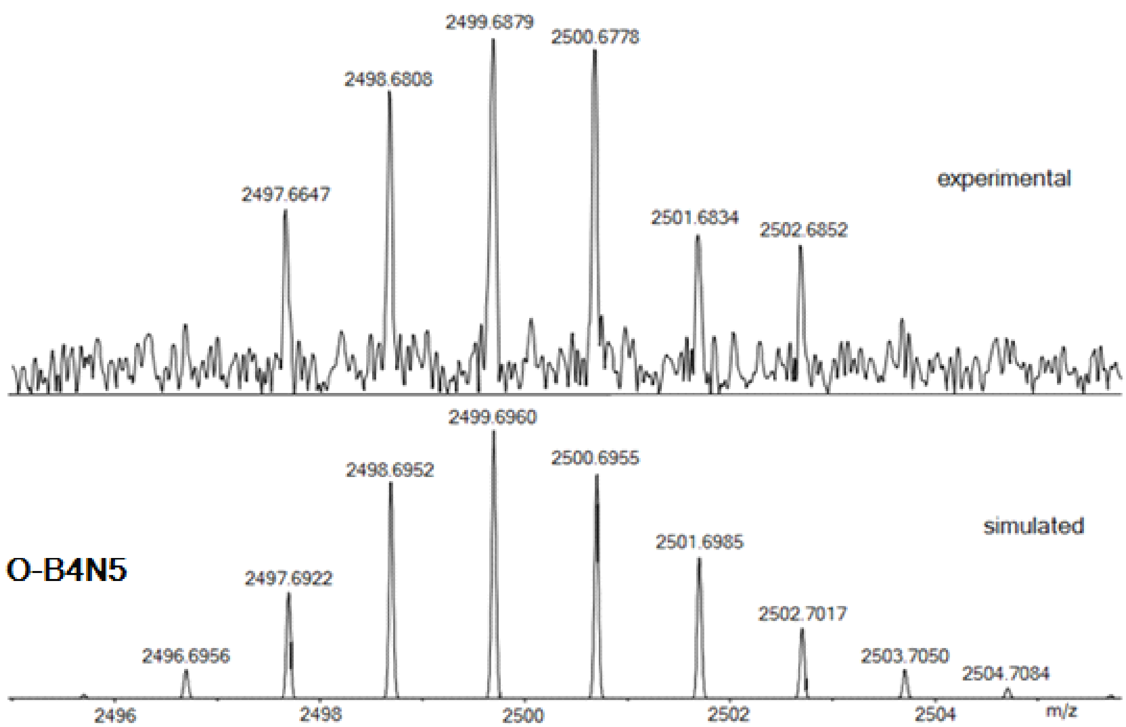
2499.6879
2500.6778
2498.6808
experimental
2497.6647
2501.6834
2502.6852
2499.6960
2498.6952
2500.6955
simulated
2501.6985
O-B4N5
2497.6922
2502.7017
2496.6956
2503.7050
2504.7084
2496
2498
2500
2502
2504
m/z

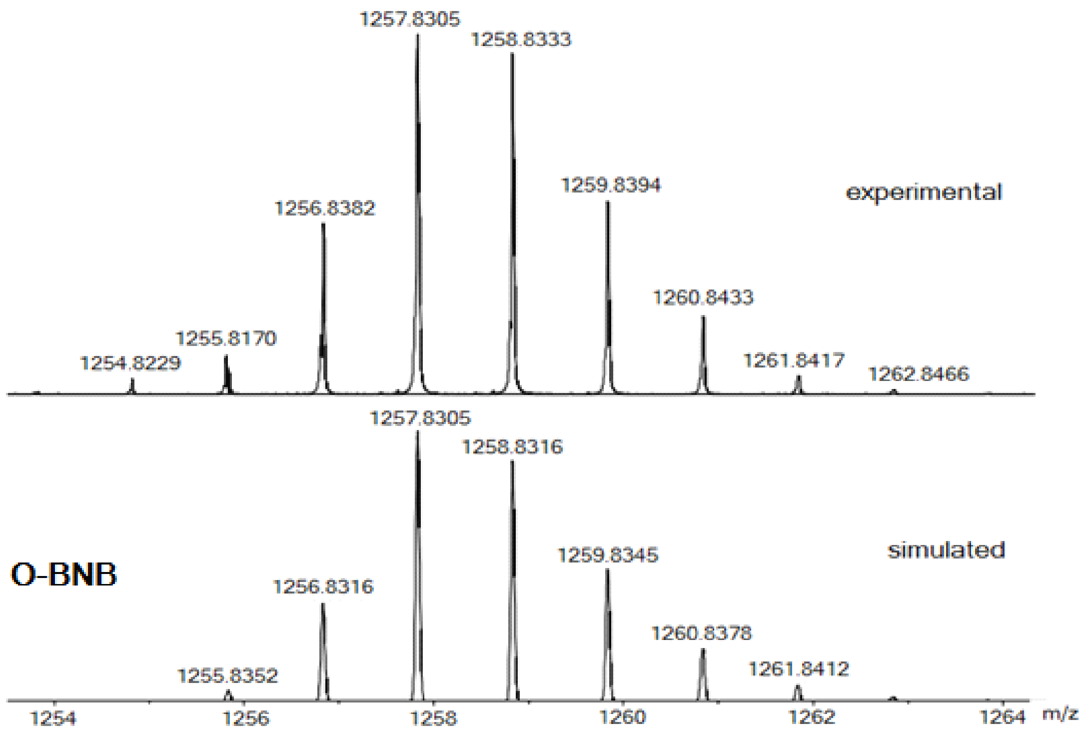

Figure 2-2. (+) MALDI-MS spectra of **O-B*n*N*m*** and **O-BNB** showing molecular ion peaks.

Spectroscopic characterization by multinuclear NMR corroborates the proposed structures (**Figures 2-3**, **2-4**, and **2-5**). Integration of the proton signals in the ^{1}H NMR spectra of the higher oligomers confirms gradual chain elongation (**Figure 2-3**). For example, the integral ratio between the protons due to the Tip groups at 6.96 ppm and the terminal phenylene protons adjacent to the silyl groups at 7.40 ppm increases from 2:4 (**O-B1N2**) to 4:4 (**O-B2N3**), 6:4 (**O-B3N4**) and 8:4 (**O-B4N5**). Two-dimensional NMR data were acquired for **O-B1N2**, and NOE correlations between the aromatic protons and the *t*-Bu, $SiMe_3$, and *i*-Pr substituents allow for unequivocal signal assignments (Appendix). Sharp single peaks ranging from –3.72 to –4.56 ppm in the ^{29}Si NMR spectra correspond to the trimethylsilyl moieties attached to the terminal aryl groups. The presence of broad ^{11}B chemical signals at ca. 70 ppm is consistent with boron in a tricoordinate environment (**Figure 2-5**). Peak broadening in the ^{11}B NMR spectra is in part due to overlap of multiple borane resonances from non-equivalent internal and terminal boron sites. Furthermore, the quadrupole-broadened B-bound carbon NMR signals can readily be identified in the ^{13}C NMR and their number is consistent with the expected one (**Figure 2-4**).

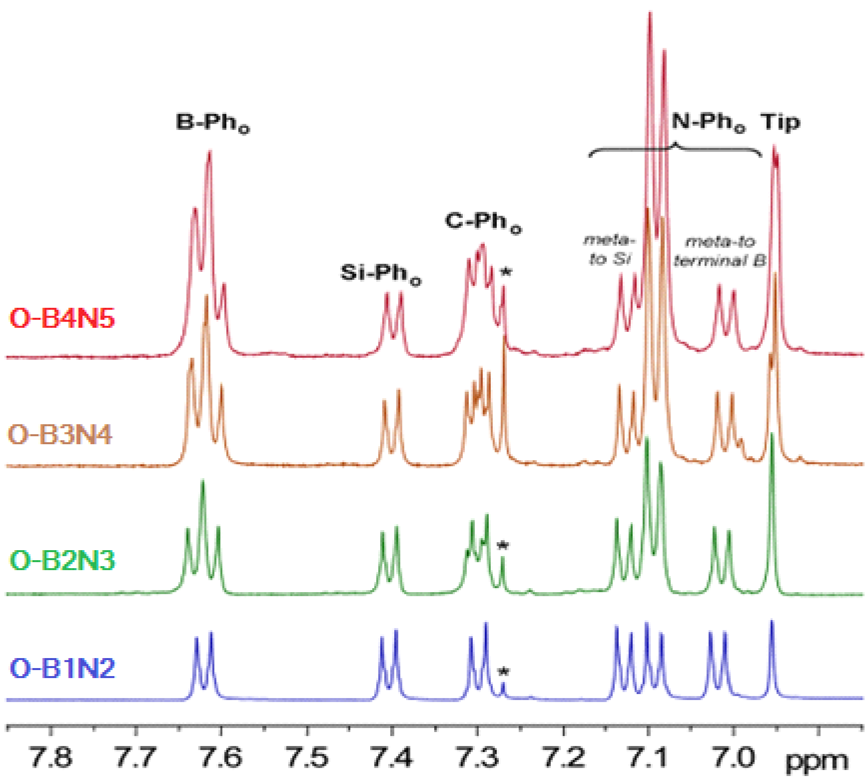

Figure 2-3. Overlay of the aromatic region of the ^1H NMR spectra for **O-B*n*N*m*** ($CDCl_3$, 25 °C).

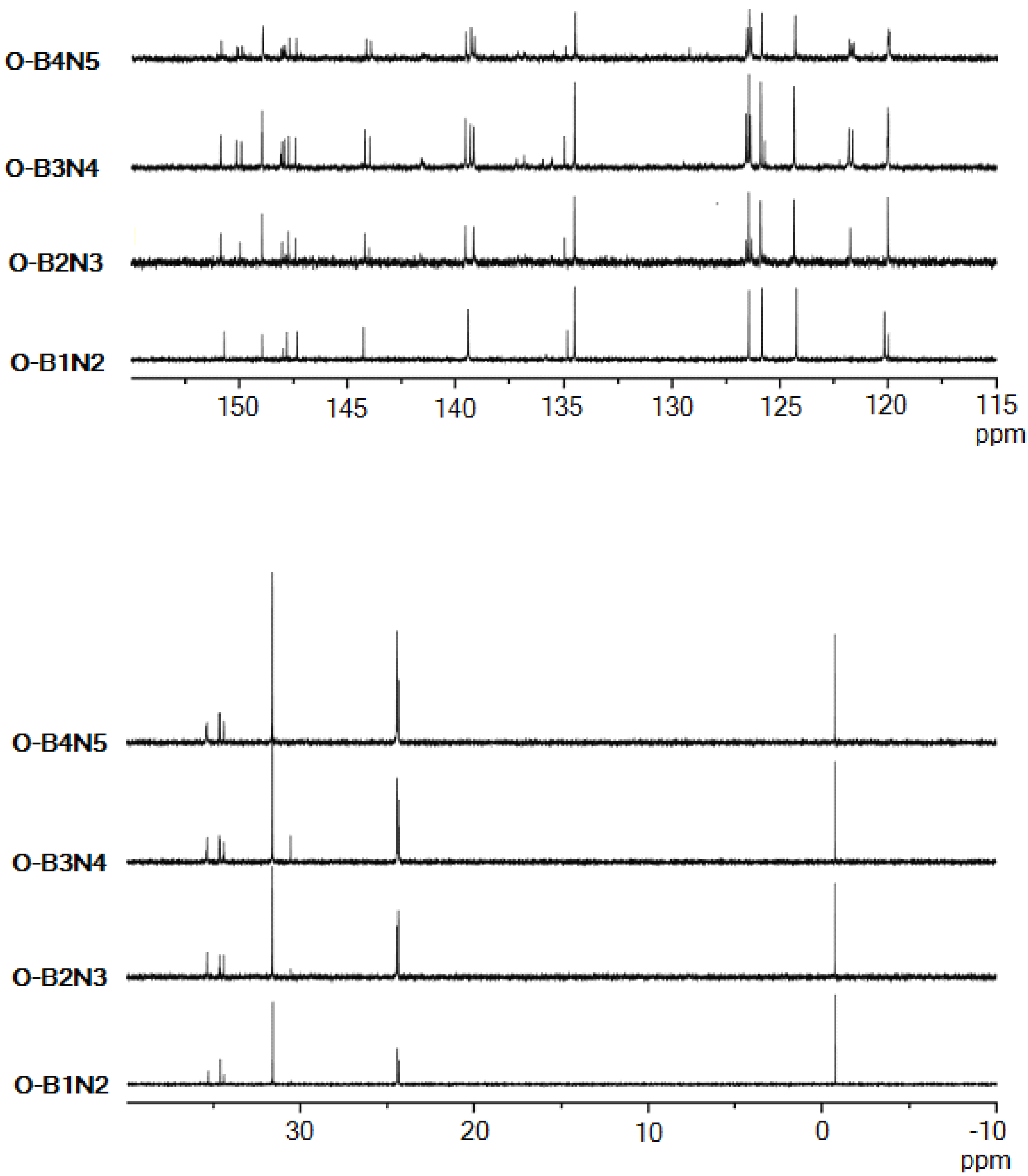

Figure 2-4. Overlays of the aromatic and aliphatic regions of the ^{13}C NMR spectra of the oligomers **O-B*n*N*m***, normalized to the $SiMe_3$ end group signal at –0.8 ppm ($CDCl_3$, 25 °C). The peaks at 31 ppm and 126.5 ppm for **O-B3N4** are due to a trace of butylate hydroxytoluene (BHT).

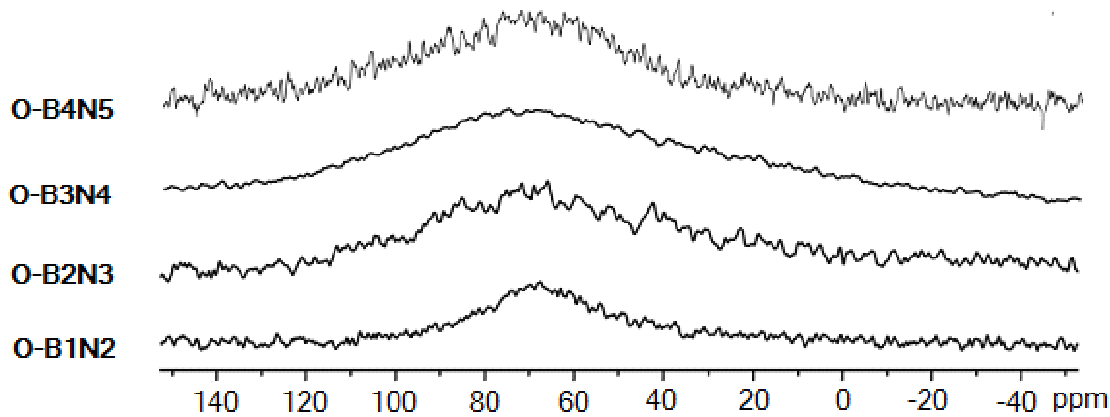

Figure 2-5. ^{11}B NMR spectra for oligomers **O-B*n*N*m*** ($CDCl_3$, 25 °C).

2.3 Photophysical, Electrochemical and Computational Studies of Oligomers **O-B*n*N*m*** and **O-BNB**

UV-vis absorption spectra were recorded to investigate the photophysical characteristics and determine the optical energy gaps. Vibronically split bands are observed in hexanes with absorption maxima shifting from 397 nm for **O-B1N2** to 422 nm for **O-B4N5** (**Figure 2-6** and **Table 2-2**). Such a red-shifted absorption of the lowest energy transition is attributed to increasing π-conjugation and is possibly also affected by D to A charge transfer processes (see below).[31] The spectral difference between **O-B3N4** and **O-B4N5** is very small, indicating that the effective conjugation length has been reached for **O-B3N4** with its 3 borane and 4 arylamine moieties. A comparable effective conjugation length of n_{ecl} = 5 has been deduced for the organoborane oligomers **O-B*n***,[58] but no such data analysis has been reported for oligoanilines **O-A*n***.[53,54] Exponential fit of the absorption data in hexanes to Meier's equation as described in Chapter 1 gives a n_{ecl} =

4 for **O-B*n*N*m*** (R^2 = 0.9999). An excellent linear correlation (R^2 = 0.9996) and extrapolation to $n\rightarrow\infty$ predicts an absorption maximum at λ_∞ = 430 nm for an infinite polymer chain (**Figure 2-7**).

Table 2-2. Comparison of Experimental Photophysical Properties and Calculation Data

	λ_{abs} [nm] [a]	λ_{edge} [nm] [a]	ε_{max} [b]	λ_{em} [nm] [a,c]	Φ [c,d]
O-B1N2	397	420	39,000	427	0.64
O-B2N3	414	433	73,000	433	0.67
O-B3N4	420	439	97,000	438	0.55
O-B4N5	422	441	120,000	439	0.49
O-BNB	407	431	48,500	434	0.63

[a] Measured in hexanes. [b] Determined in toluene. [c] Excited at λ_{max}. [d] Measured in CH_2Cl_2.

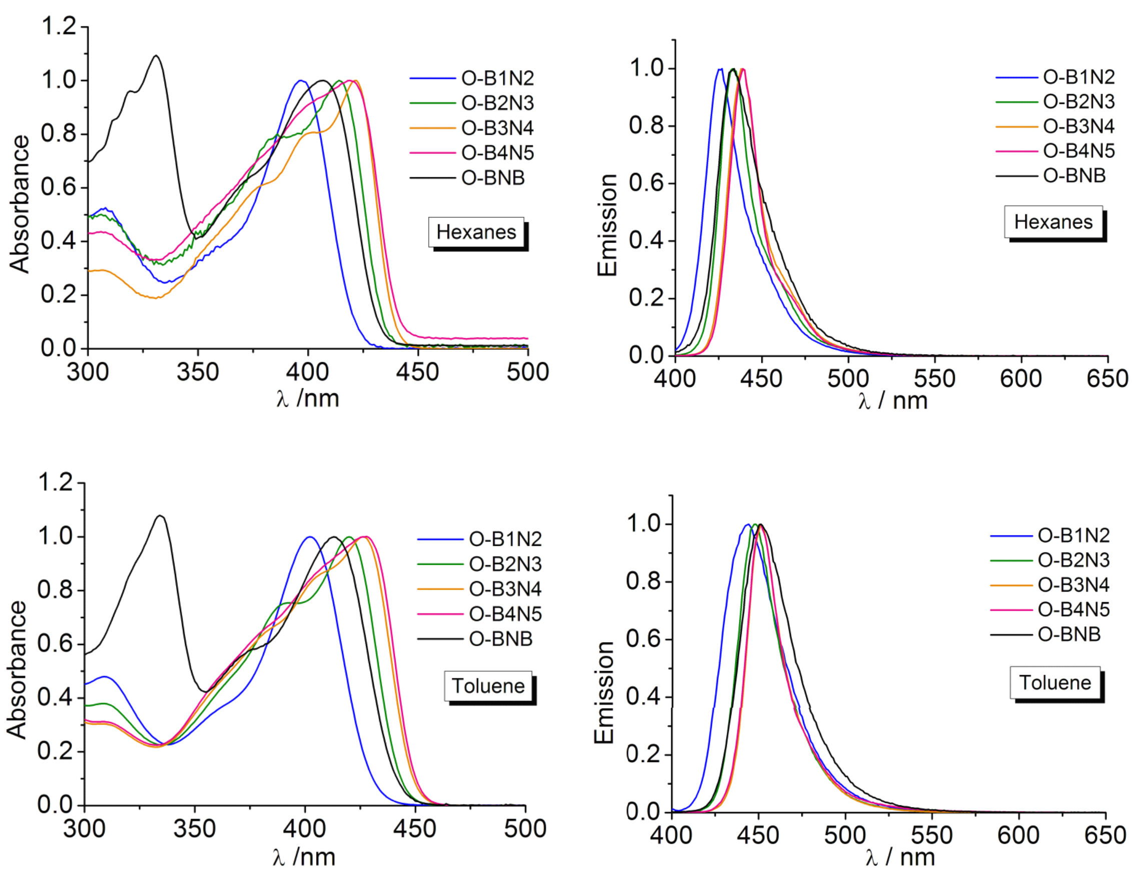

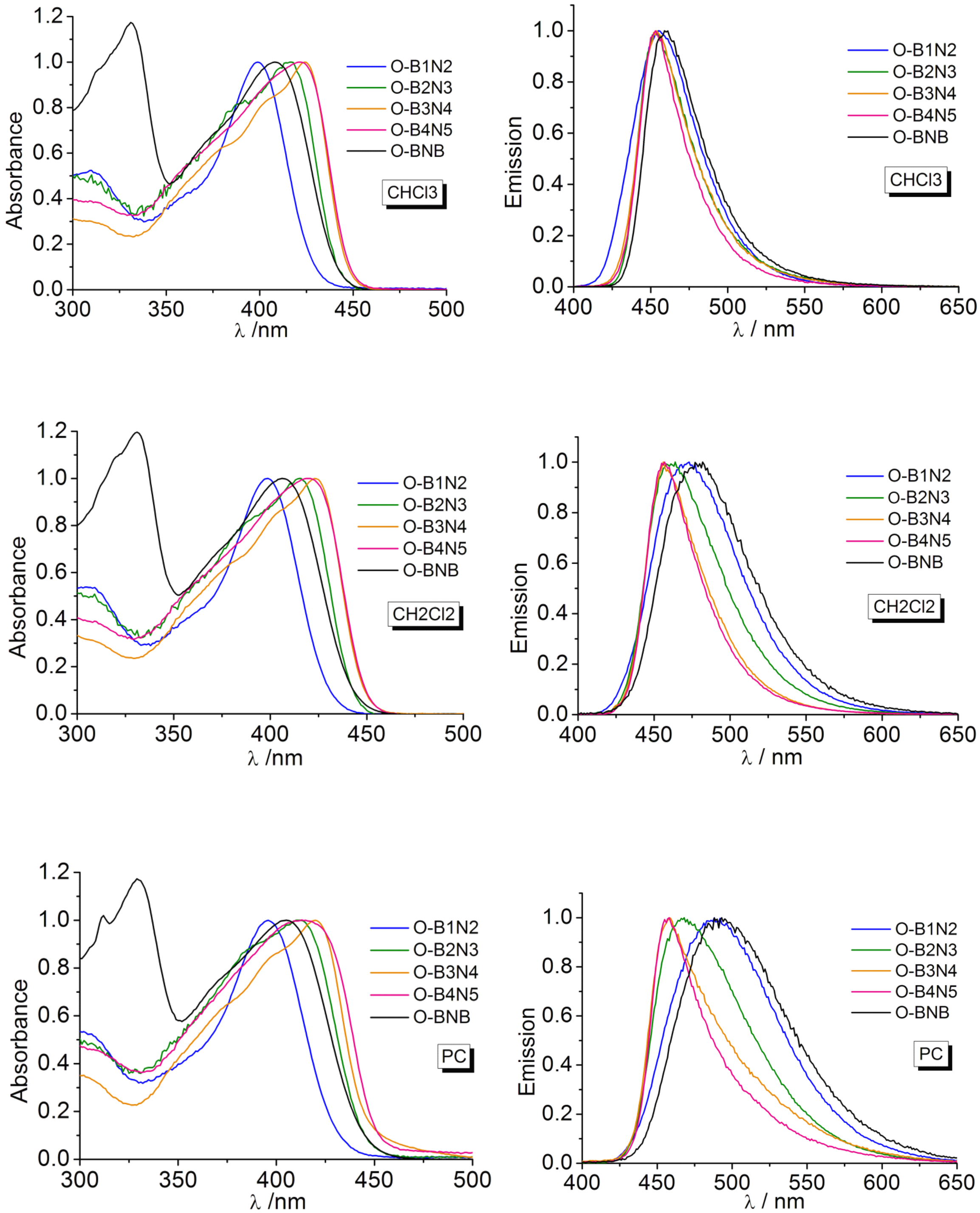

Figure 2-6. UV-vis and fluorescence spectra of **O-B*n*N*m*** and **O-BNB** (excited at λ_{max}) in different polar solvents ranging from hexanes, toluene, $CHCl_3$, CH_2Cl_2 to propylene carbonate (PC).

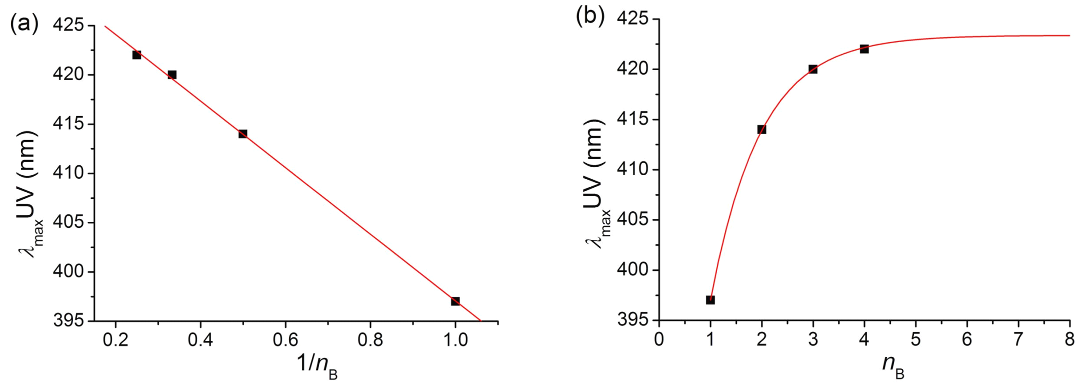

Figure 2-7. (a) Linear and (b) exponential fits of absorption data in hexanes for **O-B*n*N*m***.

According to DFT calculations (B3LYP/6-31G*), the HOMOs are localized on the π spacers with contributions from the nitrogen p-orbitals, while the LUMOs are localized on the empty p-orbitals of the boron centers with smaller contributions of the conjugated organic π-systems but not the nitrogen atoms (**Figure 2-8** and **Table 2-3**). Notably, the terminal diarylamine moieties are almost not at all involved in the LUMO levels; they also contribute less to the HOMO of **O-B4N5**, therefore indicating that the effective conjugation length is reached for **O-B3N4**, in agreement with the small absorption difference of only ~2 nm between **O-B3N4** and **O-B4N5**. Consistent is also that the calculated HOMO−LUMO energy gaps narrow from 3.41 to 3.19 eV with only a small difference between **O-B3N4** and **O-B4N5** (**Table 2-2**). Interestingly, according to the calculations, the HOMOs stay at the same level of –4.93 eV, while the LUMOs gradually decrease in energy. This phenomenon, which is consistent with our observations for the fluoreneborane oligomers **O-B*n***,[58] implies that chain extension with an increasing number of D and A sites stabilizes the LUMOs considerably more than the HOMOs, leading to lowered HOMO – LUMO gaps that converge toward a constant value. The vertical excitation energies to the first singlet excited state based on TD-DFT calculations similarly decrease with increasing length of **O-B*n*N*m***. The experimental optical energy gaps for the oligomers determined from the absorption onsets are consistent with the values calculated by TD-DFT. For compound **O-BNB**, ICT occurs from the central borane moiety to the terminal arylamine groups, in a reversal to the situation for **O-B1N2** (**Figure 2-8**). The excitation energy for **O-BNB** is slightly lower than that for **O-B1N2**, but higher than for **O-B2N3**. This effect is again due to lowering of the LUMO with increasing number of arylborane groups. It is to be noted that the silyl groups make essentially no contributions to the frontier orbitals of these oligomers.[59]

Table 2-3. Summary of Results from TD-DFT calculations (B3LYP, 6-31G(d)) on Oligomers [a]

	transition	λ_{max} nm (eV)	oscillator strength, f	orbital contributions
O-B1N2	$S_1 \leftarrow S_0$	423.7 (2.926)	0.821	**192→193(HOMO→LUMO), 0.683**
O-B2N3	$S_1 \leftarrow S_0$	445.6 (2.782)	1.159	277→280 (HOMO-2→LUMO), 0.125 278→281 (HOMO-1→LUMO+1), 0.172 **279→280 (HOMO→LUMO), 0.656**
O-B3N4	$S_1 \leftarrow S_0$	454.0 (2.731)	1.447	364→367 (HOMO-2→LUMO), -0.149 365→368 (HOMO-1→LUMO+1), -0.234 **366→367 (HOMO→LUMO), 0.623**
O-B4N5	$S_1 \leftarrow S_0$	458.3 (2.705)	1.997	451→454 (HOMO-2→LUMO), 0.201 451→456 (HOMO-2→LUMO+2), -0.128 452→454 (HOMO-1→LUMO), -0.109 452→455 (HOMO-1→LUMO+1), 0.261 **453→454 (HOMO→LUMO), 0.567**

O-BNB	$S_1 \leftarrow S_0$	423.9 (2.925)	0.681	**151→152 (HOMO→LUMO), 0.703**

[a] The ^{i}Pr on Tip and ^{t}Bu on TPA are replaced with H. The fluorene units are replaced with phenyl groups in **O-BNB**.

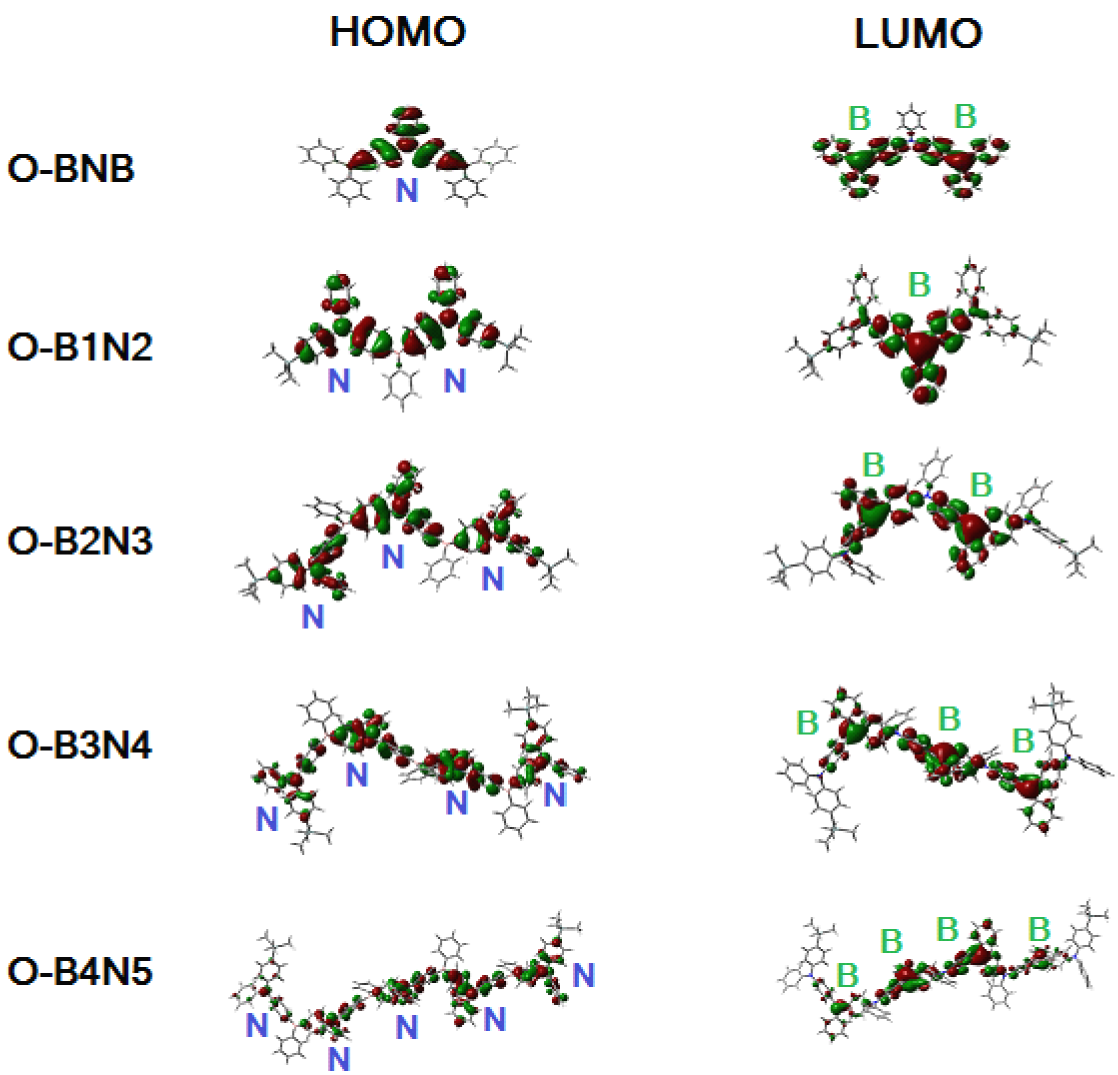

Figure 2-8. Computed HOMO and LUMO orbital plots for **O-B*n*N*m*** and **O-BNB** (B3LYP, 6-31G(d)) in the gas phase.

Photoexcitation in toluene resulted in blue emission with maxima at ~440-450 nm. Quantum yields in the range of Φ = 0.49−0.67 were measured in CH_2Cl_2 (**Table 2-2**). Surprisingly, the bathochromic shift with chain extension from **O-B1N2** to **O-B4N5** proved to be far less pronounced than in the absorption spectra (**Figure 2-6**). Moreover, in the more polar solvents CH_2Cl_2 and propylene carbonate (PC), an unusual hypsochromic shift was detected upon chain extension (**Figure 2-6**). These unexpected results can be traced back to a solvatochromic emission effect, which for the smaller oligomers is more pronounced than for the larger ones (**Figure 2-9**). The results of solvent-dependent absorption and emission studies of the oligomers are summarized in a Lippert-Mataga plot in **Figure 2-10**, in which the Stokes shift is plotted versus the solvent polarity, expressed in terms of $f(D) - f(n^2)$ with D as the solvent permittivity and n the solvent refractive index. The slope for each oligomer is correlated to the difference in the dipole moment in the excited state (μ_1) and the ground state (μ_0) according to equations (1) and (2) [60]

$$\Delta\nu = \frac{2}{hc}\frac{(\mu_1 - \mu_0)^2}{a^3}\Delta f + k \qquad (1)$$

$$\Delta f = f(D) - f(n^2) = \frac{D-1}{2D+1} - \frac{n^2-1}{2n^2+1} \qquad (2)$$

in which h is the Planck constant, c the velocity of light, and a is the Onsager radius of the chromophore. The key observation in the Lippert-Mataga plots is that the slope decreases significantly with increasing chain length from **O-B1N2** to **O-B4N5**. This observation indicates a decreasing polarity of the excited state as the ratio of D to A sites gets smaller from 2:1 for **O-B1N2** to 5:4 for **O-B4N5**.

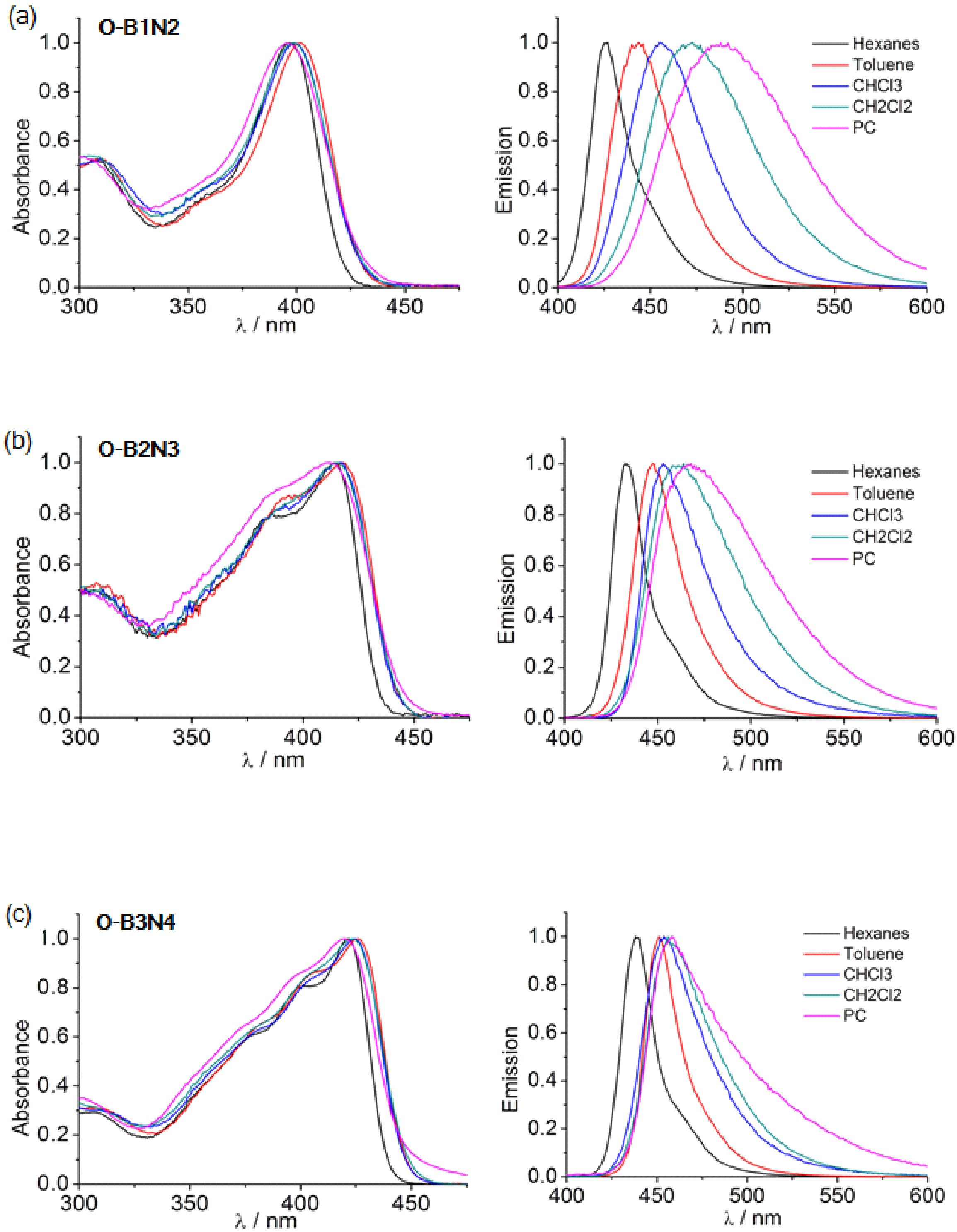

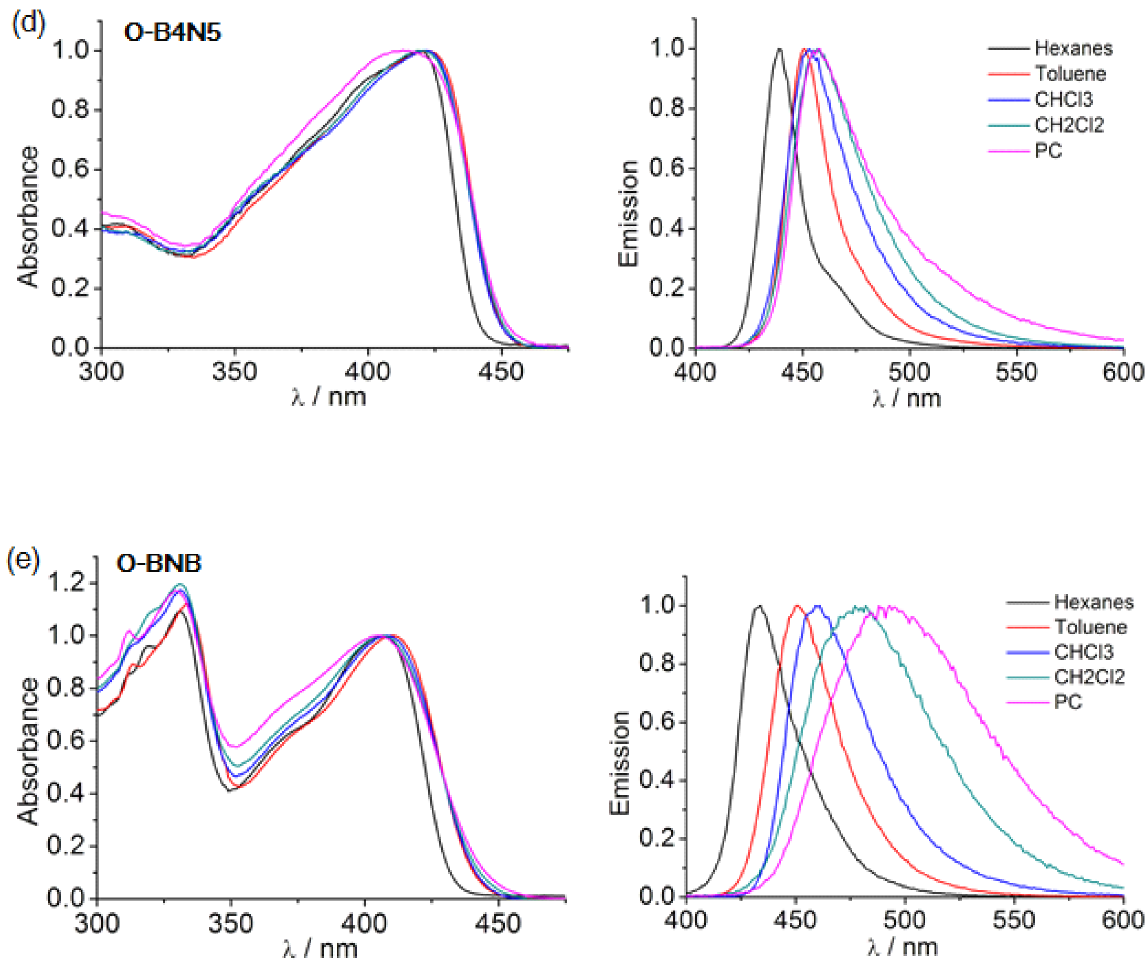

Figure 2-9. Absorption and emission spectra of oligomers in different solvents.

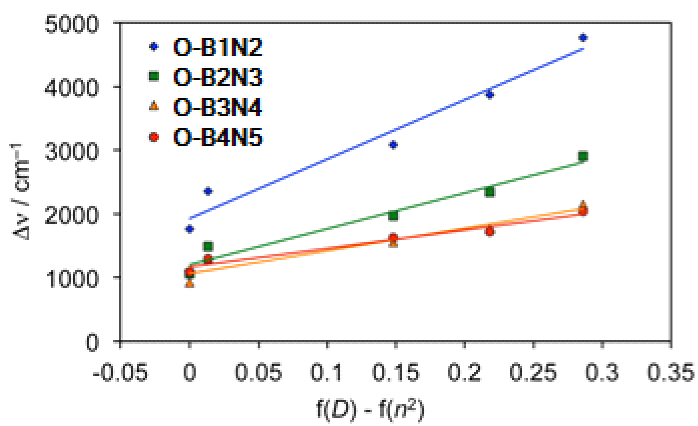

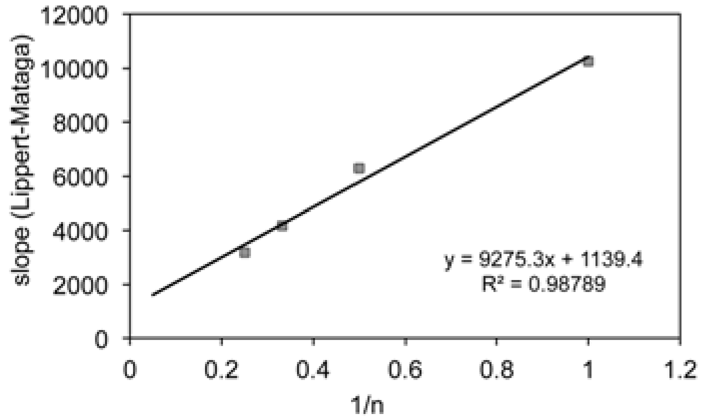

Figure 2-10. (Top) Lippert-Mataga plots for oligomers **O-B*n*N*m***. (Bottom) Plot of Lippert- Mataga slopes versus the number of repeating units *n* in oligomers **O-B*n*N*m***.

Electrochemical measurements provide an alternative method to probe the HOMO/LUMO energy levels, and can also provide information on the stability of radical ions in the solution. Electrochemical experiments were carried out in THF for reduction and CH_2Cl_2 for oxidation processes both by cyclic and square wave voltammetry, and the results are summarized in **Table 2-4**. All the oligomers are reversibly reduced and the redox potentials are reported relative to the Fc/Fc^+ couple at 298 K in **Figure 2-11**. The first reduction wave for **O-B1N2** was observed at $E_{1/2} = -2.60$ V, and those for the higher oligomers occur at gradually less negative potentials approaching –2.47 V for **O-B4N5**, which is in line with the results from DFT calculations. In the higher oligomers, successive reduction of the individual boron sites gives rise to multiple reduction waves as a consequence of electronic interactions between the resulting radical anions in the conjugated chain. The square wave voltammetry plots are consistent with separate one-electron transfer reduction processes, although the redox waves partially overlap in the voltammogram for **O-B4N5** (**Figure 2-12**). The first reduction wave at $E_{1/2} = -2.43$ V for **O-BNB** is slightly less negative than that for **O-B1N2**. This is attributed to the relative orientation of electron donor and acceptor sites. In the case of **O-BNB**, each boron accepts electron density from one N donor, whereas in **O-B1N2** one boron acceptor shows strong interaction with two donor sites.

In contrast to the reduction processes, which are generally well separated, the oxidation profiles in CH_2Cl_2 are more complex. The smaller oligomers show reversibly oxidation waves. For example, two oxidation waves are detected for **O-B1N2** with its two N donors. **O-BNB** is oxidized at $E_{1/2} = 0.55$ V. In view also of the square wave voltammograms, we assign the first two oxidations to correspond to 2e:1e, 3e:1e and 3e:2e processes for **O-B2N3**, **O-B3N4** and **O-B4N5**, respectively, in cation radical states (**Scheme 2-2**).[61] A third wave at higher potentials is attributed to further oxidation of the terminal arylamines to dication states.[62] The less than perfect reversibility of the CV waves in CH_2Cl_2 could be due to deposition of the more highly charged species on the electrode or the instability of the radical cations that are generated at the electrode and may rapidly undergo follow-up reactions.[63]

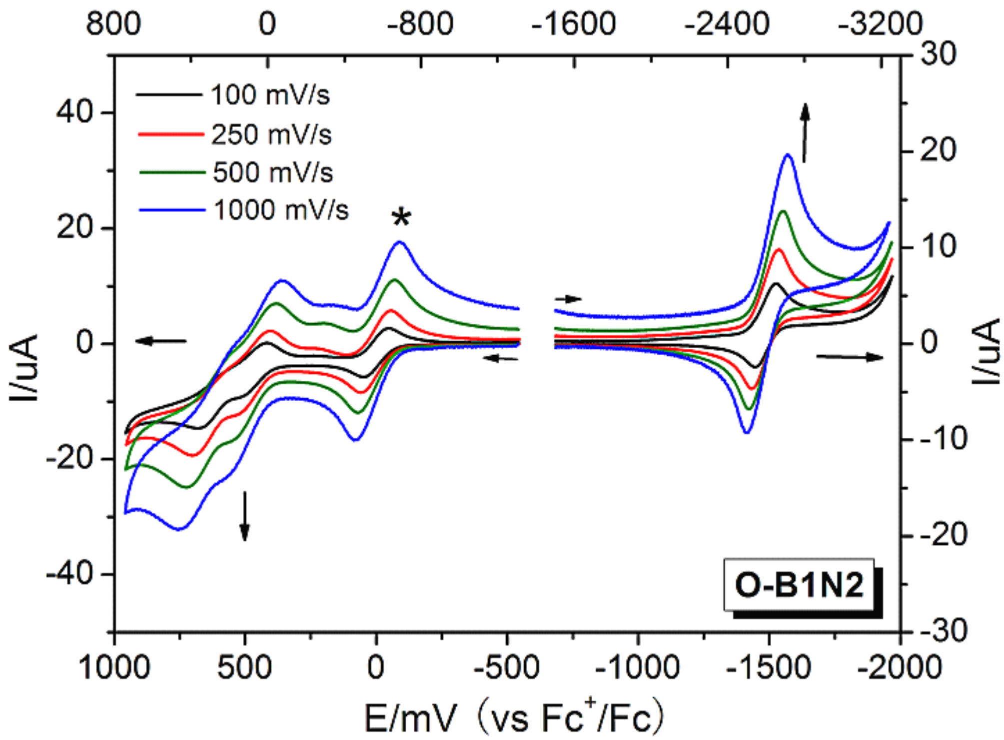
800
0
-800
-1600
-2400
-3200
100 mV/s
250 mV/s
500 mV/s
1000 mV/s
*
I/uA
E/mV (vs Fc+/Fc)
O-B1N2
1000
500
0
-500
-1000
-1500
-2000

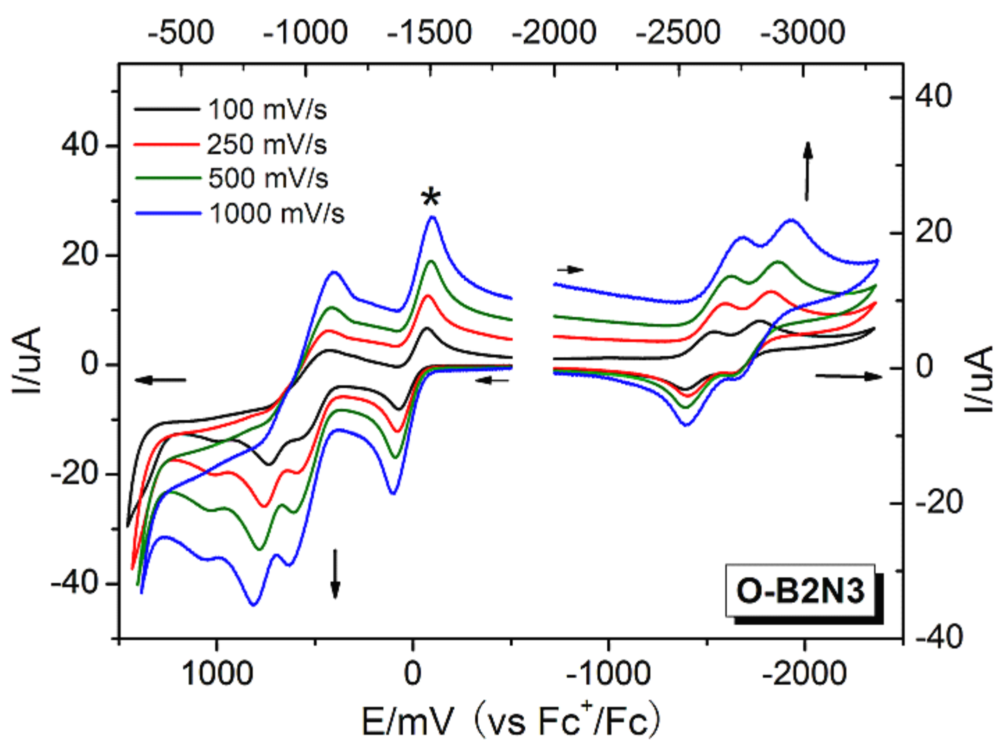
-500
-1000
-1500
-2000
-2500
-3000
100 mV/s
250 mV/s
500 mV/s
1000 mV/s
*
I/uA
E/mV (vs Fc+/Fc)
O-B2N3
1000
0
-1000
-2000

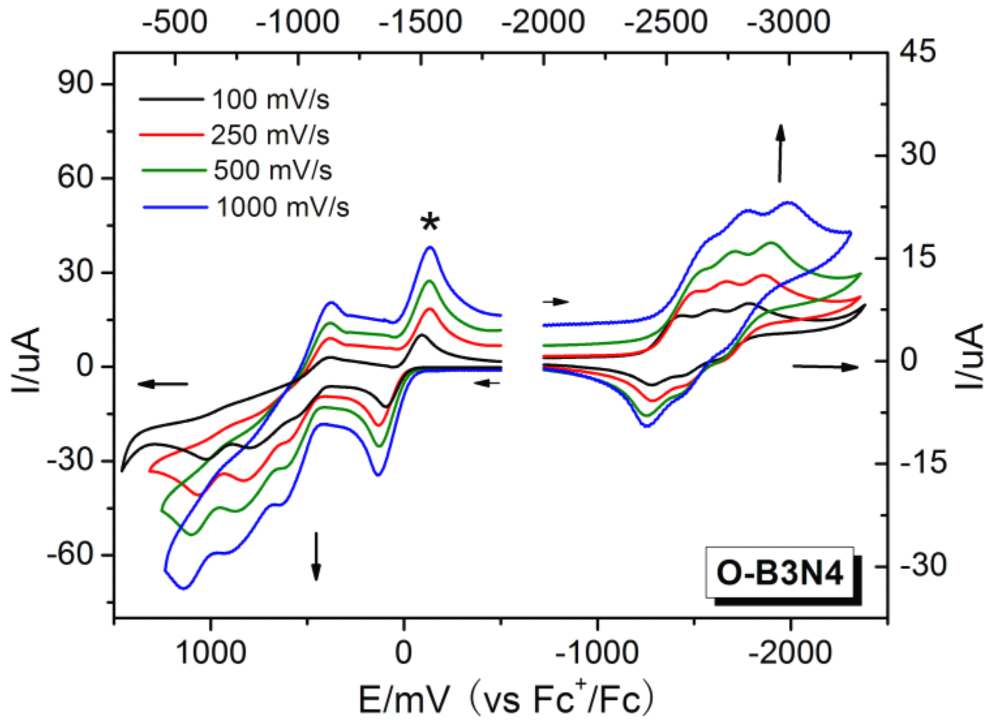
-500
-1000
-1500
-2000
-2500
-3000
100 mV/s
250 mV/s
500 mV/s
1000 mV/s
*
I/uA
O-B3N4
E/mV (vs Fc+/Fc)

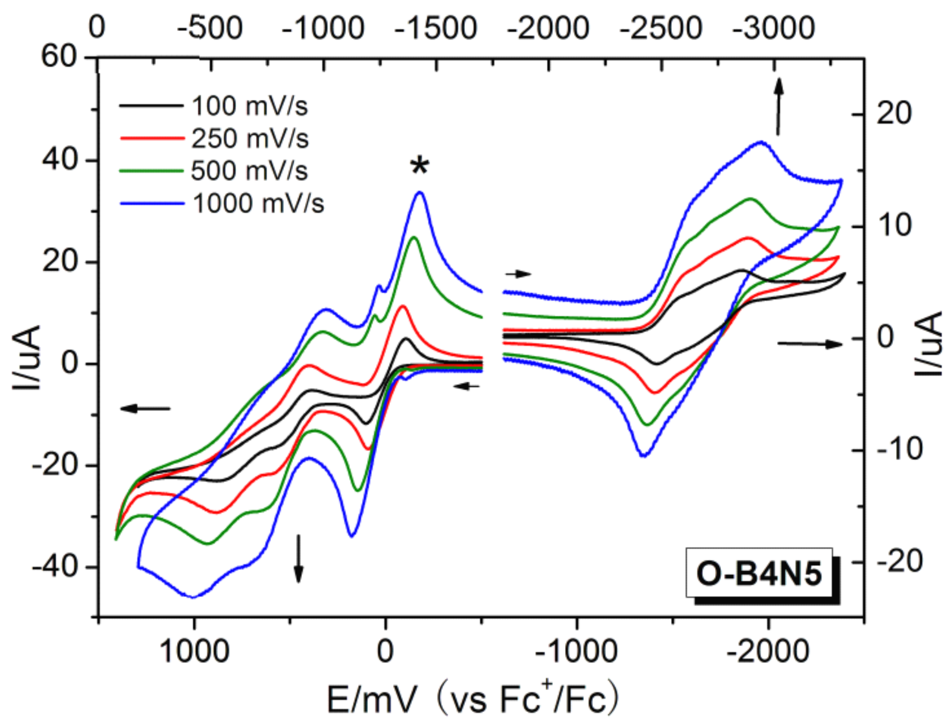
0
-500
-1000
-1500
-2000
-2500
-3000
100 mV/s
250 mV/s
500 mV/s
1000 mV/s
*
I/uA
O-B4N5
E/mV (vs Fc+/Fc)

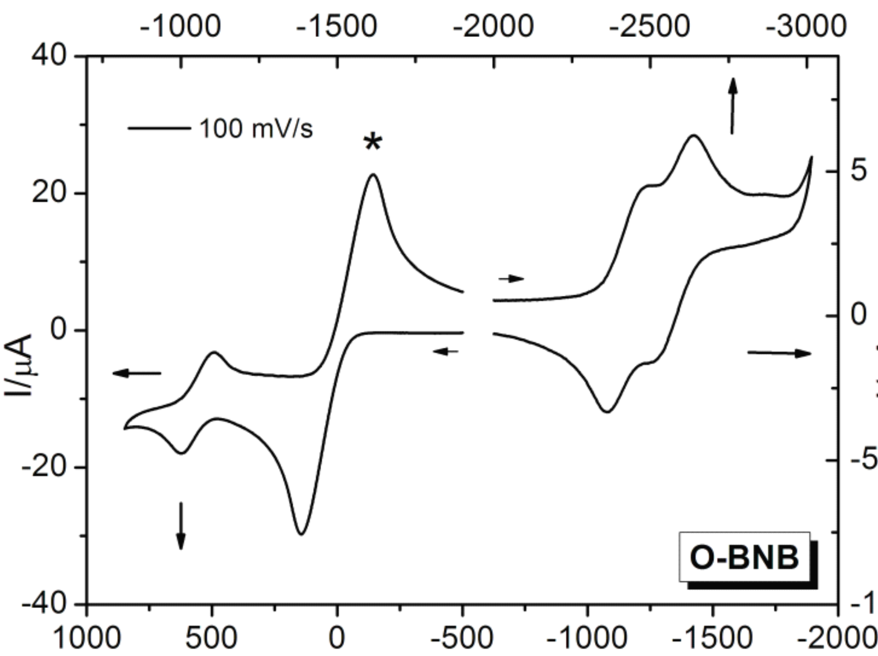

Figure 2-11. Cyclic voltammetry plots for oligomers (reduction in THF and oxidation in CH_2Cl_2 containing 0.1 M Bu_4NPF_6; recorded *vs* $Fc^{0/+}$ (Fc = $[(\eta\text{-}C_5H_5)_2Fe]$ as an internal reference (indicated with an asterisk).

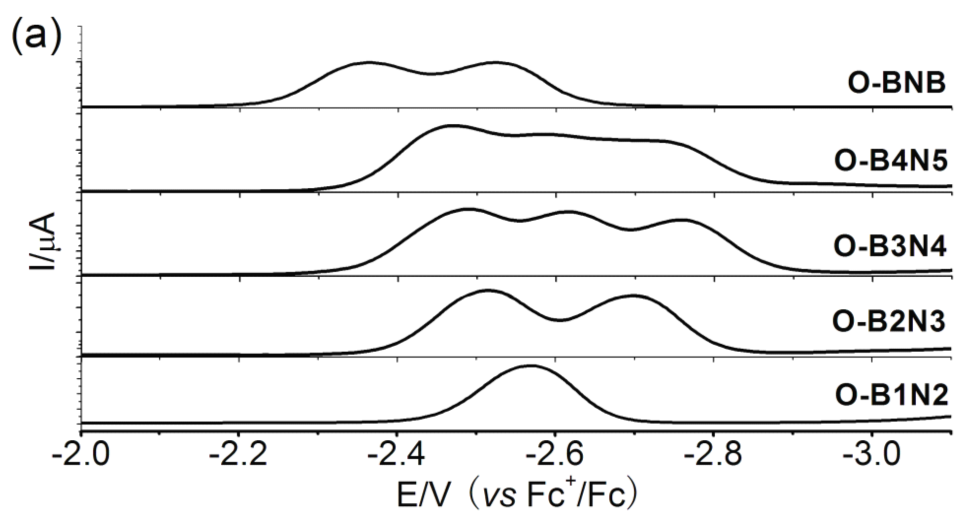

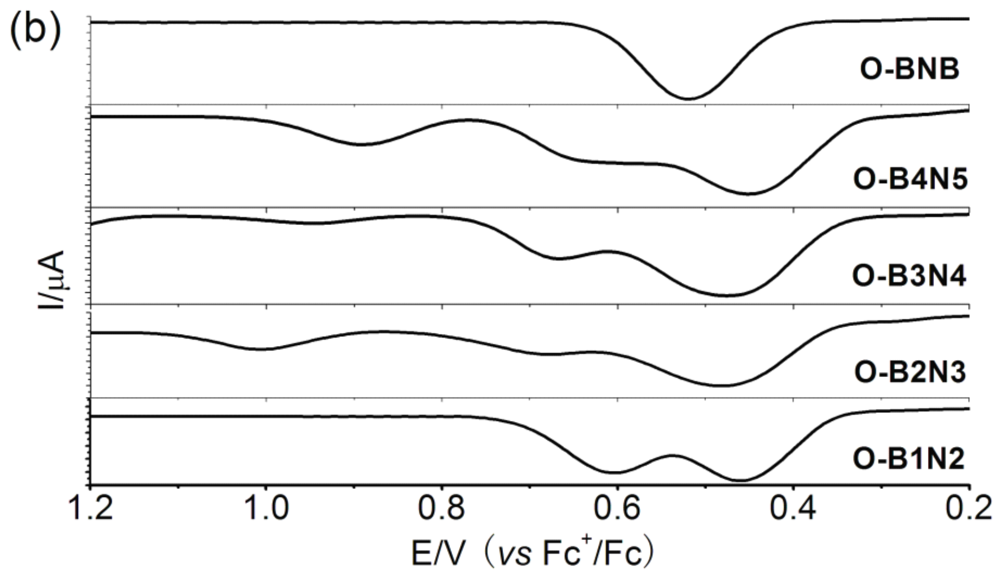

Figure 2-12. Square wave voltammograms for oligomers **O-B*n*N*m*** and **O-BNB**: (a) reduction in THF and (b) oxidation in CH_2Cl_2 /0.1 M Bu_4NPF_6 vs Fc^+/Fc.

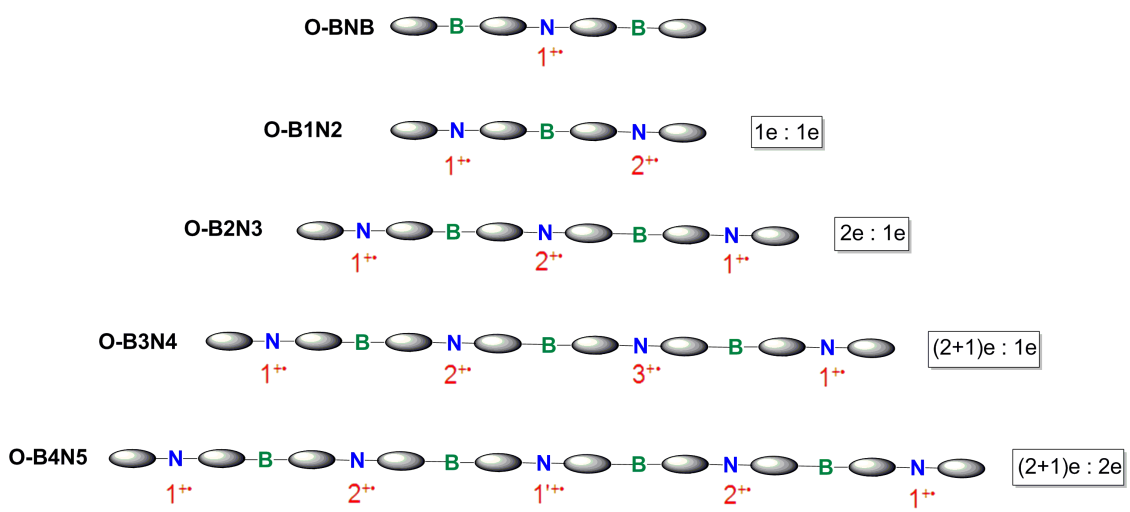

Scheme 2-2. Simplified schematic representation of assignments for electrochemical oxidation on N donor sites in oligomers **O-B*n*N*m*** and **O-BNB**; only the most probable configurations are given for the higher oligomers. The π systems are phenyl groups.

Table 2-4. Electrochemical Data Obtained from Cyclic Voltamnmetry (CV) and Square Wave Voltammetry (SWV) Measurements

	O-B1N2 (V)	**O-B2N3** (V)	**O-B3N4** (V)	**O-B4N5** (V)	**O-BNB** (V)
$E^{1}_{1/2,\,CV}$	–2.60	–2.58	–2.50	nd	–2.43
E^{p1}_{SWV}	–2.57	–2.51	–2.49	–2.47 (2e)	–2.36
$E^{2}_{1/2,\,CV}$		–2.76	nd	nd	–2.58
E^{p2}_{SWV}		–2.70	–2.62	–2.58	–2.52
$E^{3}_{1/2,\,CV}$			nd	nd	
E^{p3}_{SWV}			–2.76	–2.73	
E^{p1}_{SWV}	0.46	0.48 (2e)	0.47 (3e)	0.45 (3e)	0.52
$E^{1}_{1/2,\,CV}$	0.47	0.52	0.51	0.49	0.55
E^{pa1}_{CV}	0.52	0.63	0.64	0.67	0.61
E^{pa2}_{SWV}	0.60	0.68	0.66	0.64 (2e)	
E^{pa2}_{CV}	0.68	0.82	0.89	0.93	
E^{p3}_{SWV}		1.01 [a]	0.95 [a]	0.89 [a]	
E^{pa3}_{CV}		1.10	1.15	1.18	

[a] Attributed to double oxidation of the terminal arylamines

Even though the redox processes for the higher oligomers are not fully reversible, the electrochemical HOMO and LUMO levels can be estimated from the first square wave potentials using the equations

$$E_{HOMO} = -(E^{SWV}_{ox} + 4.8) \quad (eV)$$

$$E_{LUMO} = -(E^{SWV}_{red} + 4.8) \quad (eV)$$

As shown in **Table 2-5**, the optical HOMO-LUMO energy gaps are close to the electrochemical energy gaps. However, they slightly deviate from the DFT calculated energy gaps, because the energy levels are in general calculated on the basis of static structures that correspond to the lowest energy ground state, while the electrochemical data are measured for the time-averaged structures on the voltammetric time scale, which are dynamic probably adopting different conformations.[64]

Table 2-5. Comparison of the Orbital Energy Levels (eV) for Oligomers **O-B*n*N*m*** and **O-BNB**

	$\lambda_{edge, abs}$	DFT Results[a]				Electrochemical Results		
		HOMO	LUMO	$E_{gap, DFT}$	$\lambda_{abs,TD\text{-}DFT}$	HOMO	LUMO	$E_{gap,SWV}$
O-B1N2	2.96	–4.93	–1.52	3.41	2.93	–5.26	–2.23	3.03
O-B2N3	2.87	–4.93	–1.66	3.27	2.78	–5.28	–2.29	2.99
O-B3N4	2.83	–4.93	–1.71	3.22	2.73	–5.27	–2.31	2.96
O-B4N5	2.81	–4.93	–1.74	3.19	2.71	–5.25	–2.33	2.92
O-BNB	2.88	–5.09	–1.80	3.29	2.83	–5.32	–2.44	2.88

[a] The Me groups on fluorene, ^{i}Pr on Tip and ^{t}Bu on TPA are replaced with H.

Taking into account the fully reversible reduction and oxidation under ambient conditions, **O-B1N2** and **O-BNB** are particularly promising for applications both as p-type and as n-type charge transporting materials. Oligomers **O-B2N3**, **O-B3N4** and **O-B4N5** can potentially serve as n-type semiconducting materials in electronic devices. We estimated the reorganization energies of **O-B*n*N*m*** by plotting the LUMO energies from the DFT calculations versus the first reductive potentials determined by square wave voltammetry. In general, a linear dependence should result for structurally related compounds. As illustrated in **Figure 2-13**, a linear correlation was formulated in the equation:

$$E^{0/-}\,[V] = -1.56 + 0.44\ E_{LUMO}\ [eV]$$

The calculated LUMO energies and the reduction potentials show a reasonable correlation, thus suggesting that a small reorganization energy is needed to switch the neutral and radical anion state, which is a prerequisite for electronic applications.[65,66]

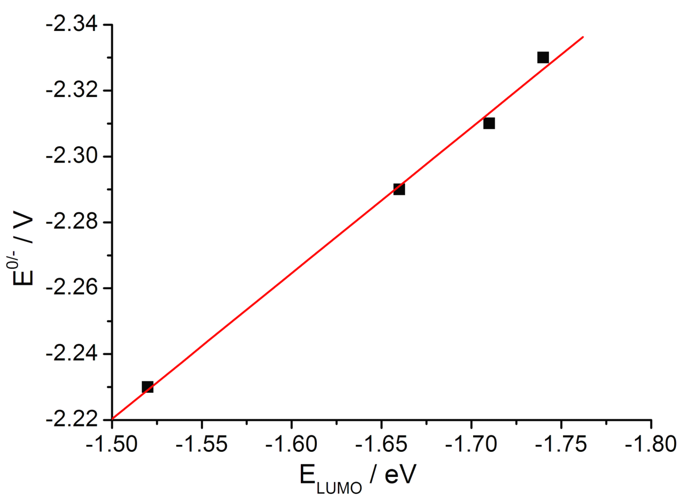

Figure 2-13. Linear correlation of LUMO energies (DFT, B3LYP/6-31G*) with first reduction potentials for oligomers **O-B*n*N*m*** (square wave, standard ferrocene).

2.4 Anion Binding Studies

The binding of small anions to these organoboranes has been investigated by UV and emission titration experiments (**Figures 2-14** to **2-18**). Stepwise addition of CN^- to a solution of **O-B1N2** in toluene leads to an attenuation both in UV absorption and emission intensity. Based on the absorption data analysis (**Table 2-6**), we found that there is no significant interaction between the boron sites in each oligomer, which is verified by the small differences generated for the binding constants. This is not too surprising because adjacent borons are separated by electron-rich N-centered π bridges. Observed here is also that the molar extinction coefficient increases as the chain extension goes further, which is consistent with the trend of the oscillator strength determined by TD-DFT calculations. An interesting observation is that intermediates that are generated from partially complexed species remain emissive, which is in contrast to what we observed for the oligomers **O-B*n*** in Chapter 1. Moreover, the oligomers that feature more than one boron center give intermediates that show a bathochromic tailing of the emission band. This could be due to stronger D-A interactions as a result of the increasing D/A ratio upon anion complexation. For instance, the ratio of 3:2 for the initial D-A-D-A-D model in **O-B2N3** turns to a ratio of 4:1 for the charged D-D-D-A-D species as the tetracoordinated boron serves as a donor rather than an acceptor.

Table 2-6. Summary of Results from Anion Binding Analysis for **O-B*n*N*m***

compound	$\lg\beta_{11}$	$\lg\beta_{12}$	$\lg\beta_{13}$	$\lg\beta_{14}$	f
O-B1N2	7.6				0.82
O-B2N3	7.5	15.4			1.16
O-B3N4	7.5	14.5	21.5		1.45
O-B4N5	7.5	15.0	22.5	29.4	2.00

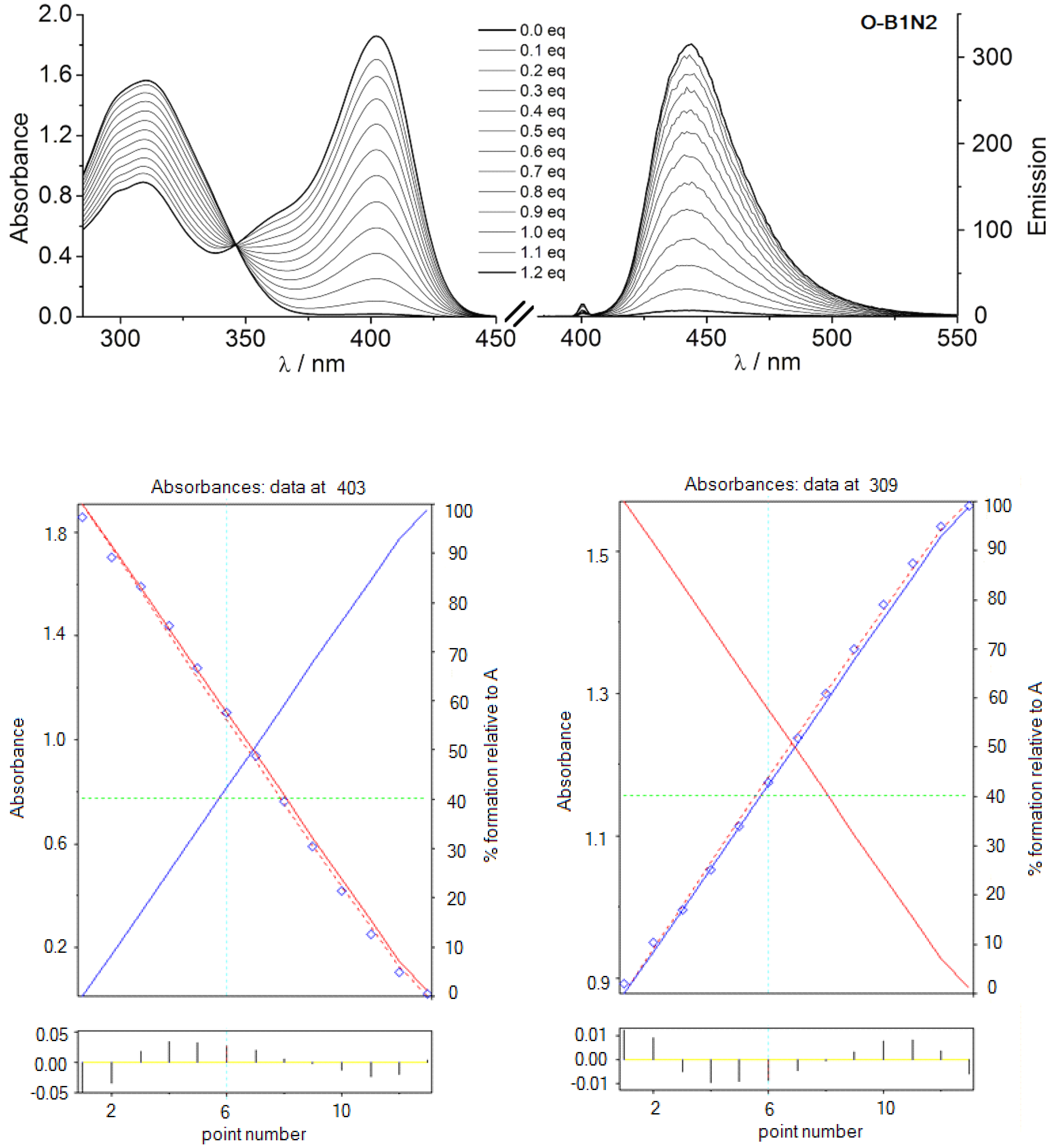

Figure 2-14. Complexation of **O-B1N2** with CN^{-} anions (1.04×10^{-3} M) in toluene, monitored by UV-vis and fluorescence spectroscopy. [**O-B1N2**] = 4.92×10^{-5} M; λ_{exc} = 403 nm. Bottom: Fit of absorption data (Hyperquad™) at λ = 403 and 309 nm.

Table 2-7. Relative concentrations of individual complexes after addition of varying amounts of CN^{-} to a solution of **O-B1N2** in toluene based on the binding constants in Table 2-6.

CN^{-} (eq)	[**O-B1N2**] (%)	[**O-B1N2**]CN (%)
1.0	15.6	84.4
1.2	1.6	98.4

Table 2-8. Relative concentrations of individual complexes after addition of varying amounts of CN^{-} to a solution of **O-B2N3** in toluene based on the binding constants in Table 2-6.

CN^{-} (eq)	[**O-B2N3**] (%)	[**O-B2N3**]CN (%)	**[O-B2N3](**$CN)_2$ (%)
1.0	43.6	23.8	32.6
2.0	2.2	8.7	89.1
2.2	0.0	1.4	98.6

Table 2-9. Relative concentrations of individual complexes after addition of varying amounts of CN^{-} to a solution of **O-B3N4** in toluene based on the binding constants in Table 2-6.

CN^{-} (eq)	[**O-B3N4**] (%)	[**O-B3N4**]CN (%)	**[O-B3N4](**$CN)_2$ (%)	[**O-B3N4](**$CN)_3$ (%)
0.96	26.3	41.9	21.1	10.7
1.92	2.7	15.8	28.7	52.8
3.36	0.0	0.0	2.1	97.9

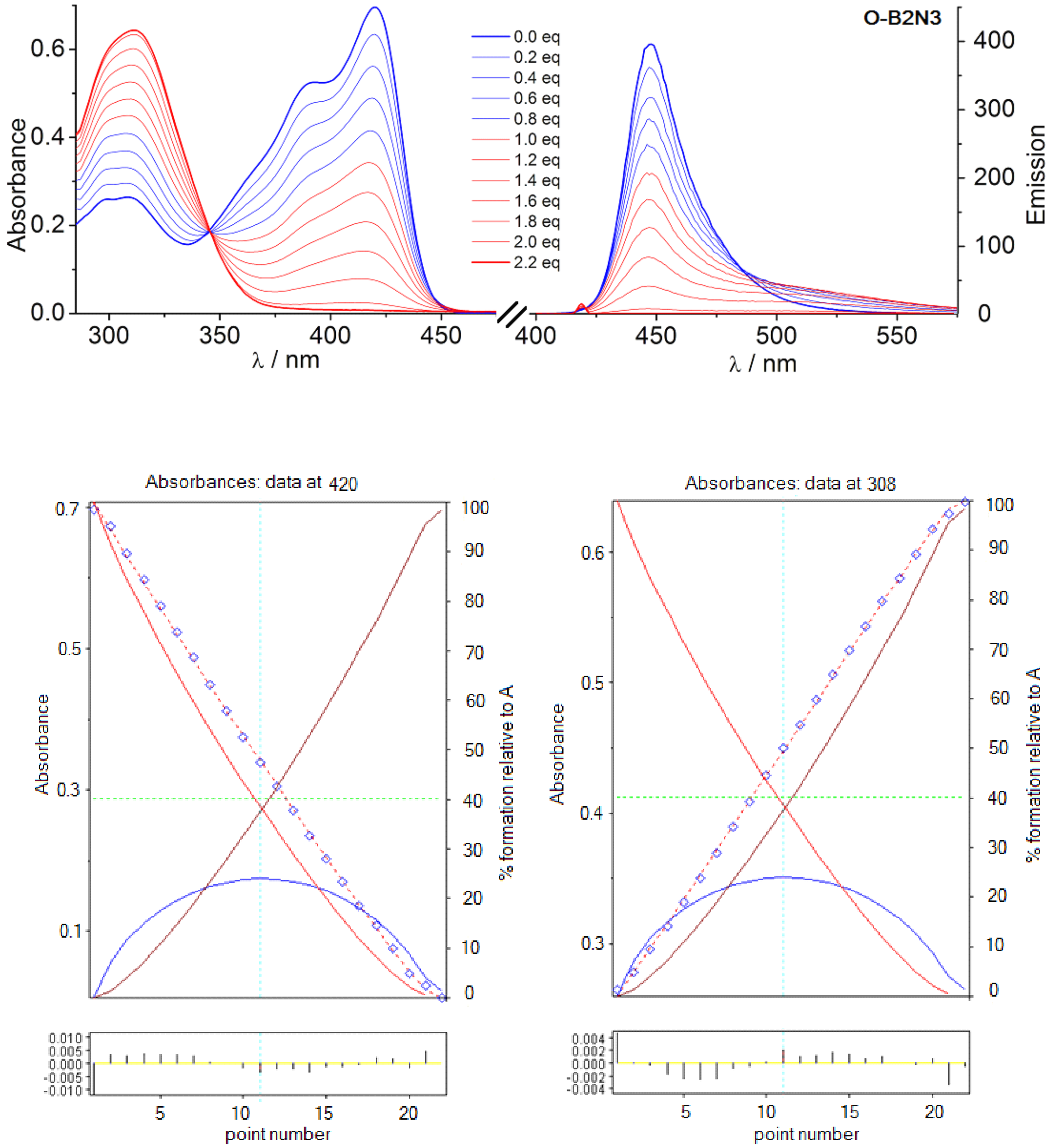

Figure 2-15. Complexation of **O-B2N3** with CN^{-} anions (1.04×10^{-3} M) in toluene, monitored by UV-vis and fluorescence spectroscopy. [**O-B2N3**] = 9.39×10^{-6} M; λ_{exc} = 420 nm. Bottom: Fit of absorption data (Hyperquad™) at λ = 420 and 308 nm.

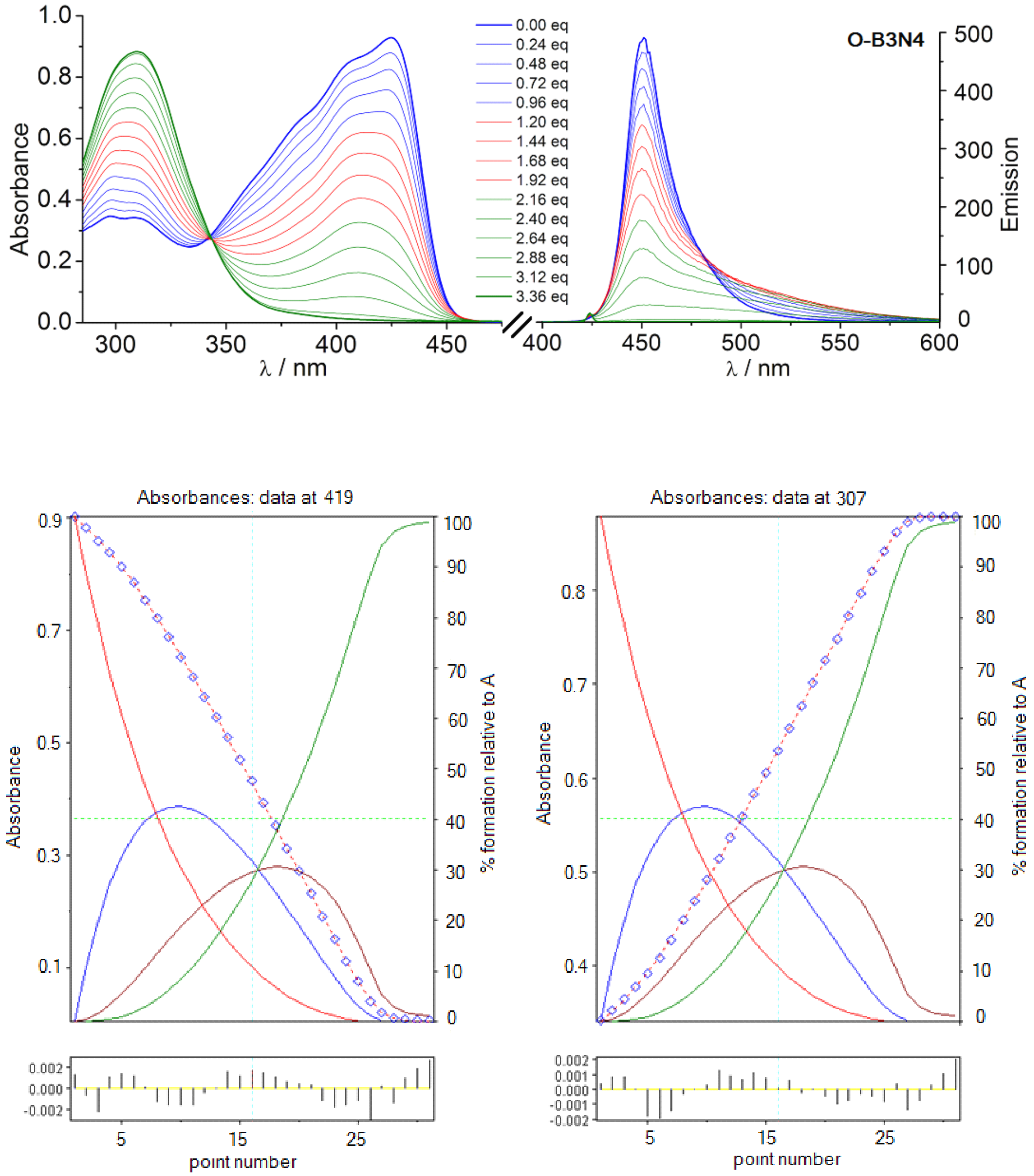

Figure 2-16. Complexation of **O-B3N4** with CN^- anions (5.20×10^{-4} M) in toluene, monitored by UV-vis and fluorescence spectroscopy. [**O-B3N4**] = 9.56×10^{-6} M; λ_{exc} = 426 nm. Bottom: Fit of absorption data (Hyperquad™) at λ = 419 and 307 nm.

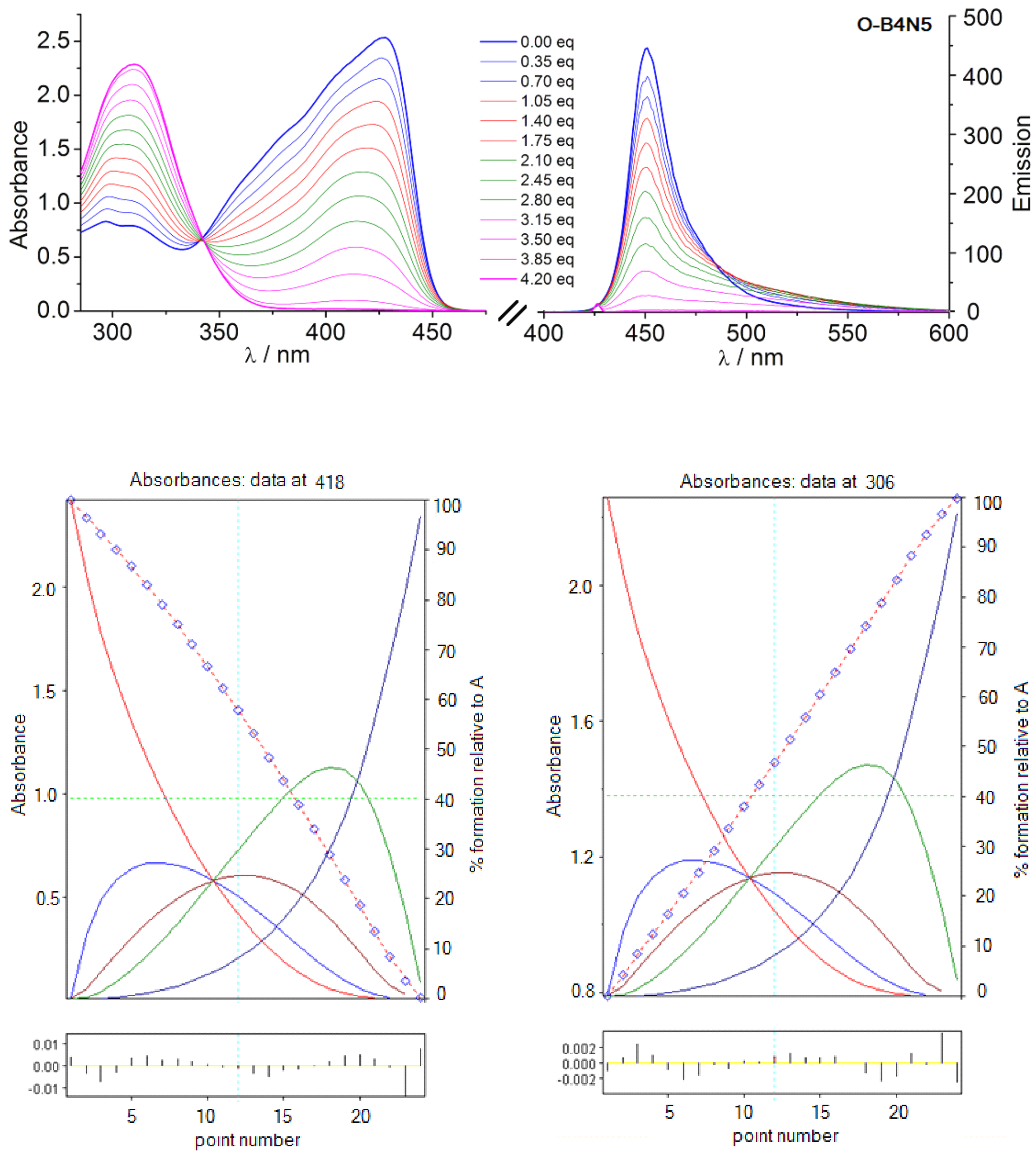

Figure 2-17. Complexation of **O-B4N5** with CN^- anions (1.04×10^{-3} M) in toluene, monitored by UV-vis and fluorescence spectroscopy. [**O-B4N5**] = 2.13×10^{-5} M; λ_{exc} = 428 nm. Bottom: Fit of absorption data (Hyperquad™) at λ = 418 and 306 nm.

Table 2-10. Relative concentrations of individual complexes after addition of varying amounts of CN^{-} to a solution of **O-B4N5** in toluene based on the binding constants in Table 2-6.

CN^{-} (eq)	[**O-B4N5**] (%)	[**O-B4N5**]CN (%)	[**O-B4N5**]$(CN)_2$ (%)	[**O-B4N5**]$(CN)_3$ (%)	[**O-B4N5**]$(CN)_4$ (%)
1.05	48.2	27.0	15.2	8.5	1.1
2.10	20.9	22.5	24.2	26.1	6.3
3.15	3.4	8.0	19.1	45.4	24.1
4.20	0.0	0.0	0.0	3.2	96.8

Table 2-11. Relative concentrations of individual complexes after addition of varying amounts of CN^{-} to a solution of **O-BNB** in toluene based on the binding constants of $\lg\beta_{11} = 8.0$ and $\lg\beta_{12} = 14.7$.

CN^{-} (eq)	[**O-BNB**] (%)	[**O-BNB**]CN (%)	[**O-BNB**]$(CN)_2$ (%)
1.0	13.6	68.8	17.6
2.0	0.0	6.9	93.0

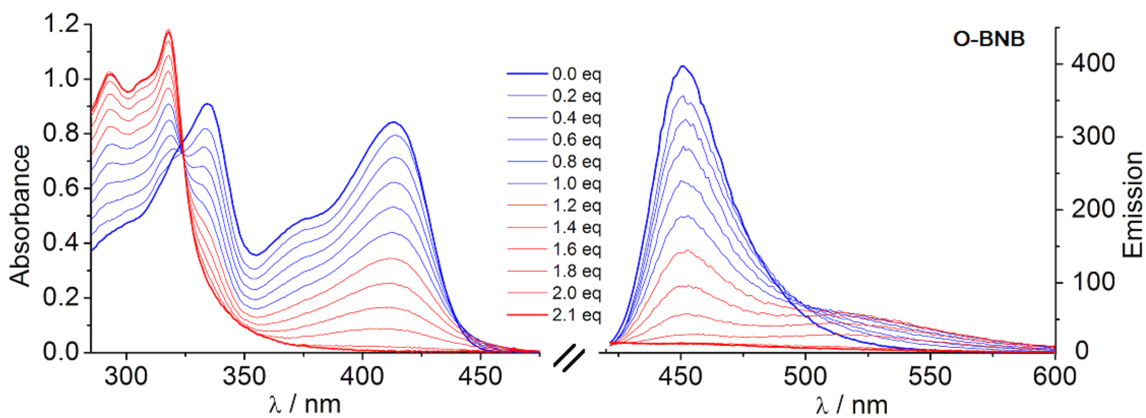

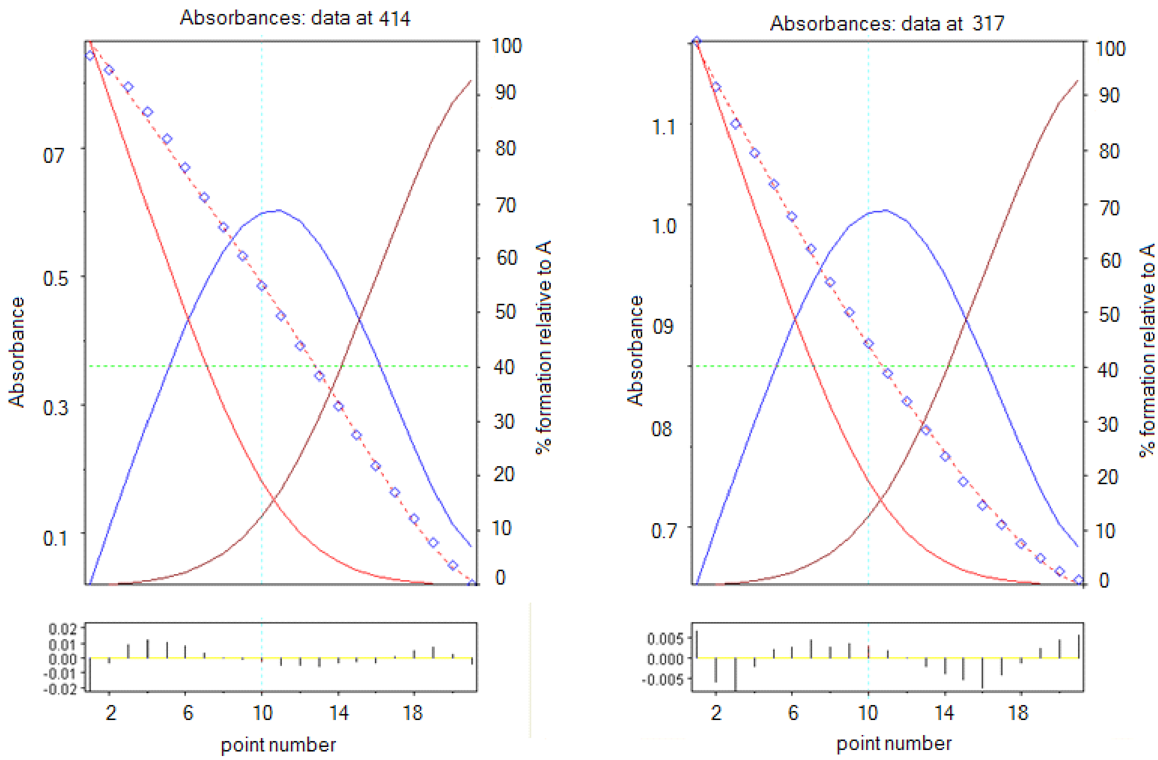

Figure 2-18. Complexation of **O-BNB** with CN^- anions (1.04×10^{-3} M) in toluene, monitored by UV-vis and fluorescence spectroscopy. [**O-BNB**] = 1.79×10^{-5} M; λ_{exc} = 414 nm. Bottom: Fit of absorption data (Hyperquad^{TM}) at λ = 414 and 317 nm.

2.5 Conclusions

Taking advantage of selective B/Si and B/Sn exchange, we have achieved a series of well-defined ambipolar oligomers in which N donors are separated from B acceptors by phenylene π bridges. Our focus has been on the electronic structure by looking into their photophysical, electrochemical characteristics in combination with DFT and TD-DFT computations. The effective conjugation length for **O-B*n*N*m*** is estimated to reach n = 4. A solvatochromic effect is apparent in the emission but not in the absorption spectra, an indication of intramolecular charge transfer (ICT) form N to B. This solvatochromic effect is much more pronounced for the shorter than the longer oligomers. It is ultimately responsible for the unusual observation that in polar solvents the emission wavelength experiences a hypsochromic shift with extension of the chain length. The anion binding of oligomers **O-B*n*N*m*** leads to a gradual decrease in the emission intensity and the partially charged intermediates stay emissive. Moreover, a cooperative binding effect was observed for this series of ambipolar oligomers. However, these characteristics were not detected in the electron-deficient fluoreneborane oligomers **O-B*n***. These oligomers are also promising to be used for n- and p-type semiconductor materials.

2.6 Experimental Section

Materials and General Methods. *n*-BuLi (1.6 M in hexanes), BBr_3, and tetrabutylammonium cyanide (TBACN) were purchased from Aldrich, Me_3SiCl and 1,3,5-triisopropylbenzene from Acros, Me_3SnCl from Strem chemicals, benzo[a]pyrene from TCI chemicals, propylene carbonate (PC) from Alfa Aesar, and Bio-Beads S-X Beads from Bio-Rad Laboratories (Hercules, CA, USA). Me_3SiCl was distilled under vacuum and all other commercially available chemicals were used as received without further purification. *t*-Butyl-N,N-bis(4-bromophenyl)aniline,[67] 7-dibromoboryl-2-trimethylsilyl-9,9-dimethyl-fluorene[58] (Fl-SiB), and 2,4,6-triisopropylphenyl copper[68] (TipCu) were prepared according to the previously published procedures. Tetrahydrofuran (THF) was distilled from Na/benzophenone prior to use. Hexanes and toluene were purified using a solvent purification system (Innovative Technologies;

alumina/copper columns). Dichloromethane (DCM) and $CDCl_3$ were distilled from CaH_2 and degassed via several freeze-pump-thaw cycles for use with air-sensitive compounds. All reactions and manipulations were carried out under an atmosphere of prepurified nitrogen using either Schlenk techniques or an inert-atmosphere glove box.

All 499.893 MHz ^{1}H, 125.7 MHz ^{13}C, 160.4 MHz ^{11}B NMR, 99.25 MHz ^{29}Si NMR, and 186.455 MHz ^{119}Sn NMR spectra were recorded on a Varian INOVA spectrometer equipped with a boron-free 5 mm dual broadband gradient probe (Nalorac, Varian Inc., Martinez, CA). ^{11}B NMR spectra were acquired with boron-free quartz NMR tubes and the spectra were referenced externally to $BF_3 \cdot Et_2O$ (δ = 0). ^{29}Si NMR spectra were referenced to $SiMe_4$ (δ = 0). All NMR spectra were obtained at ambient temperature.

High resolution MALDI-MS measurements were performed on an Apex-ultra 7T Hybrid FT-MS (Bruker Daltonics) in linear (+) mode. Benzo[a]pyrene (10 mg/mL) used as the matrix was mixed with the samples (10 mg/mL in toluene) in a 10:1 ratio, and then spotted on the wells of a target plate inside a glove box.

GPC analyses were performed in THF (1 mL/min) using a Waters Breeze system equipped with a 717 plus autosampler, a 1525 binary HPLC pump, a 2998 photodiode array detector, and a 2414 refractive index detector. For separation, the samples were passed through a series of styragel columns (Polymer Laboratories; two columns: Plgel 5 μm 100 Å and 500 Å), which were kept in a column heater at 35 °C. The columns were calibrated with low molecular weight polystyrene standards (Polymer Laboratories, range from 1300 to 5780 Da).

UV-visible absorption data were acquired on a Varian Cary 500 UV-Vis/NIR spectrophotometer. The fluorescence data and quantum yields were measured on a Varian Cary Eclipse fluorescence spectrophotometer using optically dilute solutions (A < 0.1). The quantum yields (Φ) in DCM were calculated using 9,10-diphenylanthracene as a standard (Φ = 0.92 in CH_2Cl_2).[69] Sample solutions were prepared using a microbalance (± 0.1 mg) and volumetric flasks. For titration experiments, cyanide ion solutions were prepared by dissolving the desired amount of solid TBACN in toluene; stock solutions of the samples were prepared in toluene in the glove box. Addition of cyanide to the sample solution was performed through a microsyringe (± 0.1 μL) to minimize exposure to air. Binding constants β_{1n} are given in units of M^{-n}. In the case of lower oligomers **O-B1N2** and **O-B2N3**, all the constants are automatically generated from the Hyperquad™. However, in higher oligomers, the binding constant lgβ_{11} had to be manually fixed to allow for a stable refinement.

Cyclic voltammetry (CV) and square wave voltammetry (SWV) experiments were carried out on a BAS CV-50W analyzer. The three-electrode system consisted of an Au disk as working electrode, a Pt wire as secondary electrode and an Ag wire as a pseudo reference electrode. The voltammograms were recorded with ca. 10^{-3} to 10^{-4} M sample solution in THF with $Bu_4N[PF_6]$ (0.1 M) as the supporting electrolyte for the reduction and in CH_2Cl_2 with $Bu_4N[PF_6]$ (0.1 M) for the oxidation scans. The scans were referenced after the addition of a small amount of ferrocene as an internal standard. The potentials are reported relative to the Fc/Fc^+ couple.

DFT calculations (gas phase) were performed with the Gaussian03 program. Geometries and electronic properties were calculated by means of hybrid density functional B3LYP with the basis set of 6-31G(d). The input files and orbital representations were generated with Gaussview 3.07 (scaling radii of 75%, isovalue of 0.02). Excitation data were calculated using TD-DFT (B3LYP, 6-31G(d)).

Synthesis of t-butyl-N,N-bis(4-trimethylsilylphenyl)aniline (TPA-Si2). t-Butyl-N,N-bis-(4-bromophenyl)aniline (4.6 g, 10.0 mmol) was dissolved in 150 mL of dry THF. The solution was cooled to –78 °C and *n*-BuLi (15.6 mL, 1.6 M in hexanes, 25.0 mmol) was added through an addition funnel under N_2. At this temperature the reaction mixture was stirred for one more hour followed by stirring at R.T. for 0.5 h. The reaction mixture was cooled back to –78 °C, and then dry Me_3SiCl (3.2 mL, 25.0 mmol) was added via syringe. The reaction mixture was kept stirring at R.T. overnight. After standard workup the crude material was purified by recrystallization from ethanol/hexanes mixture solvent to give colorless block-shaped crystals (3.4 g, 76%). ^{1}H NMR (600 MHz, $CDCl_3$): δ 0.26 (s, 18H), 1.32 (s, 9H), 7.05–7.07 (m, 6H), 7.28 (d, J = 9.0 Hz, 2H), 7.37 (d, J = 8.4 Hz, 4H). ^{29}Si NMR (99.25 MHz, $CDCl_3$): δ –4.74. High res. MALDI-MS (pos.) *m/z*: calcd. for $C_{28}H_{39}NSi_2$ [M^+] 445.2616, found 445.2616.

Synthesis of 4-(t-butyl)-N-(4-(trimethylsilyl)phenyl)-N-(4-(trimethylstannyl)phenyl)-aniline (TPA-SiSn). 4-Bromo-N-(4-(t-butyl)phenyl)-N-(4-(trimethylsilyl)phenyl)aniline (9.5 g, 21 mmol) was dissolved in 200 mL of dry THF. The solution was cooled to –78 °C and *n*-BuLi (17.0 mL, 1.6 M in hexanes, 27.2 mmol) was added through an addition funnel under N_2. At this temperature the reaction mixture was stirred for one more hour followed by stirring at R.T. for 0.5 h. The reaction mixture was cooled back to –78 °C, and then Me_3SnCl (5.4 g, 27 mmol) in 10 mL of dry THF was added via syringe. The reaction mixture was kept stirring at R.T. overnight. After standard workup the crude material was purified by recrystallization from hexanes to give colorless block-shaped crystals (7.6 g, 67%). ^{1}H NMR (499.893 MHz, $CDCl_3$): δ 0.25 (s, 9H), 0.28 (s/d, $J(^{117/119}$Sn, H) = 53.0/55.0 Hz, 9H), 1.32 (s, 9H), 7.05–7.09 (m, 6H), 7.27 (d, J = 8.5 Hz, 2H), 7.35 (d, J = 6.5 Hz, 2H), 7.37 (d, J = 6.5 Hz, 2H). ^{29}Si NMR (99.25 MHz, $CDCl_3$): δ –4.77. ^{119}Sn NMR (186.455 MHz, $CDCl_3$): δ –25.7. High res. MALDI-MS (pos.) *m/z*: calcd. for $C_{28}H_{39}NSiSn$ [M^+] 537.1873, found 537.1812.

Synthesis of t-butyl-N,N-bis(4-(trimethylstannyl)phenyl)aniline (TPA-Sn2). t-Butyl-N,N-bis-(4-bromophenyl)aniline (1.0 g, 2.2 mmol) was dissolved in 80 mL of dry THF. The solution was cooled to –78 °C and *n*-BuLi (3.4 mL, 1.6 M in hexanes, 5.5 mmol) was added through an addition funnel under N_2. At this temperature the reaction mixture was stirred for one more hour followed by stirring at R.T. for 0.5 h. The reaction mixture was cooled back to –78 °C, and then Me_3SnCl (1.1 g, 5.5 mmol) in 3 mL of THF was added via syringe. The reaction mixture was kept stirring at R.T. overnight. After standard workup the crude material was purified by recrystallization from ethanol to give colorless block-shaped crystals (0.76 g, 56%). ^{1}H NMR (499.893 MHz, $CDCl_3$): δ 0.27 (s/d, $J(^{117/119}$Sn, H) = 52.5/54.5 Hz, 18H), 1.32 (s, 9H), 7.03–7.08 (m, 6H), 7.25 (d, J = 8.5 Hz, 2H), 7.34 (d/dd, J(H, H) = 8.0 Hz, $J(^{117/119}$Sn, H) = 44 Hz, 4H). ^{119}Sn NMR

(186.455 MHz, $CDCl_3$): δ –26.1. High res. MALDI-MS (pos.) *m/z*: calcd. for $C_{28}H_{39}NSn_2$ [M^+] 627.1131, found 627.1120.

Synthesis of 4-(t-butyl)-N-(4-(trimethylsilyl)phenyl)-N-(4-(dibromoboryl)phenyl)-aniline (TPA-SiB). To a solution of **TPA-Si2** (1.00 g, 2.24 mmol) in 15 mL of CH_2Cl_2 was added a solution of BBr_3 (0.56 g, 2.24 mmol) in 10 mL of CH_2Cl_2 at 0 °C with stirring. The reaction mixture was kept stirring overnight, and then all volatile components were removed under high vacuum. The crude product was purified by recrystallization from hexanes at –35 °C to give **TPA-SiB** as a yellow solid (0.92 g, 76%). ^{1}H NMR (499.893 MHz, $CDCl_3$): δ 0.28 (s, 9H), 1.34 (s, 9H), 6.92 (d, J = 9.0 Hz, 2H), 7.12 (d, J = 9.0 Hz, 2H), 7.17 (d, J = 8.0 Hz, 2H), 7.37 (d, J = 9.0 Hz, 2H), 7.49 (d, J = 8.5 Hz, 2H), 8.02 (d, J = 9.0 Hz, 2H). ^{13}C NMR (125.7 MHz, $CDCl_3$): δ –0.83, 31.60, 34.79, 117.82, 125.65, 126.64, 126.89, 134.90, 137.50, 139.99, 143.00, 146.39, 149.06, 154.45. ^{11}B NMR (160.4 MHz, $CDCl_3$): δ 53 ($w_{1/2}$ = 730 Hz). ^{29}Si NMR (99.25 MHz, $CDCl_3$): δ –4.09.

Synthesis of t-Butyl-N,N-bis(4-dibromoborylphenyl)aniline (TPA-B2). To BBr_3 (0.81 g, 3.25 mmol) in 10 mL of CH_2Cl_2 was added a solution of **TPA-Si2** (0.70 g, 1.57 mmol) in 25 mL CH_2Cl_2 with stirring. The reaction mixture was kept stirring overnight, and then all volatile components were removed under high vacuum. The crude product was purified by recrystallization from toluene at –35 °C to give **TPA-B2** as a yellow solid (0.91 g, 91%). ^{1}H NMR (499.893 MHz, $CDCl_3$): δ 1.37 (s, 9H), 7.10–7.14 (m, 6H), 7.42 (d, J = 8.5 Hz, 2H), 8.13 (d, J = 8.5 Hz, 4H). ^{13}C NMR (125.7 MHz, $CDCl_3$): δ 31.58, 34.92, 121.70, 127.21, 127.31, 139.81, 142.38, 150.24, 152.85. ^{11}B NMR (160.4 MHz, $CDCl_3$): δ 55 ($w_{1/2}$ = 1,000 Hz).

Synthesis of Monomer O-B1N2. To a solution of compound **TPA-SiB** (0.83 g, 1.53 mmol) in 20 mL of CH_2Cl_2 was added a solution of **TPA-SiSn** (0.82 g, 1.53 mmol) in 10 mL of CH_2Cl_2 and the mixture was kept stirring overnight. All volatile components were removed under vacuum, leaving behind a yellowish solid. Without further purification the crude product was dissolved in toluene (10 mL) and then treated with TipCu (0.41 g, 1.53 mmol) in 10 mL of toluene. The reaction mixture was refluxed at 120 °C under N_2 for 2 d. A solid precipitate (CuBr) was removed by filtration through a fritted glass disk. All volatile components were removed under high vacuum. The crude product was purified by preparative column chromatography on Bio-Beads S-X beads using THF as the eluent, and then precipitated from hexanes/toluene mixture (10:1) at –35 °C to give **O-B1N2** as a yellow powdery solid (0.96 g, 66%). ^{1}H NMR (499.893 MHz, $CDCl_3$): δ 0.26 (s, 18H), 1.01 (d, J = 6.5 Hz, 12H), 1.29 (d, J = 6.5 Hz, 6H), 1.33 (s, 18H), 2.49 (sept, J = 7.0 Hz, 2H), 2.91 (sept, J = 7.0 Hz, 1H), 6.96 (s, 2H), 7.02 (d, J = 8.5 Hz, 4H), 7.10 (d, J = 9.0 Hz, 4H), 7.13 (d, J = 8.5 Hz, 4H), 7.30 (d, J = 9.0 Hz, 4H), 7.40 (d, J = 8.5 Hz, 4H), 7.62 (d, J = 8.5 Hz, 4H). ^{13}C NMR (125.7 MHz, $CDCl_3$): –0.75, 24.39, 24.45, 31.64, 34.42, 34.62, 35.35, 120.18, 124.27, 125.84, 126.46, 134.51, 134.84, 135.83 (B-C), 139.42, 141.73 (B-C), 144.26, 147.34, 147.80, 147.97, 148.93, 150.70. ^{11}B NMR (160.4 MHz, $CDCl_3$): δ 71 ($w_{1/2}$ = 870 Hz). ^{29}Si NMR (99.25 MHz, $CDCl_3$): δ –4.43. High res. MALDI-MS (pos.) m/z: calcd. for $C_{65}H_{83}BN_2Si_2$ [M^+] 958.6193, found

958.6198.

Synthesis of Dimer O-B2N3. To solution of **TPA-B2** (0.91 g, 1.42 mmol) in 20 mL of CH_2Cl_2 was added a solution of **TPA-SiSn** (1.52 g, 2.84 mmol) in 10 mL of CH_2Cl_2 with stirring. The reaction mixture was kept stirring overnight, followed by the removal of all volatile components under high vacuum, leaving behind a yellow solid. Without further purification the crude product was dissolved in toluene (10 mL) and then treated with TipCu (0.75 g, 2.84 mmol) in 10 mL of toluene. The reaction mixture was refluxed at 120 °C under N_2 for 2 d. A solid precipitate (CuBr) was removed by filtration through a fritted glass disk. All volatile components were removed under high vacuum. The crude product was purified by preparative column chromatography on Bio-Beads S-X beads using THF as the eluent, and then precipitated from hexanes/toluene mixture at –35 °C to give **O-B2N3** as a yellow solid (1.29 g, 62%). ^{1}H NMR (499.893 MHz, $CDCl_3$): δ 0.26 (s, 18H), 1.00 (d, J = 8.5 Hz, 24H), 1.29 (d, J = 7.0 Hz, 12H), 1.32 (2 overlapping signals, 27H), 2.47 (sept, J = 6.5 Hz, 4H), 2.90 (sept, J = 7.0 Hz, 2H), 6.95 (s, 4H), 7.02 (d, J = 9.0 Hz, 4H), 7.10 (m, 10H), 7.13 (d, J = 8.5 Hz, 4H), 7.30 (m, 6H), 7.40 (d, J = 8.5 Hz, 4H), 7.62 (m, 8H). ^{13}C NMR (125.7 MHz, $CDCl_3$): –0.77, 24.37, 24.43, 31.63, 34.40, 34.63, 34.67, 35.39, 120.02, 121.76, 124.36, 125.89, 126.35, 126.48, 126.57, 134.52, 134.96, 135.58 (B-C), 137.11 (B-C), 139.19, 139.56, 141.62 (B-C), 144.00, 144.20, 147.41, 147.74, 147.87, 148.03, 148.94, 149.97, 150.88. ^{11}B NMR (160.4 MHz, $CDCl_3$): δ 71 ($w_{1/2}$ = 1,400 Hz). ^{29}Si NMR (99.25 MHz, $CDCl_3$): δ –4.5. High res. MALDI-MS (pos.) m/z: calcd. for $C_{102}H_{127}B_2N_3Si_2$ [M^+] 1471.9757, found 1471.9766.

Synthesis of Trimer O-B3N4. To a solution of BBr_3 (0.45 g, 1.80 mmol) in 5 mL of CH_2Cl_2 was added a solution of **O-B1N2** (0.80 g, 0.83 mmol) in 15 mL of CH_2Cl_2 with stirring. The reaction mixture was kept stirring overnight, and then all volatile components were removed under high vacuum. The crude product was purified by recrystallization from toluene at –35 °C to give **O-B1N2-BBr2** as a yellow solid (0.81 g, 81%). ^{1}H NMR (499.893 MHz, $CDCl_3$): δ 1.02 (d, J = 6.5 Hz, 12H), 1.30 (d, J = 7.0 Hz, 6H), 1.35 (s, 18H), 2.43 (sept, J = 6.5 Hz, 2H), 2.92 (sept, J = 6.5 Hz, 1H), 6.99 (s, 2H), 7.04 (d, J = 9.0 Hz, 4H), 7.12 (d, J = 9.0 Hz, 4H), 7.19 (d, J = 8.5 Hz, 4H), 7.38 (d, J = 9.0 Hz, 4H), 7.72 (d, J = 8.5 Hz, 4H), 8.06 (d, J = 9.0 Hz, 4H). ^{11}B NMR (160.4 MHz, $CDCl_3$): δ 53 (two overlapping B signals: $w_{1/2}$ = 2,000 Hz). To a solution of **O-B1N2-BBr2** (0.60 g, 0.52 mmol) in 20 mL of CH_2Cl_2 was added a solution of **TPA-SiSn** (0.56 g, 1.04 mmol) in 15 mL of CH_2Cl_2 with stirring. The reaction mixture was stirred overnight and all volatile components were removed under high vacuum, leaving behind a yellowish solid. Without further purification the crude product was dissolved in toluene (10 mL) and then treated with TipCu (0.28 g, 1.04 mmol) in 10 mL of toluene. The reaction mixture was refluxed at 120 °C under N_2 for 2 d. A solid precipitate (CuBr) was removed by filtration through a fritted glass disk. All volatile components were removed under high vacuum. The crude product was purified by preparative column chromatography on Bio-Beads S-X beads using THF as the eluent, and then precipitated from hexanes/toluene mixture at –35 °C to give **O-B3N4** as a yellow solid (0.59 g, 57%). ^{1}H NMR (499.893 MHz, $CDCl_3$): δ 0.26 (s, 18H), 1.00 (m, 36H), 1.29 (m, 18H), 1.32 (2 × s, 36H), 2.47 (m, 6H), 2.90 (m, 3H), 6.96 (2 × s, 6H), 7.02 (d, J = 8.5 Hz, 4H), 7.10 (m, 16H), 7.13 (d, J = 8.5 Hz, 4H), 7.30 (m, 8H), 7.41 (d, J = 8.0 Hz, 4H), 7.62 (m, 12H). ^{13}C NMR (125.7 MHz, $CDCl_3$): –0.77, 24.37, 24.42, 31.63, 34.40, 34.63, 34.68, 35.39, 35.43, 120.02, 121.65, 121.84, 124.36, 125.89, 126.39, 126.47, 126.58, 134.51, 134.97, 135.55 (B-C), 136.85 (B-C), 137.18 (B-C), 139.18, 139.34, 139.56, 141.51 (B-C), 141.60 (B-C), 143.97, 144.19, 147.42, 147.73, 147.92, 148.04, 148.10, 148.94, 149.91, 150.14, 150.88. ^{11}B NMR (160.4 MHz, $CDCl_3$): δ 72 (two overlapping B signals: $w_{1/2}$ = 2,100 Hz). ^{29}Si NMR (99.25 MHz, $CDCl_3$): δ –4.5. High res. MALDI-MS (pos.) *m/z*: calcd. for $C_{139}H_{171}B_3N_4Si_2$ [M^+] 1986.3377, found 1986.3349.

Synthesis of Tetramer O-B4N5. To a solution of BBr_3 (0.37 g, 1.50 mmol) in 5 mL of CH_2Cl_2 was added a solution of **O-B2N3** (1.00 g, 0.68 mmol) in 15 mL of CH_2Cl_2 with stirring. The reaction mixture was kept stirring overnight, and then all volatile components were removed under high vacuum. The crude product was purified by recrystallization from toluene at –35 °C to give **O-B2N3-BBr2** as a yellow solid (0.87 g, 77%). ^{1}H NMR (499.893 MHz, $CDCl_3$): δ 1.01 (d, J = 6.5 Hz, 24H), 1.30 (d, J = 7.0 Hz, 12H), 1.33 (s, 9H), 1.34 (s, 18H), 2.45 (sept, J = 7.0 Hz, 4H), 2.90 (sept, J = 7.0 Hz, 2H), 6.98 (s, 4H), 7.02 (d, J = 8.5 Hz, 4H), 7.12 (m, 8H), 7.18 (m, 8H), 7.38 (m, 6H), 7.66 (d, J = 8.0 Hz, 2H), 7.71 (d, J = 8.0 Hz, 4H), 8.05 (d, J = 9.0 Hz, 4H). ^{11}B NMR (160.4 MHz, $CDCl_3$): δ 54 (two overlapping B signals: $w_{1/2}$ = 2,300 Hz). To a solution of **O-B2N3-BBr2** (0.67 g, 0.40 mmol) in 20 mL of CH_2Cl_2 was added a solution of

TPA-SiSn (0.43 g, 0.80 mmol) in 15 mL of CH_2Cl_2 with stirring. The reaction mixture was stirred overnight and all volatile components were removed under high vacuum, leaving behind a yellow solid. Without further purification the crude product was dissolved in toluene (10 mL) and then treated with TipCu (0.21 g, 0.80 mmol) in 10 mL of toluene. The reaction mixture was refluxed at 120 °C under N_2 for 2 d. A solid precipitate (CuBr) was removed by filtration through a fritted glass disk. All volatile components were removed under high vacuum. The crude product was purified by preparative column chromatography on Bio-Beads S-X beads using THF as the eluent, and then precipitated from hexanes/toluene mixture at –35 °C to give **O-B4N5** as a yellow solid (0.52 g, 53%). ^{1}H NMR (499.893 MHz, $CDCl_3$): δ 0.26 (s, 18H), 1.00 (m, 48H), 1.30 (m, 24H), 1.33 (3 overlapping s, 45H), 2.47 (m, 8H), 2.91 (m, 4H), 6.96 (2 overlapping s, 8H), 7.02 (d, J = 8.5 Hz, 4H), 7.10 (m, 22H), 7.14 (d, J = 8.0 Hz, 4H), 7.31 (m, 10H), 7.41 (d, J = 8.5 Hz, 4H), 7.63 (m, 16H). ^{13}C NMR (125.7 MHz, $CDCl_3$): –0.76, 24.37, 24.43, 31.64, 34.40, 34.63, 34.68, 35.39, 35.43, 120.03, 121.65, 121.74, 121.86, 124.37, 125.90, 126.40, 126.48, 126.59, 134.52, 134.97, 135.54 (B-C), 136.85 (B-C), 136.92 (B-C), 137.19 (B-C), 139.19, 139.35, 139.57, 141.50 (B-C), 141.60 (B-C), 143.97, 144.19, 147.42, 147.73, 147.92, 148.04, 148.11, 148.96, 149.91, 150.10, 150.16, 150.88. ^{11}B NMR (160.4 MHz, $CDCl_3$): δ 69 (2 overlapping B signals: $w_{1/2}$ = 2,700 Hz).^{29}Si NMR (99.25 MHz, $CDCl_3$): δ –4.5. High res. MALDI-MS (pos.) *m/z*: calcd. for $C_{176}H_{215}B_4N_5Si_2$ [M^+] 2499.6960, found 2499.6879.

Synthesis of O-BNB. To a solution of compound **Fl-SiB** (0.41 g, 0.94 mmol) in 20 mL of CH_2Cl_2 was added a solution of **TPA-Sn2** (0.30 g, 0.47 mmol) in 10 mL of CH_2Cl_2 and the mixture was kept stirring overnight. All volatile components were removed under vacuum, leaving behind a yellowish solid. Without further purification the crude product was dissolved in toluene (10 mL) and then treated with TipCu (0.25 g, 0.94 mmol) in 10 mL of toluene. The reaction mixture was refluxed at 120 °C under N_2 for 2 d. A solid precipitate (CuBr) was removed by filtration through a fritted glass disk. All volatile components were removed under high vacuum. The crude product was purified by preparative column chromatography on Bio-Beads S-X beads using THF as the eluent, and then precipitated from hexanes/toluene mixture at –35 °C to give **O-BNB** as a yellow solid (0.84 g, 71%). ^{1}H NMR (499.893 MHz, $CDCl_3$): δ 0.33 (s, 18H, TMS), 1.00 (d, J = 7.0 Hz, 24H, Tip), 1.33 (d, J = 7.0 Hz, 12H, Tip), 1.35 (s, 9H, *t*-Bu), 1.50 (s, 12H, Fl), 2.48 (sept, J = 7.0 Hz, 4H, Tip), 2.95 (sept, J =7.0 Hz, 2H, Tip), 7.00 (s, 4H, Tip), 7.18 (m, 6H, TPA), 7.36 (d, J = 9.0 Hz, 2H, TPA), 7.54 (d, J = 8.5 Hz, 2H, Fl), 7.59 (s, 2H, Fl), 7.72 (d, J = 8.5 Hz, 4H, TPA), 7.78 (m, 6H, Fl), 7.82 (s, 2H, Fl). ^{13}C NMR (125.7 MHz, $CDCl_3$): –0.64, 24.34 (Tip_*C*H_3), 24.37 (Tip_*C*H_3), 27.34 (Fl_*C*H_3), 31.64 (C(*C*H_3)$_3$), 34.42 (*p*-Tip_*C*H(CH_3)$_2$), 34.72 (*C*(CH_3)$_3$), 35.54 (*o*-Tip_*C*H(CH_3)$_2$), 47.02 (Fl_*C*(CH_3)$_2$), 119.42, 120.14, 121.90, 126.47, 126.67, 127.54, 131.75, 132.32, 136.48, 136.98, 137.21, 139.71, 139.89, 140.56, 141.40 (B-C), 142.36, 142.60, 143.86, 148.14, 148.33, 149.02, 150.40, 152.95, 153.95. ^{11}B NMR (160.4 MHz, $CDCl_3$): δ 72 ($w_{1/2}$ = 1,750 Hz). ^{29}Si NMR (99.25 MHz, $CDCl_3$): δ –3.7. High res. MALDI-MS (pos.) *m/z*: calcd. for $C_{88}H_{109}B_2NSi_2$ [M^+] 1257.8305, found 1257.8305.

2.7 Reference

(1) Meijer, E. J.; Deleeuw, D. M.; Setayesh, S.; van Veenendaal, E.; Huisman, B. H.; Blom, P. W. M.; Hummelen, J. C.; Scherf, U.; Klapwijk, T. M. *Nat. Mater.* **2003**, *2*, 678.

(2) Forrest, S. R. *Nature* **2004**, *428*, 911.

(3) Yan, H.; Chen, Z.; Zheng, Y.; Newman, C. E.; Quin, J.; Dötz, F.; Kastler, M.; Facchetti, A. *Nature* **2009**, *457*, 679.

(4) Tsao, H. N.; Cho, D. M.; Park, I.; Hansen, M.; Mavrinskiy, A.; Yoon, D. Y.; Graf, R.; Pisula, W.; Spiess, H. W.; Müllen, K. *J. Am. Chem. Soc.* **2011**, *133*, 2605.

(5) Zaumseil, J.; Sirringhaus, H. *Chem. Rev.* **2007**, *107*, 1296.

(6) Günes, S.; Neugebauer, H.; Sariciftci, N. S. *Chem. Rev.* **2007**, *107*, 1324.

(7) Li, C.; Liu, M.; Pschirer, N. G.; Baumgarten, M.; Müllen, K. *Chem. Rev.* **2010**, *110*. 6817.

(8) Wang, C.; Dong, H.; Hu, W.; Liu, Y.; Zhu, D. *Chem. Rev.* **2012**, *112*, 2208.

(9) Beaujuge, P. M.; Fréchet, J. M. J. *J. Am. Chem. Soc.* **2011**, *133*, 20009.

(10) Szarko, J. M.; Guo, J.; Rolczynski, B. S.; Chen, L. X. *J. Mater. Chem.* **2011**, *21*, 7849.

(11) Tada, A.; Geng, Y.; Wei, Q.; Hashimoto, K.; Tajima, K. *Nat. Mater.* **2011**, *10*, 450.

(12) Didier, P.; Ulrich, G.; Mely, Y.; Ziessel, R. *Org. Biomol. Chem.* **2009**, *7*, 3639.

(13) Andrade, C. D.; Yanez, C. O.; Rodriguez, L.; Belfield, K. D. *J. Org. Chem.* **2010**, *75*, 3975.

(14) Velusamy, M.; Shen, J. Y.; Lin, J. T.; Lin, Y. C.; Hsieh, C. C.; Lai, C. H.; Lai, C. W.; Ho, M. L.; Chen, Y. C.; Chou, P .T.; Hisao, J. K. *Adv. Funct. Mater.* **2009**, *19*, 2388.

(15) Kwon, O.; Barlow, S.; Odom, S. A.; Beverina, L.; Thompson, N. J.; Zojer, E.; Brédas, J. L.; Marder, S. R. *J. Phys. Chem. A*. **2005**, *109*, 9346.

(16) Roquet, S.; Cravino, A.; Leriche, P.; Alévêque, O.; Frère, P.; Roncali, J. *J. Am. Chem. Soc.* **2006**, *128*, 3459.

(17) Zheng, R.; Häussler, M.; Dong, H.; Lam, J. W. Y.; Tang, B. Z. *Macromolecules* **2006**, *39*, 7973.

(18) Yamaguchi, S.; Akiyama, S.; Tamao, K. *J. Am. Chem. Soc.* **2001**, *123*, 11372.

(19) Yamaguchi, S.; Shirasaka, T.; Akiyama, S.; Tamao, K. *J. Am. Chem. Soc.* **2002**, *124*, 8816.

(20) Jäkle, F. *Coord. Chem. Rev.* **2006**, *250*, 1107.

(21) Jäkle, F. *Chem. Rev.* **2010**, *110*, 3985.

(22) Chiu, C. W.; Kim, Y.; Gabbai, F. P. *J. Am. Chem. Soc.* **2009**, *131*, 60.

(23) Kim, Y.; Gabbai, F. P. *J. Am. Chem. Soc.* **2009**, *131*, 3363.

(24) Hudnall, T. W.; Chiu, C. W.; Gabbai, F. P. *Acc. Chem. Res.* **2009**, *42*, 388.

(25) Wade, C. R.; Broomsgrove, A. E. J.; Aldridge, S.; Gabbaï, F. P. *Chem. Rev.* **2010**, *110*, 3958.

(26) Entwistle, C. D.; Marder, T. B. *Angew. Chem. Int. Ed.* **2002**, *41,* 2927.

(27) Entwistle, C. D.; Marder, T. B. *Chem. Mater.* **2004**, *16*, 4574.

(28) Liu, X. Y.; Bai, D. R.; Wang, S. *Angew. Chem. Int. Ed.* **2006,** *45,* 5475.

(29) Bai, D. R.; Liu, X. Y.; Wang, S. *Chem. Eur. J.* **2007**, *13*, 5713.

(30) Hudson, Z.; Liu, X. Y.; Wang, S. *Org. Lett.* **2011**, *13*, 300.

(31) Hudson, Z.; Wang, S. *Acc. Chem. Res.* **2009**, *42*, 1584.

(32) Lambert, C.; Stadler, S.; Bourhill, G.; Bräuchle, C. *Angew. Chem. Int. Ed. Engl.* **1996**, *35*, 644.

(33) Stahl, R.; Lambert, C.; Kaiser, C.; Wortmann, R.; Jakober, R. *Chem. Eur. J.* **2006**, *12*, 2358.

(34) Reitzenstein, D.; Lambert, C. *Macromolecules* **2009**, *42*, 773.

(35) Heckmann, A.; Lambert, C. *Angew. Chem. Int. Ed.* **2012**, *51*, 326.

(36) Yuan, M. S.; Liu, Z. Q.; Fang, Q. *J. Org. Chem.* **2007**, *72*, 7915.

(37) Zhou, G.; Baumgarten, M.; Müllen, K. *J. Am. Chem. Soc.* **2008**, *130*, 12477.

(38) Proń, A.; Zhou, G.; Norouzi-Arasi, H.; Baumgarten, M.; Müllen, K. *Org. Lett.* **2009**, *11*, 3550.

(39) Proń, A.; Baumgarten, M.; Müllen, K. *Org. Lett.* **2010**, *12*, 4236.

(40) Makarov, N. S.; Mukhopadhyay, S.; Yesudas, K.; Brédas, J.; Perry, J. W.; Pron, A.; Kivala, M.; Müllen, K. *J. Phys. Chem. A.* **2012**, *116*, 3781.

(41) Schmidt, H. C.; Reuter, L. G.; Hamacek, J.; Wenger, O. S. *J. Org. Chem.* **2011**, *76*, 9081.

(42) Agou, T.; Kojima, T.; Kobayashi, J.; Kawashima, T. *Org. Lett.* **2009**, *11,* 3534.

(43) Li, H.; Jäkle, F. *Macromol. Rapid Commun.* **2010**, *31*, 915.

(44) Geng, Y.; Trajkovska, A.; Katsis, D.; Ou, J. J.; Culligan, S. W.; Chen, S. H. *J. Am. Chem. Soc.* **2002**, *124*, 8337.

(45) Jo, J.; Chi, C.; Höger, S.; Wegner, G.; Yoon, D. Y. *Chem. -Eur. J.* **2004**, *10*, 2681.

(46) Wang, Q.; Qu, Y.; Tian, H.; Geng, Y.; Wang, F. *Macromolecules* **2011**, *44*, 1256.

(47) Anémian, R.; Mulatier, J.; Andraud, C.; Stéphan, O.; Vial, J. *Chem. Commun.* **2002**, 1608.

(48) Ohkubo, K.; Sakamoto, Y.; Suzuki, T.; Tsuzuki, T.; Kumaki, D.; Tokito, S. *Chem. Eur. J.* **2008**, *14*, 4472.

(49) Ma, C.; Mena-Osteritz, E.; Debaerdemaeker, T.; Wienk, M. M.; Janssen, R. A. J.; Bäuerle, P. *Angew. Chem. Int. Ed.* **2007**, *46*, 1679.

(50) Allard, S.; Forster, M.; Souharce, B.; Thiem, H.; Scherf, U. *Angew. Chem. Int. Ed.* **2008**, *47*, 4070.

(51) Mishra, A.; Ma, C.; Bäuerle, P. *Chem. Rev.* **2009**, *109*, 1141.

(52) Mishra, A.; Bäuerle, P. *Angew. Chem. Int. Ed.* **2012**, *51*, 2020.

(53) Sadighi, J. P.; Singer, R. A.; Buchwald, S. L. *J. Am. Chem. Soc.* **1998**, *120*,

4960.

(54) Wang, Y.; Tran, H. D.; Liao, L.; Duan, X.; Kaner, R. B. *J. Am. Chem. Soc.* **2010**, *132*, 10365.

(55) Wang, Y.; Liu, J.; Tran, H. D.; Mecklenburg, M.; Guan, X. N.; Stieg, A. Z.; Regan, B. C.; Martin, D. C.; Kaner, R. B. *J. Am. Chem. Soc.* **2012**, *134*, 9251.

(56) Nepomnyashchii, A. B.; Bröring, M.; Ahrens, J.; Bard, A. J. *J. Am. Chem. Soc.* **2011**, *133*, 8633.

(57) Rihn, S.; Erdem, M.; De Nicola, A.; Retailleau, P.; Ziessel, R. *Org. Lett.* **2011**, *13*, 1916.

(58) Chen, P.; Lalancette, R. A.; Jäkle, F. *J. Am. Chem. Soc.* **2011**, *133*, 8802.

(59) Chen, P.; Jäkle, F. *J. Am. Chem. Soc.* **2011**, *133*, 20142.

(60) Lakowicz, J. R. *Principles of Fluorescence Spectroscopy*, 3rd ed., Springer, Berlin, **2006**, pp. 205–213.

(61) Zhou, G.; Baumgarten, M.; Müllen, K. *J. Am. Chem. Soc.* **2007**, *129*, 12211.

(62) Leliège, A.; Blanchard, P.; Rousseau, T.; Roncali, J. *Org. Lett.* **2011**, *13*, 3098.

(63) Suk, J.; Wu, Z.; Wang, L.; Bard, A. J. *J. Am. Chem. Soc.* **2011***, 133,* 14675.

(64) Iwamoto, T.; Watanabe, Y.; Sakamoto, Y.; Suzuki, T.; Yamago, S. *J. Am. Chem. Soc.* **2011***, 133,* 8354.

(65) Winkler, M.; Houk, K. N. *J. Am. Chem. Soc.* **2007***, 129,* 1805.

(66) Lindner, B. D.; Engelhart, J. U.; Tverskoy, O.; Appleton, A. L.; Rominger, F.; Peters, A.; Himmel, H.; Bunz, U. H. *Angew. Chem. Int. Ed.* **2011**, *50*, 8588.

(67) Jiang, Z.; Zhang, W.; Yao, H.; Yang, C.; Cao, Y.; Qin, J.; Yu, G.; Liu,Y. *J. Polym. Sci. Part A: Polym. Chem.* **2009**, *47*, 3651.

(68) Sasaki, S.; Sutoh, K.; Murakami, F.; Yoshifuji, M. *J. Am. Chem. Soc.* **2002**, *124*, 14830.

(69) Murov, S. L.; Carmichael, I.; Hug, G. L. *Handbook of Photochemistry*, 2nd ed., Marcel Dekker: New York, **1993**.

Appendix

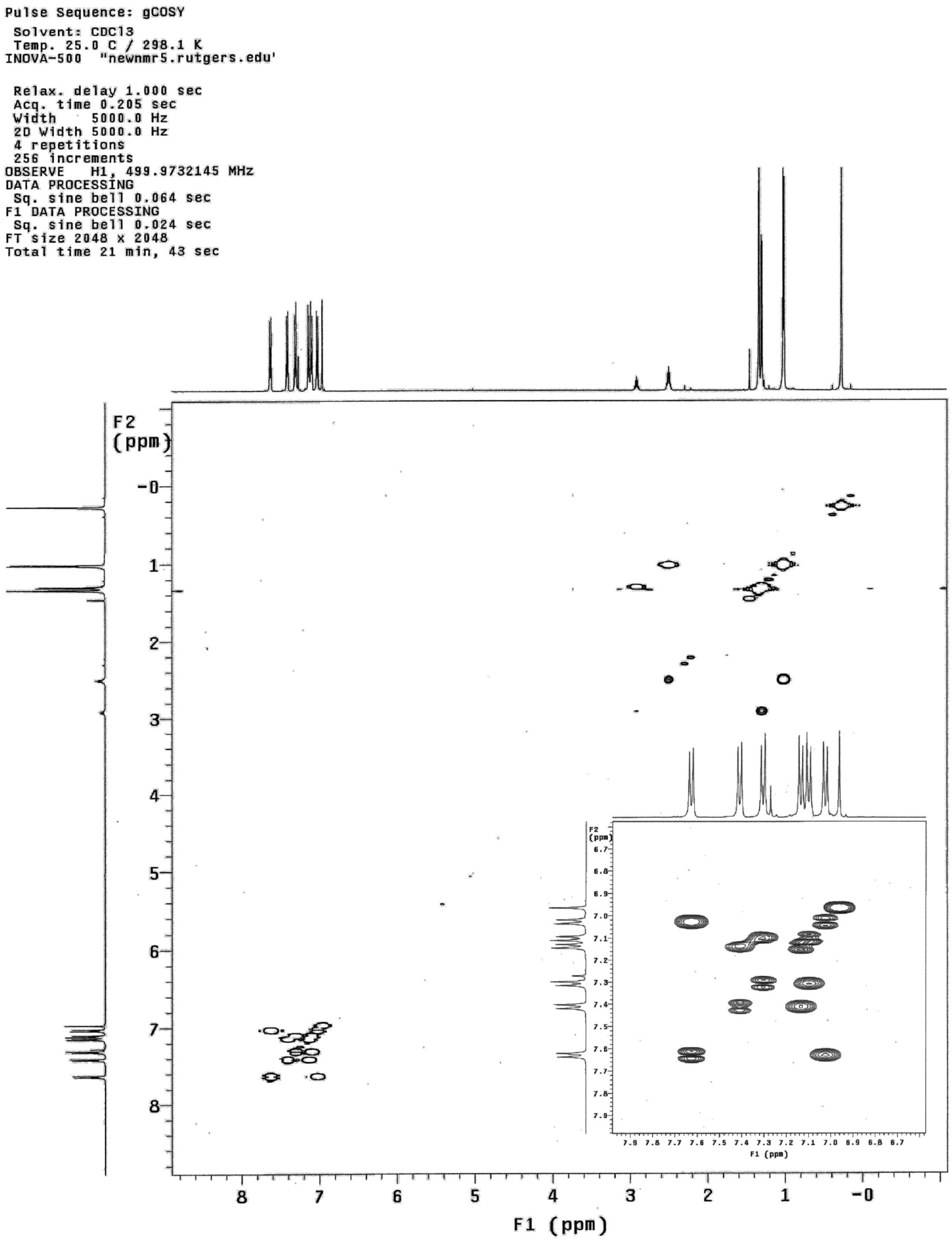

Figure 1. gCOSY NMR spectrum of **O-B1N2** and expansion of the aromatic region.

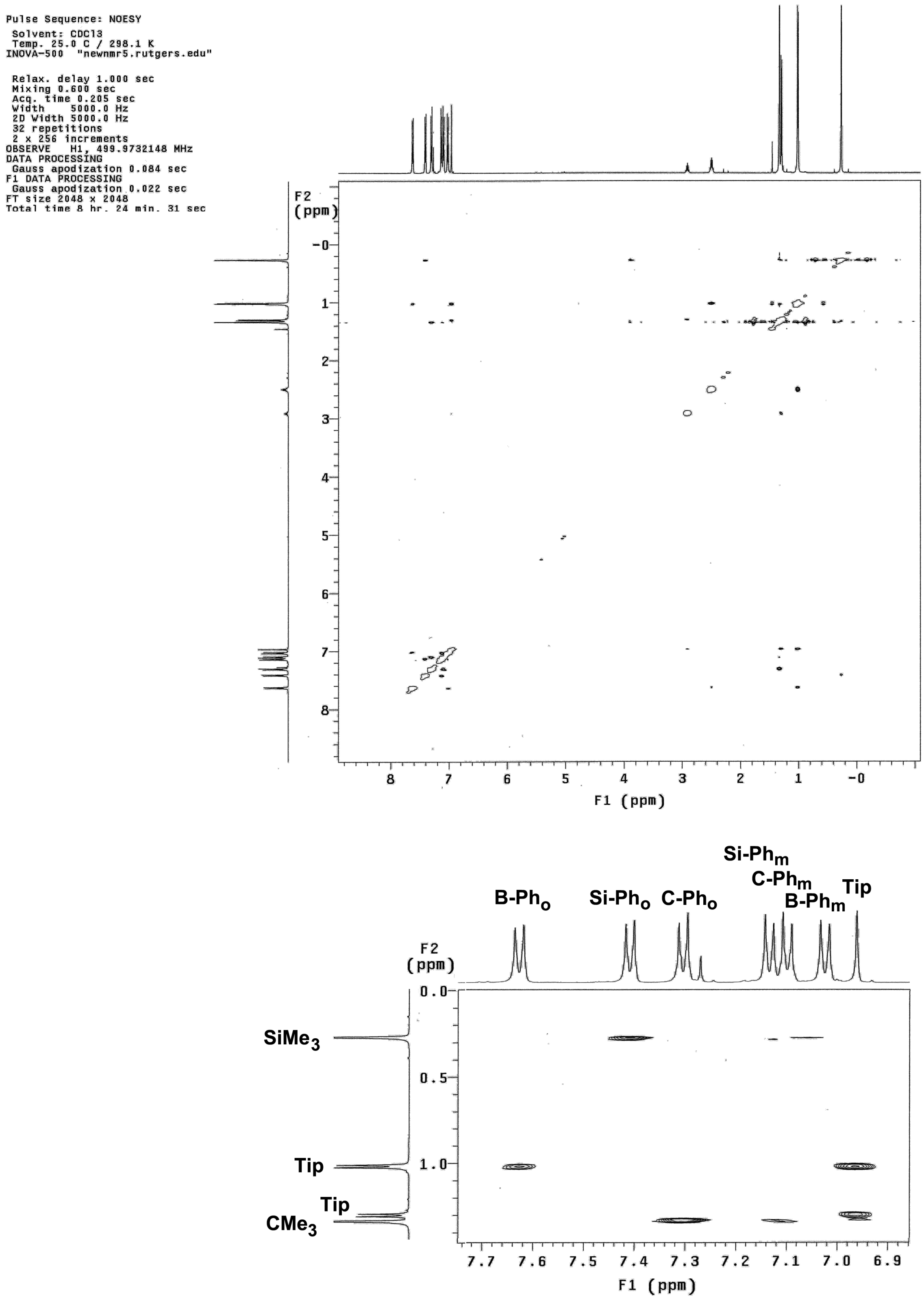

Figure 2. HH-NOESY spectrum of **O-B1N2** and expansion in the aromatic region.

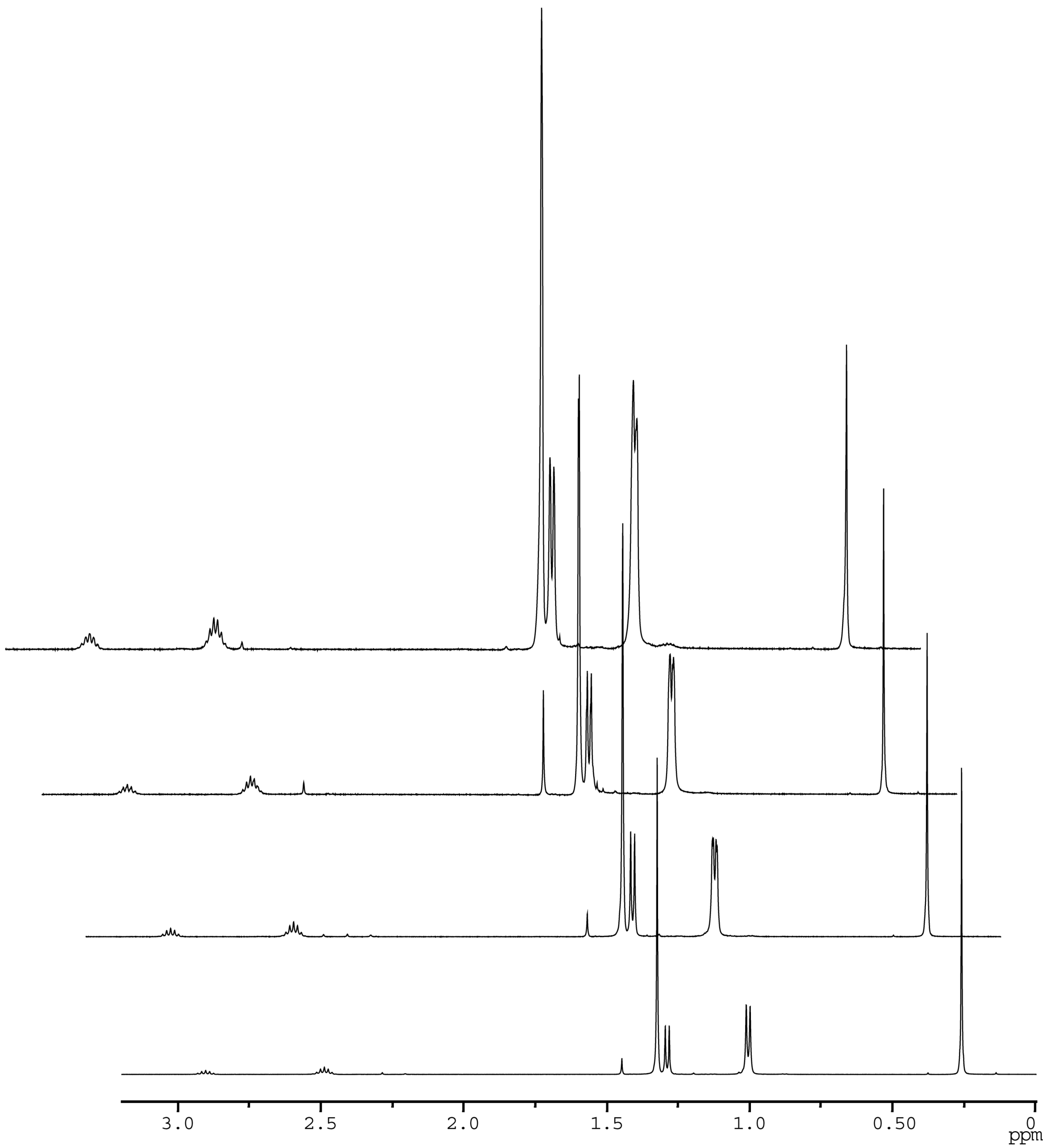

Figure 3. Overlay of the aliphatic region of the [1]H NMR spectra of the oligomers **O-B*n*N*m***, normalized to the $SiMe_3$ end group signal at 0.26 ppm ($CDCl_3$, 25 °C). The peak at 1.42 ppm for **O-B3N4** is due to a trace of butylate hydroxytoluene (BHT).

Table 1. Coordinates (Å) for the Optimized Structure of **O-B1N2**

atom	x	y	z	atom	x	y	z
C	5.091446	2.758203	-0.183351	C	-1.513016	0.483582	-0.617271
C	4.272026	3.435690	-1.099235	C	-2.499916	-1.322438	0.606795
C	4.288883	4.828054	-1.159315	C	-2.723138	1.166140	-0.606983
C	5.132508	5.564101	-0.324387	H	-0.669942	0.936227	-1.132176
C	5.955756	4.891347	0.581018	C	-3.708147	-0.639200	0.662024
C	5.932182	3.500092	0.660280	H	-2.433180	-2.291965	1.092876
H	3.625925	2.865344	-1.759136	C	-3.843503	0.618155	0.044658
H	3.648461	5.338070	-1.874166	H	-2.811170	2.126099	-1.105369
H	6.612604	5.451544	1.241331	H	-4.555118	-1.072238	1.184171
H	6.563986	2.979998	1.373398	C	0.010022	-3.133869	-0.070585
N	5.078469	1.334495	-0.114990	C	1.004691	-3.878902	0.599385
C	6.314671	0.633251	-0.058897	C	-0.983318	-3.868129	-0.754342
C	6.485509	-0.453561	0.814129	C	1.002571	-5.273518	0.599910
C	7.393823	1.024274	-0.864579	C	-0.978027	-5.262451	-0.781889
C	7.701770	-1.127866	0.863313	C	0.013145	-5.969669	-0.097878
H	5.662445	-0.761857	1.451382	H	1.773935	-5.818197	1.138988
C	8.609301	0.346312	-0.789960	H	-1.748304	-5.798354	-1.331220
H	7.275298	1.860511	-1.546661	N	-5.072009	1.316598	0.080647
C	8.802178	-0.750389	0.068862	C	-5.086807	2.740327	0.153091
H	7.793300	-1.963502	1.555284	C	-5.941193	3.481689	-0.677024
H	9.421519	0.680253	-1.431234	C	-4.257626	3.417708	1.060185
C	3.850451	0.633828	-0.102276	C	-5.968612	4.872660	-0.593228
C	2.721491	1.171621	0.542626	H	-6.580470	2.961264	-1.383256
C	3.725951	-0.616589	-0.735559	C	-4.278600	4.809807	1.124864
C	1.514064	0.484283	0.533857	H	-3.600713	2.847513	1.709470
H	2.801353	2.126622	1.051908	C	-5.135799	5.545376	0.303366
C	2.519478	-1.304388	-0.701080	H	-6.636141	5.432609	-1.242938
H	4.580201	-1.040403	-1.253562	H	-3.630634	5.319969	1.832775
C	1.363351	-0.781668	-0.077211	C	-6.309355	0.615356	0.052417
H	0.664432	0.927684	1.045913	C	-6.504245	-0.468482	-0.816324
H	2.460847	-2.268186	-1.199394	C	-7.367312	1.006243	0.888640
B	0.007563	-1.560501	-0.056935	C	-7.722532	-1.145199	-0.833585
C	-1.351514	-0.788116	-0.021361	H	-5.698793	-0.776721	-1.475778

C	-8.581906	0.328305	0.845887	H	-12.822586	-0.938421	-0.445195
H	-7.229416	1.841185	1.568629	H	-11.877945	0.384850	0.251476
C	-8.798812	-0.769436	-0.009717	H	-11.694340	-0.023019	-1.459216
H	-7.833247	-1.980256	-1.521329	C	-10.797745	-2.402837	1.692933
H	-9.375751	0.662559	1.511920	H	-11.770752	-2.908903	1.722838
Si	10.442705	-1.688312	0.170083	H	-10.031361	-3.136042	1.970524
Si	-10.460681	-1.673850	-0.024169	H	-10.805902	-1.626319	2.467261
C	11.722379	-0.869786	-0.960717	C	-10.426824	-3.069056	-1.303430
H	12.678290	-1.404481	-0.902020	H	-10.258740	-2.690899	-2.318783
H	11.407978	-0.878021	-2.011176	H	-9.643262	-3.804513	-1.08587
H	11.912046	0.172113	-0.676607	H	-11.384642	-3.603466	-1.307572
C	11.072075	-1.660354	1.957845	H	-5.154712	6.629939	0.361747
H	11.257956	-0.634158	2.296062	H	5.148399	6.648899	-0.379141
H	10.348377	-2.108696	2.649143	H	-1.765952	-3.331295	-1.283993
H	12.011000	-2.219374	2.056043	H	0.014449	-7.056925	-0.108430
C	10.179118	-3.485198	-0.372166	H	1.785781	-3.350745	1.139939
H	9.833164	-3.538310	-1.411160	H	9.429411	-3.988372	0.250168
H	11.109651	-4.061938	-0.299812	C	-11.840742	-0.449059	-0.459694

Table 2. Coordinates (Å) for the Optimized Structure of **O-B2N3**

atom	x	y	z	atom	x	y	z
C	0.382111	4.445400	-1.042038	C	6.279700	0.984630	0.293147
C	1.480226	5.247671	-0.697462	C	6.586037	-1.383204	0.481634
C	1.803335	6.362660	-1.468788	C	7.561799	1.119987	-0.224585
C	1.029680	6.703573	-2.580340	H	5.685238	1.882524	0.438159
C	-0.068895	5.911004	-2.919802	C	7.857690	-1.273355	-0.066463
C	-0.388549	4.784109	-2.164347	H	6.221169	-2.372569	0.743432
H	2.074629	4.991349	0.173913	C	8.371834	-0.013189	-0.423300
H	2.656657	6.975069	-1.189590	H	7.947412	2.102884	-0.475576
H	-0.675183	6.161356	-3.786333	H	8.461266	-2.161126	-0.225411
H	-1.234875	4.161687	-2.437446	C	3.987267	-1.579883	2.271667
N	0.055373	3.297718	-0.260123	C	2.742158	-2.245713	2.270898
C	-1.289403	3.072999	0.125741	C	4.938468	-2.009605	3.222488
C	-1.825433	1.773374	0.149391	C	2.465794	-3.287916	3.155362
C	-2.120991	4.149080	0.482446	C	4.660889	-3.032458	4.128936

C	-3.152857	1.569578	0.507805	C	3.423909	-3.679796	4.092822
H	-1.198360	0.931093	-0.124814	H	1.502666	-3.791127	3.118349
C	-3.441119	3.922358	0.853701	H	5.409383	-3.328873	4.859767
H	-1.722069	5.158439	0.473770	N	9.669694	0.112248	-0.970384
C	-4.011976	2.630010	0.873638	C	9.933421	1.089163	-1.973773
H	-3.537958	0.553537	0.506207	C	11.088612	1.882874	-1.904426
H	-4.052984	4.775131	1.135156	C	9.047445	1.264141	-3.048174
C	1.080341	2.391566	0.108672	C	11.352019	2.826975	-2.895432
C	2.117656	2.081993	-0.788193	H	11.774019	1.753392	-1.072784
C	1.090127	1.790487	1.379819	C	9.309839	2.222959	-4.024916
C	3.134071	1.212111	-0.412136	H	8.156774	0.646943	-3.110807
H	2.116229	2.525282	-1.778927	C	10.463859	3.006630	-3.958006
C	2.097847	0.898138	1.725094	H	12.250996	3.433978	-2.827357
H	0.305897	2.030951	2.090655	H	8.613981	2.346446	-4.850631
C	3.163899	0.580590	0.852193	C	10.723624	-0.737860	-0.534646
H	3.915668	0.989550	-1.133164	C	10.896066	-1.027675	0.826749
H	2.075467	0.451876	2.715437	C	11.618701	-1.296842	-1.460788
N	4.300066	-0.415012	1.261783	C	11.929639	-1.865333	1.241576
C	5.740284	-0.266124	0.672389	H	10.217424	-0.594916	1.555292
C	12.654422	-2.118510	-1.025955	C	-6.063730	4.689500	4.372189
H	11.494396	-1.084977	-2.518276	C	-7.410879	5.035178	4.244456
C	12.841684	-2.433636	0.334062	H	9.200474	4.810621	3.061266
H	12.028745	-2.066378	2.305650	H	-5.481528	5.067857	5.208882
H	13.324591	-2.534285	-1.776632	N	-8.573472	-1.932628	-1.173578
Si	14.254995	-3.564966	0.884658	C	-7.930413	-2.855650	-2.049339
C	15.916113	-2.760931	0.451073	C	-8.526770	-3.209249	-3.269256
H	16.755208	-3.410061	0.730871	C	-6.698244	-3.428349	-1.698594
H	15.998519	-2.559495	-0.623710	C	-7.903308	-4.124570	-4.115542
H	16.042869	-1.806479	0.975426	H	-9.477622	-2.764595	-3.545581
C	14.113459	-5.228654	-0.012637	C	-6.073442	-4.329400	-2.558920
H	14.941595	-5.895113	0.258811	H	-6.238052	-3.162276	-0.752283
H	13.177096	-5.738013	0.243632	C	-6.672703	-4.686398	-3.768890
H	14.133854	-5.105286	-1.102100	H	-8.377539	-4.388712	-5.057108
C	14.162969	-3.849444	2.754384	H	-5.119493	-4.764945	-2.273452
H	14.261243	-2.913954	3.317919	C	-9.963878	-2.076641	-0.913260
H	13.218536	-4.321211	3.050460	C	-10.806893	-0.956485	-0.862707
H	14.975151	-4.511931	3.077845	C	-10.523521	-3.349064	-0.714010

B	-5.507422	2.392591	1.272729	C	-12.168244	-1.111883	-0.608444
C	-6.325120	1.230436	0.620840	H	-10.391351	0.033372	-1.023914
C	-7.386354	0.585805	1.297317	C	-11.888263	-3.485398	-0.478202
C	-6.055657	0.763489	-0.686188	H	-9.883075	-4.225034	-0.744011
C	-8.111916	-0.454262	0.730235	C	-12.753491	-2.375932	-0.413766
H	-7.629637	0.892317	2.310934	H	-12.786825	-0.218023	-0.576006
C	-6.791592	-0.251790	-1.283932	H	-12.281762	-4.489231	-0.326976
H	-5.264173	1.234207	-1.262826	Si	-14.603898	-2.602418	-0.089937
C	-7.831554	-0.885722	-0.579414	C	-15.385487	-3.567889	-1.522117
H	-8.899025	-0.941944	1.296242	H	-14.910717	-4.547543	-1.654271
H	-6.570643	-0.558462	-2.301288	H	-16.454707	-3.739952	-1.346106
C	-6.188652	3.335253	2.331724	H	-15.286260	-3.023613	-2.468680
C	-7.551016	3.694277	2.238734	C	-15.443060	-0.911997	0.061475
C	-5.463542	3.864245	3.421740	H	-15.027577	-0.323007	0.887685
C	-8.152883	4.540442	3.169779	H	-15.343492	-0.319104	-0.855540
H	-16.515645	-1.036176	0.254367	H	1.279857	7.577397	-3.175237
C	-14.849327	-3.571945	1.520467	H	-8.143218	3.311496	1.411734
H	-14.358274	-4.551874	1.485373	H	-7.879517	5.686852	4.977876
H	-14.436653	-3.027847	2.378185	H	-4.411936	3.611619	3.529318
H	-15.914758	-3.745665	1.716461	H	5.908754	-1.521036	3.257445
H	10.668881	3.747945	-4.725115	H	1.983009	-1.946546	1.552888
H	-6.186321	-5.394567	-4.433702	H	3.207806	-4.484721	4.791071

Table 3. Coordinates (Å) for the Optimized Structure of **O-B3N4**

atom	x	y	z	atom	x	y	z
C	4.567799	2.161230	4.376196	C	-1.610997	-0.038691	2.100283
C	3.446657	2.759016	4.971177	C	-2.091740	-1.532867	0.290390
C	3.375822	2.891718	6.356833	C	-2.723553	-0.501864	2.791840
C	4.424531	2.448600	7.165718	H	-1.015806	0.750750	2.550762
C	5.545069	1.861215	6.574407	C	-3.189420	-2.032587	0.980352
C	5.616427	1.708608	5.190875	H	-1.857775	-1.955158	-0.682939
H	2.637235	3.116510	4.342475	C	-3.527055	-1.518033	2.244895
H	2.501408	3.357292	6.803803	H	-2.980590	-0.080259	3.758366
H	6.365206	1.506296	7.192905	H	-3.789998	-2.827217	0.549278
H	6.482392	1.240724	4.733345	C	0.000013	0.000008	-1.525221

N	4.642997	2.017756	2.958880	C	1.172342	-0.268609	-2.264789
C	5.835712	2.382442	2.284244	C	-1.172315	0.268647	-2.264783
C	6.322891	1.611821	1.214201	C	1.173849	-0.283284	-3.659276
C	6.563602	3.517071	2.682025	C	-1.173823	0.283353	-3.659270
C	7.506349	1.966910	0.576871	C	0.000013	0.000041	-4.360931
H	5.773629	0.731411	0.895846	H	2.089931	-0.509479	-4.199460
C	7.735729	3.865015	2.020808	H	-2.089904	0.509562	-4.199449
H	6.198905	4.124770	3.504112	N	-4.642973	-2.017760	2.958892
C	8.257656	3.103431	0.951209	C	-4.567746	-2.161307	4.376195
H	7.860435	1.344601	-0.240517	C	-5.616410	-1.708824	5.190909
H	8.267239	4.755482	2.345376	C	-3.446547	-2.759021	4.971142
C	3.527082	1.518017	2.244893	C	-5.545030	-1.861496	6.574430
C	2.723571	0.501863	2.791851	H	-6.482419	-1.240990	4.733411
C	3.189451	2.032554	0.980340	C	-3.375691	-2.891787	6.356790
C	1.611012	0.038687	2.100297	H	-2.637094	-3.116412	4.342421
H	2.980598	0.080268	3.758384	C	-4.424435	-2.448809	7.165706
C	2.091771	1.532829	0.290384	H	-6.365195	-1.506684	7.192951
H	3.790034	2.827172	0.549253	H	-2.501231	-3.357304	6.803729
C	1.251161	0.528869	0.823989	C	-5.835681	-2.382446	2.284243
H	1.015815	-0.750742	2.550790	C	-6.322877	-1.611774	1.214242
H	1.857813	1.955107	-0.682952	C	-6.563543	-3.517113	2.681957
N	0.000016	-0.000016	0.047528	C	-7.506325	-1.966855	0.576891
C	-1.251139	-0.528894	0.823983	H	-5.773634	-0.731333	0.895941
C	-7.735666	-3.865045	2.020721	H	-11.519597	0.844708	0.191566
H	-6.198836	-4.124848	3.504014	H	-12.829074	-1.893915	-2.857456
C	-8.257611	-3.103409	0.951170	C	-9.977126	-5.020634	0.101939
H	-7.860425	-1.344506	-0.240461	C	-11.318640	-5.454020	0.178698
H	-8.267155	-4.755542	2.345242	C	-8.995938	-6.016976	-0.093287
B	9.590565	3.501520	0.231087	C	-11.661586	-6.802194	0.079428
B	-9.590518	-3.501488	0.231037	C	-9.332107	-7.364349	-0.220698
C	10.536941	2.402197	-0.349880	C	-10.667912	-7.761326	-0.127796
C	10.613102	1.104344	0.206499	H	-12.702741	-7.105474	0.158550
C	11.379946	2.645629	-1.458708	H	-8.553994	-8.105456	-0.386392
C	11.470274	0.128606	-0.285916	N	13.154247	-0.592809	-1.917768
H	10.003674	0.864752	1.073544	N	-13.154261	0.592842	-1.917716
C	12.219755	1.673367	-1.987005	C	12.781111	-1.965493	-1.904938
H	11.354130	3.620344	-1.938081	C	13.712683	-2.953262	-1.547713

C	12.285725	0.395504	-1.401402	C	11.482885	-2.361333	-2.258296
H	11.519590	-0.844696	0.191507	C	13.346143	-4.295795	-1.551458
H	12.829112	1.893990	-2.857438	H	14.719738	-2.660867	-1.266772
C	9.977195	5.020664	0.102036	C	11.130058	-3.709499	-2.241237
C	11.318714	5.454031	0.178814	H	10.754470	-1.609363	-2.545756
C	8.996022	6.017024	-0.093180	C	12.046620	-4.717988	-1.893113
C	11.661678	6.802203	0.079583	H	14.097321	-5.030094	-1.265452
C	9.332209	7.364396	-0.220553	H	10.113543	-3.975325	-2.521622
C	10.668019	7.761354	-0.127625	C	14.421123	-0.223580	-2.456877
H	12.702836	7.105467	0.158722	C	14.857729	-0.765076	-3.675478
H	8.554108	8.105517	-0.386238	C	15.251727	0.676620	-1.771846
C	-10.536904	-2.402158	-0.349904	C	16.104152	-0.415622	-4.192185
C	-10.613085	-1.104321	0.206509	H	14.216070	-1.458527	-4.209976
C	-11.379898	-2.645572	-1.458745	C	16.488864	1.034100	-2.304716
C	-11.470264	-0.128579	-0.285885	H	14.921385	1.091190	-0.824648
H	-10.003667	-0.864748	1.073566	C	16.924740	0.488235	-3.514131
C	-12.219720	-1.673307	-1.987016	H	16.428107	-0.843462	-5.137288
H	-11.354068	-3.620274	-1.938142	H	17.120836	1.732571	-1.762502
C	-12.285707	-0.395461	-1.401382	C	-12.781158	1.965532	-1.904907
C	-13.712762	2.953287	-1.547718	C	-12.643023	7.480217	-3.153688
C	-11.482939	2.361401	-2.258256	H	-13.714253	7.365343	-2.949115
C	-13.346255	4.295828	-1.551479	H	-12.418826	8.554214	-3.145873
H	-14.719814	2.660875	-1.266786	H	-12.459992	7.108343	-4.168705
C	-11.130147	3.709576	-2.241219	C	-9.754971	6.760091	-2.316837
H	-10.754500	1.609450	-2.545703	H	-9.102535	6.248801	-1.599176
C	-12.046738	4.718050	-1.893124	H	-9.524517	6.369840	-3.315352
H	-14.097458	5.030114	-1.265504	H	-9.479721	7.821862	-2.310618
H	-10.113636	3.975424	-2.521597	C	-11.912398	7.275408	-0.159614
C	-14.421145	0.223571	-2.456778	H	-12.961984	7.160948	0.137085
C	-14.857787	0.764988	-3.675401	H	-11.299144	6.779797	0.602097
C	-15.251715	-0.676606	-1.771677	H	-11.677971	8.346831	-0.132175
C	-16.104216	0.415479	-4.192059	H	-17.892751	-0.763848	-3.922760
H	-14.216154	1.458421	-4.209954	H	-4.369190	-2.560375	8.244850
C	-16.488857	-1.034142	-2.304497	H	4.369303	2.560116	8.244868
H	-14.921340	-1.091115	-0.824463	H	17.892717	0.763687	-3.922994
C	-16.924771	-0.488354	-3.513933	H	-12.104002	-4.718675	0.332718
H	-16.428202	0.843258	-5.137180	H	-7.951283	-5.723969	-0.157993

H	-17.120802	-1.732596	-1.762228	H	-10.932934	-8.812141	-0.215810
Si	11.585998	-6.553300	-1.881728	H	2.095595	-0.482387	-1.732590
Si	-11.586156	6.553372	-1.881727	H	0.000013	0.000053	-5.448196
C	9.754745	-6.759952	-2.316587	H	-2.095568	0.482418	-1.732580
H	9.102414	-6.248636	-1.598849	C	12.104065	4.718670	0.332817
H	9.524186	-6.369695	-3.315076	H	7.951364	5.724032	-0.157909
H	9.479456	-7.821713	-2.310337	H	10.933055	8.812167	-0.215613
C	12.642634	-7.480132	-3.153890	H	12.962115	-7.160922	0.136875
H	13.713900	-7.365301	-2.949477	C	11.912497	-7.275416	-0.159697
H	12.418398	-8.554120	-3.146078	H	11.678132	-8.346854	-0.132291
H	12.459461	-7.108216	-4.168867	H	11.299316	-6.779885	0.602124

Table 4. Coordinates (Å) for the Optimized Structure of **O-B4N5**

atom	x	y	z	atom	x	y	z
C	-0.256870	0.854680	4.956428	C	-6.519123	-0.479751	2.252625
C	-1.322821	1.545838	5.551283	C	-7.041189	-1.792752	0.318118
C	-1.453043	1.573326	6.938689	C	-7.703825	-0.881092	2.857450
C	-0.516943	0.929509	7.750846	H	-5.877290	0.215767	2.786308
C	0.549598	0.248094	7.160420	C	-8.213397	-2.233315	0.920090
C	0.677683	0.201204	5.773235	H	-6.797680	-2.167112	-0.672393
H	-2.043344	2.057694	4.921055	C	-8.567415	-1.777563	2.202789
H	-2.283711	2.112953	7.385807	H	-7.970579	-0.503843	3.839475
H	1.281136	-0.262567	7.781042	H	-8.860572	-2.935908	0.404919
H	1.500238	-0.338965	5.314976	C	-4.725673	-0.339731	-1.282407
N	-0.125492	0.817817	3.535884	C	-3.546122	-0.661499	-1.988641
C	1.132429	1.090318	2.943720	C	-5.829927	0.091216	-2.049595
C	1.567624	0.377001	1.812860	C	-3.474511	-0.572184	-3.378477
C	1.979185	2.074145	3.483935	C	-5.758872	0.209435	-3.437329
C	2.812946	0.640487	1.254680	C	-4.580803	-0.129078	-4.106667
H	0.928510	-0.388349	1.384464	H	-2.556152	-0.842454	-3.893970
C	3.214113	2.333605	2.901304	H	-6.622136	0.559661	-3.997932
H	1.657292	2.636330	4.354721	N	-9.758236	-2.217830	2.828717
C	3.683746	1.625909	1.771855	C	-9.771536	-2.452373	4.236036
H	3.121715	0.064674	0.386436	C	-10.816489	-1.952597	5.027457
H	3.838161	3.108988	3.337267	C	-8.742508	-3.187201	4.843787

C	-1.254795	0.504176	2.740356	C	-10.832067	-2.192018	6.400453
C	-2.184982	-0.459116	3.168760	H	-11.611459	-1.379991	4.560064
C	-1.478816	1.154642	1.513749	C	-8.756983	-3.407154	6.220035
C	-3.305939	-0.743276	2.398242	H	-7.936668	-3.581448	4.232622
H	-2.018920	-0.982047	4.105230	C	-9.802037	-2.915566	7.005292
C	-2.588175	0.831790	0.741742	H	-11.648073	-1.798795	7.000969
H	-0.780194	1.913317	1.175445	H	-7.953268	-3.978323	6.677156
C	-3.550849	-0.118085	1.154297	C	-10.940168	-2.437668	2.076359
H	-4.001157	-1.497185	2.756911	C	-11.306433	-1.565249	1.036922
H	-2.730798	1.353931	-0.200374	C	-11.777056	-3.529180	2.365174
N	-4.806609	-0.455834	0.283704	C	-12.479869	-1.780571	0.323111
C	-6.140510	-0.912713	0.961245	H	-10.671648	-0.716447	0.802889
C	-12.937206	-3.737333	1.628174	H	8.183844	-6.954507	-1.127116
H	-11.505180	-4.213813	3.162332	H	4.605091	-5.090205	-2.618365
C	-13.339047	-2.870752	0.587328	C	9.432745	-2.152235	-1.904916
H	-12.739268	-1.081925	-0.467666	C	10.337527	-1.345810	-1.192101
H	-13.555364	-4.598424	1.867158	C	9.867353	-2.755902	-3.097806
B	5.084038	1.918182	1.136255	C	11.631609	-1.159110	-1.663674
C	5.896104	0.771166	0.449445	H	10.021171	-0.876194	-0.266295
C	6.782081	1.019277	-0.623905	C	11.161664	-2.546253	-3.559140
C	5.794037	-0.575852	0.865513	H	9.181315	-3.380064	-3.661424
C	7.495632	0.006236	-1.252683	C	12.095236	-1.746610	-2.862329
H	6.891043	2.034562	-0.995266	H	12.306890	-0.534524	-1.085266
C	6.527061	-1.597446	0.274265	H	11.460830	-3.018169	-4.491029
H	5.142125	-0.823870	1.698599	B	13.550877	-1.518964	-3.392435
C	7.386760	-1.322453	-0.804248	B	-14.660532	-3.107147	-0.219880
H	8.140481	0.235307	-2.094972	C	14.730869	-1.279840	-2.394607
H	6.441788	-2.614330	0.643780	C	14.754080	-1.850153	-1.101630
C	5.677487	3.373128	1.191813	C	15.843354	-0.476352	-2.732765
C	7.062541	3.602867	1.341131	C	15.800532	-1.642511	-0.211261
C	4.849013	4.512511	1.096636	H	13.926003	-2.479095	-0.785950
C	7.590281	4.892115	1.406236	C	16.891980	-0.242712	-1.851747
C	5.371009	5.805082	1.133256	H	15.884663	-0.018395	-3.717271
C	6.744754	5.998076	1.295376	C	16.888442	-0.825883	-0.571169
H	8.659988	5.035560	1.537787	H	15.778169	-2.101685	0.771750
H	4.707965	6.661854	1.041223	H	17.725522	0.384323	-2.151177
N	8.114939	-2.364449	-1.428316	C	13.826594	-1.525744	-4.941241

C	7.510921	-3.648377	-1.583548	C	15.024789	-2.047123	-5.475757
C	8.216010	-4.810432	-1.237115	C	12.888608	-1.010971	-5.862372
C	6.206029	-3.762179	-2.085622	C	15.268430	-2.068065	-6.848699
C	7.625710	-6.062626	-1.399389	C	13.135569	-1.002821	-7.234875
H	9.224063	-4.724688	-0.843779	C	14.325409	-1.538692	-7.732474
C	5.616790	-5.017243	-2.228206	H	16.194572	-2.491212	-7.230046
H	5.661239	-2.864555	-2.360837	H	12.399612	-0.584392	-7.917133
C	6.323194	-6.173727	-1.890826	C	-15.165039	-4.576211	-0.467972
C	-16.540305	-4.895046	-0.483147	H	18.484496	-0.327810	2.932360
C	-14.261934	-5.640049	-0.683089	C	18.977119	-3.942403	1.628958
C	-16.989750	-6.199266	-0.688181	H	18.376105	-3.165943	-0.291459
C	-14.703125	-6.942251	-0.916018	C	19.234190	-3.651309	2.970530
C	-16.070573	-7.226448	-0.912432	H	19.252604	-2.105198	4.475109
H	-18.055423	-6.414844	-0.678286	H	19.114245	-4.953398	1.254331
H	-13.982463	-7.736597	-1.094468	C	-17.326116	2.733409	-2.079178
C	-15.482012	-1.896874	-0.768765	C	-18.210519	3.742609	-1.667022
C	-15.486191	-0.637119	-0.126374	C	-15.991749	3.073929	-2.343639
C	-16.281282	-1.995923	-1.931009	C	-17.763148	5.053360	-1.530620
C	-16.240251	0.434893	-0.586324	H	-19.244961	3.491205	-1.453962
H	-14.905825	-0.505614	0.782765	C	-15.558445	4.389408	-2.187338
C	-17.014299	-0.925809	-2.427725	H	-15.299265	2.304915	-2.672084
H	-16.306152	-2.935392	-2.476342	C	-16.426235	5.419304	-1.781378
C	-17.015762	0.310155	-1.754212	H	-18.480176	5.805356	-1.205369
H	-16.240128	1.373725	-0.042177	H	-14.516356	4.613206	-2.402979
H	-17.591161	-1.037695	-3.340026	C	-19.036753	1.163496	-2.872846
N	17.953281	-0.598079	0.330421	C	-19.362356	1.839851	-4.058328
N	-17.782739	1.394635	-2.235438	C	-19.965482	0.268816	-2.318932
C	18.612162	0.662595	0.367899	C	-20.595624	1.626789	-4.671715
C	20.008969	0.734316	0.466773	H	-18.645606	2.530227	-4.491807
C	17.877260	1.858295	0.321854	C	-21.189074	0.048548	-2.948758
C	20.647171	1.972245	0.521442	H	-19.721482	-0.249677	-1.397092
H	20.589627	-0.182448	0.500396	C	-21.513718	0.727679	-4.125142
C	18.533094	3.084970	0.363289	H	-20.832978	2.158015	-5.589699
H	16.794364	1.817744	0.255976	H	-21.897574	-0.647627	-2.507609
C	19.934558	3.183414	0.467265	Si	20.786895	4.871988	0.528534
H	21.731971	1.985666	0.596192	Si	-15.853569	7.211795	-1.578066
H	17.926747	3.988657	0.328924	C	20.434264	5.816121	-1.076702

C	18.378559	-1.628546	1.218313	H	20.837292	5.283707	-1.946292
C	18.629639	-1.340072	2.568476	H	19.357649	5.945368	-1.240200
C	18.561593	-2.940247	0.753948	H	20.887654	6.815030	-1.057047
C	19.062254	-2.344642	3.432184	C	20.112932	5.862882	1.997173
H	20.323247	5.356826	2.946733	H	-15.901964	8.831245	0.337772
H	20.567793	6.860255	2.042147	H	-22.471207	0.558814	-4.609627
H	19.026869	5.999105	1.930290	H	-9.813926	-3.094907	8.076617
C	22.655951	4.644571	0.728715	H	-0.617336	0.958653	8.832101
H	22.905701	4.101437	1.647882	H	5.863791	-7.150896	-2.009644
H	23.095713	4.097290	-0.113530	H	19.565115	-4.433469	3.647839
H	23.154161	5.620432	0.779791	H	-17.267662	-4.104755	-0.317187
C	-13.999012	7.337647	-1.937083	H	-13.194335	-5.436099	-0.679119
H	-13.406751	6.712584	-1.258348	H	-16.417736	-8.242632	-1.082821
H	-13.759582	7.036155	-2.963789	H	-2.674435	-1.000588	-1.435061
H	-13.655919	8.372016	-1.812691	H	-6.756254	0.350029	-1.543444
C	-16.804756	8.322189	-2.784641	H	-4.525275	-0.048245	-5.189506
H	-17.887746	8.258848	-2.624319	H	7.734032	2.752013	1.421054
H	-16.514466	9.373561	-2.665819	H	3.776938	4.377938	0.979294
H	-16.608904	8.037603	-3.825167	H	7.153942	7.004633	1.335038
C	-16.195869	7.783702	0.196346	H	11.954461	-0.598142	-5.490499
H	-17.259904	7.704142	0.449457	H	15.771988	-2.454027	-4.799411
H	-15.639132	7.179792	0.922467	H	14.516720	-1.543657	-8.802783

Table 5. Coordinates (Å) for the Optimized Structure of **O-BNB**

atom	x	y	z	atom	x	y	z
H	-8.477526	1.572152	1.226370	C	-7.279304	-2.202649	-2.937674
C	-4.333049	0.312317	-0.943356	C	-6.686523	-4.223604	-1.774588
C	-5.423549	-0.590355	-0.917954	C	-8.316211	-2.873756	-3.584933
C	-6.683831	-0.077257	-0.525772	H	-7.113512	-1.150489	-3.153710
C	-6.827334	1.253895	-0.163534	C	-7.738865	-4.895387	-2.395998
C	-5.721759	2.130166	-0.208711	H	-6.057021	-4.762599	-1.071463
C	-4.469110	1.658309	-0.609596	C	-8.552581	-4.222588	-3.310115
H	-3.357447	-0.054641	-1.249745	H	-8.943629	-2.345577	-4.298735
H	-7.542785	-0.743491	-0.498260	H	-7.921938	-5.943630	-2.172773
H	-3.611252	2.324658	-0.657219	C	-9.366924	-4.746234	-3.804909

C	-8.061503	2.001642	0.304269	N	-0.266024	-4.911876	-0.150019
H	-8.868508	1.971723	-0.441164	C	0.869698	-4.226322	0.346378
C	-7.538264	3.408795	0.519518	C	1.191578	-2.936285	-0.112081
C	-8.207279	4.546614	0.949924	C	1.708362	-4.828599	1.300791
C	-7.523887	5.774001	1.088463	C	2.319765	-2.282806	0.368728
C	-6.149874	5.801495	0.774786	H	0.558042	-2.458187	-0.852220
C	-5.463899	4.665890	0.339985	C	22.822923	-4.151741	1.78127
C	-6.161905	3.464029	0.212593	H	1.473564	-5.822826	1.667070
H	-9.269799	4.485275	1.183620	C	3.177232	-2.859037	1.333412
H	-5.597401	6.732856	0.872240	H	2.544647	-1.291208	-0.014216
H	-4.403226	4.722775	0.107284	H	3.443053	-4.641635	2.526875
B	-5.248162	-2.098143	-1.311837	C	-0.198169	-6.321183	-0.366915
C	-3.911370	-2.847341	-1.001504	C	0.887860	-6.881622	-1.055234
C	-3.091204	-2.498112	0.096044	C	-1.218089	-7.160007	0.105879
C	-3.450733	-3.919748	-1.799271	C	0.953253	-8.259243	-1.257240
C	-1.912125	-3.171427	0.390580	H	1.674941	-6.233042	-1.426971
H	-3.404726	-1.693999	0.755994	C	-1.153322	-8.534608	-0.115461
C	-2.256992	-4.582484	-1.541586	H	-2.056187	-6.728052	0.643825
H	-4.033449	-4.223836	-2.664415	C	-0.067146	-9.092304	-0.793354
C	-1.469615	-4.221376	-0.433943	H	1.800449	-8.680318	-1.792012
H	-1.327528	-2.892214	1.261375	H	-1.950246	-9.173029	0.256570
H	-1.924424	-5.381847	-2.196120	H	-0.016321	-10.164794	-0.958291
C	-6.427823	-2.857582	-2.021186	B	4.442510	-2.115425	1.874257
C	5.216717	-1.096830	0.967067	Si	-8.446003	7.318538	1.682281
C	5.300560	-1.271038	-0.435645	C	10.318012	5.738806	-4.125195
C	5.867732	0.031578	1.522035	H	10.928107	6.621804	-4.351502
C	5.997074	-0.388214	-1.258509	H	10.862126	4.861697	-4.495062
H	4.816920	-2.133990	-0.884851	H	9.390256	5.825522	-4.703076
C	6.542067	0.932594	0.711456	C	9.055767	7.184087	-1.700182
H	5.825140	0.194146	2.596290	H	8.814110	7.145558	-0.631234
C	6.615683	0.724731	-0.682596	H	9.656538	8.086120	-1.870579
H	6.052944	-0.564871	-2.329946	H	8.112826	7.302446	-2.246778
C	7.284683	2.200792	1.086119	C	11.630645	5.512583	-1.333158
C	7.394967	1.814664	-1.279268	H	11.475926	5.422290	-0.251307
H	8.100439	2.006440	1.796407	H	12.207069	4.638113	-1.657158
H	6.624917	2.935763	1.568202	H	12.248700	6.402674	-1.504957
C	7.800335	2.693615	-0.252094	C	-9.824325	7.745778	0.452970

C	7.754939	2.072022	-2.603079	H	-10.532286	6.916761	0.334888
C	8.561213	3.816065	-0.548904	H	-10.393782	8.621305	0.788781
C	8.518937	3.205886	-2.886486	H	-9.415044	7.973339	-0.538301
H	7.448708	1.403953	-3.404559	C	-7.246495	8.777752	1.814891
C	8.939188	4.098000	-1.879408	H	-7.774697	9.673744	2.163250
H	8.867290	4.482484	0.257035	H	-6.437538	8.576942	2.527189
H	8.794944	3.398299	-3.920418	H	-6.789092	9.022893	0.849055
C	4.945689	-2.388780	3.338727	C	-9.209442	6.977201	3.383513
C	4.044773	-2.637466	4.396996	C	5.855959	-2.877436	5.978832
C	6.321181	-2.393849	3.657255	H	6.205024	-3.064810	6.991354
C	4.487560	-2.864492	5.699761	H	7.840645	-2.661823	5.161375
H	2.977197	-2.638533	4.193195	H	-9.884956	6.113805	3.358605
C	6.773913	-2.648101	4.951484	H	-8.434624	6.767072	4.130133
H	7.046563	-2.206757	2.869809	H	-9.788820	7.839356	3.736599
Si	9.983868	5.630738	-2.264773	H	3.767785	-3.036497	6.496290

Chapter 3 Luminescent Electron-Deficient Organoborane Macrocycles[a]

3.1 Introduction

Macrocycles continue to attract tremendous interest, in part because of their ability to act as hosts for guest molecules and their pronounced tendency to form well-defined porous supramolecular structures in the solid state.[1,2] The channels generated during the assembly process can, for example, be used for selective ion transport, as catalytically active sites or for photochemical reactions in a confined environment, leading to unexpected selectivities.[3] Conjugated macrocycles in particular have received much attention in recent years as they also offer desirable optical, electronic, or sensory properties; in addition, they are important from a fundamental standpoint, because they represent polymer chains without the presence of end groups, which tend to influence the photophysical and electronic characteristics of the linear counterparts.[4-12]

Conjugated organoborane macrocycles would be especially interesting in that they feature an "anti-crown"-like structure, in which more commonly encountered donor atoms (e.g. O, S, N, P) are replaced with Lewis acid sites.[13-15] Such an arrangement could be beneficial for the selective detection of anions and other electron-rich substrates.[16-18] In addition, the unusual electronic properties of conjugated organoborane oligomers and polymers that result from p-π overlap of the empty p-orbital on boron with π-conjugated

[a] This chapter is adapted from a journal publication (ref.60).

organic groups continue to fascinate researchers as they suggest potential applications in optoelectronic devices.[19-32] However, although several reports on boron-containing macrocycles have appeared in the literature, in most cases the Lewis acidity of boron is low due to π-overlap with amino or alkoxy substituents or the borons are tetracoordinate, and thus no significant electron delocalization is present (**Figure 3-1**).[33-42]

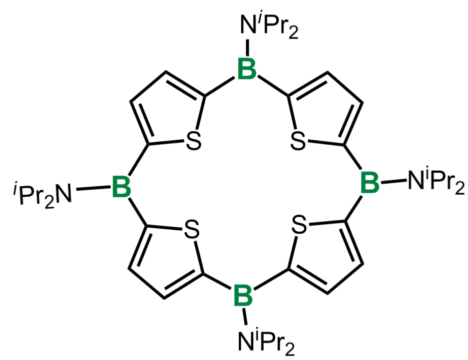

Figure 3-1. Molecular structure of a boron-containing conjugated macrocycle.[42]

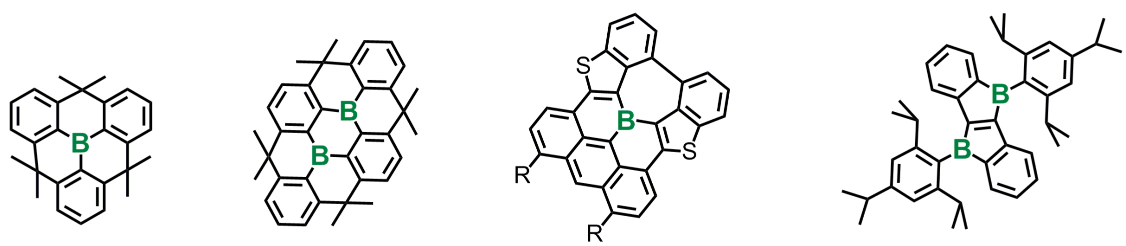

Figure 3-2. Recent examples of planarized boron-containing π-conjugated systems.[43-45]

From the viewpoint of conjugation extension, a recent advance in boron chemistry is the preparation of planarized boron-containing π-conjugated systems. Yamaguchi and co-workers discovered that kinetic stabilization (structural constraint) can serve as an alternative strategy to steric stabilization of tricoordinate boron (**Figure 3-2A and 3-2B**).

More recently, the same group synthesized a fully π-conjugated planarized triarylborane (**Figure 3-2C**) that is similar to the well-know polycyclic aromatic hydrocarbons (PAHs).[43,44] Another interesting compound that represents a planarized boron-containing acene analog was reported by Piers and co-workers (**Figure 3-2D**).[45] However, larger highly electron-deficient ring systems have not been reported.

Herein we describe a rational approach to hitherto unprecedented bora-cyclophanes that feature multiple highly electron-deficient organoborane moieties as an integral part of the ring system and thus constitute the first "charge-reverse" analogues of electron-donating macrocycles such as porphyrins, phthalocyanines, calixarenes, oligopyrrols, and recently introduced triarylamine-based aza-cyclophanes.[3,46-50] We also discuss the effect of cyclization on optical and electronic characteristics and present preliminary results on the complexation of anions, which can act as a stimulus to turn the electron-deficient into an electron-rich one.

3.2 Synthesis and Structural Characterization of Fluoreneborane Macrocycles

Treatment of Br_2B-Fl-BBr_2 (Fl = 9,9-dihexyl-2,7-fluorenediyl) with Me_3Sn-Fl-$SnMe_3$ is known to lead to polycondensation, and the resulting polymer [Fl-B(Br)]$_n$ can be converted with TipCu (Tip = 2,4,6-triisopropylphenyl) to a Lewis acidic organoboron polymer [Fl-B(Tip)]$_n$ that is highly luminescent and exhibits good stability in air.[51] As discussed in chapter 1, we have recently succeeded in the preparation of a series of well-defined conjugated fluoreneborane oligomers Me_3Si-[Fl-B(Tip)]$_n$-Fl-$SiMe_3$ (**O-B*n***, n = 1-6; Fl = 9,9-dimethylfluorene-2,7-diyl) using a novel iterative procedure.[52] We reasoned that some of the longer monodisperse oligomers should be promising as precursors for macrocycles because the formation of so-called "overshooting oligomers"[53] that lead to larger linear structures rather than cyclics can be prevented. Moreover, the number of possible cyclic products is limited since ring closure of, for example, a tetraboryl precursor with a fluorene linker can only lead to a tetramer, octamer, dodecamer, etc., while a hexaboryl species would result in a hexamer, dodecamer, etc., without any of the intermediate ring sizes. This should greatly facilitate isolation of a specific desired cyclic product.

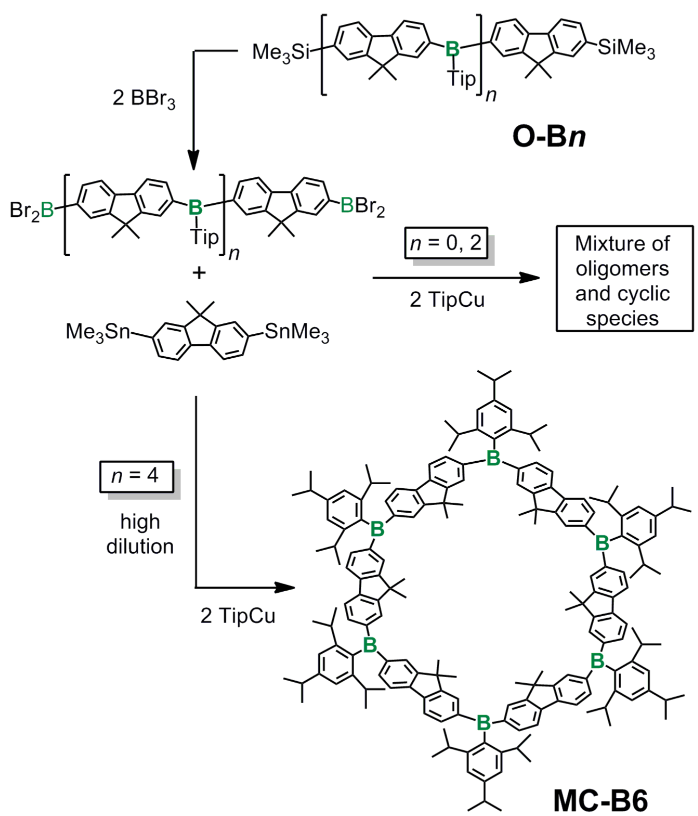

Scheme 3-1. Synthesis of the bora-cyclophane **MC-B6**.

We first converted the oligo(fluoreneborane)s **O-B*n*** (n = 2,4)[52] into species Br_2B-[Fl-B(Tip)]$_n$-Fl-BBr_2 (n = 2, 4) by reaction with 2 equiv of BBr_3 in CH_2Cl_2 at RT (**Scheme 3-1**). The resulting BBr_2-terminated species were then treated *in situ* with 2,7-distannyl-9,9-dimethylfluorene under dilute conditions, followed by reaction with TipCu, which serves to replace the reactive Br substituents with bulky groups that sterically stabilize the borane centers. The gel permeation chromatography (GPC) trace of the product obtained from the precursor **O-B2** revealed a polymodal profile with distinct peaks at 1300, 2000, 3800, 6500 Da, and MALDI-TOF MS data suggested the presence of multiple linear and cyclic species, including the tetrameric and octameric macrocycles (**MC-B4**, **MC-B8**) (**Figure 3-3a** and **Figure 3-4**). In contrast, a similar reaction sequence starting from the longer oligomer **O-B4** led to highly efficient cyclization with formation of **MC-B6** as the major product in >80% yield based on NMR and GPC analysis of the crude mixture (**Figure 3-3b**). Column chromatography on silica gel followed by crystallization from a 10/1 mixture of hexanes/toluene at –35 °C gave monodisperse **MC-B6** as a white microcrystalline solid.

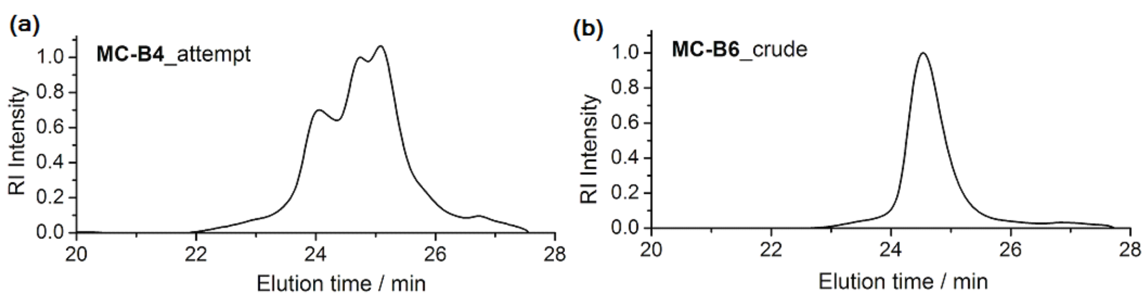

Figure 3-3. GPC-RI trace for (a) the purified product from the attempted synthesis of **MC-B4** and (b) the crude macrocycle **MC-B6** [PDI = 1.06] (THF, 1 mL/min).

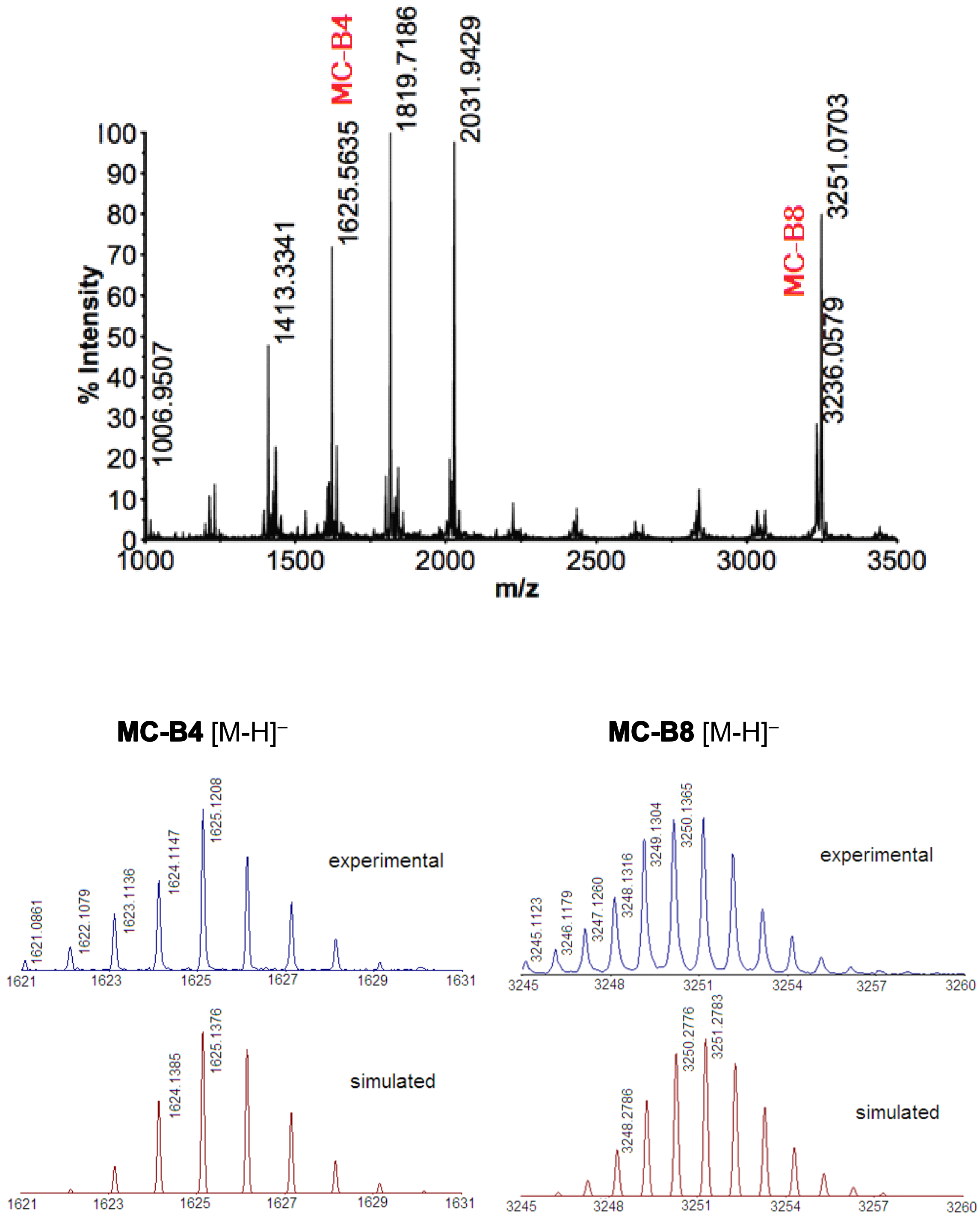

Figure 3-4. MALDI-TOF MS (neg. mode) of the product from attempted synthesis of **MC-B4**. The product was purified by column chromatography and subsequent precipitation from hexanes/toluene mixture.

Single crystals suitable for X-ray diffraction analysis could not be obtained. Polyfunctional arylboranes of relatively large size such as the macrocycle described here are known to be difficult to crystallize and amorphous molecular materials are often obtained instead.[54] The presence of the triisopropylphenyl substituents is also unfavorable. However, the identity of macrocycle **MC-B6** was unequivocally confirmed by GPC analysis, high-resolution mass spectrometry, and multinuclear NMR spectroscopy; moreover, the cyclic arrangement of 6 Lewis acidic boron centers in **MC-B6** is reflected in the electrochemical and anion-binding behavior (see later discussion). Based on GPC against PS standards (**Figure 3-5a**), **MC-B6** has a molecular weight of M_n = 2470 Da (M_w/M_n = 1.01), which is close to the expected value of 2437 Da, but significantly lower than that of the respective linear hexamer **O-B6** (M_n = 3360 Da). This observation is consistent with a more compact cyclic structure that gives rise to a relatively smaller hydrodynamic volume. The structure of **MC-B6** was further confirmed by multinuclear NMR. Most strikingly, the ^{1}H and ^{13}C NMR spectra (**Figure 3-6** and **Figure 3-7**) show only one distinct set of signals for the fluorene and Tip moieties, which is in stark contrast to the linear precursor, for which complex patterns arise from multiple nonequivalent repeating units. In the ^{11}B NMR a single broad resonance is observed at 70 ppm, which is in the expected chemical shift range and consistent with the presence of only one type of triarylborane moieties. Finally, the negative ion mode MALDI-TOF MS shows a major peak with a mass of 2437.667 (calcd for $[M-H]^-$ 2437.701) and an isotope pattern that suggests an overlap of $[M]^-$ and $[M-H]^-$ ions (**Figure 3-5b**). A smaller peak to the left corresponds to fragment ions of $[M–CH_3]^-$ overlapping with $[M–CH_3–H]^-$. No other signals were observed.

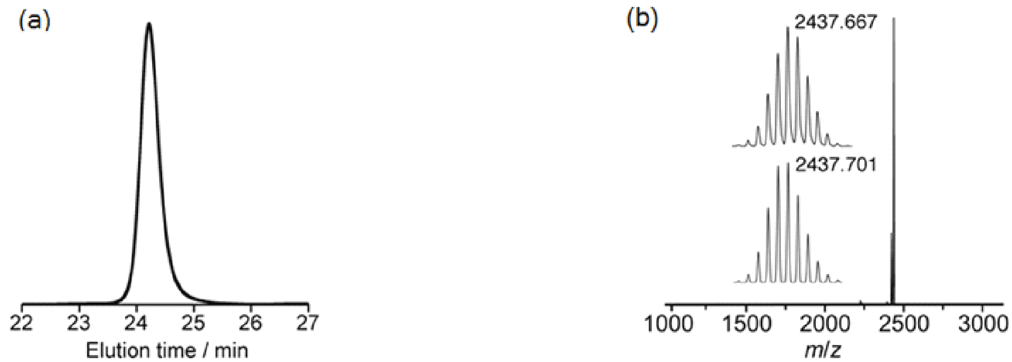

Figure 3-5. (a) GPC trace of **MC-B6** in THF. (b) MALDI-TOF MS data of **MC-B6**. Insets: Comparison of experimental (top) and calculated (bottom: $[M-H]^-$) peak patterns.

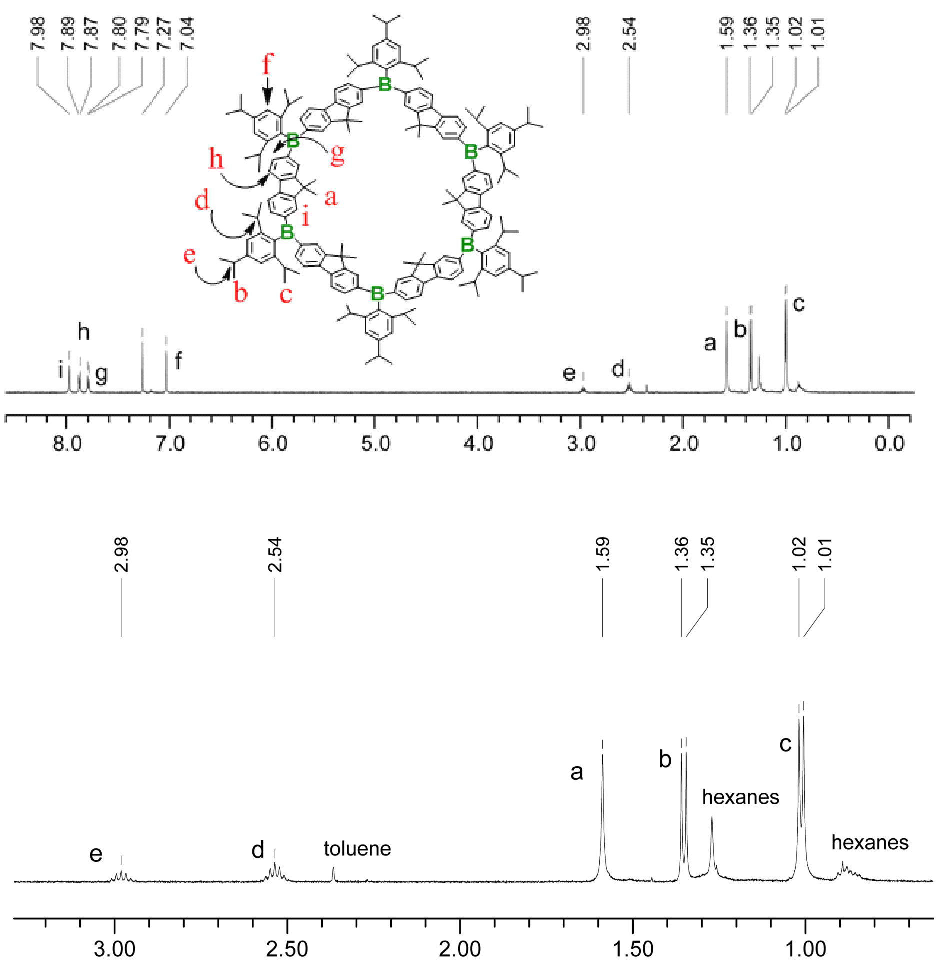

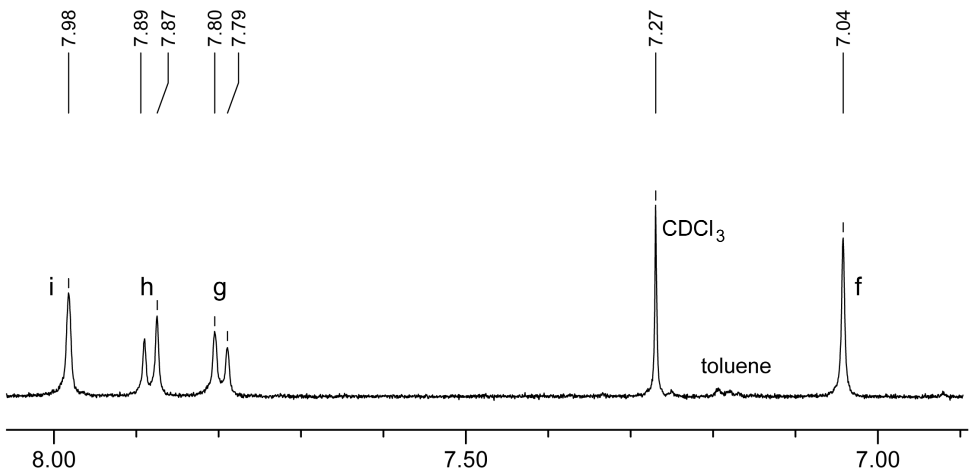

Figure 3-6. [1]H NMR spectrum of purified **MC-B6** and corresponding magnifications in $CDCl_3$ at RT.

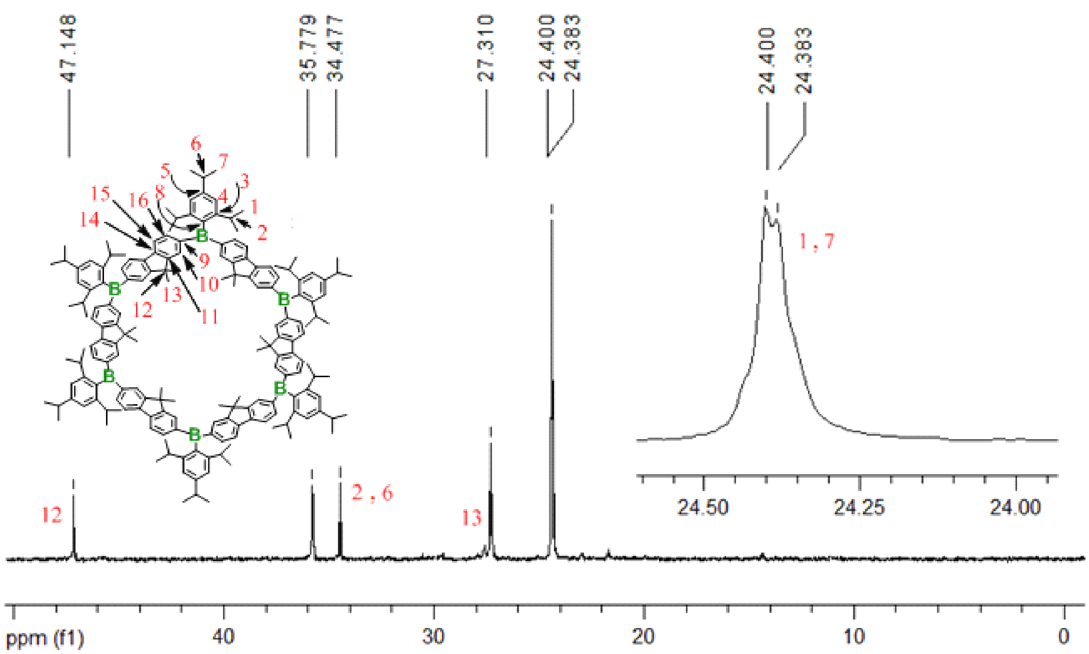

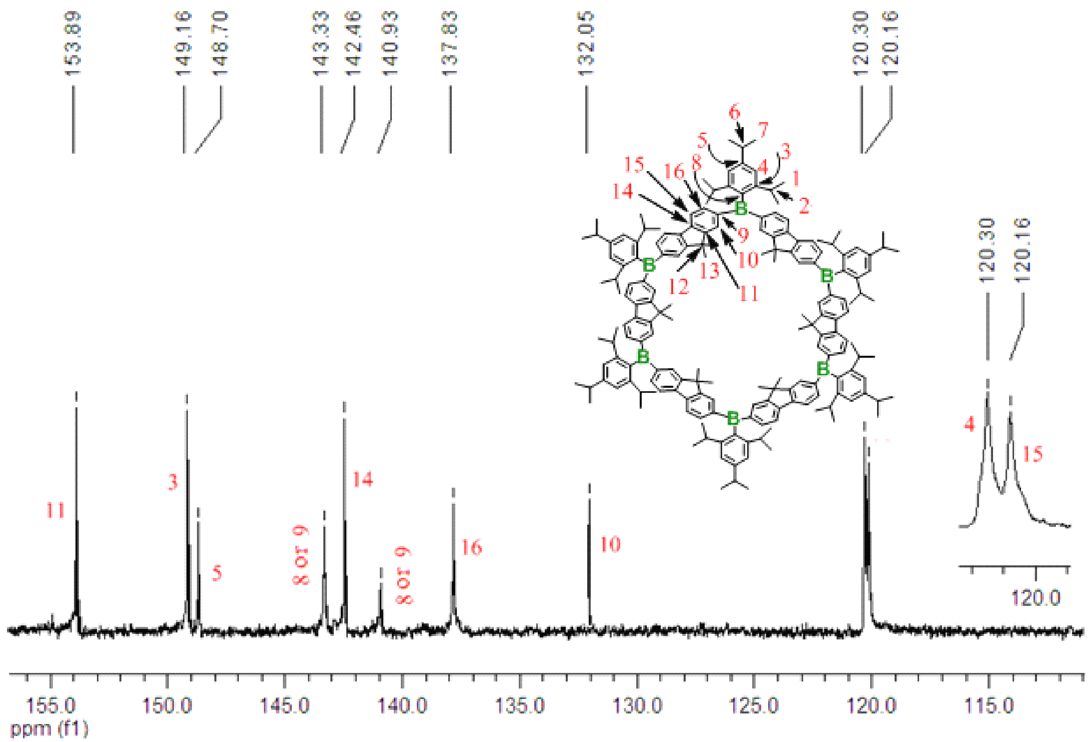

Figure 3-7. Magnifications for aliphatic and aromatic regions of the ^{13}C NMR spectrum of **MC-B6** in $CDCl_3$ at RT.

3.3 Photophysical, Electrochemical and Computational Studies of Macrocycle **MC-B6**

Analysis of the electronic structure of the macrocycle revealed characteristic differences in comparison to the respective linear oligomers. Both cyclic and square wave voltammograms show six distinct peaks, where the first two processes to give [**MC-B6**]$^{2-}$ occur almost simultaneously, whereas reduction of the following four boron centers occurs at increasingly cathodic potentials (**Figure 3-8** and **Table 3-1**). In comparison to the linear analogue **O-B6** (**Figure 3-8b**), all reductions except for the first one occur at more negative potentials, which is attributed to larger Coulombic repulsion in the cyclic framework (in the fully reduced cyclic species every boron center experiences the effect of two neighboring boron radical anions, while in the linear species the terminal borons only have one neighboring boron radical anion).

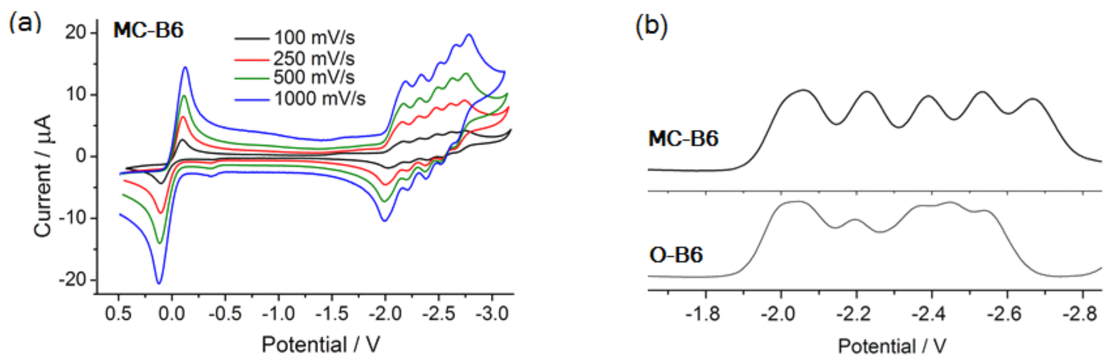

Figure 3-8. (a) Cyclic voltammetry plots for **MC-B6** (THF, 0.1M Bu_4NPF_6, vs. Fc/Fc^+) and (b) comparison of square wave voltamograms of **MC-B6** and the linear hexamer **O-B6** (THF, 0.1M Bu_4NPF_6, 100 mV/s).

Table 3-1. Summary of Cyclic and Square Wave Voltammetry Results (V) for **MC-B6**

CV	$E_{1/2}^{1\&2}$	$E_{1/2}^{3}$	$E_{1/2}^{4}$	$E_{1/2}^{5}$	$E_{1/2}^{6}$
MC-B6	-2.098	-2.270	-2.438	-2.577	-2.700
Square Wave	$E_p^{1\&2}$	E_p^{3}	E_p^{4}	E_p^{5}	E_p^{6}
MC-B6	-2.060	-2.228	-2.392	-2.532	-2.668

The macrocycle **MC-B6** absorbs at a slightly shorter wavelength than linear **O-B6** (**Figure 3-9**). This effect could be due to a more restricted conformation, which may not allow for optimal overlap of the empty *p* orbitals on B with the adjacent fluorene π-systems. However, this is unlikely as the calculated structure (DFT, B3LYP 6-31G(d); alkyl groups were omitted)[55] shows little strain with endocyclic B-C bond lengths of 1.568 Å and angles about B that range from 120.3 to 120.4° (see appendix). Moreover, the HOMO for **MC-B6-calc** is localized on the six fluorene moieties, while the LUMO shows delocalization of all six empty *p* orbitals on B with the organic π-systems (**Figure 3-10**). This stands in contrast to the observations for **O-B6-calc**,[52] for which the LUMO is mostly concentrated on just four of the six available boron centers. The difference is attributed to the absence of fluorene end groups and the resulting higher symmetry in the cyclic system. In comparison to **MC-B6**, the formation of **MC-B4** is considerably less favorable (**Figure 3-11**). This is attributed to significant ring strain in **MC-B4** as confirmed by DFT calculations on **MC-B4-calc**. The calculated endocyclic B-C bond distances for **MC-B4-calc** amount to 1.570 Å, while the C-B-C bond angles of 118.1° are smaller than in **MC-B6-calc** (see appendix).

TD-DFT calculations were also performed, and they suggest another reason for the differences in the absorption profiles, which is that, in contrast to **O-B6-calc**, the lowest energy absorption for **MC-B6-calc** is symmetry-forbidden (HOMO→LUMO, 415 nm, f = 0.000), making higher energy transitions that involve contributions primarily from the HOMO–1 and HOMO–2 to the LUMO orbital (389 nm, f = 2.439; 388 nm, f = 2.434) and the 0-1 vibronic transition dominant (**Table 3-2** and **Table 3-3**).[56,57] Indeed, the experimental absorption onsets (**O-B6**, 402 nm *vs* **MC-B6,** 404 nm) and the calculated HOMO-LUMO gaps follow the expected trend with a decrease from linear **O-B6-calc** (3.51 eV) to the "infinite chain" of **MC-B6-calc** (3.49 eV). Also consistent is that similar blue emissions are observed in both cases and the maxima are even slightly red-shifted for the cyclic species. A remarkable quantum yield of Φ = 0.98 was measured for

MC-B6. A relatively modest solvatochromic effect is consistent with some degree of polarization of the excited state, and the emission profiles proved to be slightly concentration-dependent, suggesting possibly the formation of aggregates at high concentrations (**Figure 3-12**).

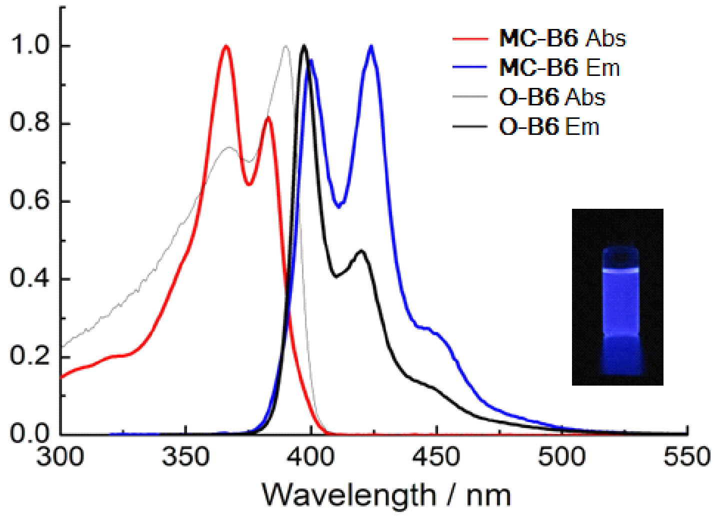

Figure 3-9. Comparison of the UV-vis and fluorescence spectra of **MC-B6** with those of **O-B6** in CH_2Cl_2 (λ_{exc} = 366 nm). Inset: Photograph of **MC-B6** in CH_2Cl_2 exposed to a UV lamp (365 nm).

Table 3-2. Calculated Orbital Energies for **MC-B6-calc** in Comparison to **MC-B4-calc** and **O-B6-calc** (DFT, B3LYP, 6-31G(d)) [a]

Compound	**HOMO (eV)**	**LUMO (eV)**	**HOMO-LUMO gap (eV)**
MC-B4-calc	–5.69	–2.18	3.51
MC-B6-calc	–5.69	–2.20	3.49
O-B6-calc	–5.66	–2.15	3.51
O-B6-calc, no $SiMe_3$	–5.66	–2.15	3.51

[a] The Me groups on fluorene and ^{i}Pr on Tip are replaced with H.

Table 3-3. Comparison of Results from TD-DFT calculations (B3LYP, 6-31G(d)) for **MC-B6-calc** with Data for the More Strained Cycle **MC-B4-calc** and the Linear Analogue of **O-B6-calc**

compound	transition	λ, nm (eV)	oscillator strength, f	orbital contributions
MC-B4-calc	$S_1 \leftarrow S_0$	414.3 (2.993)	0.000	262→266 (HOMO-2→LUMO+1), 0.165 263→267 (HOMO-1→LUMO+2), 0.165 **264→265 (HOMO→LUMO), 0.657**
	$S_2 \leftarrow S_0$	373.7 (3.318)	1.298	**263→265 (HOMO-1→LUMO), 0.651** 264→267 (HOMO→LUMO+2), 0.178
	$S_3 \leftarrow S_0$	373.5 (3.319)	1.381	**262→265 (HOMO-2→LUMO), 0.650** 264→266 (HOMO→LUMO+1), 0.181
MC-B6-calc	$S_1 \leftarrow S_0$	414.6 (2.991)	0.000	394→399 (HOMO-2→LUMO+2), 0.256 395→398 (HOMO-1→LUMO+1), 0.257 **396→397 (HOMO→LUMO), 0.580**
	$S_2 \leftarrow S_0$	388.5 (3.191)	2.439	394→397 (HOMO-2→LUMO), 0.136 **395→397 (HOMO-1→LUMO), 0.528** 396→398 (HOMO→LUMO+1), 0.374
	$S_3 \leftarrow S_0$	388.45 (3.192)	2.434	**394→397 (HOMO-2→LUMO), 0.529** 395→397 (HOMO-1→LUMO), -0.136 396→399 (HOMO→LUMO+2), 0.372
O-B6-calc	$S_1 \leftarrow S_0$	406.1 (3.053)	1.867	477→482 (HOMO-3→LUMO+1), -0.144 478→481 (HOMO-2→LUMO), -0.251 478→483 (HOMO-2→LUMO+2), 0.155 479→482 (HOMO-1→LUMO+1), 0.276 **480→481 (HOMO→LUMO), 0.523**
O-B6-calc , without $SiMe_3$ groups	$S_1 \leftarrow S_0$	405.9 (3.054)	1.923	437→442 (HOMO-3→LUMO+1), -0.124 438→441 (HOMO-2→LUMO), -0.200 438→443 (HOMO-2→LUMO+2), 0.156 439→442 (HOMO-1→LUMO+1), 0.278 **440→441 (HOMO→LUMO), 0.550**

The Me groups on fluorene and ^{i}Pr on Tip are replaced with H.

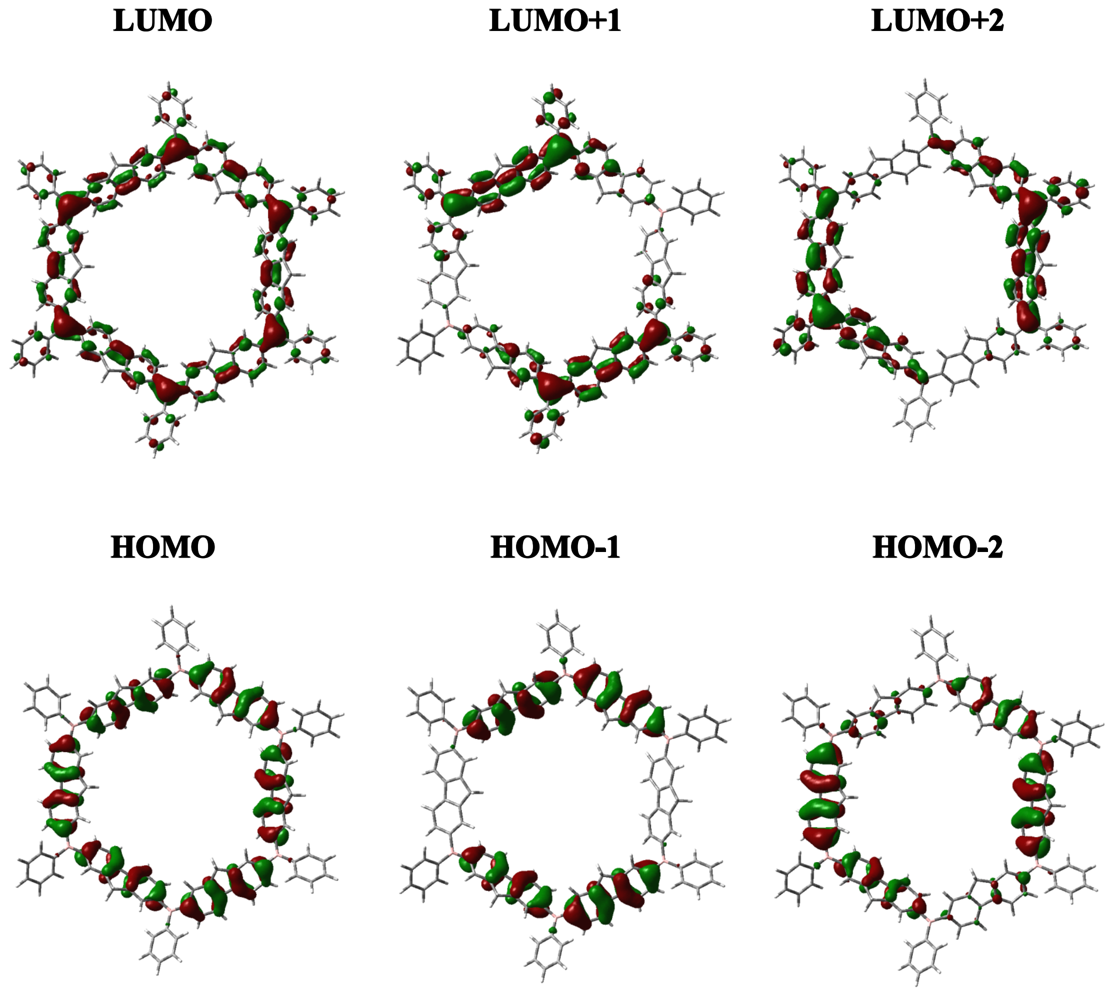

Figure 3-10. Computed orbital plots for **MC-B6-calc** (DFT, B3LYP, 6-31G(d)). The Me groups on fluorene and ^{i}Pr on Tip are replaced with H.

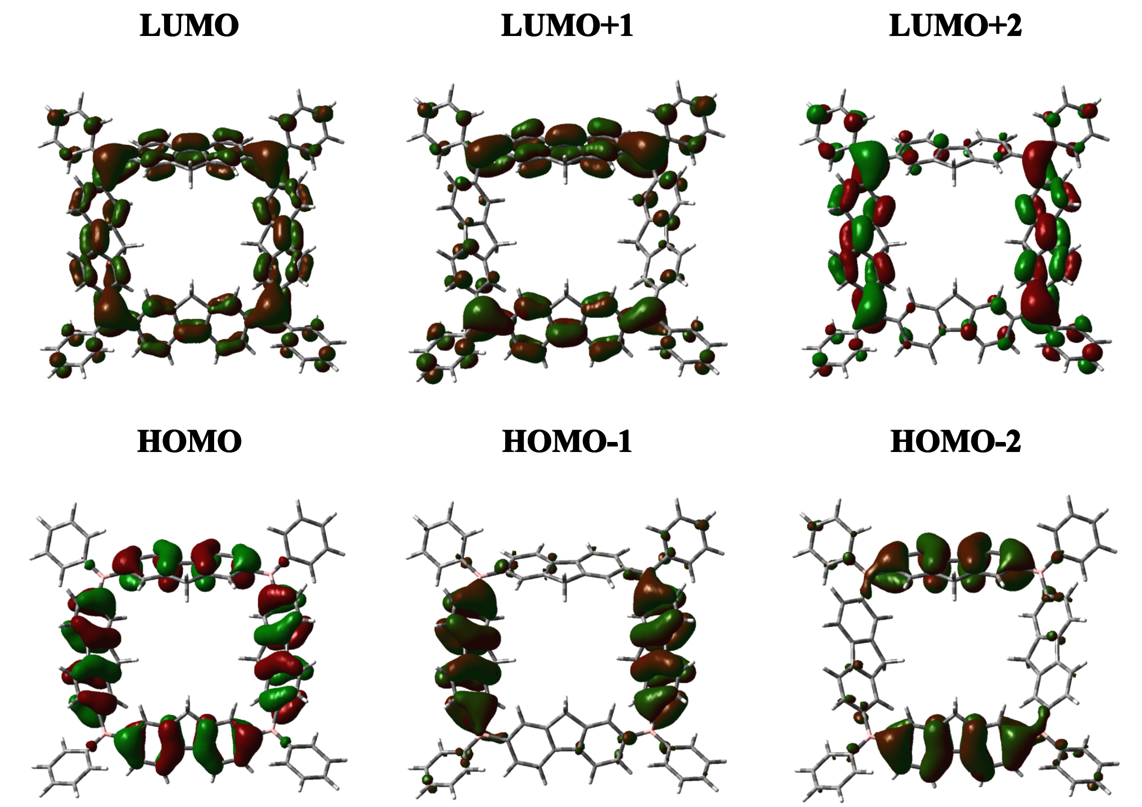

Figure 3-11. Computed orbital plots for **MC-B4-calc** (DFT, B3LYP, 6-31G(d)).

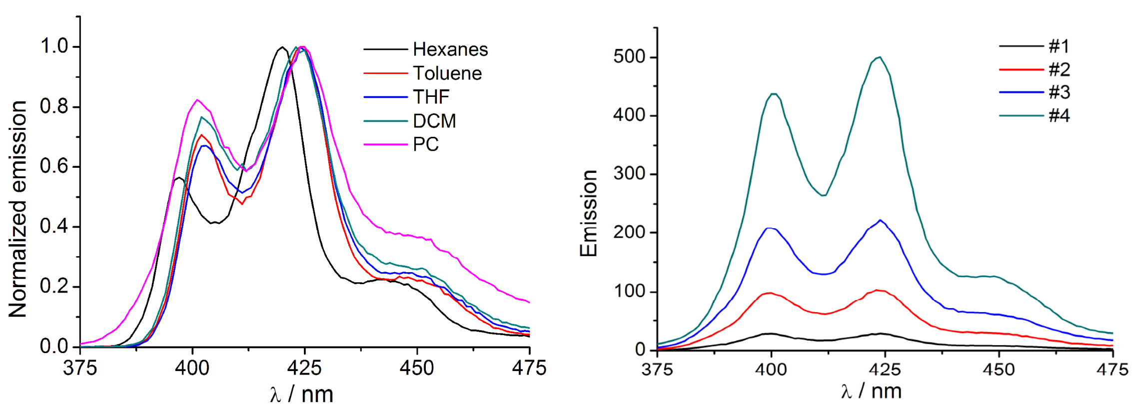

Figure 3-12. (Left) solvent-dependent emission of **MC-B6** ($c = 6.0 \times 10^{-7}$ M, $\lambda_{exc} = 366$ nm, PC = propylene carbonate) and (Right) concentration-dependent emission in CH_2Cl_2 ($c_{\#1} = 1 \times 10^{-8}$, $c_{\#2} = 5 \times 10^{-8}$, $c_{\#3} = 2 \times 10^{-7}$ M, $c_{\#4} = 6 \times 10^{-6}$, $\lambda_{exc} = 366$ nm).

3.4 Anion Binding Studies

The presence of electron-deficient boron centers allows for binding of electron-rich substrates. For instance, borate cycles should be generated in the presence of F^- or CN^-.[16-18] This process is very effective with large stepwise binding constants that are in the range typical of highly electron-deficient triarylboranes (~10^5–10^8 M^{-1}) and decrease slightly as the cycle becomes more highly charged. Another interesting aspect is that the presence of only 1 equiv of the anion for each hexameric macrocycle results in ca. 75% quenching of the luminescence, although the absorbance decreases by less than 40% (**Figure 3-13**). Based on the fitting of the absorption data (**Table 3-4**), at a 1:6 ratio of F/B, the relative abundance of species [**MC-B6**], [**MC-B6**]F, [**MC-B6**]F_2, [**MC-B6**]F_3, [**MC-B6**]F_4, [**MC-B6**]F_5, [**MC-B6**]F_6 is 29:49:20:2:0:0:0, while the amount of free [**MC-B6**] decreases to 4% after addition of 2 equiv of F^-. This suggests that the emission of all the cycles that are complexed with even just one anion is effectively quenched, consistent with an amplified quenching mechanism (**Scheme 3-2**).[51] Addition of an excess of $[Bu_4N]F$ or $[Bu_4N]CN$ leads to highly charged species $\{[(\textbf{MC-B6})X_6](Bu_4N)_n\}^{(6-n)-}$ (X = F, CN), which were also identified by high resolution ESI-MS analysis (**Figure 3-14** and **Table 3-5**).

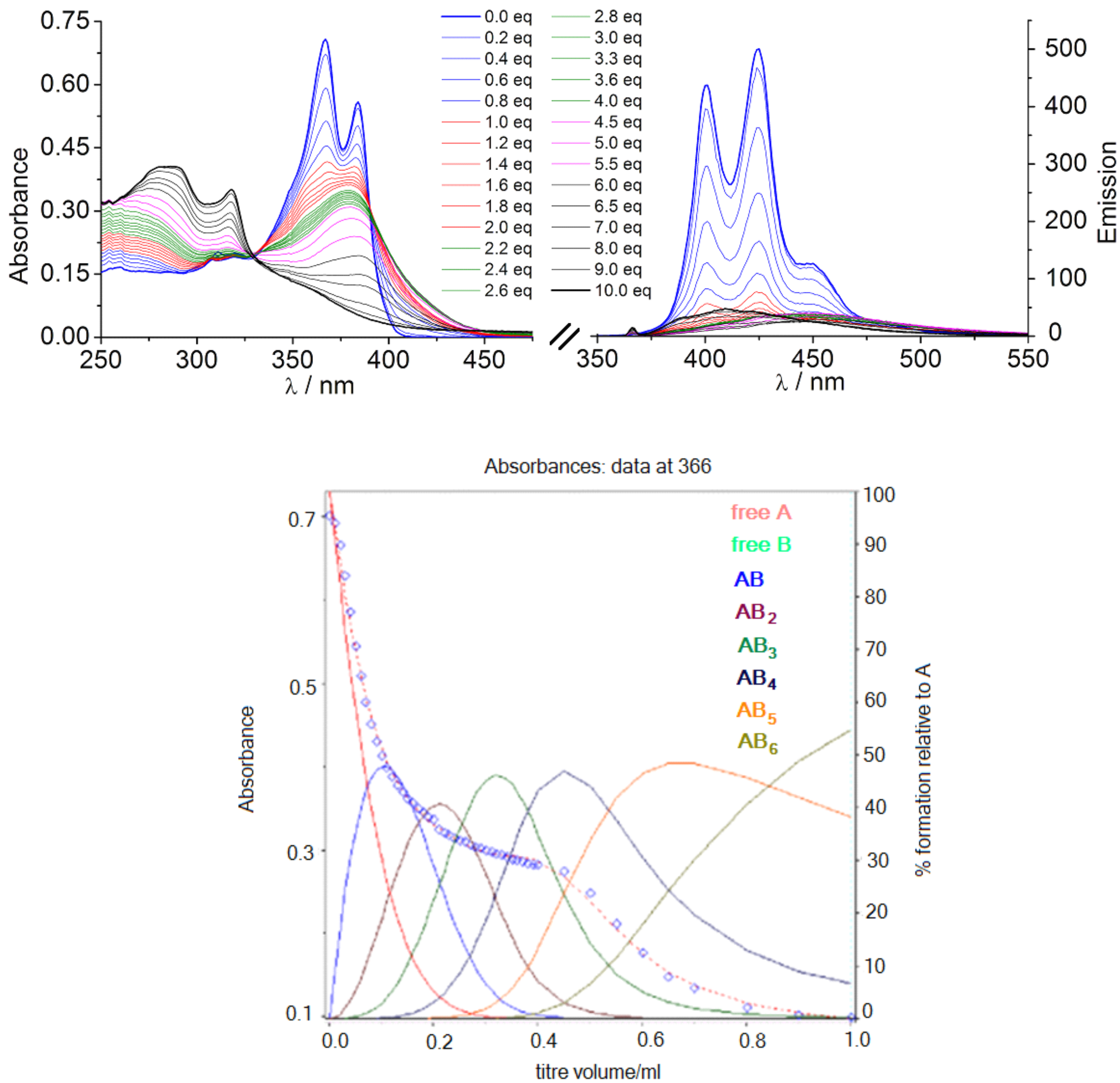

Figure 3-13. Complexation of **MC-B6** with F^- anions (1.34×10^{-4} M) in THF, monitored by UV-vis and fluorescence spectroscopy. [**MC-B6**] = 4.474×10^{-6} M; λ_{exc} = 366 nm.

Table 3-4. Relative concentrations of individual complexes after addition of varying amounts of F^-. Fit of absorption data (Hyperquad™) at λ_{max} (366 nm) with the following binding constants: $\lg\beta_{11} = 7.8$, $\lg\beta_{12} = 15.0$, $\lg\beta_{13} = 21.8$, $\lg\beta_{14} = 28.0$, $\lg\beta_{15} = 33.6$, $\lg\beta_{16} = 38.6$. These binding constants β_{1n} are given in units of M^{-n}. They are all based on a manual fit to achieve convergence using this program.

F^- (eq.)	[**MC-B6**] (%)	[**MC-B6**]F (%)	[**MC-B6**]F_2 (%)	[**MC-B6**]F_3 (%)	[**MC-B6**]F_4 (%)	[**MC-B6**]F_5 (%)	[**MC-B6**]F_6 (%)
1	29.1	**48.5**	20.2	2.1	0.1	0.0	0.0
2	3.9	26.9	**46.6**	20.3	2.2	0.1	0.0
3	0.2	4.8	29.5	**45.8**	17.9	1.7	0.0
4	0.0	0.6	10.1	**39.7**	**39.3**	9.8	0.6
5	0.0	0.0	1.2	14.2	**43.9**	**34.0**	6.6
6	0.0	0.0	0.2	5.0	**30.5**	**46.5**	17.8
7	0.0	0.0	0.1	2.0	19.5	**48.4**	**30.1**
8	0.0	0.0	0.0	0.9	12.9	**45.6**	**40.5**
9	0.0	0.0	0.0	0.5	9.0	**41.8**	**48.7**
10	0.0	0.0	0.0	0.3	6.7	38.2	**54.9**

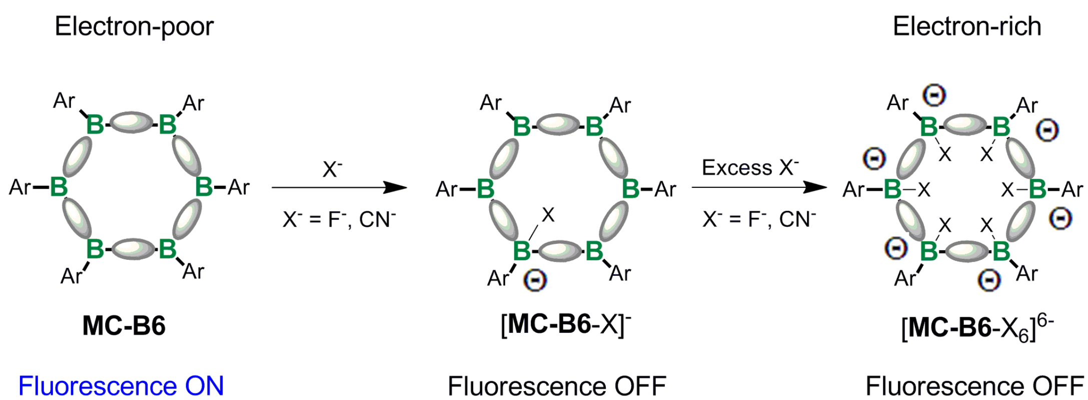

Scheme 3-2. Conversion of electron-poor to electron-rich **MC-B6** by anion binding.

3.5 Conclusions

In conclusion, we have succeeded in the preparation of the first example of a highly electron-deficient bora-cyclophane. The macrocycle is strongly blue luminescent and can be reversibly reduced in six separate redox steps. Important differences in comparison to the electronic structure of the respective linear species were deduced. Another unique aspect is the presence of multiple electron-deficient organoborane moieties, which leads to high affinity for electron-rich substrates. There has been immense recent interest in the binding of anions to organoborane Lewis acid receptors, and **MC-B6** binds strongly to F^- and CN^- as evidenced by UV-vis titration and ESI FT-MS, thus suggesting potential use in anion recognition and as stimuli-responsive optoelectronic materials. Anion binding to **MC-B6** results in amplified fluorescence quenching with formation of a highly charged hexaborate species. This offers a facile means to convert an electron-deficient macrocycle into an electron-rich one using anion addition as an external stimulus.

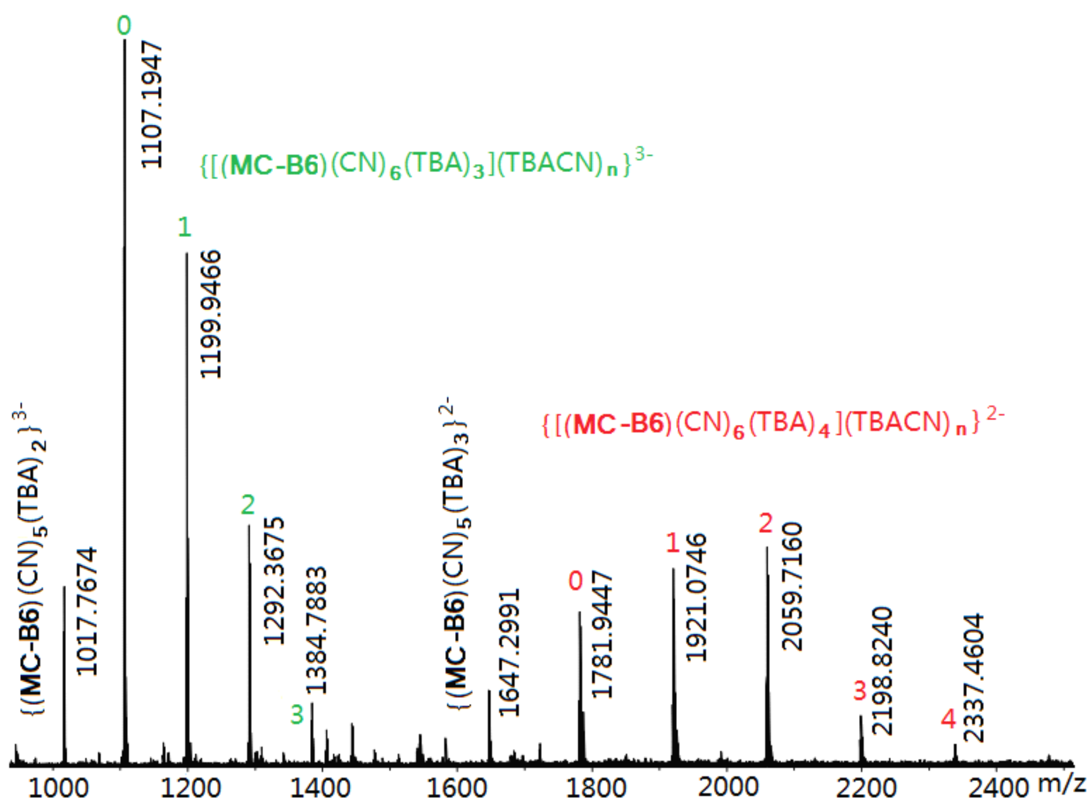

Figure 3-14. High resolution (-) ESI FT-MS analysis for the anion complex of **MC-B6** with CN^- in THF ($c = 1.4 \times 10^{-4}$ M) in the presence of 12 equiv tetrabutylammonium cyanide (TBACN).

Table 3-5. Summary of Data from High Resolution (-) ESI FT-MS Analysis of **MC-B6** in THF ($c = 1.435 \times 10^{-4}$ M) in the Presence of 12 Equiv TBACN

Cyanide Complexes	Formula	Calcd (m/z)	Found (m/z)
$[M+6CN^{-}+3TBA^{+}]^{3-}$	**$C_{180}H_{210}B_6(C_{16}H_{36}N)_3(CN)_6$**	**1107.1938**	**1107.1947**
$[M+6CN^{-}+3TBA^{+}]^{3-}$ x TBACl	$C_{180}H_{210}B_6(C_{16}H_{36}N)_3(CN)_6(C_{16}H_{36}NCl)$	1199.9453	1199.9466
$[M+6CN^{-}+3TBA^{+}]^{3-}$ x 2TBACl	$C_{180}H_{210}B_6(C_{16}H_{36}N)_3(CN)_6(C_{16}H_{36}NCl)_2$	1292.3630	1292.3675
$[M+6CN^{-}+3TBA^{+}]^{3-}$ x 3TBACl	$C_{180}H_{210}B_6(C_{16}H_{36}N)_3(CN)_6(C_{16}H_{36}NCl)_3$	1384.7808	1384.7883
$[M+6CN^{-}+3TBA^{+}]^{3-}$ x 4TBACl	$C_{180}H_{210}B_6(C_{16}H_{36}N)_3(CN)_6(C_{16}H_{36}NCl)_4$	1477.8656	1477.8755
$[M+6CN^{-}+4TBA^{+}]^{2-}$	**$C_{180}H_{210}B_6(C_{16}H_{36}N)_4(CN)_6$**	**1781.9335**	**1781.9447**
$[M+6CN^{-}+4TBA^{+}]^{2-}$ x TBACl	$C_{180}H_{210}B_6(C_{16}H_{36}N)_4(CN)_6(C_{16}H_{36}NCl)$	1921.0608	1921.0746
$[M+6CN^{-}+4TBA^{+}]^{2-}$ x 2TBACl	$C_{180}H_{210}B_6(C_{16}H_{36}N)_4(CN)_6(C_{16}H_{36}NCl)_2$	2059.6874	2059.7160
$[M+6CN^{-}+4TBA^{+}]^{2-}$ x 3TBACl	$C_{180}H_{210}B_6(C_{16}H_{36}N)_4(CN)_6(C_{16}H_{36}NCl)_3$	2198.8144	2198.8240
$[M+6CN^{-}+4TBA^{+}]^{2-}$ x 4TBACl	$C_{180}H_{210}B_6(C_{16}H_{36}N)_4(CN)_6(C_{16}H_{36}NCl)_4$	2337.4390	2337.4604
$[M+5CN^{-}+2TBA^{+}]^{3-}$	$C_{180}H_{210}B_6(C_{16}H_{36}N)_2(CN)_5$	1017.7644	1017.7674
$[M+5CN^{-}+3TBA^{+}]^{2-}$	$C_{180}H_{210}B_6(C_{16}H_{36}N)_3(CN)_5$	1647.2844	1647.2991

3.6 Experimental Section

Materials and General Methods. BBr_3, tetrabutylammonium fluoride (TBAF; 1.0 M in THF) and tetrabutylammonium cyanide (TBACN) were purchased from Aldrich, and benzo[α]pyrene from TCI chemicals. BBr_3 was distilled under vacuum and all other commercially available chemicals were used as received without further purification. 2,7-Bis(trimethylstannyl)-9,9-dimethylfluorene,[52] 2,4,6-triisopropylphenylcopper (TipCu),[58] **O-B2**,[52] and **O-B4**[52] were prepared according to literature procedures. Hexanes and toluene were purified using a solvent purification system (Innovative Technologies; alumina/copper columns). Dichloromethane (DCM) and $CDCl_3$ were distilled from CaH_2 and degassed via several freeze-pump-thaw cycles. All reactions and manipulations were carried out under an atmosphere of prepurified nitrogen using either Schlenk techniques or an inert-atmosphere glove box.

499.9 MHz ^{1}H and 160.4 MHz ^{11}B NMR spectra were recorded at ambient temperature on 500 MHz Varian INOVA spectrometer equipped with a boron-free 5 mm dual broadband gradient probe (Nalorac, Varian Inc., Martinez, CA) and the 150.0 MHz ^{13}C NMR spectrum was recorded on a 600 MHz Varian INOVA spectrometer. ^{11}B NMR spectra were acquired with boron-free quartz NMR tubes and the spectra were referenced externally to $BF_3 \cdot Et_2O$ ($\delta = 0$). Chemical shifts are given in ppm.

MALDI-TOF measurements were performed on an Applied Biosystems 4800 Proteomics Analyzer as specified either in linear or in reflection (-) mode with delayed extraction. Benzo[a]pyrene (10 mg/mL) was used as the matrix and mixed with the samples (10 mg/mL in toluene) in a 10:1 ratio, and then spotted on the wells of a target plate inside a glove box. Electrospray ionization mass spectra (ESI-MS) experiments were recorded on an Apex-ultra 7T Hybrid FT-MS (Bruker Daltonics).

GPC analyses were performed in THF (1 mL/min) using a Waters Empower system equipped with a 717 plus autosampler, a 1525 binary HPLC pump, a 2998 photodiode array detector, and a 2414 refractive index detector. For separation the samples were passed through a series of styragel columns (Polymer Laboratories; two PLgel 5 μm Mixed-C and one PLgel 5 μm Mixed-D), which were kept in a column heater at 35 °C. The columns were calibrated with narrow polystyrene standards (Polymer Laboratories).

UV-visible absorption data were acquired on a Varian Cary 500 UV-Vis/NIR spectrophotometer. The fluorescence data and quantum yields were measured on a Varian Cary Eclipse fluorescence spectrophotometer with optically dilute solutions ($A < 0.1$). Quantum yields (Φ) in dichloromethane were calculated based on that of 9,10-diphenylanthracene as a standard, for which $\Phi = 0.92$ in dichloromethane.[59] Sample solutions were prepared using a microbalance (± 0.1 mg) and volumetric flasks.

Cyclic voltammetry (CV) and square wave voltammetry experiments were carried out on a CV-50W analyzer from BAS. The three-electrode system consisted of an Au disk as working electrode, a Pt wire as secondary electrode and an Ag wire as the reference electrode. The voltammograms were recorded with ca. 10^{-3} to 10^{-4} M solution in THF and $Bu_4N[PF_6]$ (0.1 M) was used as the supporting electrolyte. The scans were referenced after the addition of a small amount of ferrocene as internal standard. The potentials are reported relative to the ferrocene/ferrocenium couple.

DFT calculations (gas phase) have been performed with the Gaussian03 program. Geometries and electronic properties are calculated using the hybrid density functional B3LYP with the basis set of 6-31G(d). The input files were generated using Chem3D and orbital representations were plotted with Gaussview 3.07 (scaling radii of 75%, isovalue of 0.02). Excitation data were calculated using TD-DFT (B3LYP, 6-31G(d)).

Synthesis of MC-B6: To BBr_3 (40 mg, 160 μmol) in 5 mL of CH_2Cl_2 was added a solution of **O-B4** (120 mg, 60 μmol) in 15 mL of CH_2Cl_2 with stirring. The reaction mixture was kept stirring overnight, and then all volatile components were removed under high vacuum. The crude product was purified by recrystallization from hexanes/toluene mixture at –35 °C to give a white solid (100 mg, 75%). A solution of the borylated product (100 mg, 46 μmol) in 50 mL of toluene and a solution of 2,7-bis(trimethylstannyl)-9,9-dimethylfluorene (24 mg, 46 μmol) in 50 mL of toluene were simultaneously added through two different addition funnels to a three-necked round bottom flask containing 350 mL of toluene under N_2 over a period of 12 h with stirring. After stirring for 2 d at RT, the reaction solution was evaporated to dryness, leaving behind a light yellow solid. The solid was redissolved in toluene and treated with TipCu (25 mg, 94 μmol) in 10 mL of toluene. The reaction mixture was refluxed at 115 °C under N_2 for 2 d. A solid precipitate (CuBr) that had formed was removed by filtration through a fritted glass disk. The crude product was examined by GPC and ^{1}H NMR. All volatile components were then removed under high vacuum and the crude product was purified by column chromatography on silica gel using hexanes/toluene (5:1) as the eluent. A solution of the purified product in a 10/1 hexanes/toluene mixture was kept at –35 °C to give a microcrystalline white solid (34 mg, 31%). ^{1}H NMR (499.893 MHz, $CDCl_3$): δ 1.01 (d, J = 7.0 Hz, 72H), 1.35 (d, J = 7.5 Hz, 36H), 1.59 (s, 36H), 2.54 (septet, J = 6.5 Hz, 12H), 2.98 (septet, J = 6.5 Hz, 6H), 7.04 (s, 12H), 7.80 (d, J = 8.0 Hz, 12H), 7.88 (d, J = 8.0 Hz, 12H), 7.98 (s, 12H). ^{11}B NMR (160.4 MHz, $CDCl_3$): δ 70 ($w_{1/2}$ = 5700 Hz). ^{13}C NMR (150.0 MHz, $CDCl_3$): δ 24.4, 24.4, 27.3, 34.5, 35.8, 47.2, 120.2, 120.3, 132.1, 137.8, 140.9 (B-C), 142.5, 143.3 (B-C), 148.7, 149.2, 153.9. MALDI-TOF MS (neg.) m/z: calcd. for $C_{180}H_{209}B_6$ $[M–H]^-$ 2437.701 found 2437.667. ESI MS (neg.)

m/z: calcd. for $\{[(C_{180}H_{210}B_6)(CN)_6](C_{16}H_{36}N)_3\}^{3-}$ 1107.1938 found 1107.1947.

Attempted Synthesis of MC-B4. To BBr_3 (50 mg, 200 μmol) in 5 mL of CH_2Cl_2 was added a solution of **O-B2** (90 mg, 80 μmol) in 15 mL of CH_2Cl_2 with stirring. The reaction mixture was kept stirring overnight, and then all volatile components were removed under high vacuum. The crude mixture was recrystallized from hexanes/toluene mixture at –35 °C to give a white microcrystalline solid (75 mg, 71%). A solution of the borylated product (75 mg, 56 μmol) in 50 mL of toluene and a solution of 2,7-bis(trimethylstannyl)-9,9-dimethylfluorene (29 mg, 56 μmol) in 50 mL of toluene were simultaneously added through two different addition funnels to a three-necked round bottom flask containing 350 mL of toluene under N_2 over a period of 12 h with stirring. After stirring for 2 d at RT, the reaction solution was evaporated to dryness, leaving behind a light yellow solid. The solid was redissolved in toluene and treated with TipCu (30 mg, 112 μmol) in 10 mL of toluene. The reaction mixture was refluxed at 115 °C under N_2 for 2 d. A solid precipitate (CuBr) that had formed was removed by filtration through a fritted glass disk. All volatile components were removed under high vacuum and the crude product was purified by column chromatography on silica gel using hexanes/toluene (5:1) as the eluent. A solution in hexanes/toluene mixture was kept at –35 °C to give a microcrystalline white solid. The product was examined by GPC and MALDI-TOF MS.

3.7 References

(1) Ramaiah, D.; Neelakandan, P. P.; Nair, A. K.; Avirah, R. R. *Chem. Soc. Rev.* **2010**, *39*, 4158.

(2) Gong, B. *Acc. Chem. Res.* **2008**, *41*, 1376.

(3) Xu, Y.; Smith, M. D.; Krause, J. A.; Shimizu, L. S. *J. Org. Chem.* **2009**, *74*, 4874.

(4) Iyoda, M. *Pure Appl. Chem.* **2010**, *82*, 831.

(5) Mishra, A.; Ma, C.-Q.; Bäuerle, P. *Chem. Rev.* **2009**, *109*, 1141.

(6) Zang, L.; Che, Y.; Moore, J. S. *Acc. Chem. Res.,* **2008**, *41*, 1596.

(7) Tykwinski, R. R.; Gholami, M.; Eisler, S.; Zhao, Y.; Melin, F.; Echegoyen, L. *Pure Appl. Chem.* **2008**, *80*, 621.

(8) MacLachlan, M. J. *Pure Appl. Chem.* **2006**, *78*, 873.

(9) Zhang, W.; Moore, J. S. *Angew. Chem., Int. Ed.* **2006**, *45*, 4416.

(10) Höger, S. *Chem. Eur. J.* **2004**, *10*, 1320.

(11) Zhao, D.; Moore, J. S. *Chem. Commun.* **2003**, 807.

(12) Grave, C.; Schlüter, A. D. *Eur. J. Org. Chem.* **2002**, 3075.

(13) Gabbaï, F. P. *Angew. Chem. Int. Ed.* **2003**, *42*, 2218.

(14) Wedge, T. J.; Hawthorne, M. F. *Coord. Chem. Rev.* **2003**, *240*, 111.

(15) Aldridge, S.; Fallis, I. A.; Howard, S. T. *Chem. Commun.* **2001**, 231.

(16) Wade, C. R.; Broomsgrove, A. E. J.; Aldridge, S.; Gabbai, F. P. *Chem. Rev.* **2010**, *110*, 3958.

(17) Hudson, Z. M.; Wang, S. *Acc. Chem. Res.* **2009**, *42*, 1584.

(18) Yamaguchi, S.; Akiyama, S.; Tamao, K. *J. Organomet. Chem.* **2002**, *652*, 3.

(19) Jäkle, F. *Chem. Rev.* **2010**, *110*, 3985.

(20) Entwistle, C. D.; Marder, T. B. *Chem. Mater.* **2004**, *16*, 4574.

(21) Entwistle, C. D.; Marder, T. B. *Angew. Chem. Int. Ed.* **2002**, *41*, 2927.

(22) Caruso, A.; Siegler, M. A.; Tovar, J. D. *Angew. Chem. Int. Ed.* **2010**, *49*, 4213.

(23) Wood, T. K.; Piers, W.; Keay, B. A.; Parvez, M. *Chem.-Eur. J.* **2010**, *16*, 12199.

(24) Pron, A.; Baumgarten, M.; Müllen, K. *Org. Lett.* **2010**, *12*, 4236.

(25) Li, H.; Jäkle, F. *Macromol. Rap. Commun.* **2010**, *31*, 915.

(26) Baik, C.; Murphy, S. K.; Wang, S. *Angew. Chem. Int. Ed.* **2010**, *49*, 8224.

(27) Lorbach, A.; Bolte, M.; Li, H.; Lerner, H.-W.; Holthausen, M. C.; Jäkle, F.; Wagner, M. *Angew. Chem. Int. Ed.* **2009**, *48*, 4584.

(28) Braunschweig, H.; Herbst, T.; Rais, D.; Ghosh, S.; Kupfer, T.; Radacki, K.; Crawford, A. G.; Ward, R. M.; Marder, T. B.; Fernandez, I.; Frenking, G. *J. Am. Chem. Soc.* **2009**, *131*, 8989.

(29) Weber, L.; Werner, V.; Fox, M. A.; Marder, T. B.; Schwedler, S.; Brockhinke, A.; Stammler, H. G.; Neumann, B. *Dalton Trans.* **2009**, 1339.

(30) Chai, J.; Wang, C.; Jia, L.; Pang, Y.; Graham, M.; Cheng, S. Z. D. *Synth. Met.* **2009**, *159*, 1443.

(31) Nagai, A.; Murakami, T.; Nagata, Y.; Kokado, K.; Chujo, Y. *Macromolecules* **2009**, *42*, 7217.

(32) Zhao, C.; Sakuda, E.; Wakamiya, A.; Yamaguchi, S. *Chem. -Eur. J.* **2009**, *15*, 10603.

(33) Lorbach, A.; Bolte, M.; Lerner, H.-W.; Wagner, M. *Chem. Commun.* **2010**, *46*, 3592.

(34) Severin, K. *Dalton Trans.* **2009**, 5254.

(35) Salazar-Mendoza, D.; Guerrero-Alvarez, J.; Höpfl, H. *Chem. Commun.* **2008**, 6543.

(36) Zhang, D.; Tanaka, H.; Pelton, R. *Langmuir* **2007**, *23*, 8806.

(37) Day, J. K.; Bresner, C.; Fallis, I. A.; Ooi, L. L.; Watkin, D. J.; Coles, S. J.; Male, L.; Hursthouse, M. B.; Aldridge, S. *Dalton Trans.* **2007**, 3486.

(38) Iwasawa, N.; Takahagi, H. *J. Am. Chem. Soc.* **2007**, *129*, 7754.

(39) Barba, V.; Villamil, R.; Luna, R.; Godoy-Alcantar, C.; Höpfl, H.; Beltran, H. I.; Zamudio-Rivera, L. S.; Santillan, R.; Farfan, N. *Inorg. Chem.* **2006**, *45*, 2553.

(40) Scheibitz, M.; Winter, R. F.; Bolte, M.; Lerner, H. W.; Wagner, M. *Angew. Chem. Int. Ed.* **2003**, *42*, 924.

(41) Eckert, A.; Pritzkow, H.; Siebert, W. *Eur. J. Inorg. Chem.* **2002**, 2064.

(42) Carre, F. H.; Corriu, R. J.-P.; Deforth, T.; Douglas, W. E.; Siebert, W. S.; Weinmann, W. *Angew. Chem. Int. Ed. Engl.* **1998**, *37*, 652.

(43) Zhou, Z.; Wakamiya, A.; Kushida, T.; Yamaguchi, S. *J. Am. Chem. Soc.* **2012**, *134*, 4529.

(44) Saito, S.; Matsuo, K.; Yamaguchi, S. *J. Am. Chem. Soc.* **2012**, *134*, 9130.

(45) Araneda, J. F.; Neue, B.; Piers, W. E.; Parvez, M. *Angew. Chem. Int. Ed.* **2012**, *51*, 8546.

(46) Rambo, B. M.; Sessler, J. L. *Chem.-Eur. J.* **2011**, *17*, 4946.

(47) Ito, A.; Yokoyama, Y.; Aihara, R.; Fukui, K.; Eguchi, S.; Shizu, K.; Sato, T.; Tanaka, K. *Angew. Chem., Int. Ed.* **2010**, *49*, 8205.

(48) Zhang, E.-X.; Wang, D.-X.; Zheng, Q.-Y.; Wang, M.-X. *Org. Lett.* **2008**, *10*, 2565.

(49) Gong, H.-Y.; Zhang, X.-H.; Wang, D.-X.; Ma, H.-W.; Zheng, Q.-Y.; Wang, M.-X. *Chem. Eur. J.* **2006**, *12*, 9262.

(50) König, B.; Fonseca, M. H. *Eur. J. Inorg. Chem.* **2000**, 2303.

(51) Li, H.; Jäkle, F. *Angew. Chem. Int. Ed.* **2009**, *48*, 2313.

(52) Chen, P.; Lalancette, R. A.; Jäkle, F. *J. Am. Chem. Soc.* **2011**, *133*, 8802.

(53) Feng, W.; Yamato, K.; Yang, L.; Ferguson, J. S.; Zhong, L.; Zou, S.; Yuan, L.; Zeng, X. C.; Gong, B. *J. Am. Chem. Soc.* **2009**, *131*, 2629.

(54) Noda, T.; Shirota, Y. *J. Am. Chem. Soc.* **1998**, *120*, 9714.

(55) Frisch, M. J. et al. Gaussian 03, Revision C.02, Gaussian Inc., Wallingford, CT, **2004**.

(56) Bednarz, M.; Reineker, P.; Mena-Osteritz, E.; Bäuerle, P. *J. Luminescence* **2004**,

110, 225.

(57) Hoffmann, M.; Kärnbratt, J.; Chang, M.-H.; Herz, L. M.; Albinsson, B.; Anderson, H. L. *Angew. Chem. Int. Ed.* **2008**, *47*, 4993.

(58) Sasaki, S.; Sutoh, K.; Murakami, F.; Yoshifuji, M. *J. Am. Chem. Soc.* **2002**, *124*, 14830.

(59) Murov, S. L.; Carmichael, I.; Hug, G. L. *Handbook of Photochemistry*, 2nd ed., Marcel Dekker: New York, **1993**.

(60) Chen, P.; Jäkle, F. *J. Am. Chem. Soc.* **2011**, *133*, 20142.

Appendix

Table 1. Selected Bond Distances and Angles for **MC-B4-calc** (DFT, B3LYP, 6-31G(d))

Bond Distances (Å)				Bond Angles (°)			
B14-C6	1.570	B30-C27	1.570	C6-B14-C16	118.1	C42-B44-C54	118.1
B14-C16	1.570	B30-C31	1.570	C6-B14-C57	121.0	C42-B44-C60	120.9
B14-C57	1.567	B30-C58	1.567	C16-B14-C57	120.9	C54-B44-C60	121.0
B15-C12	1.570	B44-C42	1.570	C12-B15-C17	118.1	C27-B30-C31	118.1
B15-C17	1.570	B44-C54	1.570	C12-B15-C59	120.9	C27-B30-C58	121.0
B15-C59	1.567	B44-C60	1.567	C17-B15-C59	121.0	C31-B30-C58	120.9

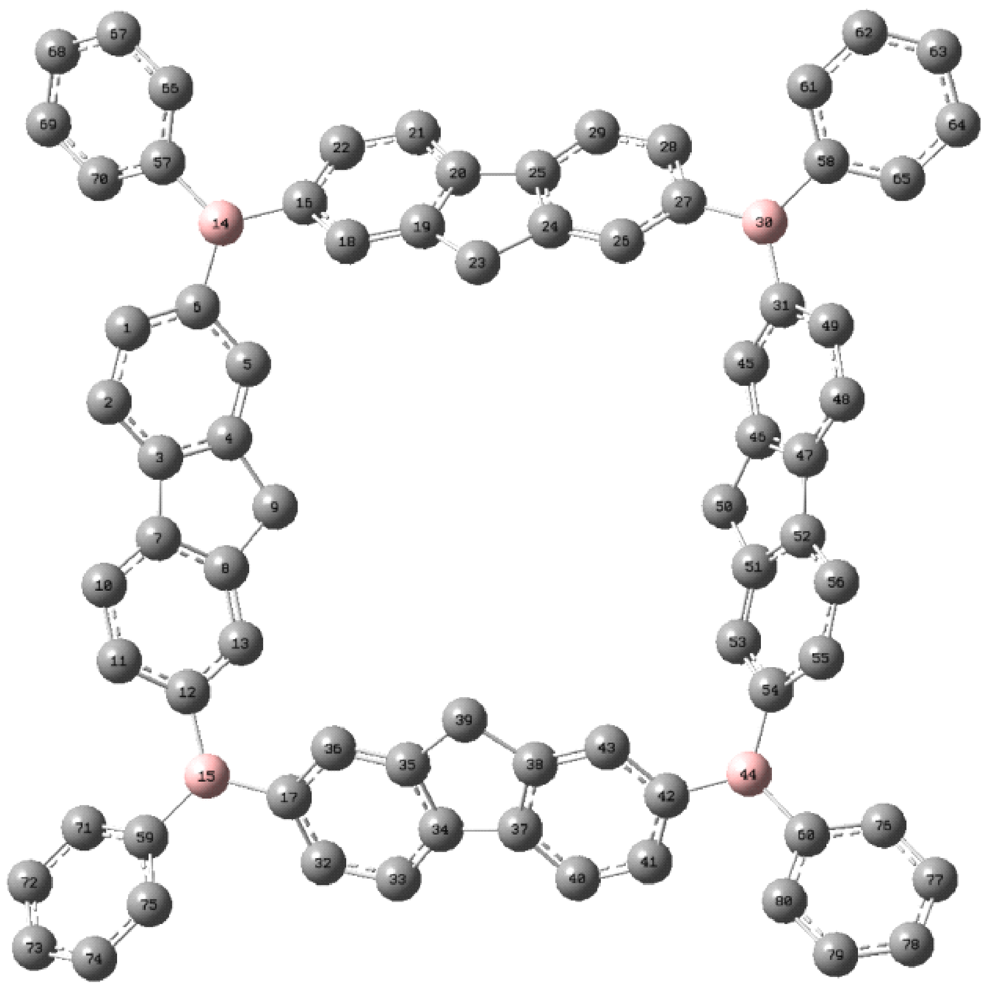

Table 2. Selected bond distances and angles for **MC-B6-calc** (DFT, B3LYP, 6-31G(d))

Bond Distances (Å)				Bond Angles (°)			
B22-C2	1.568	B56-C33	1.568	C2-B22-C24	120.4	C33-B56-C79	120.3
B22-C24	1.568	B56-C79	1.568	C2-B22-C162	119.8	C33-B56-C151	119.8
B22-C162	1.571	B56-C151	1.571	C24-B22-C162	119.9	C79-B56-C151	119.8
B23-C11	1.568	B100-C89	1.568	C11-B23-C40	120.3	C89-B100-C102	120.4
B23-C40	1.568	B100-C102	1.568	C11-B23-C173	119.7	C89-B100-C140	119.7
B23-C173	1.571	B100-C140	1.571	C40-B23-C173	119.9	C102-B100-C140	119.9
B57-C49	1.568	B101-C68	1.568	C49-B57-C58	120.3	C68-B101-C111	120.3
B57-C58	1.568	B101-C111	1.568	C49-B57-C118	119.8	C68-B101-C129	119.8
B57-C118	1.571	B101-C129	1.571	C58-B57-C118	119.9	C111-B101-C129	119.9

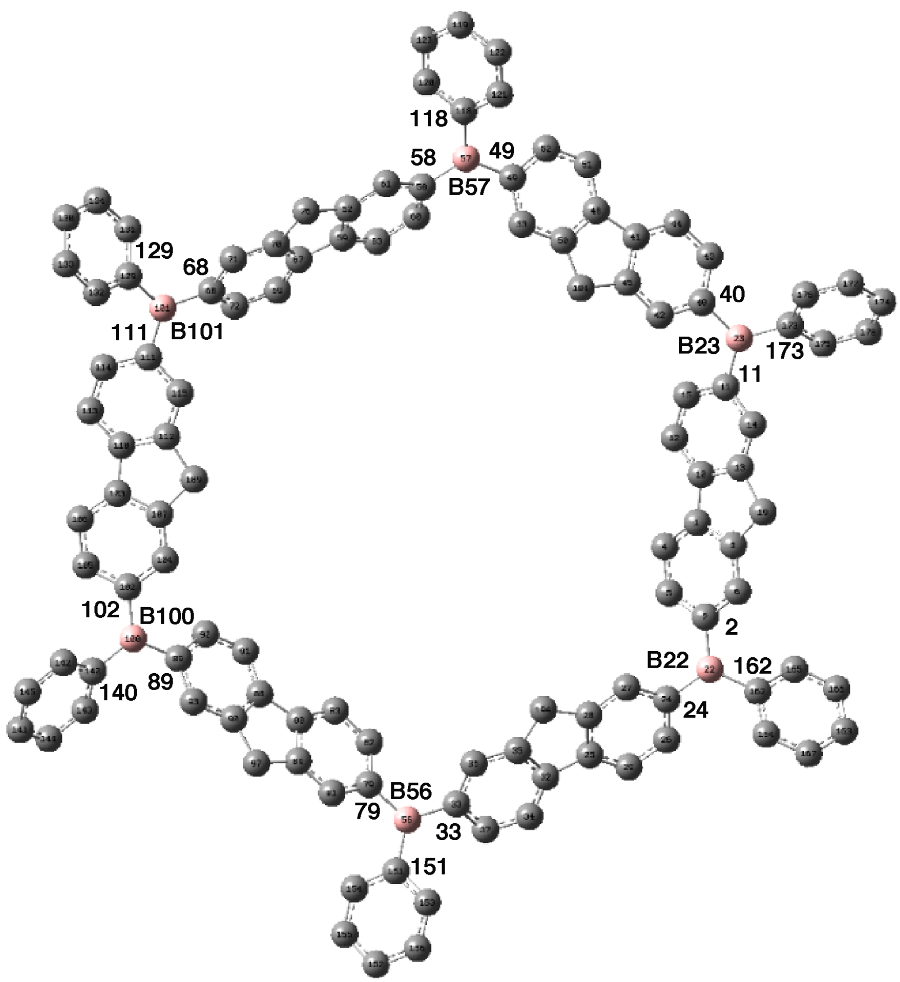

Table 3. Coordinates (Å) for the Optimized Structure of **MC-B6**

atom	x	y	z	atom	x	y	z
C	8.003668	-1.203484	-0.653868	C	3.232375	-10.130587	-0.743599
C	8.271844	-3.989589	-0.261718	C	2.662117	-7.936561	0.146717
C	8.957436	-1.709023	0.255948	C	1.329014	-8.307076	0.248141
C	7.181432	-2.079690	-1.368233	C	1.896069	-10.499019	-0.607913
C	7.314934	-3.450050	-1.155408	H	0.595972	-7.599685	0.628361
C	9.098448	-3.076947	0.437203	H	1.597089	-11.502086	-0.898614
H	6.448097	-1.703114	-2.077155	C	7.870713	5.593048	-0.190517
H	6.672939	-4.130977	-1.707200	C	5.847541	7.555527	-0.387136
H	9.843838	-3.458734	1.130521	C	6.540976	5.303545	0.200717
C	8.088962	0.259672	-0.657411	C	8.138310	6.894879	-0.679602
C	8.680055	2.997408	-0.279661	C	7.147645	7.866987	-0.795141
C	7.373495	1.222088	-1.375809	C	5.550114	6.270966	0.117284
C	9.095963	0.655305	0.249443	H	6.303334	4.314002	0.583701
C	9.395957	1.998320	0.423091	H	9.150739	7.139328	-0.988161
C	7.665723	2.568606	-1.169925	C	4.623296	8.360410	-0.372778
H	6.600616	0.929900	-2.082549	C	2.022427	9.436162	-0.123514
H	10.181907	2.294212	1.113639	C	3.569900	7.571793	0.138439
H	7.106793	3.316898	-1.724986	C	4.387707	9.682521	-0.760182
C	9.713613	-0.565334	0.903285	C	3.104363	10.204914	-0.617977
H	9.586043	-0.554866	1.994784	C	2.289783	8.095763	0.246181
H	10.795273	-0.629250	0.720513	H	2.923005	11.235469	-0.909701
B	8.419108	-5.537653	-0.058642	H	1.481333	7.479562	0.632203
B	9.007199	4.518665	-0.085000	B	-0.589843	-10.051478	0.006030
C	7.165941	-6.473505	-0.165429	B	0.586204	10.051274	0.008793
C	4.928709	-8.187832	-0.366398	C	-0.681719	9.152529	-0.200007
C	7.282367	-7.799838	-0.648424	C	-2.961625	7.532498	-0.607404
C	5.876932	-6.029616	0.217596	C	-0.671823	8.063286	-1.105071
C	4.780647	-6.875543	0.132459	C	-1.884613	9.404918	0.502941
C	6.185685	-8.650346	-0.766066	C	-2.999341	8.601410	0.313980
H	8.260836	-8.162026	-0.950858	C	-1.792431	7.265557	-1.325642
H	5.754056	-5.017517	0.595626	H	0.238265	7.853106	-1.659782
C	3.618815	-8.844152	-0.357014	H	-1.925463	10.233614	1.205566
C	0.908790	-9.607977	-0.120770	H	-1.752704	6.449296	-2.042792

C	-4.271830	6.875849	-0.617412	B	-9.008477	-4.519729	-0.090600
C	-6.939020	6.017267	-0.248885	B	-8.420598	5.538778	-0.059575
C	-4.748440	5.783454	-1.347821	C	-9.191279	-2.967586	-0.211095
C	-5.117052	7.540779	0.297166	C	-9.556499	-0.174204	-0.432615
C	-6.430714	7.128784	0.466001	C	-8.165888	-2.070656	0.174889
C	-6.060876	5.361993	-1.146185	C	-10.393401	-2.408712	-0.709438
H	-4.109353	5.267535	-2.060248	C	-10.581153	-1.034568	-0.837427
H	-7.079413	7.654841	1.162030	C	-8.350174	-0.698965	0.079831
H	-6.429992	4.509521	-1.709492	H	-7.231232	-2.467494	0.563707
C	-4.367398	8.678098	0.963303	H	-11.193077	-3.077289	-1.015499
H	-4.311771	8.549759	2.053356	C	-9.471310	1.288628	-0.427224
H	-4.852382	9.649172	0.792245	C	-8.783978	4.019280	-0.187891
C	-1.743824	-9.011372	-0.207029	C	-8.212106	1.666141	0.087428
C	-3.818461	-7.137574	-0.623380	C	-10.389482	2.264931	-0.824346
C	-2.969460	-9.119979	0.493710	C	-10.043586	3.607166	-0.687329
C	-1.605065	-7.932816	-1.114401	C	-7.869474	3.006535	0.190489
C	-2.624484	-7.010319	-1.339194	H	-10.760470	4.366071	-0.987651
C	-3.982702	-8.192858	0.299888	H	-6.894577	3.289484	0.580090
H	-3.108125	-9.936241	1.198354	C	0.417165	11.575403	0.349724
H	-0.675412	-7.831592	-1.667336	C	0.114893	14.325915	0.965167
H	-2.488296	-6.205858	-2.057860	C	-0.652175	12.336335	-0.171711
C	-5.043050	-6.332372	-0.637480	C	1.329072	12.249082	1.191727
C	-7.592446	-5.167746	-0.276215	C	1.176020	13.598307	1.508427
C	-5.962411	-6.892980	0.275510	C	-0.796468	13.692853	0.116975
C	-5.386981	-5.192284	-1.369674	H	-1.373561	11.855182	-0.826754
C	-6.641590	-4.620073	-1.171402	H	2.165451	11.698225	1.613612
C	-7.219312	-6.330197	0.440703	H	1.885757	14.084555	2.173128
H	-4.690269	-4.755187	-2.080809	H	-1.620547	14.255851	-0.314230
H	-6.907292	-3.730854	-1.736257	H	-0.000890	15.380934	1.201050
H	-7.926662	-6.775700	1.135944	C	-9.544276	6.588998	0.259953
C	-5.352122	-8.108649	0.945320	C	-11.571791	8.484499	0.834747
H	-5.285072	-7.986071	2.035388	C	-9.507176	7.895789	-0.274096
H	-5.946473	-9.016870	0.773874	C	-10.637874	6.271019	1.094793
C	-11.629886	7.204890	1.391476	C	12.266026	-6.154359	-0.031140
C	-10.510099	8.826571	-0.005789	C	11.231589	-7.813668	1.387509
H	-8.682072	8.178916	-0.922186	H	9.093896	-7.724391	1.538748
H	-10.701234	5.276251	1.527676	H	10.940241	-4.740589	-0.949784

H	-12.450686	6.934960	2.051321	H	13.155242	-5.721074	-0.482353
H	-10.462521	9.819367	-0.446385	H	11.313941	-8.669202	2.053283
H	-12.349626	9.211499	1.055098	H	13.356549	-7.682088	1.033949
C	-10.247860	-5.433088	0.220903	C	10.482164	4.965763	0.218594
C	-12.484509	-7.081948	0.779393	C	13.143872	5.772980	0.764855
C	-11.298117	-4.995228	1.057072	C	11.589171	4.283004	-0.331573
C	-10.363078	-6.731068	-0.323116	C	10.763111	6.069328	1.053788
C	-11.468654	-7.539799	-0.062784	C	12.071188	6.460794	1.336664
C	-12.393329	-5.808486	1.345806	C	12.899669	4.685645	-0.077103
H	-11.245077	-4.003084	1.497426	H	11.414629	3.429425	-0.981246
H	-9.575952	-7.103901	-0.973081	H	9.938243	6.620220	1.497861
H	-11.537044	-8.527973	-0.510981	H	12.255327	7.304471	1.997174
H	-13.178025	-5.449055	2.006882	H	13.730563	4.150239	-0.529846
H	-13.342525	-7.714468	0.993478	H	14.164827	6.082771	0.974134
C	-0.936708	-11.544067	0.351996	C	4.083633	6.189922	0.494682
C	-1.561430	-14.237554	0.976505	H	7.387716	8.850777	-1.190784
C	-0.113704	-12.315877	1.201297	H	5.189414	10.298204	-1.160512
C	-2.085061	-12.177250	-0.172240	H	3.557777	5.398544	-0.057290
C	-2.388399	-13.506227	0.120992	H	3.946317	5.964126	1.561405
C	-0.425041	-13.636518	1.522530	C	-7.410767	0.431727	0.452811
H	0.779170	-11.864494	1.625499	H	-7.149862	0.412863	1.520178
H	-2.742082	-11.618119	-0.833057	H	-6.460803	0.377789	-0.096934
H	-3.270607	-13.970976	-0.312302	H	-11.360326	1.987489	-1.227509
H	0.219712	-14.199417	2.192922	H	-11.512574	-0.643531	-1.239351
H	-1.800918	-15.270718	1.215950	C	3.331620	-6.623015	0.502535
C	9.831016	-6.151417	0.253729	H	6.311320	-9.656965	-1.157214
C	12.379190	-7.257664	0.817765	H	3.958959	-10.836560	-1.138218
C	9.978837	-7.275275	1.095881	H	3.216714	-6.380062	1.568152
C	11.012018	-5.604655	-0.294565	H	2.904120	-5.777217	-0.053608

Table 4. Coordinates (Å) for the Optimized Structure of **MC-B4**

atom	x	y	z	atom	x	y	z
C	-2.585162	6.684223	0.833086	C	-4.669520	-3.786311	-0.299907
C	-3.732139	5.900277	0.959038	C	-4.248359	-2.697599	0.494574

C	-3.786949	4.669154	0.298005	C	-5.025078	-1.554345	0.591479
C	-2.697355	4.247967	-0.495293	C	-3.613153	-4.805838	-0.290252
C	-1.553841	5.024488	-0.590458	C	-2.547210	-4.338375	0.509212
C	-1.460350	6.267013	0.081124	C	-2.891903	-2.988084	1.102290
C	-4.806018	3.612363	0.288093	C	-3.507780	-6.040536	-0.938397
C	-4.337721	2.546415	-0.510877	C	-2.334490	-6.781244	-0.794027
C	-2.987229	2.891532	-1.103332	C	-1.232201	-6.315679	-0.037278
C	-6.041258	3.506838	0.935119	C	-1.377132	-5.071707	0.622115
C	-6.781569	2.333355	0.790303	B	0.128007	-7.097766	0.027162
C	-6.315567	1.231254	0.033608	C	5.072088	-1.376049	-0.621800
C	-5.070948	1.376314	-0.624756	C	4.338173	-2.545710	-0.508109
B	-0.128597	7.097983	0.036432	C	4.803378	-3.610071	0.294813
B	-7.098657	-0.128362	-0.032976	C	6.036255	-3.503417	0.946186
C	1.230381	6.314107	-0.030391	C	6.777826	-2.330749	0.800847
C	-6.267195	-1.459662	-0.080699	C	2.989544	-2.891486	-1.104253
C	1.375421	5.069900	0.628512	C	2.697671	-4.247088	-0.495330
C	2.545098	4.336178	0.513959	C	3.784053	-4.666661	0.303134
C	3.610654	4.803773	-0.286036	C	1.554782	-5.024034	-0.594316
C	3.504993	6.038645	-0.933755	C	1.458443	-6.265051	0.079655
C	2.331836	6.779436	-0.788418	C	2.580056	-6.680787	0.837014
C	2.890224	2.985970	1.106915	C	3.726464	-5.896530	0.966356
C	4.247495	2.696674	0.500415	C	-0.152744	8.664338	0.055719
C	4.668069	3.785339	-0.294390	C	8.664595	0.153330	-0.057090
C	5.024594	1.553691	0.597355	C	-8.665159	-0.153966	-0.055057
C	6.266970	1.459835	-0.074364	C	0.155326	-8.664109	0.050887
C	6.683764	2.583789	-0.827843	C	9.397301	1.238403	0.472795
C	5.899160	3.730065	-0.955609	C	10.791219	1.257099	0.459915
B	7.098459	0.128779	-0.027458	C	11.496984	0.194429	-0.109170
C	6.314743	-1.230434	0.039810	C	10.801977	-0.888609	-0.652365
C	-6.684268	-2.583541	-0.834165	C	9.408607	-0.910400	-0.613668
C	-5.900603	-3.730600	-0.960979	C	0.908013	9.411335	0.614088
C	0.887473	10.804917	0.642897	H	-2.935259	-3.023189	2.200267
C	-0.191194	11.497214	0.087614	H	-2.149103	-2.219894	0.847892
C	-1.250396	10.788504	-0.484174	H	-4.318868	-6.415917	-1.557653
C	-1.232976	9.394491	-0.487466	H	-2.251906	-7.735636	-1.307097
C	-9.412950	0.910889	-0.604519	H	-0.552958	-4.685956	1.216688
C	-10.806468	0.888261	-0.636331	H	4.688301	-0.553059	-1.219345

C	-11.498048	-0.197081	-0.093388	H	6.410406	-4.313642	1.567310
C	-10.788595	-1.260930	0.468811	H	7.731312	-2.247407	1.315525
C	-9.394657	-1.241154	0.475044	H	2.220468	-2.148495	-0.852815
C	1.241782	-9.392843	-0.481586	H	3.027536	-2.936303	-2.202076
C	1.264023	-10.786744	-0.472113	H	0.714431	-4.675485	-1.189256
C	0.203604	-11.496567	0.096066	H	2.534241	-7.631028	1.362131
C	-0.880934	-10.805623	0.641419	H	4.553774	-6.235180	1.585281
C	-0.906275	-9.412225	0.606150	H	8.860125	2.073949	0.913435
H	-2.541373	7.635089	1.357234	H	11.328077	2.099727	0.888426
H	-4.561496	6.239713	1.574808	H	12.583950	0.210137	-0.128974
H	-0.710644	4.674330	-1.180427	H	11.346952	-1.715526	-1.100795
H	-3.022309	2.935253	-2.201304	H	8.879859	-1.761522	-1.034185
H	-2.218866	2.148816	-0.849007	H	1.755614	8.884655	1.044246
H	-6.417778	4.318106	1.553425	H	1.711921	11.352108	1.093193
H	-7.736066	2.250370	1.303088	H	-0.206083	12.584281	0.099848
H	-4.684982	0.552494	-1.219679	H	-2.089173	11.323138	-0.922869
H	0.551999	4.684788	1.224662	H	-2.065414	8.855247	-0.931388
H	4.316289	6.414796	-1.552258	H	-8.887019	1.763541	-1.025501
H	2.249185	7.734428	-1.300432	H	-11.354222	1.716318	-1.079273
H	2.932013	3.020477	2.204953	H	-12.585079	-0.213759	-0.108071
H	2.148454	2.217178	0.850966	H	-11.322625	-2.105467	0.897149
H	4.675239	0.711442	1.189139	H	-8.854842	-2.077211	0.911356
H	7.634874	2.539701	-1.351567	H	2.075488	-8.852457	-0.921703
H	6.238456	4.559105	-1.571882	H	2.107831	-11.320376	-0.902384
H	-7.634942	-2.539031	-1.358602	H	0.222184	-12.583527	0.113501
H	-6.239994	-4.559335	-1.577602	H	-1.706297	-11.353821	1.088794
H	-4.675399	-0.712272	1.183338	H	-1.758222	-8.886652	1.028924

Chapter 4 Conjugated Ambipolar B-π-N Macrocycles[a]

4.1 Introduction to BN Functionalized Organic Systems

Electronic isosterism is a common phenomenon observed in nature. CC and BN units have the same number of valence electrons, leading to essentially similar properties (**Figure 4-1**).[1] For example, boron nitride exists in the form of two allotropes that are structurally related to graphite and diamond, respectively. More recently, boron nitride nanotubes (BNNTs) were discovered as a structural analogue of carbon nanotubes (CNTs). They were reported to show desirable mechanical properties and exceptionally high thermal and chemical stability (**Figure 4-2**).[2,3]

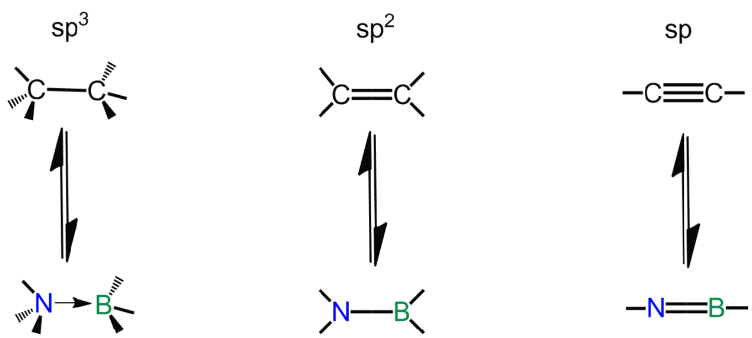

Figure 4-1. Isoelectronic relationship between CC and BN units.[1]

Figure 4-2. Structural models of carbon nanotubes (CNTs) and boron nitride nanotubes (BNNTs). The alternating B and N atoms are shown in blue and pink, respectively, in the BNNT model.[3]

[a] This chapter is in part adapted from a journal publication (ref.57).

In reference to its isoelectronic and isostructural relationship with benzene, borazine is commonly referred to as “inorganic benzene”.[4,5] This concept has generated renewed interest in recent years, as the judicious replacement of C=C double bonds with isoelectronic and isosteric B-N fragments has resulted in a plethora of interesting molecules for applications ranging from hydrogen storage materials to analogs of aromatic natural products, and new optical and electronic materials (**Figure 4-3**).[6-14] For instance, introduction of a B-N fragment in benzene results in polarization of the molecule, which in turn leads to unusual reactivity, including nucelophilic substitution and hydrogenation under mild conditions.[11,12,15] B-N functionalization of extended organic π-systems alters the electronic structure, resulting for example in low-lying LUMO levels and corresponding bathochromic shifts in the emission spectra (**Figure 4-4**).[13,14,16,17] In the previous examples, B and N are directly connected or located in the same ring system. An alternative design has borane acceptor (A) moieties separated from amine donors (D) by an organic π-conjugated linker. This D-π-A approach has proven very successful for the development of non-linear optical materials, ambipolar charge carriers in organic light emitting devices (OLEDs), and fluorescent anion sensors.[18-27]

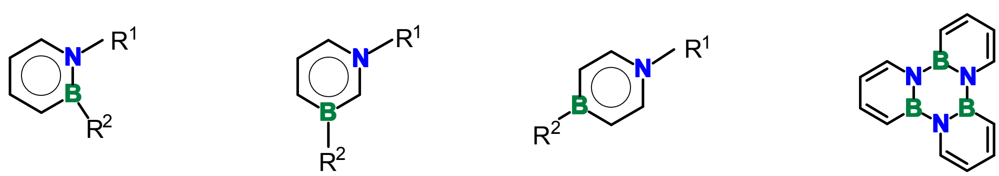

Figure 4-3. Molecular structures of BN functionalized aromatic compounds.[1]

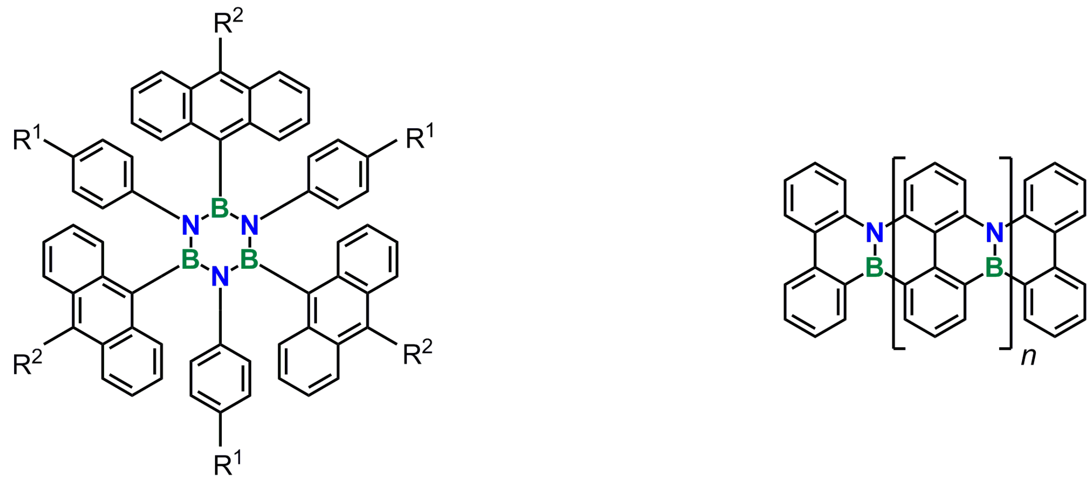

Figure 4-4. Examples of BN functionalization of extended organic π-systems.[16,17]

As already discussed in Chapter 3, conjugated macrocycles are an attractive class of materials for optoelectronic applications as they comprise discrete, monodisperse structures, representative of an infinite polymer chain without any end groups.[28-32] Another interesting feature is their ability to self-assemble into tubular supramolecular structures and to form well-defined and highly symmetric arrays upon deposition on surfaces.[33,34] Numerous conjugated organic cyclics have been explored. More recently, heteroatom-containing systems have attracted interest because the added functionality can offer unique properties and possibly open the door to new applications.[35-43] As an example, Tanaka's cyclic hexaanilines **MC-N6** (π = phenylene) provide a platform for studies on the aromaticity and molecular magnetism that results from spin delocalization in the radical cation and dication.[35] In Chapter 3, we have introduced an electron-deficient charge-reverse analogue[44] to **MC-N6**, the conjugated macrocyclic organoborane **MC-B6** with fluorene as the π-system.[45] We describe here the first ambipolar macrocycle, which contains nitrogen as donor and boron as acceptor sites, bridged by π-conjugated phenylene groups. This new type of macrocycle **MC-B3N3** may be viewed as a π-expanded borazine (**Figure 4-5**); however, introduction of the phenylene bridges results in remarkably different properties in comparison to borazine, including strong blue fluorescence, solvatochromic emission, and redox processes that reflect the ambipolar structure of this unique D-π-A type macrocycle. In addition to **MC-B3N3**, we also discuss two related ambipolar macrocycles **MC-B4N2** and **MC-B2N2** that incorporate N donor and B acceptor separated by hybrid π systems.

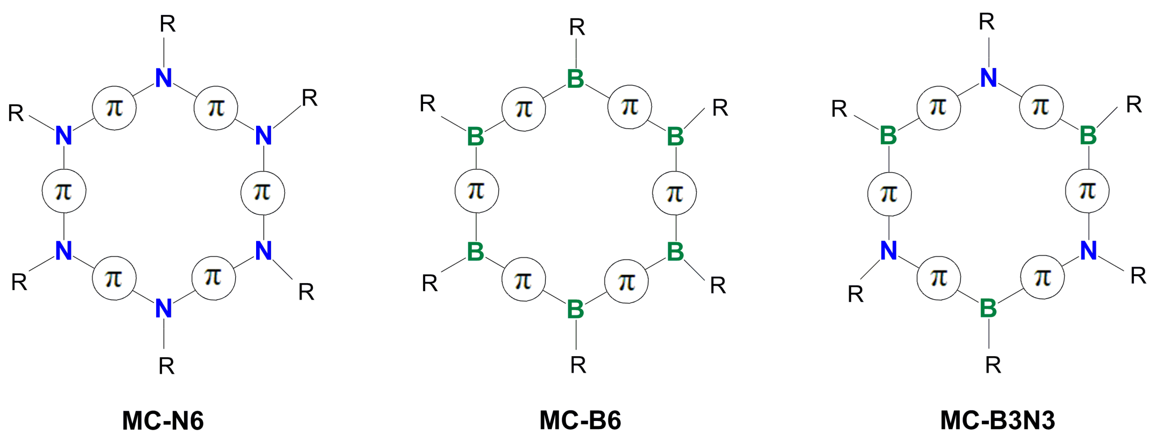

Figure 4-5. Representations of conjugated all-nitrogen (**MC-N6**), all-boron (**MC-B6**) and boron-alt-nitrogen ambipolar (**MC-B3N3**) macrocycles.

Phenylene π system

4.2 Synthesis and Structural Characterization of **MC-B3N3**

Initially, the linear oligomer **O-B1N2** was prepared in 66% overall yield by Sn/B exchange of the stannyl group in **TPA-SiSn** with the boryl group in **TPA-SiB**, followed by treatment with triisopropylphenyl copper (TipCu) for steric protection of the boron center (**Scheme 4-1**). The selectivity of the Sn/B exchange relies on the much higher reactivity[46,47] of the Sn-C in comparison to the Si-C bond in **TPA-SiSn**. Formation of the ambipolar macrocycle **MC-B3N3** was accomplished by reaction of **O-B1N2** with 2 equivalents of BBr_3, followed by cyclization under pseudo-high dilution conditions upon simultaneous addition of stoichiometric amounts of the resulting borylated species and **TPA-Sn2** (1:1) to a large quantity of toluene. Treatment of the initially generated B-Br functionalized macrocycle with 2 equivalents of TipCu in refluxing toluene for 2 days gave the desired product **MC-B3N3**. GPC analysis indicated that the crude sample after standard workup consists of the targeted macrocycle as the major product in addition to a small amount of larger cyclics and/or higher linear polymers (**Figure 4-6**). Purification by preparative size exclusion column chromatography on Bio-beads™ with THF as the eluent gave analytically pure **MC-B3N3** as a pale yellow powdery solid in 38% overall yield over 3 steps.

GPC analysis of purified **MC-B3N3** revealed a single, monodisperse band corresponding to a molecular weight of M_n = 1483 Da (PDI = M_w/M_n = 1.01), which is close to the theoretical value of 1540 Da (**Figure 4-6**). Successful synthesis of the macrocyclic species was further confirmed by high-resolution MALDI-MS (**Figure 4-7**), which showed a single signal at m/z = 1540.0705 that can be assigned to the molecular ion peak (calcd 1540.0706). Consistent with the highly symmetric cyclic structure, only one set of sharp signals was observed in the ^1H (**Figure 4-8**) and ^{13}C NMR spectra, and a broad ^{11}B NMR resonance at 72 ppm is indicative of tricoordinate B centers (**Figure 4-9**).

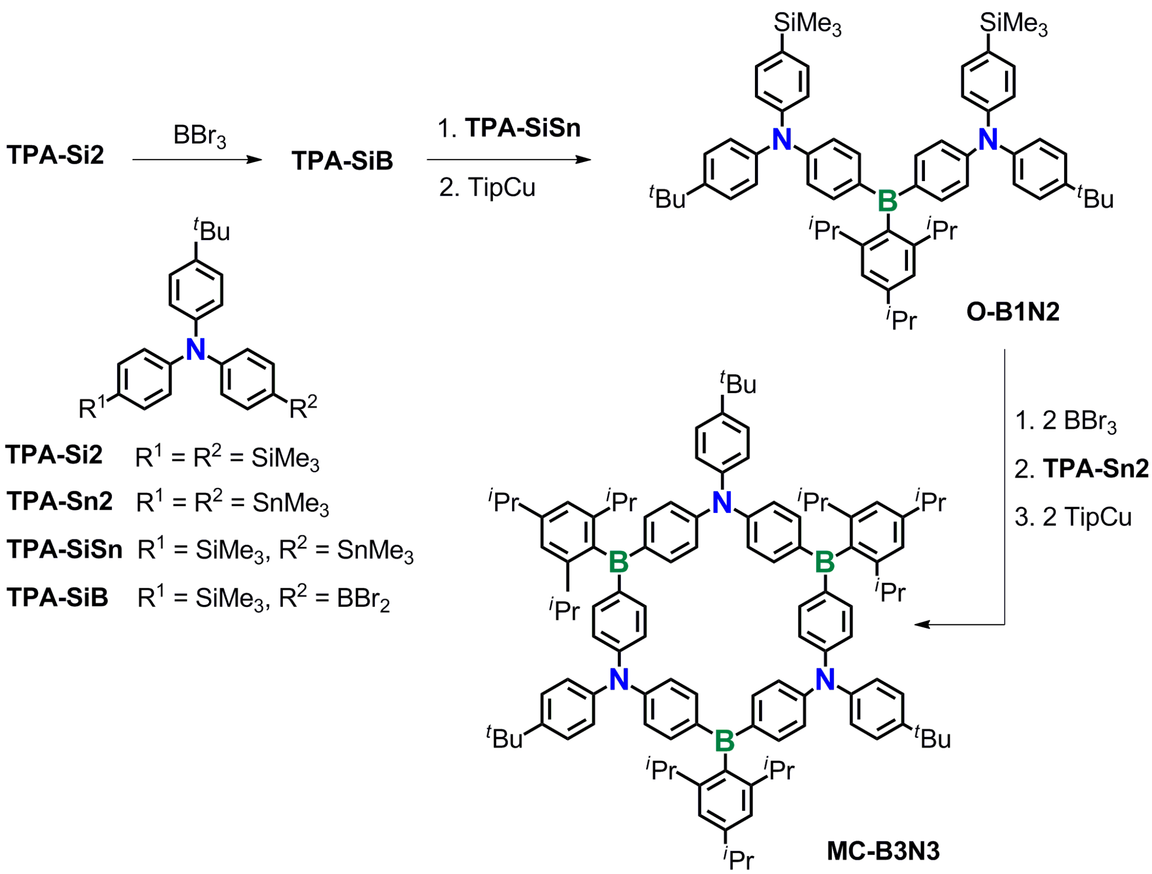

Scheme 4-1. Synthesis of the donor-π-acceptor macrocycle **MC-B3N3**.

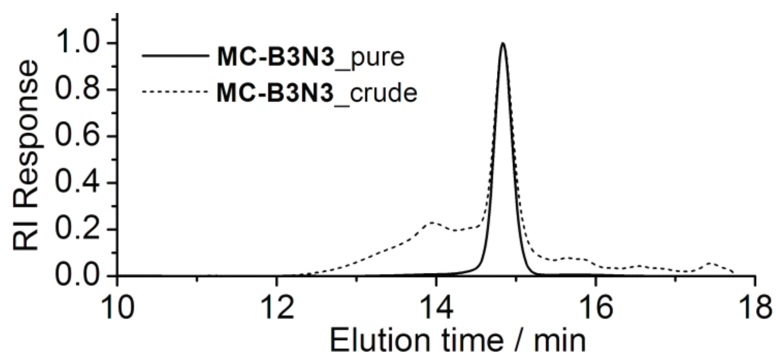

Figure 4-6. GPC traces for macrocycle **MC-B3N3** in THF (1 mL min^{-1}).

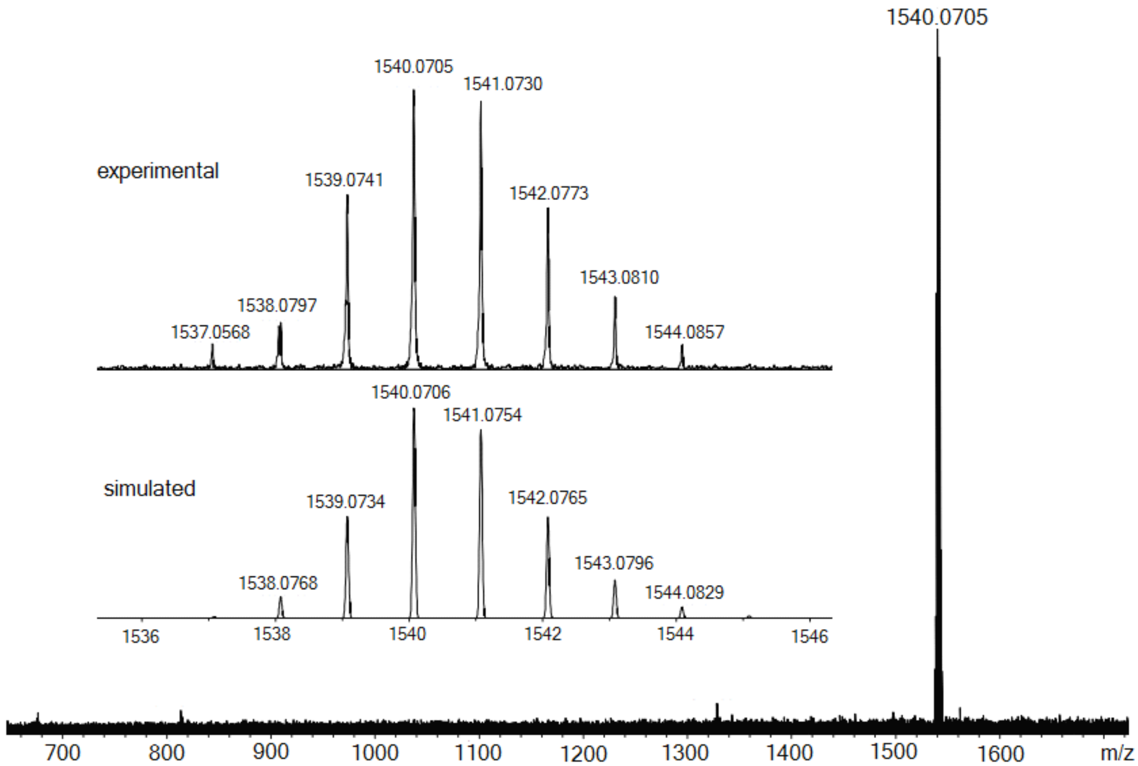

Figure 4-7. High resolution MALDI-MS (positive mode) of the isolated **MC-B3N3**.

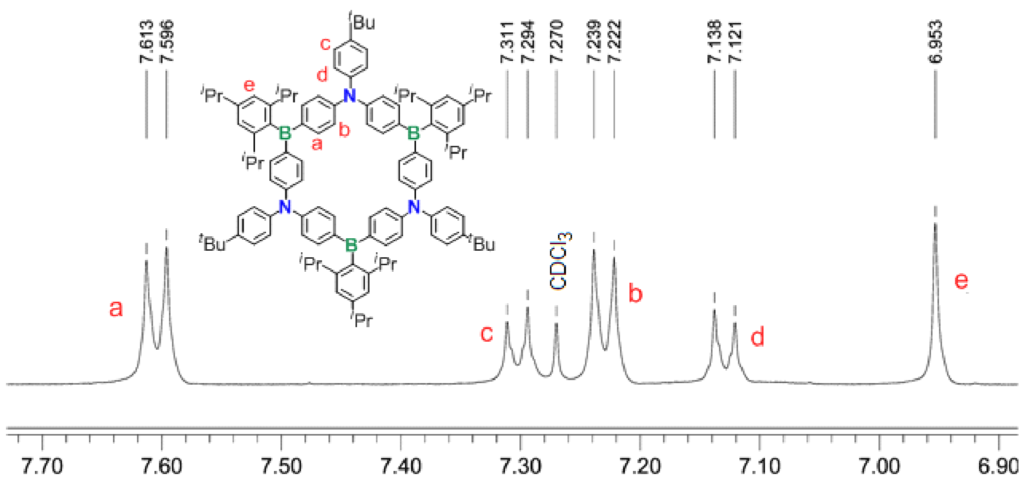

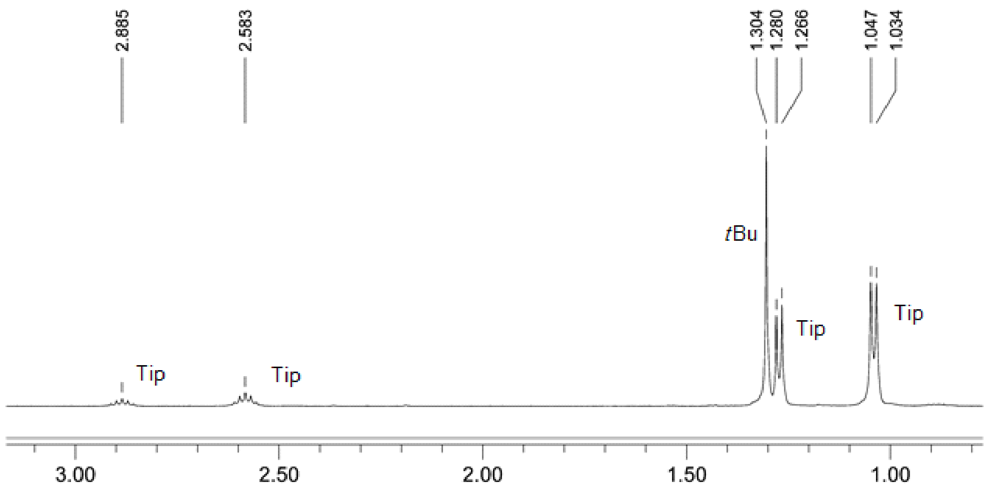

Figure 4-8. ^{1}H NMR spectrum of macrocycle **MC-B3N3** ($CDCl_3$, 25 °C).

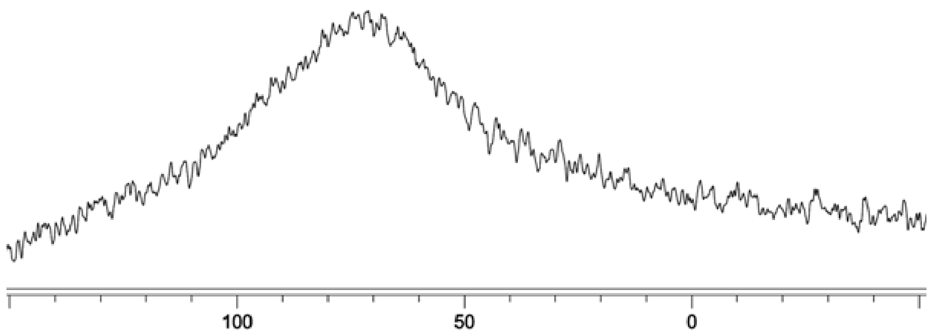

Figure 4-9. ^{11}B NMR spectrum of macrocycle **MC-B3N3** ($CDCl_3$, 25 °C).

Colorless hexagon-shaped single crystals that show blue fluorescence were obtained by slow vapor diffusion of dichloroethane into a solution of **MC-B3N3** in toluene (**Figure 4-10**). Compound **MC-B3N3** crystallizes in the trigonal space group R $\bar{3}$ with eight molecules of dichloroethane per macrocycle for a total of six macrocycles and 48 solvent molecules per unit cell (see Appendix). Due to the large size and exceedingly fast solvent evaporation from the crystals, and despite the use of dichloroethane in place of dichloromethane, the uncertainties are relatively large and only allow for a qualitative discussion. The endocyclic B-C (1.546(6), 1.560(6) Å) and N-C (1.414(5), 1.426(5) Å) distances are similar to the exocyclic ones of 1.571(6) and 1.427(5) Å, respectively, and the endocyclic C-B-C (119.7(3)°) and C-N-C (121.5(3)°) angles are close to 120°, indicating that the ring system is not significantly strained. However, as evident from the side view in **Figure 4-10b**, rather than adopting perfect D_3 symmetry, the B_3N_3 core is distorted towards a chair-like conformation, and all the exocyclic substituents point into one direction relative to the mean plane described by the B_3N_3 core. Six of the dichloroethane solvent molecules are located in layers that alternate with layers consisting of the main molecules **MC-B3N3** (**Figure 4-11**). The remaining two solvent molecules are highly disordered and are positioned in channels that propagate along the crystallographic *c* axis. The channels are smaller than the cavity of the individual macrocycles, because the aryl substituents and solvents in layers above and below each macrocycle reach into the channels (**Figure 4-10c**).

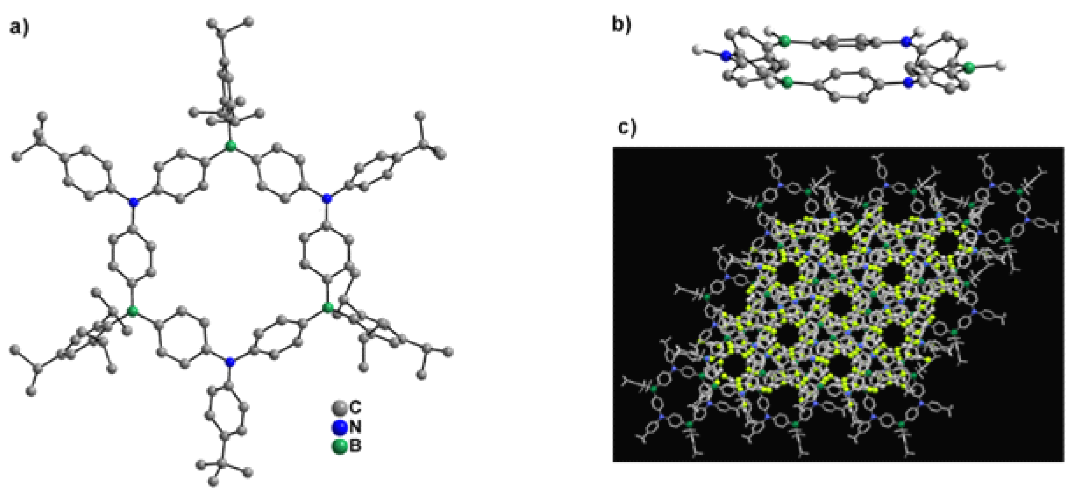

Figure 4-10 a) X-ray structure of **MC-B3N3** (solvents and hydrogens omitted). b) Side view without exocyclic substituents. c) Supramolecular structure of **MC-B3N3** viewed along the crystallographic *c* axis (only solvent outside the channels shown).

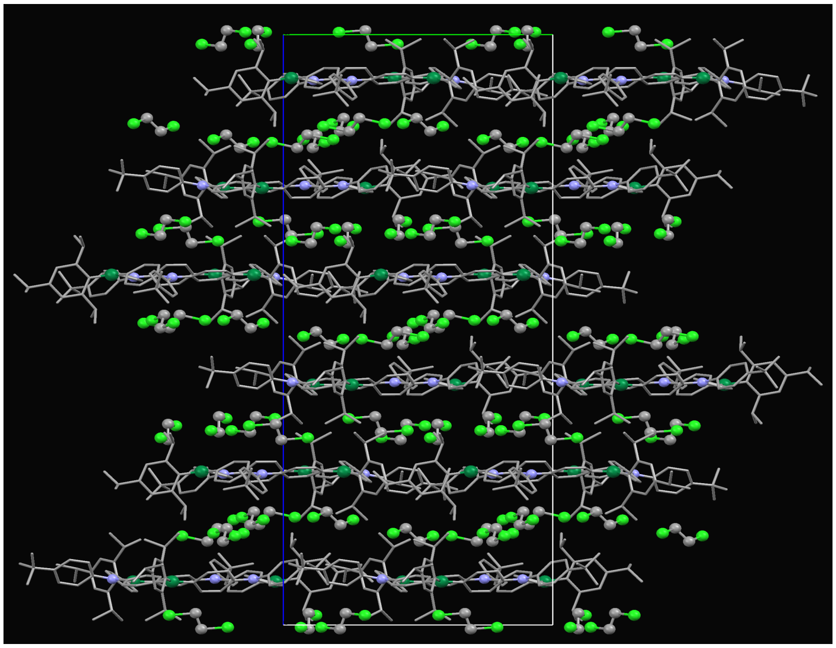

Figure 4-11. The extended structure of macrocycle **MC-B3N3** viewed along the crystallographic *a* axis, showing solvent molecules between the layers.

4.3 Photophysical, Electrochemical and Computational Studies of Ambipolar Macrocycle **MC-B3N3**

Compound **MC-B3N3** forms colorless crystals that are blue-emissive when exposed to UV light. In solution, the absorption spectra of **MC-B3N3** show two distinct bands around 420 and 390 nm, independent of the solvent (**Figure 4-12**). These bands are attributed to intramolecular charge transfer (ICT) from triarylamine donor sites (n/π) to triarylborane acceptor sites (n/π*). Photoexcitation gives rise to an intense emission (CH_2Cl_2: λ_{em} = 460 nm, Φ = 0.76), which experiences a pronounced red-shift with increasing solvent polarity. This solvatochromic effect in the emission, but not the absorption spectra, suggests a more polarized excited state upon ICT, a phenomenon that is consistent with the formation of a B/N D-π-A system.[18-26]

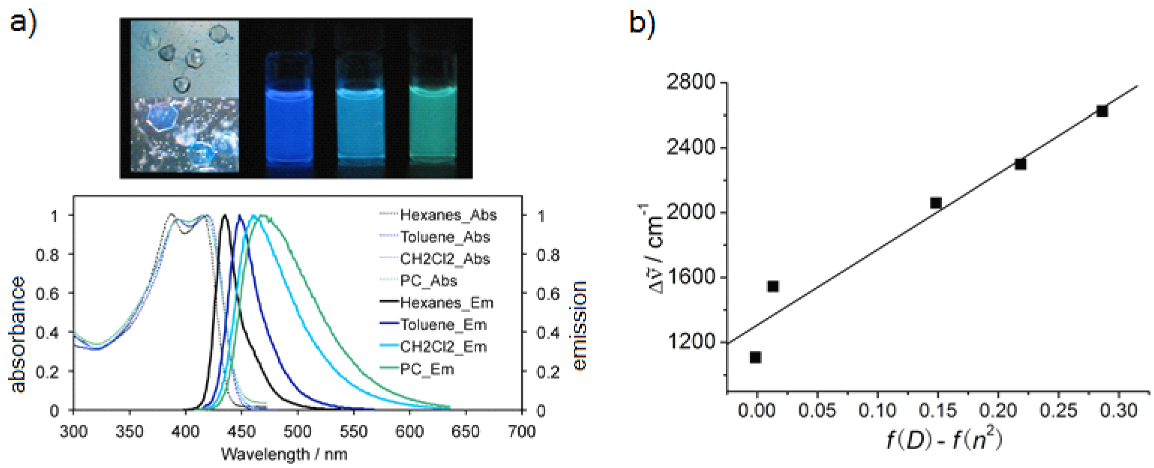

Figure 4-12. a) Top left: photographs of crystals of **MC-B3N3** without (top) and with (bottom) UV irradiation at 365 nm and photographs of solutions of **MC-B3N3** in (left to right) toluene, CH_2Cl_2 (DCM), and propylene carbonate (PC) irradiated at 365 nm. Bottom left: UV-vis absorption and fluorescence spectra (λ_{ex} = 419 nm) of **MC-B3N3** in solvents of different polarity. b) Lippert-Mataga plot for the solvatochromic emission of macrocycle **MC-B3N3** (hexanes, toluene, $CHCl_3$, CH_2Cl_2, propylene carbonate). The Stokes shifts in different solvents are plotted relative to the solvent polarity function f(D) – f(n^2) with f(D) = (D-1)/(2D+1) and f(n^2) = (n^2-1)/(2n^2+1); D = permittivity; n = refractive index of the solvent (see also the detailed discussion in Chapter 2 about the Lippert-Mataga analysis).

Table 4-1. Computational and Experimental Data for **MC-B3N3**

	CV[a] [eV]	SWV[a] [eV]	DFT[b] [eV]	UV/Vis [nm] ([eV])	TD-DFT [b] [nm] ([eV])
E_{LUMO}	–2.27	–2.30	–1.69		
E_{HOMO}	–5.26	–5.30	–5.01		
$\Delta E_{gap/uv}$	2.99	3.00	3.32	420 (2.96)	432 (2.87)[c]

[a] Reference: ferrocene at 4.80 eV below vacuum, CV = cyclic voltammetry, SWV = square-wave voltammetry. [b] Computations performed on a simplified analog of **MC-B3N3** (^{i}Pr and ^{t}Bu groups omitted). [c] Allowed $S_2 \leftarrow S_0$ transition.

DFT and TDDFT calculations (B3LYP/6-31G*) were carried out on a simplified analog of **MC-B3N3** (R = Ph, phenylene π-system) in D_3 symmetry (minimization in C_3 symmetry gave slightly higher energy) and the results are summarized in **Table 4-1** and **Table 4-2**. The HOMO of **MC-B3N3** is degenerate (e) with contributions of the nitrogen atoms and the bridging phenylene rings, while the degenerate LUMOs (e) are mostly localized on the boron p orbitals with smaller contributions of the exocyclic phenyl rings (**Figure 4-13**). The HOMO-2 and LUMO+2 orbitals are totally symmetric (a_2) and thus feature contributions from all of the filled N and empty B p-orbitals, respectively. Again, p-π delocalization into the bridging phenylene rings is more pronounced in the N-centered HOMO-2 than the B-centered LUMO+2. This is in contrast to results for the corresponding simplified hexabora and hexaaza analogs **MC-N6** and **MC-B6** (R = Ph, phenylene π-system), for which both the HOMO and LUMO show delocalization throughout the ring system (**Figures 4-14** and **4-15**). Based on TDDFT calculations, the $S_1 \leftarrow S_0$ transition (HOMO-1 to LUMO+1 / HOMO to LUMO) is symmetry forbidden because of cancellation of the transition dipole moments, as is typically observed for highly symmetric macrocycles, including **MC-N6** and **MC-B6**.[45] While in solution lower symmetry conformations may be adopted, the structure of the cycle is expected to be quite rigid. The experimentally observed absorption bands are therefore assigned to doubly degenerate nπ–nπ* transitions to S_2 and S_3, for which HOMO-2 and LUMO+2 contributions are mixed in (**Table 4-3**). GIAO calculations suggest less aromatic character for **3** in comparison to the corresponding hexabora and hexaaza species (**Table 4-4** and **Figure 4-16**).

Table 4-2. Calculated Orbital Energies (eV) (DFT, B3LYP, 6-31G(d)) of the Simplified Macrocycles (R = Ph, phenylene π-system)

	MC-B3N3	**MC-N6**	**MC-B6**
LUMO+2	–1.39 (a_2)	–0.41 (e_u)	–2.10 (e_g)
LUMO+1	–1.69 (e)	–0.57 (a_{1u})	–2.10 (e_g)
LUMO	–1.69 (e)	–0.57 (a_{1g})	–2.39 (a_{2u})
HOMO	–5.01 (e)	–4.22 (a_{2g})	–6.45 (a_{1u})
HOMO-1	–5.01 (e)	–4.65 (e_u)	–6.50 (e_g)
HOMO-2	–5.20 (a_2)	–4.65 (e_u)	–6.50 (e_g)
HOMO-LUMO gap	3.32	3.65	4.06

Table 4-3. Comparison of Results from TD-DFT Calculations (B3LYP, 6-31G(d)) on the Simplified Macrocycles (R = Ph, phenylene π-system)

Compound	Transition	λ, nm (eV)	Oscillator Strength, f	Orbital Contributions
MC-B3N3	$S_1 \leftarrow S_0$	471.0 (2.632)	0.000	**HOMO-1→LUMO+1, 0.494** **HOMO→LUMO, 0.494**
	$S_2 \leftarrow S_0$	432.0 (2.870)	0.8837	HOMO–2→LUMO, –0.115 **HOMO-1→LUMO, 0.469** HOMO-1→LUMO+2, –0.109 **HOMO→LUMO+1, 0.469**
	$S_3 \leftarrow S_0$	432.0 (2.870)	0.8835	HOMO–2→LUMO+1, –0.115 **HOMO-1→LUMO+1, 0.469** **HOMO→LUMO, 0.469** HOMO→LUMO+2, 0.109
MC-N6	$S_1 \leftarrow S_0$	406.0 (3.054)	0.000	HOMO-2→LUMO+2, –0.134 HOMO-1→LUMO+3, –0.134 **HOMO→LUMO, 0.669**
	$S_2 \leftarrow S_0$	389.9 (3.180)	0.025	HOMO-2→LUMO+4, 0.117 HOMO-1→LUMO+5, 0.177 **HOMO→LUMO+1, 0.672**
	$S_5 \leftarrow S_0$	365.9 (3.342)	1.211	HOMO–2→LUMO, –0.139 **HOMO→LUMO+2, 0.659**

	$S_6 \leftarrow S_0$	365.9 (3.342)	1.211	HOMO–1→LUMO, –0.139 **HOMO→LUMO+3, 0.659**
MC-B6	$S_1 \leftarrow S_0$	356.2 (3.480)	0.000	HOMO-2→LUMO+1, 0.169 HOMO-1→LUMO+2, –0.169 **HOMO→LUMO, 0.631**
	$S_2 \leftarrow S_0$	338.8 (3.659)	0.9205	HOMO-4→LUMO+2, 0.109 HOMO-3→LUMO+1, 0.109 **HOMO-2→LUMO, 0.640** HOMO→LUMO+1, –0.134
	$S_3 \leftarrow S_0$	338.8 (3.659)	0.9205	HOMO-4→LUMO+1, 0.109 HOMO-3→LUMO+2, 0.109 **HOMO-1→LUMO, 0.640** HOMO→LUMO+2, –0.134

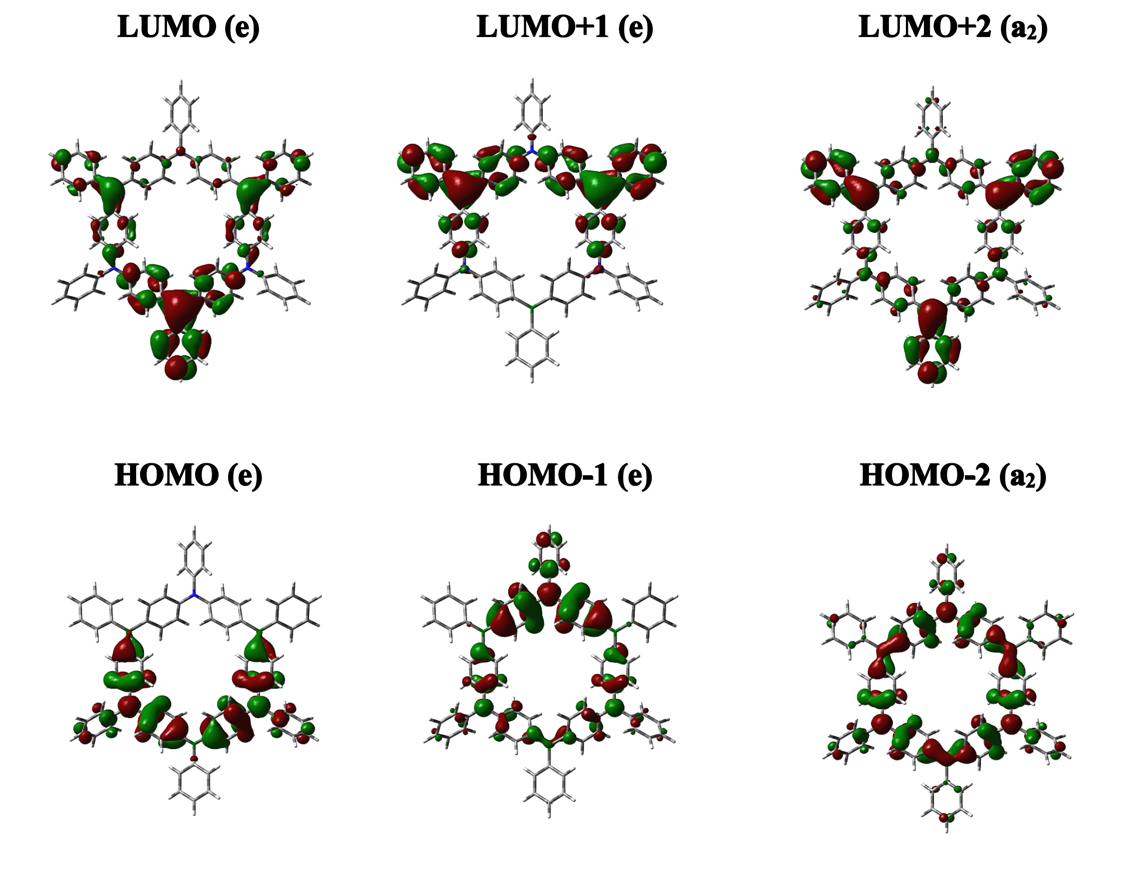

Figure 4-13. Kohn-Sham orbital representation for the ground state frontier orbitals of **MC-B3N3** (D_3). The ^{i}Pr and ^{t}Bu groups are replaced with H.

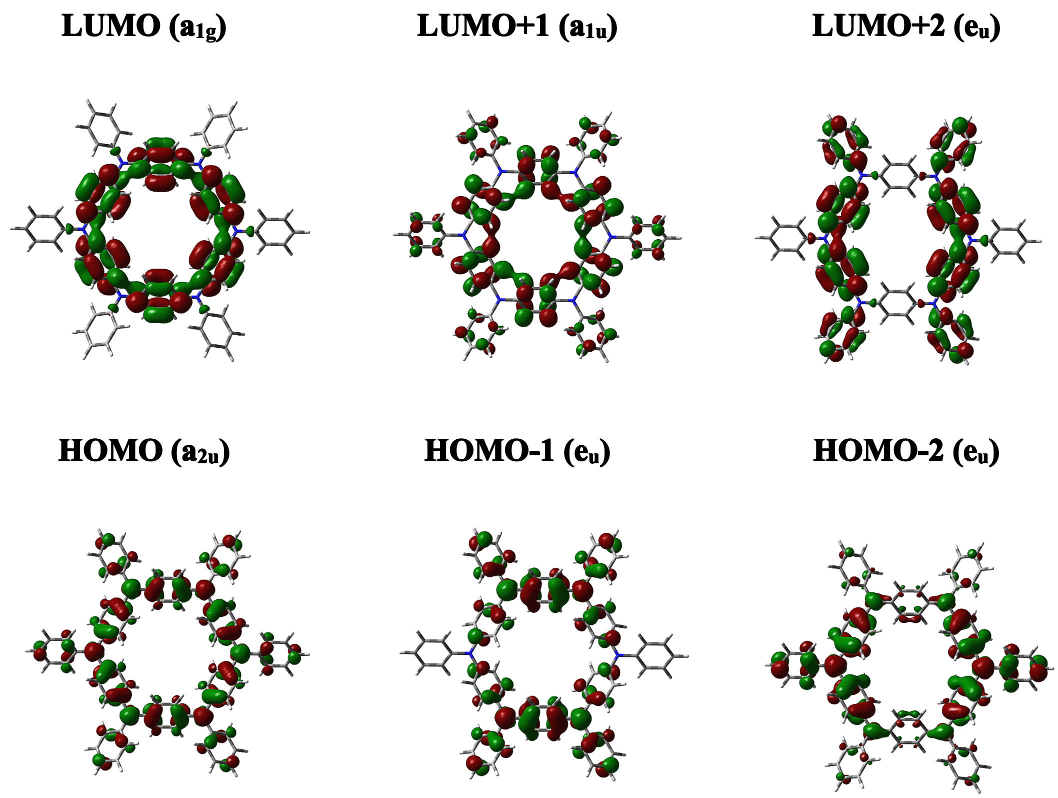

Figure 4-14. Kohn-Sham orbital representation for the ground state frontier orbitals of **MC-N6** (six nitrogens, phenylene π-system, D_{3d}).

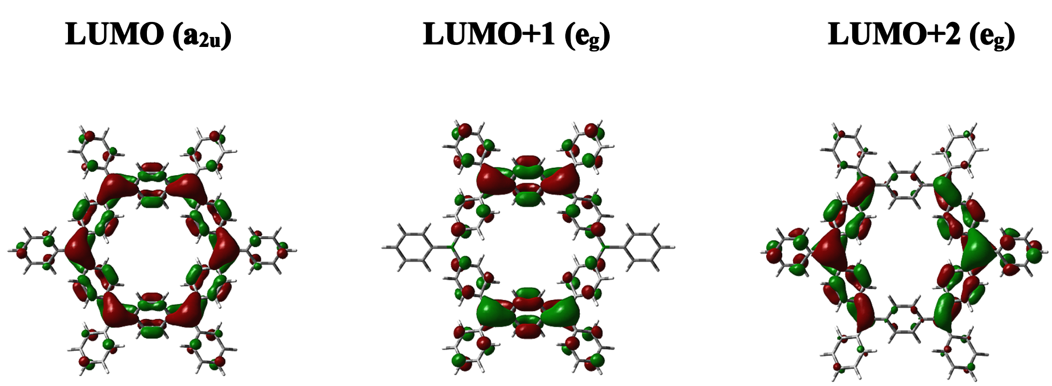

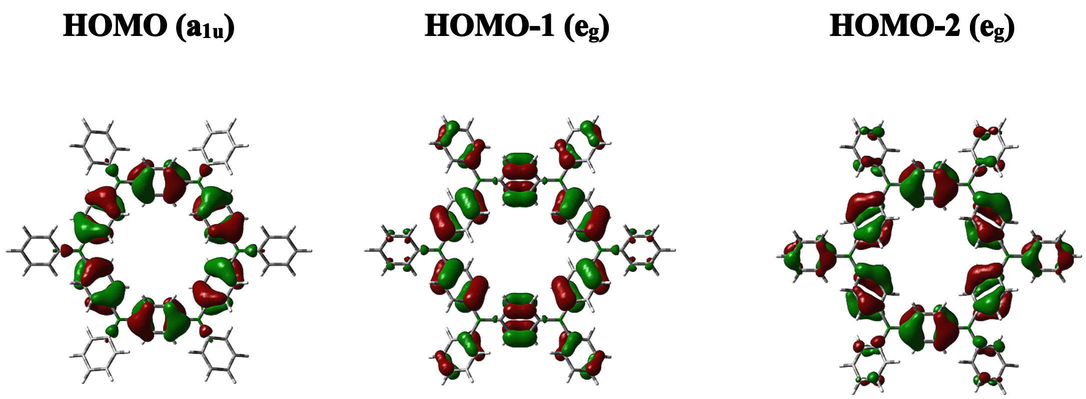

Figure 4-15. Kohn-Sham orbital representation for the ground state frontier orbitals of **MC-B6** derivative (six borons, phenylene π-system, D_{3d}).

Table 4-4. Results from GIAO Calculations (GIAO-B3LYP/6-311G*//B3LYP/6-31G*) on the Simplified Macrocycles (R = Ph, phenylene π-system)

	MC-B3N3	**MC-N6**	**MC-B6**
NICS(0)	0.239	–0.694	0.573
NICS(1)	0.221	–0.978	0.497
NICS(2)	0.151	–1.375	0.308
NICS (center of Ph rings)	–6.270	–7.630	–5.996

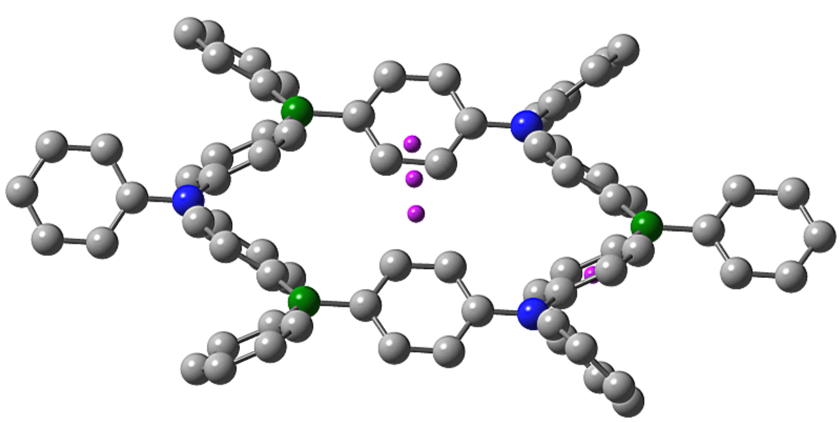

Figure 4-16. Illustration of structure used for NICS calculations on simplified **MC-B3N3**; NICS values determined at the center of the molecule (NICS(0)), and at distances of 1.0 and 2.0 Å above the plane for NICS(1) and NICS(2), respectively.

The electrochemical properties of **MC-B3N3** were examined by cyclic and square wave voltammetry (**Figure 4-17**). Three distinct oxidation and three reduction waves were observed. A comparison of the electrochemical data with those reported for the azacyclophane **MC-N6** (phenylene π-system)[35] and boracyclophane **MC-B6** (fluorene π-system)[45] provides insights into the mutual electronic effects of the adjacent boron and nitrogen centers in the ambipolar structure of **MC-B3N3** (**Table 4-5**). Relative to the azacyclophane **MC-N6**, **MC-B3N3** is oxidized at more positive potentials, because the presence of the electron-deficient neighboring borons decreases the electron density at nitrogen. Conversely, more negative potentials are needed to reduce the boron sites in **MC-B3N3** compared with the boracyclophane **MC-B6** (fluorene π-system), because of an increase in the electron density at boron in the presence of the neighboring amine groups. These experimental findings suggest that the HOMO level is lowered, while the LUMO is elevated. We also note that the potentials for reduction of **MC-B3N3** are similar to the last three reduction steps in **MC-B6** (fluorene π-system), while the potentials for oxidation are similar to the last three oxidation steps in **MC-N6** (fluorene π-system), indicating that the electronic effect of a reduced borane moiety is comparable to that of a neutral amine and the effect of an oxidized amine to that of a neutral borane, respectively. Importantly, despite the relatively higher LUMO than in **MC-N6** (fluorene π-system) and the relatively lower HOMO than in **MC-B6** (fluorene π-system), theoretical calculations reveal that the HOMO-LUMO gap in the ambipolar species **MC-B3N3** is the smallest among these macrocycles, which is consistent with the relatively small optical gap of 2.96 eV determined by UV/Vis spectroscopy.

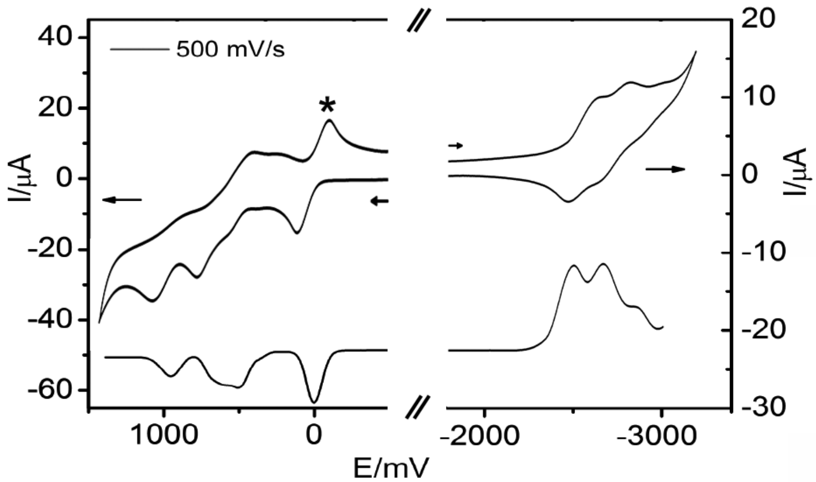

Figure 4-17. Cyclic (top) and square wave (bottom) voltammograms for **MC-B3N3**; oxidation (left) in CH_2Cl_2 and reduction (right) in THF (0.1 M $[Bu_4N][PF_6]$) *vs* $Fc^{0/+}$ (Fc = $[(\eta\text{-}C_5H_5)_2Fe]$ as an internal reference (indicated with an asterisk).

Table 4-5. Cyclic Voltammetry Data (vs $Fc^{0/+}$, ν = 100 mV s^{-1}) for **MC-B3N3** and for **MC-N6** and **MC-B6** (fluorene π-system)

Species	Event	$E^1_{1/2}$	$E^2_{1/2}$	$E^3_{1/2}$	$E^4_{1/2}$	$E^5_{1/2}$	$E^6_{1/2}$
MC-N6[a]	Ox [c]	–0.28	–0.17	+0.20	+0.45	+0.72[f]	+0.72[f]
MC-B3N3	Ox[d]				+0.46[g]	+0.65[g]	+0.94[g]
	Red[e]				–2.53	–2.72	–2.84[g]
MC-B6[b]	Red[e]	–2.10[b]	–2.10[b]	–2.27	–2.44	–2.57	–2.70

[a] From Ref. [35]. [b] From Ref. [45]. [c] 0.1M $[Bu_4N][BF_4]$ in CH_2Cl_2. [d] 0.1M $[Bu_4N][PF_6]$ in CH_2Cl_2. [e] 0.1M $[Bu_4N][PF_6]$ in THF. [f] Overlapping. [g] Determined by SWV.

4.4 Anion Binding Study of **MC-B3N3**

The presence of electron-deficient organoborane moieties also suggests possible use of these molecules in the recognition of anions.[48,49] The anion binding behavior was evaluated by titration experiments with the cyanide anion. As shown in **Figure 4-18**, stepwise addition of [nBu$_4$N]CN to a solution of **MC-B3N3** in toluene resulted in a gradual decrease in the UV absorbance and emission intensity. Three distinct regimes were observed, consistent with addition of the anion to the three available borane moieties, albeit with little or no cooperative effects[27,50] ($\lg\beta_{11} \approx 8.0$, $\lg\beta_{12} = 15.7$, $\lg\beta_{13} = 23.0$) (**Figure 4-19** and **Table 4-6**). Noteworthy is that, although the absorption wavelength does not change dramatically, in the emission spectra a clear bathochromic tailing is observed, which we attribute to new CT pathways upon generation of an electron-rich organoborate site (**Figure 4-18c**).[27,51-53] A comparison to the quenching behavior of the boracyclophane **MC-B6** provides further insights. In the case of **MC-B6**, only slightly more than 1 equivalent of quencher is needed to completely turn off the emission of the host (Chapter 3).[45] In contrast, to fully quench the fluorescence of **MC-B3N3**, more than 3 equivalents of CN^- are required, corresponding to full complexation of all three Lewis acidic B centers. This suggests that emission from CT states in the partially complexed species [**MC-B3N3**(CN)]$^-$ and [**MC-B3N3**(CN)$_2$]$^{2-}$ remains strong, whereas a very weakly emissive low-energy CT state is generated upon anion binding in [**MC-B6**(CN)]$^-$. As discussed in Chapter 3, this CT state is believed to serve as an energy trap, resulting in effective quenching of the emission.[45]

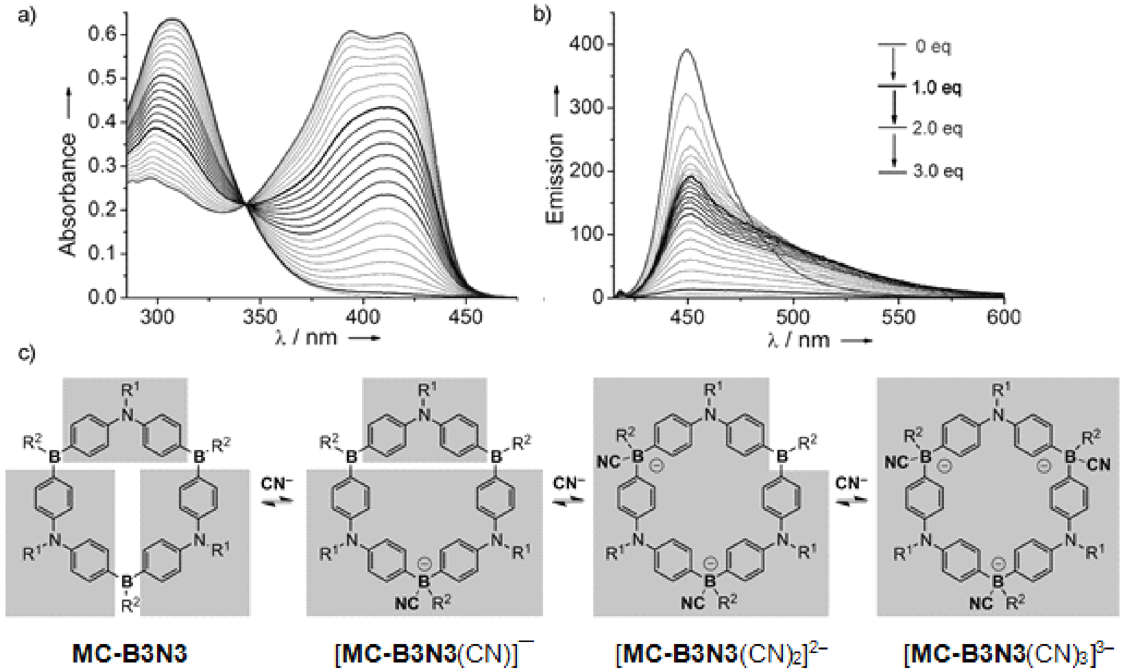

Figure 4-18. Titration of **MC-B3N3** with [nBu$_4$N]CN in toluene monitored by a) UV/Vis and b) fluorescence spectroscopy ([**MC-B3N3**]^0 = 1.429 × 10^{-5} M; [CN^-] = 1.042 × 10^{-3} M, λ_{ex} = 419 nm. c) Illustration of electron-donor segments for **MC-B3N3** and the corresponding anion complexes.

Table 4-6. Relative concentrations of individual species after addition of varying amounts of CN^- to a solution of **MC-B3N3** ([**MC-B3N3**]^0 = 1.429 × 10^{-5} M; [**CN^-**] = 1.042 × 10^{-3} M) in toluene with binding constants of lgβ_{11} = 8.0, lgβ_{12} = 15.7, lgβ_{13} = 23.0. These binding constants β_{1n} are given in units of M^{-n} and they are all automatically generated from the program of Hyperquad™ .

CN^- (equ.)	[**MC-B3N3**] (%)	[**MC-B3N3**]CN (%)	[**MC-B3N3**]$(CN)_2$ (%)	[**MC-B3N3**]$(CN)_3$ (%)
1	33.5	38	23	6
2	5.5	20.5	41	33
3	0	0	5	95

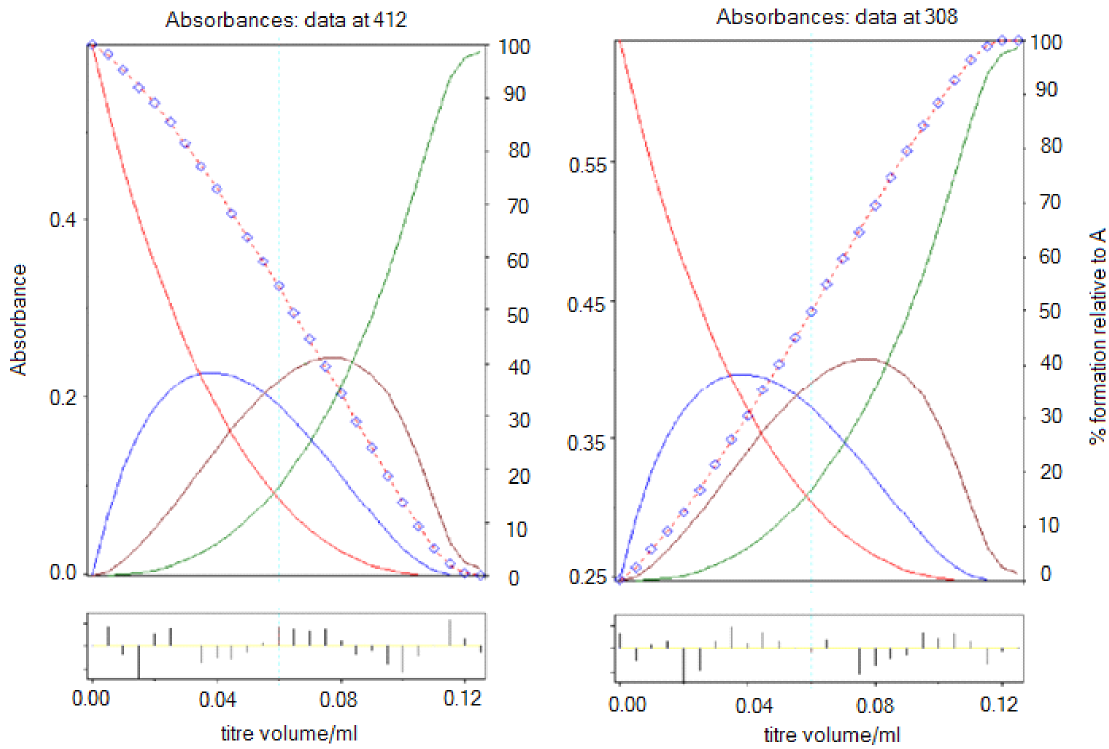

Figure 4-19. Fit of absorption data (Hyperquad^{TM} software) at $\lambda = 412$ nm and at $\lambda = 308$ nm in toluene. Note that $\lg\beta_{11}$ had to be fixed to give a reasonable refinement. Color Code: **[MC-B3N3]** (red), **[MC-B3N3]CN** (blue), **[MC-B3N3](CN)$_2$** (brown), **[MC-B3N3](CN)$_3$** (green).

Hybrid π Systems

4.5 Synthesis and Structural Characterization of **MC-B4N2**

The position and relative orientation of electron donor and acceptor sites in CT compounds has a distinct impact on the electronic properties. Therefore, we also pursued the synthesis of ambipolar macrocycles with different number of N donor and B acceptor sites. Taking advantage of the much higher reactivity of the Sn–C bond in comparison to the Si–C bond in **CzSiSn**, we prepared the linear oligomer **O-CFC** reaction of **FlB2** with 2 equiv of **CzSiSn,** followed by treatment with TipCu for steric stabilization of boron

(**Scheme 4-2**). The ambipolar macrocycle **MC-B4N2** was then prepared by reaction of **O-CFC** with 2 equivalents of BBr_3, followed by cyclization under pseudo-high dilution conditions upon simultaneous addition of stoichiometric amounts of the resulting borylated species and **FlSn2** (1:1) to a large quantity of toluene. Treatment of the initially generated B-Br functionalized macrocycle with 2 equivalents of TipCu in refluxing toluene for 2 days gave the desired product **MC-B4N2**. GPC analysis indicated that the crude sample after standard workup consists of the targeted macrocycle as the major product in addition to a higher molecular weight component which likely corresponds to larger linear or cyclic species (**Figure 4-20**). Purification by preparative size exclusion column chromatography on Bio-beads™ with THF as the eluent gave analytically pure **MC-B4N2** as a white powdery solid in 33% yield.

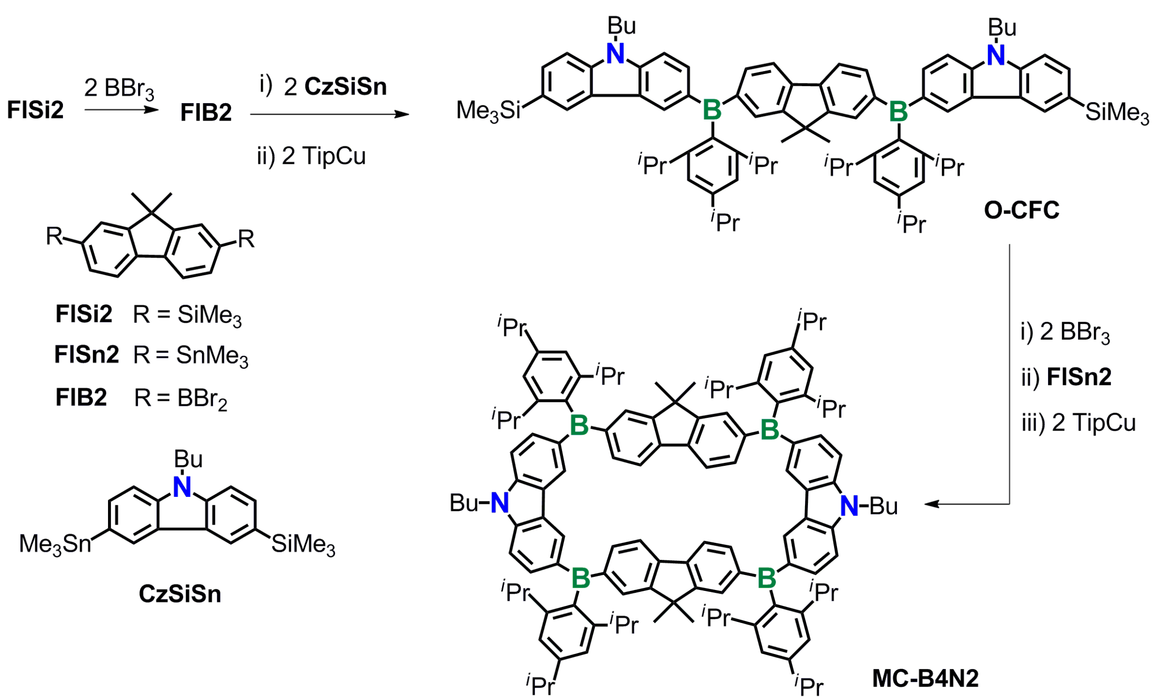

Scheme 4-2. Synthesis of the donor-π-acceptor macrocycle **MC-B4N2**.

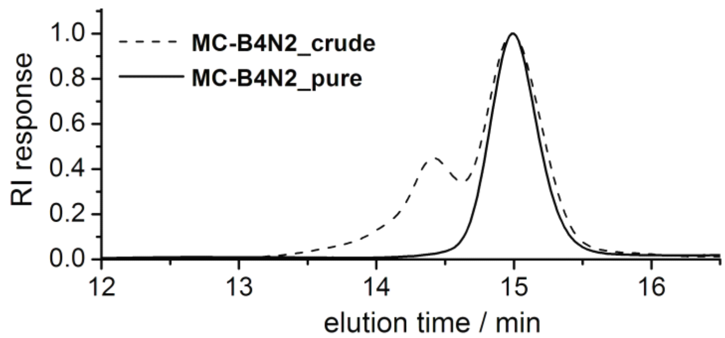

Figure 4-20. GPC traces for macrocycle **MC-B4N2** in THF (*PDI* = 1397/1372 = 1.02, vs low molecular weight polystyrene).

We also attempted to synthesize an ambipolar macrocycle **MC-B2N2**. An aryl halide functionalized boron-containing linear species **Fl2BTip** was initially prepared via the B/Sn exchange of **FlSnBr** with BBr_3, followed by the treatment with TipCu for the formed B-Br intermediate. Different from **MC-B4N2**, a standard Pd-catalyzed Stille coupling was performed under pseudo-high dilution conditions for the macrocyclization of **MC-B2N2** (**Scheme 4-3)**.

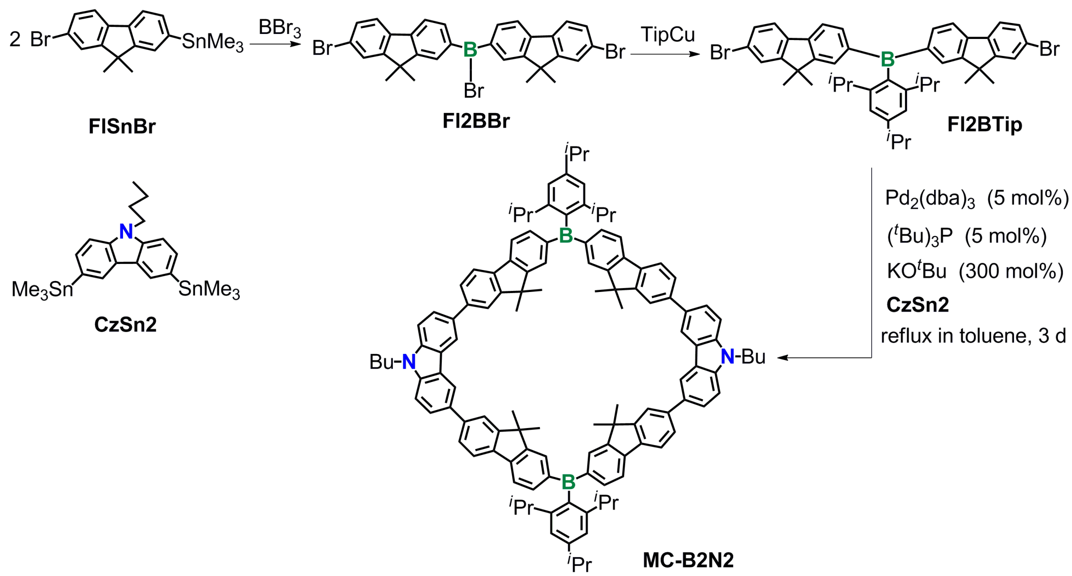

Scheme 4-3. Synthesis of the donor-π-acceptor macrocycle **MC-B2N2**.

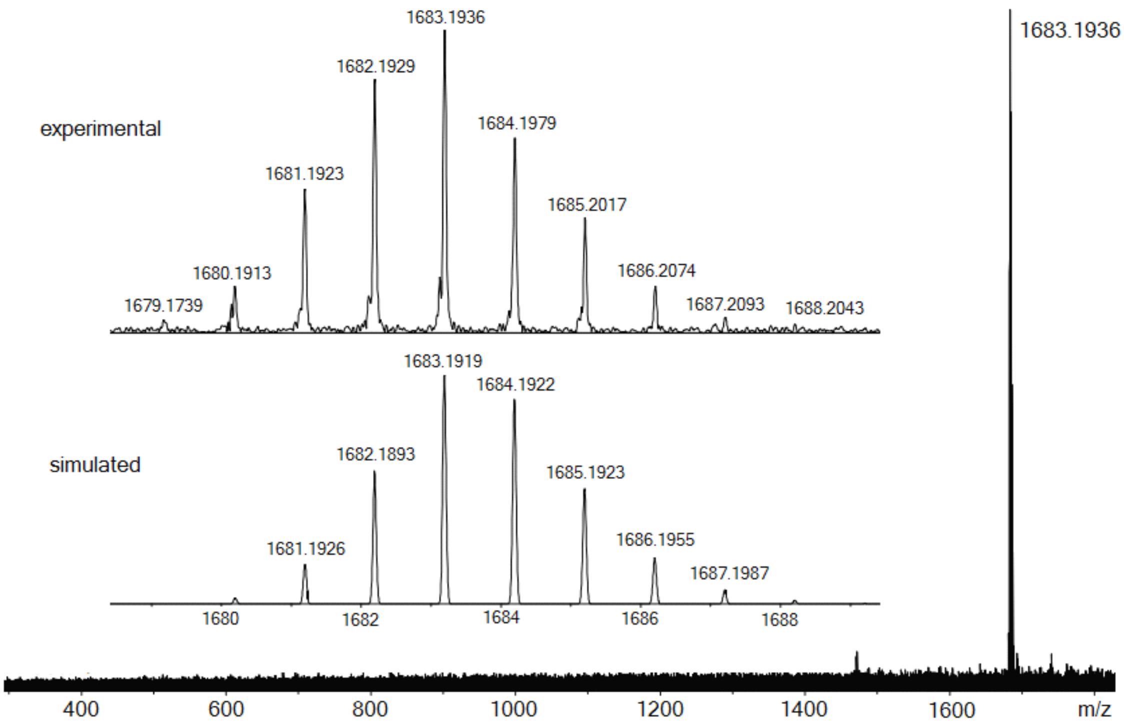

Figure 4-21. High resolution MALDI-MS of isolated **MC-B4N2** (positive mode).

As shown in **Figure 4-20**, isolation of monodisperse **MC-B4N2** after purification is verified by a single band with a narrow *PDI* = 1.02 in the GPC traces. As further evidence, the high resolution MALDI-MS spectra gives a molecular ion peak at 1683.1936 Da, which is close to the theoretical value of 1683.1919 Da. The experimental isotope pattern fits the simulated pattern well (**Figure 4-21**). **MC-B4N2** was further characterized by multinuclear NMR spectroscopy. Only one set of signals that corresponds to the cycle is observed in the ^{1}H NMR (**Figure 4-22**). The presence of a broad ^{11}B NMR signal at 77 ppm is consistent with boron in a tricoordinate environment (**Figure 4-23**). Furthermore, the quadrupole-broadened B-bound carbon NMR signals can readily be identified in the ^{13}C NMR and their number (3) is consistent with the expected one.

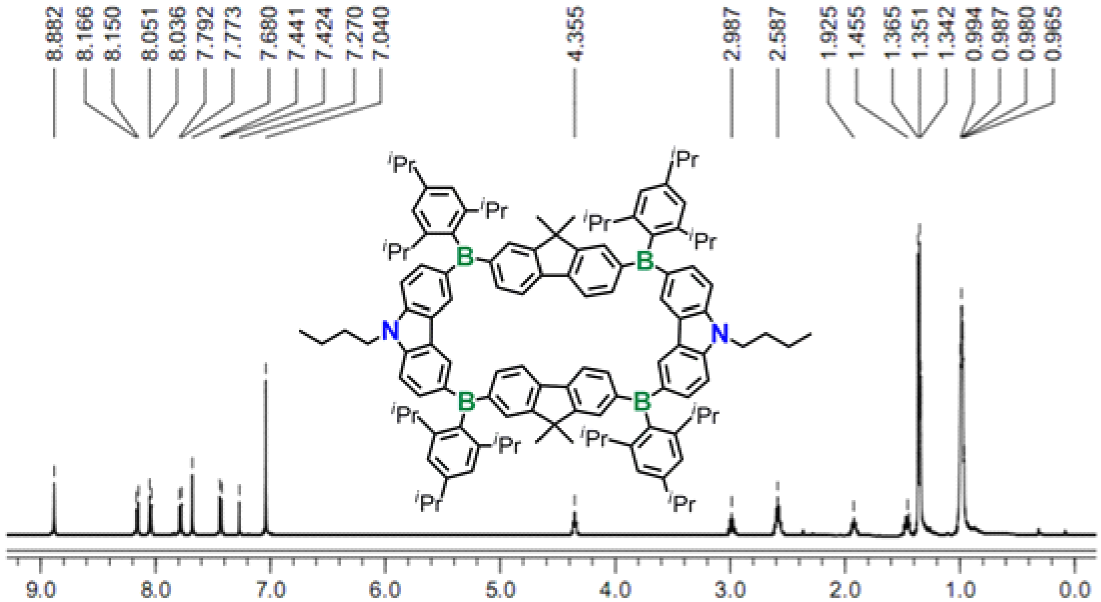

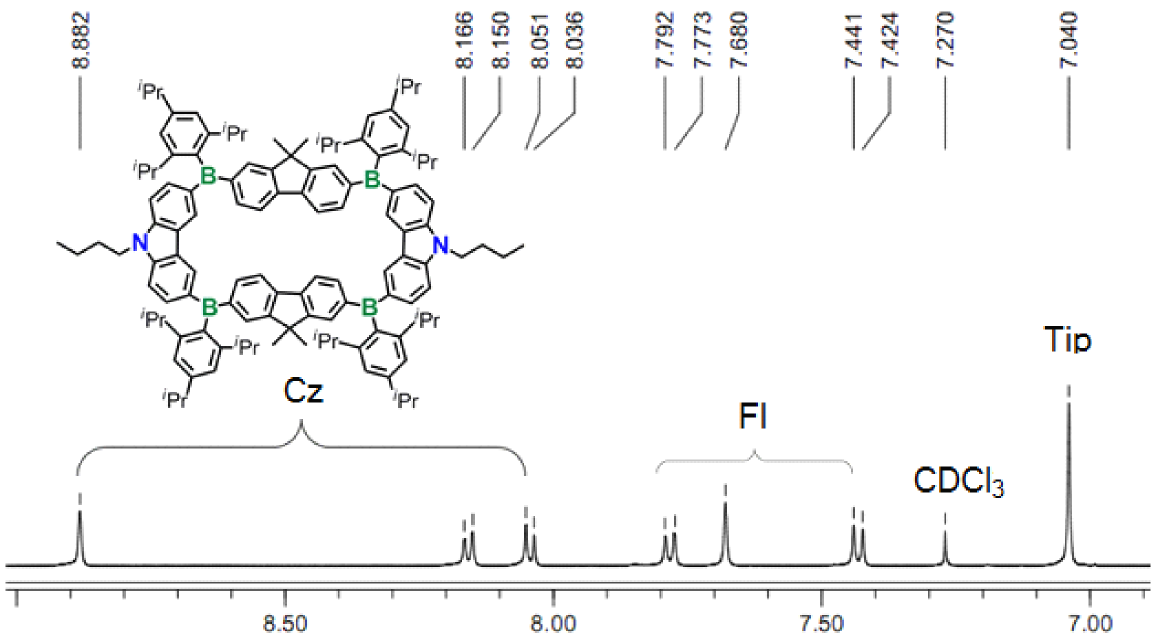

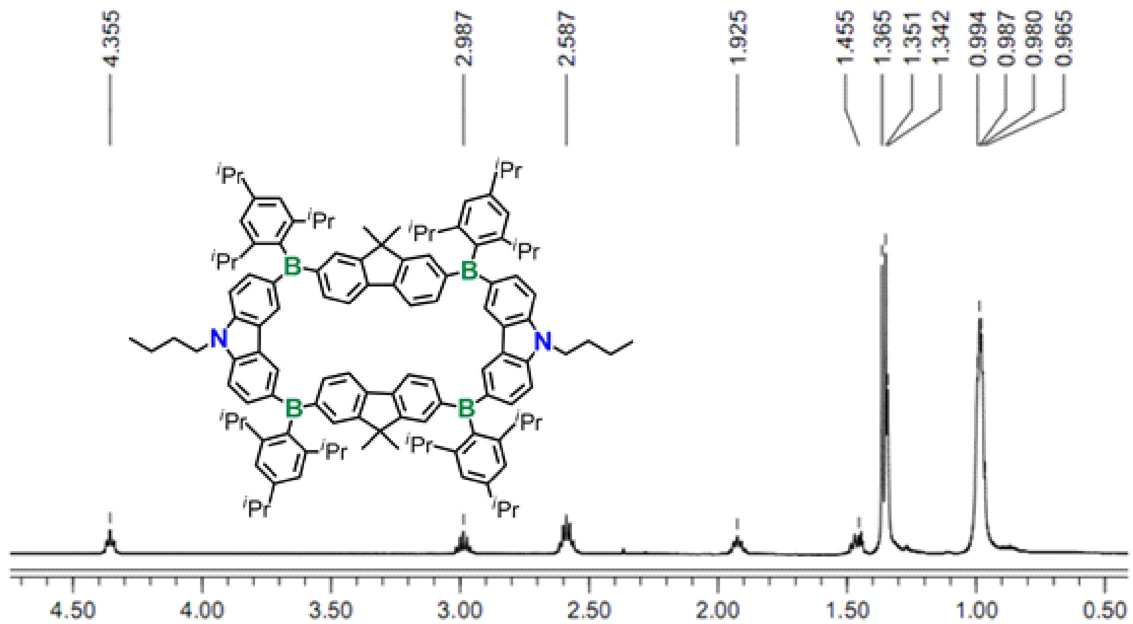

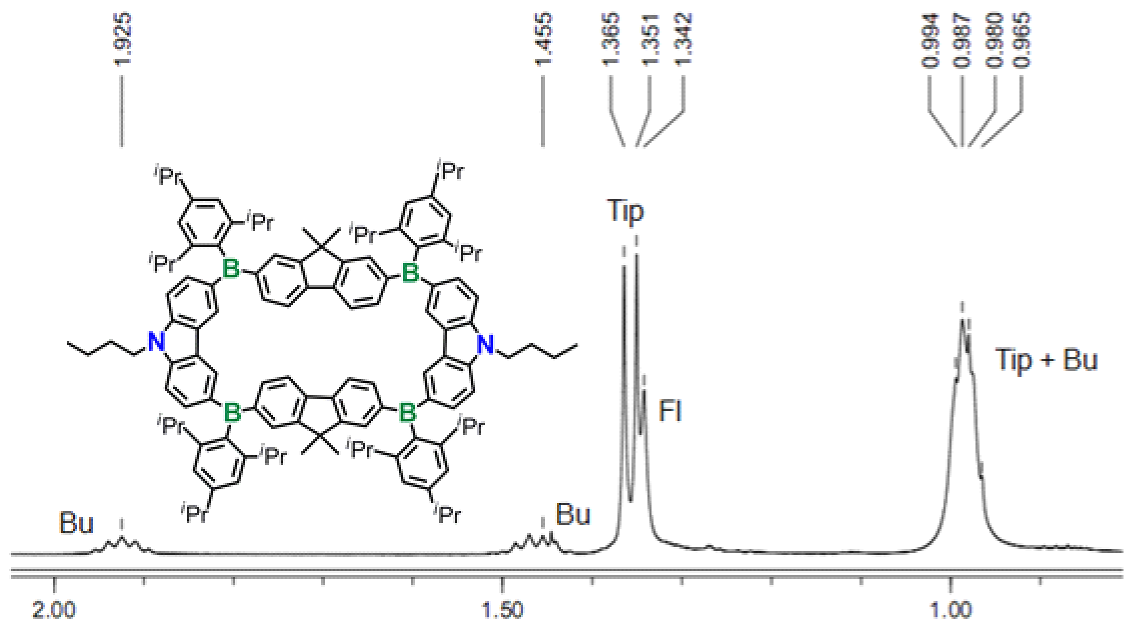

Figure 4-22. ^{1}H NMR spectrum of macrocycle **MC-B4N2** and corresponding magnifications ($CDCl_3$, 25 °C).

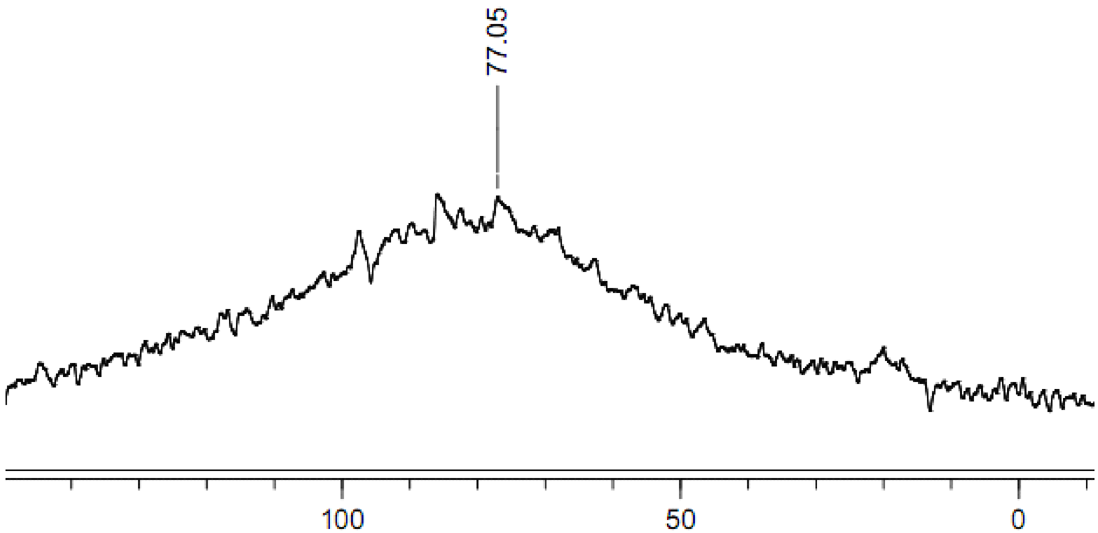

Figure 4-23. ^{11}B NMR spectrum of macrocycle **MC-B4N2** ($CDCl_3$, 25 °C).

4.6 Photophysical, Electrochemical and Computational Studies of Ambipolar Macrocycle **MC-B4N2**

UV-vis absorption spectra were recorded in different solvents to investigate the photophysical characteristics and determine the optical energy gap. In solution, the absorption spectra of **MC-B4N2** show a distinct band at 357 nm and two shoulders around 345 and 375 nm, independent of the solvent (**Figure 4-24**). These bands are attributed to intramolecular charge transfer (ICT) from carbazole donor sites (n/π) to fluoreneborane acceptor sites (n/π*). The onset of the absorption at 390 nm suggests that **MC-B4N2** absorbs at higher energy than does **MC-B3N3** (onset at 420 nm). This trend is in agreement with the relative calculated energy of the lowest allowed transition ($S_2 \leftarrow S_0$, $\lambda_{\textbf{MC-B4N2}}$ = 382 nm, $\lambda_{\textbf{MC-B3N3}}$ = 432 nm). Photoexcitation leads to an emission band at 436 nm (CH_2Cl_2: λ_{exc} = 357 nm, Φ = 0.40), which experiences a pronounced red-shift with increasing solvent polarity. The presence of a strong solvatochromic effect in the emission but only small effect in the absorption is indicative of a more polarized excited state upon ICT, a phenomenon similar to what we observed in **MC-B3N3**.

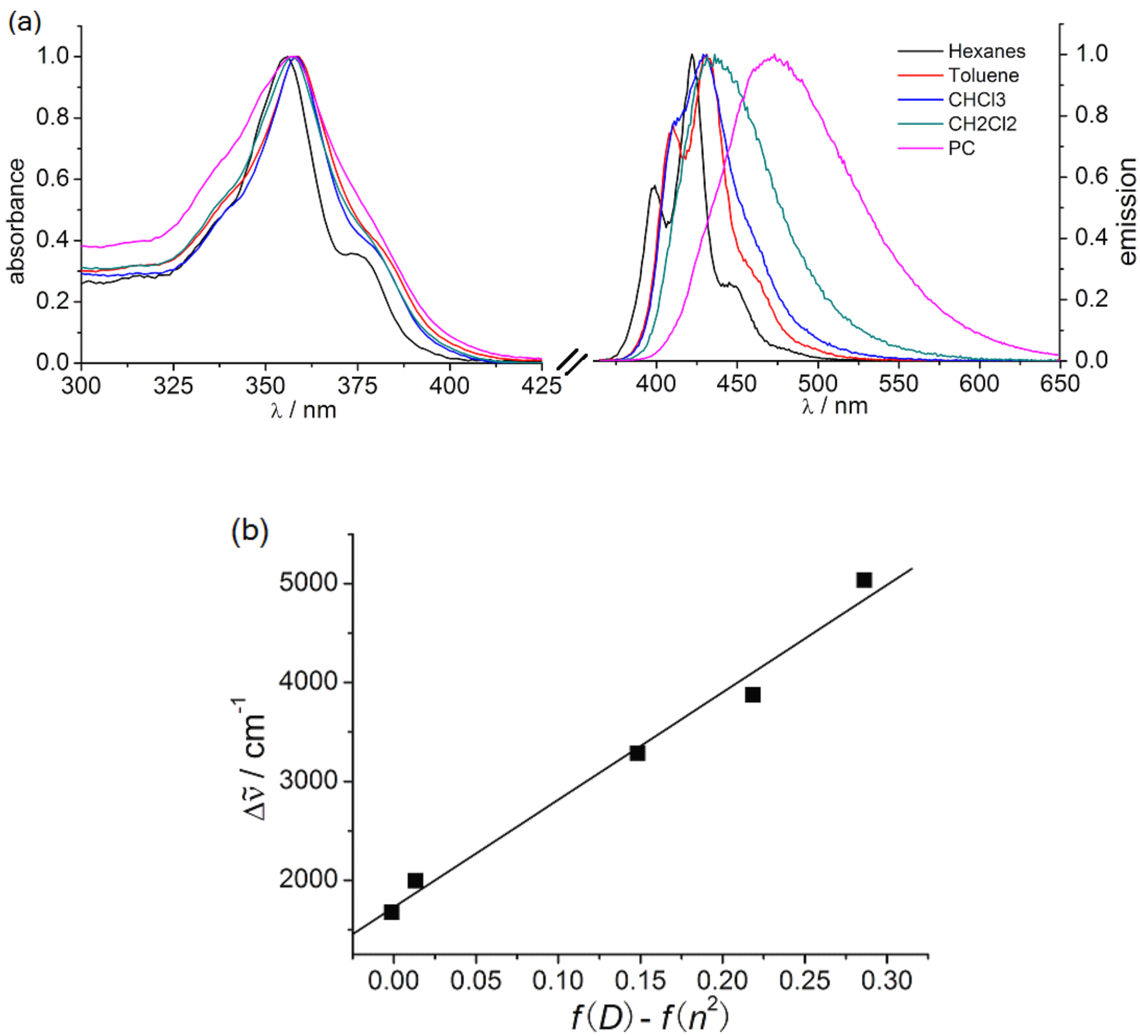

Figure 4-24. (a) UV-vis absorption (left) and fluorescence spectra (right) (λ_{ex} = 357 nm) of **MC-B4N2** in solvents of different polarity. (b) Lippert-Mataga plot for the solvatochromic emission of macrocycle **MC-B4N2** (hexanes, toluene, $CHCl_3$, CH_2Cl_2, propylene carbonate). The Stokes shifts in different solvents are plotted relative to the solvent polarity function $f(D) - f(n^2)$ with $f(D) = (D-1)/(2D+1)$ and $f(n^2) = (n^2-1)/(2n^2+1)$; D = permittivity; n = refractive index of the solvent (see also the detailed discussion in Chapter 2 about the Lippert-Mataga analysis).

DFT and TDDFT calculations (B3LYP/6-31G*) were carried out on a simplified analog of **MC-B4N2** (Me and ^{i}Pr groups are replaced with H, and ^{n}Bu groups on carbazole are replaced with Me groups) in C_{2V} symmetry and the results are summarized in **Table 4-7**. The formation of cyclic hybrid tetramer of **MC-B4N2** is favored due to less ring strain in comparison to its cyclic fluorene analog (**MC-B4**) and the respective cyclic carbazole tetramer. The endocyclic bond angles about B are calculated to be: 120.9° (hybrid) > 119.0° (carbazole) > 118.1° (fluorene) (Appendix). According to DFT calculations, the HOMO of **MC-B4N2** is localized on the π spacers with contributions from the nitrogen p-orbitals of the carbazole moieties, while the LUMO is localized on the conjugated π-system including fluorene units and the boron centers with generally small contributions from the carbazole moieties, but not the nitrogen atoms (**Figure 4-25**). Based on TDDFT calculations, the $S_1 \leftarrow S_0$ transition (HOMO to LUMO) is symmetry forbidden because of cancellation of the transition dipole moments, as is typically observed for highly symmetric macrocycles.[45,57] The lowest allowed transition ($S_2 \leftarrow S_0$) by TDDFT at 382 nm is predicted , which is close to the onset of the observed absorption at *ca.* 390 nm (**Table 4-8**). Higher transitions including $S_3 \leftarrow S_0$ and $S_4 \leftarrow S_0$ also contribute to the UV-vis absorption, and the $S_3 \leftarrow S_0$ (f = 0.9398) transition is responsible for the major band at 357 nm.

Table 4-7. Results from TD-DFT Calculations (B3LYP, 6-31G*) on the Macrocycles **MC-B4N2** (C_2v) and **MC-B2N2** (C_2)

Compound	Transition	λ, nm (eV)	Oscillator Strength, f	Orbital Contributions
MC-B4N2	$S_1 \leftarrow S_0$	409.8 (3.026)	0.0000	HOMO-2→LUMO+1, 0.166 HOMO-1→LUMO+2, 0.169 **HOMO→LUMO, 0.652**
	$S_2 \leftarrow S_0$	382.3 (3.243)	0.5366	**HOMO-1→LUMO, 0.666** HOMO→LUMO+2, 0.177
	$S_3 \leftarrow S_0$	371.3 (3.339)	0.9398	HOMO–2→LUMO, 0.104 **HOMO→LUMO+1, 0.674**
	$S_4 \leftarrow S_0$	367.0 (3.378)	0.5934	HOMO–3→LUMO+2, 0.112 **HOMO-2→LUMO, 0.662** HOMO→LUMO+1, –0.124
MC-B2N2	$S_1 \leftarrow S_0$	427.4 (2.901)	0.0010	HOMO-2→LUMO+1, –0.207 HOMO-1→LUMO+2, 0.102 **HOMO→LUMO, 0.654**
	$S_2 \leftarrow S_0$	408.9 (3.032)	0.9567	HOMO-2→LUMO, –0.147 **HOMO→LUMO+1, 0.675**
	$S_3 \leftarrow S_0$	403.0 (3.077)	0.7080	**HOMO-1→LUMO, 0.690**
	$S_5 \leftarrow S_0$	372.5 (3.328)	0.6010	**HOMO–2→LUMO, 0.669** HOMO→LUMO+1, 0.174
	$S_8 \leftarrow S_0$	354.7 (3.495)	0.3899	**HOMO–3→LUMO+1, 0.684**
	$S_9 \leftarrow S_0$	333.0 (3.724)	0.9409	HOMO–1→LUMO+6, 0.127 **HOMO→LUMO+2, 0.669**

The Me groups on fluorene and ^{i}Pr on Tip are replaced with H. ^{n}Bu groups on carbazole are replaced with Me groups.

Table 4-8. Computational and Experimental Data of the Frontier Orbital energies for **MC-B4N2**

	CV[a] [eV]	SWV[a] [eV]	DFT[b] [eV]	UV/Vis [c] [nm] ([eV])	TD-DFT [b] [nm] ([eV])
E_{LUMO}	–2.50	–2.50	–1.87		
E_{HOMO}	–5.74	–5.75	–5.41		
$\Delta E_{gap/uv}$	3.24	3.25	3.54	390 (3.18)	382 (3.24)[d]

[a] Reference: ferrocene at 4.80 eV below vacuum, CV = cyclic voltammetry, SWV = square-wave voltammetry. [b] Computations performed on simplified analog of **MC-B4N2** (Me groups on fluorene and *ⁱ*Pr on Tip are replaced with H, and *ⁿ*Bu on carbazole are replaced with Me groups). [c] Onset of the UV-vis absorption in hexanes. [d] Allowed $S_2 \leftarrow S_0$ transition.

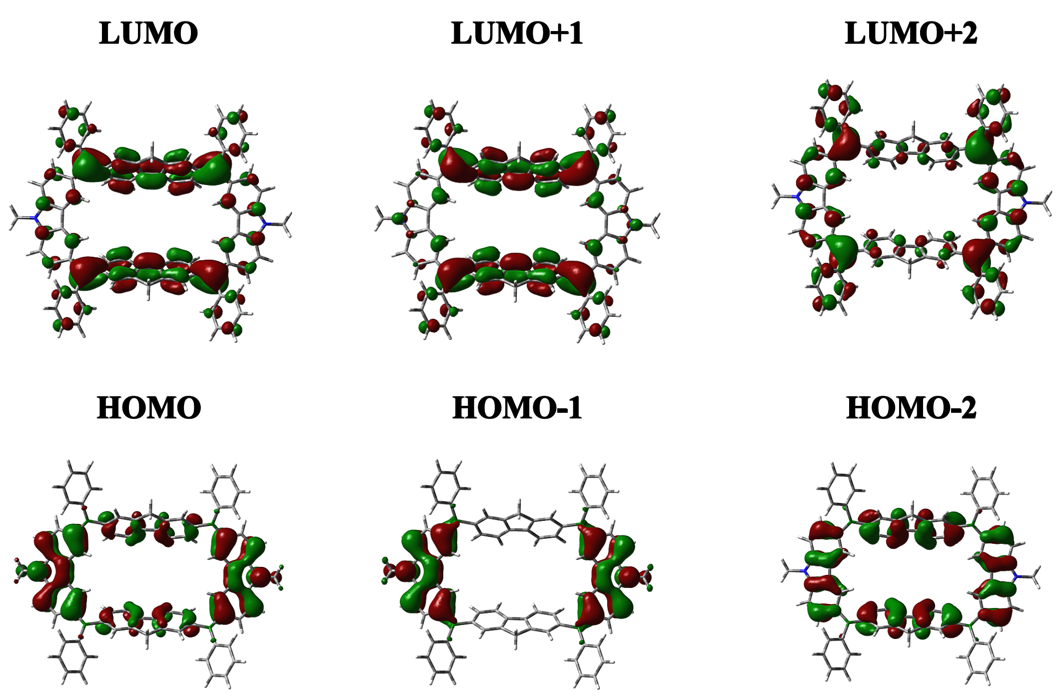

Figure 4-25. Molecular orbitals for **MC-B4N2** (C_{2V}) in the ground state. Me groups on fluorene and ^{i}Pr on Tip are replaced with H. ^{n}Bu groups on carbazole are replaced with Me groups.

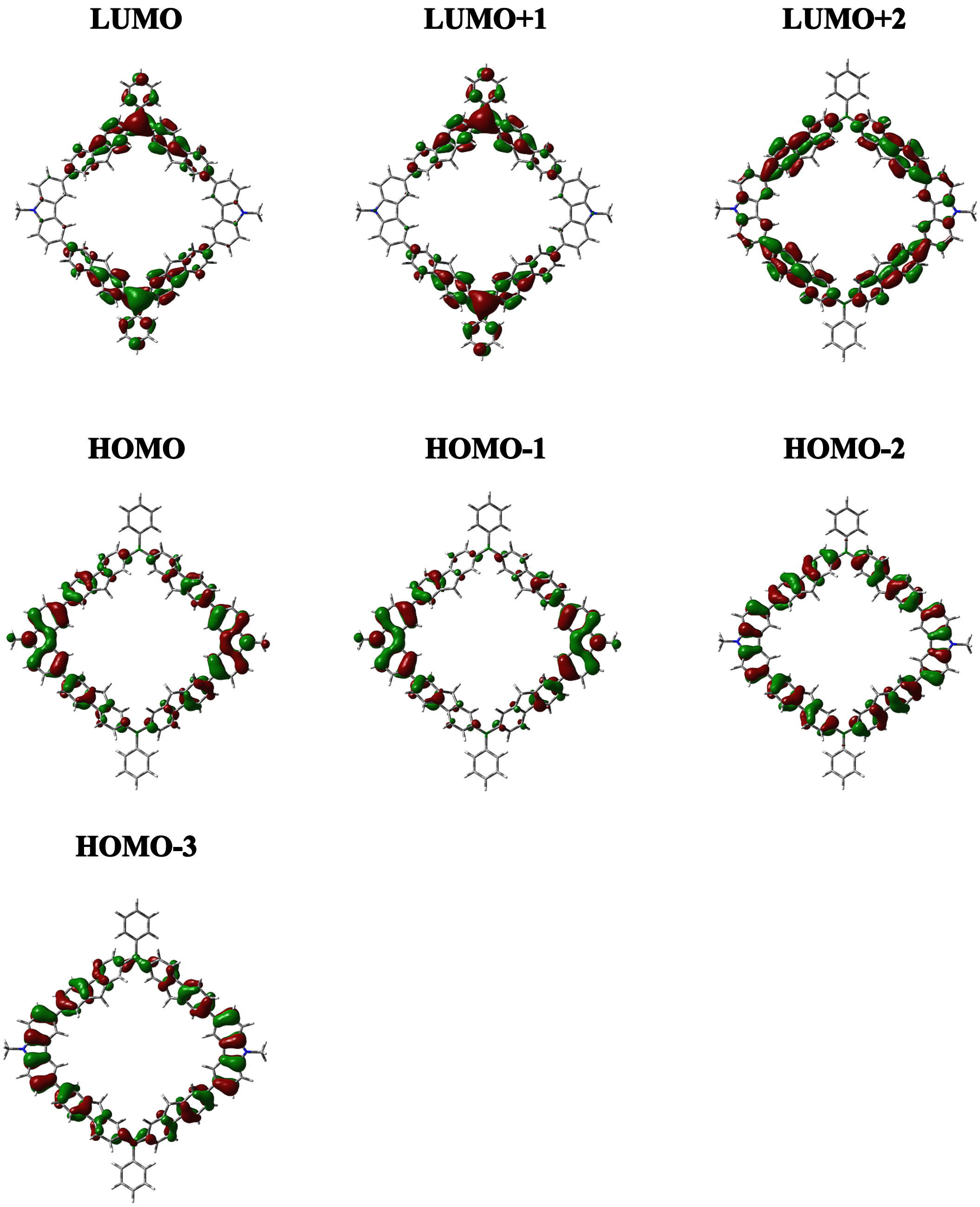

Figure 4-26. Molecular orbitals for macrocycle **MC-B2N2** (C_2) in the ground state. Me groups on fluorene and ^{i}Pr on Tip are replaced with H. ^{n}Bu groups on carbazole are replaced with Me groups.

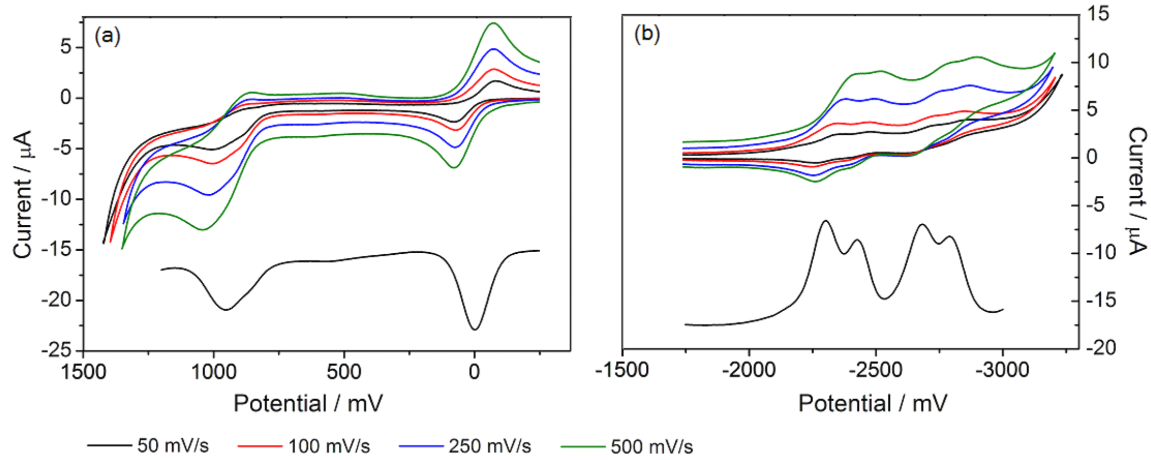

Figure 4-27. Cyclic (top) and square wave (bottom) voltammograms for **MC-B4N2**; oxidation (a) in CH_2Cl_2 and reduction (b) in THF (0.1 M $[Bu_4N][PF_6]$) *vs* $Fc^{0/+}$ (Fc = $[(\eta\text{-}C_5H_5)_2Fe]$ as an internal reference.

The electrochemical properties of **MC-B4N2** were examined by cyclic and square wave voltammetry (**Figure 4-27**, **Table 4-9**). A reversible oxidation that corresponds to a $2e^-$ process at 0.95 V was recorded in CH_2Cl_2, which suggests a very weak or no electronic communication between the two nitrogen atoms on the opposite sites. This oxidation wave is observed at more positive potential than that of 0.46 V for macrocycle **MC-B3N3**. In contrast, the boron centers in **MC-B4N2** apparently influence each other, given that four reversible reduction bands are observed that correspond to separate reductions at each boron site in the cycle. The first reduction at –2.30 V indicates that **MC-B4N2** is slightly easier to be reduced compared with –2.53 V for **MC-B3N3**. The HOMO-LUMO energy gap (~3.25 eV) is estimated from electrochemical data, and found to be consistent with that from TDDFT calculations and UV-vis measurement (**Table 4-8**). These findings indicate that **MC-B4N2** is ambipolar and potentially capable of acting as a p-type and n-type semiconducting material in organic devices.

Table 4-9. Electrochemical Data (vs $Fc^{0/+}$, $\nu = 100$ mV s^{-1}) for Macrocycle **MC-B4N2**

		Oxidation (V) [a]	Reduction (V) [b]
Cyclic Voltammetry	$E^1_{1/2,\,CV}$	0.940 (2e)	–2.297
	$E^2_{1/2,\,CV}$	O/L	N/D
	$E^3_{1/2,\,CV}$	N/A	N/D
	$E^4_{1/2,\,CV}$	N/A	N/D
Square Wave Voltammetry	E^{p1}_{SWV}	0.952 (2e)	–2.300
	E^{p2}_{SWV}	O/L	–2.424
	E^{p3}_{SWV}	N/A	–2.684
	E^{p4}_{SWV}	N/A	–2.792

[a] 0.1M $[Bu_4N][PF_6]$ in CH_2Cl_2. [b] 0.1M $[Bu_4N][PF_6]$ in THF.

4.7 Anion Binding Study of **MC-B4N2**

Complexation of **MC-B4N2** with nucleophiles was monitored by UV-vis absorption and emission spectroscopy. **Figure 4-28** reveals that the UV-vis absorption band gradually decreases upon the addition of CN^- to a **MC-B4N2** solution in CH_2Cl_2. Addition of two equiv. of CN^- leads to the disappearance of the major band at 357 nm corresponding to the $S_3 \leftarrow S_0$ transition (HOMO→LUMO+1). The spectrum after addition of 2 equiv. of CN^- shows two well-separated absorptions at 340 and 370 nm. These are likely due to charge transfer transition from electron-rich carbazole and cyanoborate sites, respectively, to the remaining electron-deficient tricoordinate borane sites (**Scheme 4-4**). These bands gradually disappear in the presence of larger amounts of CN^-. A cooperative effect was observed with relatively small binding constants ($\lg\beta_{11}$ = 7.5, $\lg\beta_{12}$ = 14.7, $\lg\beta_{13}$ = 19.8, $\lg\beta_{14}$ = 24.7) for β_{13} and β_{14}, which is probably due to interactions between the boron centers via the fluorene bridges as also observed for **MC-B6** and the related linear fluoreneborane oligomers. The initial emission band at 435 nm gradually decreases, followed by a red-shift of the band at 470 nm after addition of 2 equiv. of CN^{-}. This is distinct from the complexation of **MC-B6** and **MC-B3N3** that show only a decrease in intensity at the initial wavelength and no red-shifted bands were generated. The new emission band in **MC-B4N2** is probably due to CT from carbazole and/or cyanoborate to tricoordinate borane sites. Another important observation is that the fully complexed species [**MC-B$_4$N$_2$**$(CN)_4$]$^{4-}$ remains emissive. This uncommon phenomenon that was not found in **MC-B6** and **MC-B3N3** suggests that charge transfer occurs from carbazole moieties to fluorene units.

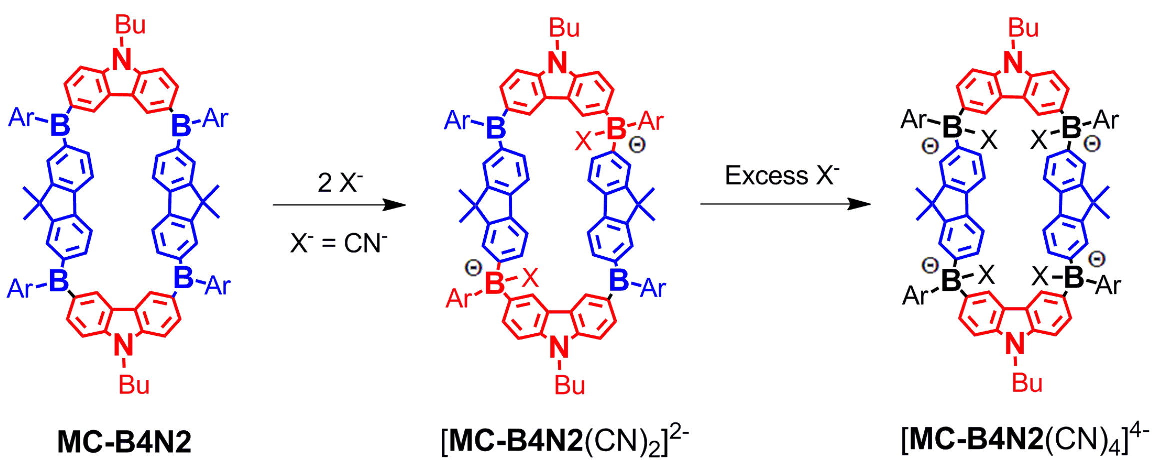

Scheme 4-4. Illustration of electron-donor (red) and electron-acceptor (blue) segments for **MC-B4N2** and the corresponding anion complexes.

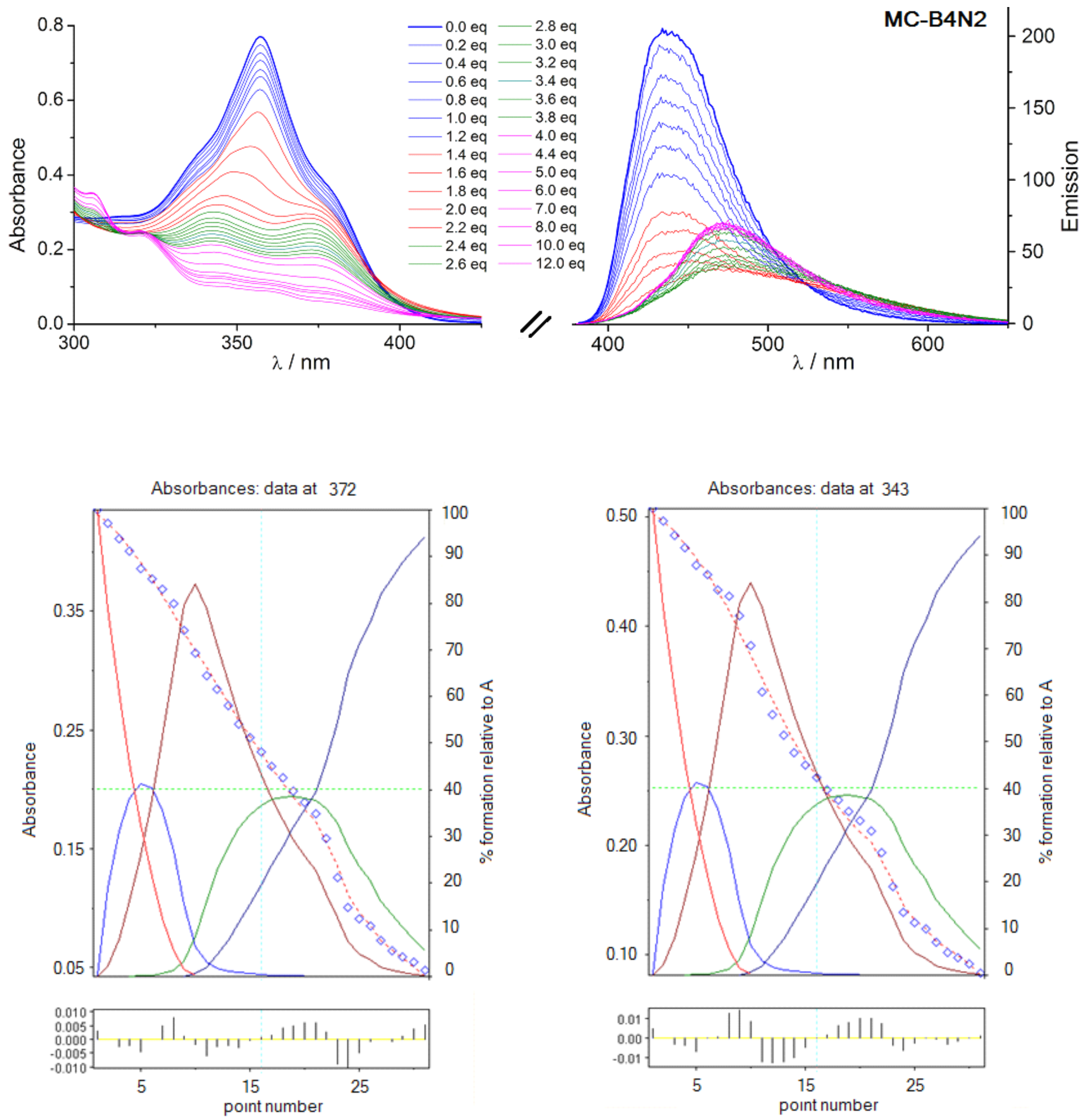

Figure 4-28. Complexation of **MC-B4N2** with CN^{-} anions (1.04×10^{-3} M) in CH_2Cl_2, monitored by UV-vis and fluorescence spectroscopy. [**MC-B4N2**] = 8.84×10^{-6} M; λ_{exc} = 375 nm. Bottom: Fit of absorption data (Hyperquad™) at λ = 372 and 343 nm.

Table 4-10. Relative concentrations of individual complexes after addition of varying amounts of CN^{-} to a solution of **MC-B4N2** in CH_2Cl_2. The binding constants are as follow: $\lg\beta_{11}$ = 7.5, $\lg\beta_{12}$ = 14.7, $\lg\beta_{13}$ = 19.8, $\lg\beta_{14}$ = 24.7. These binding constants β_{1n} are given in units of M^{-n}. They are all based on a manual fit to achieve convergence using the program of Hyperquad™.

CN^- (eq)	[**MC-B4N2**] (%)	[**MC-B4N2**]CN (%)	[**MC-B4N2**]$(CN)_2$ (%)	[**MC-B4N2**]$(CN)_3$ (%)	[**MC-B4N2**]$(CN)_4$ (%)
1.2	12.3	35.6	51.5	0.6	0.0
2.2	0.0	1.7	71.0	22.7	4.6
3.8	0.0	0.1	25.8	38.3	35.8
8.0	0.0	0.0	3.5	20.5	76.0
10	0.0	0.0	2.0	16.1	81.9
12	0.0	0.0	1.3	13.2	85.5
30	0.0	0.0	0.2	5.6	94.2

4.8 Conclusions

In conclusion, the synthesis of several ambipolar π-conjugated B–N macrocycles was accomplished by cyclization of the corresponding linear oligomers under pseudo-high dilution conditions. As confirmed by single-crystal X-ray diffraction, N donor and B acceptor sites are alternating in the highly symmetric ring system of **MC-B3N3**. The D–π–A type arrangement results in mutual interactions between B and N as is evidenced by electrochemical measurements and reflected in a pronounced solvatochromic effect on the emission. Macrocycles, such as **MC-B3N3**, combine aspects of electron-rich aza- and electron-deficient boracyclophanes suggesting possible applications as ambipolar semiconductor materials. The strong luminescence in solution also lends itself to use in anion recognition and our studies indicate that, in the presence of low levels of cyanide, fluorescence results from emissive charge-transfer states, which is in stark contrast to the respective boracyclophane **MC-B6** discussed in Chapter 3. Macrocycle **MC-B4N2** also shows a strong solvatochromic effect on the emission. Electronic communication of 4 borons is apparent from the electrochemical studies, whereas the two nitrogens are electronically independent due to a long distance between the carbazole units.

4.9 Perspective for Future Work

Incorporation of donor and acceptor units into conjugated systems is known to give rise to narrow band gaps that are of paramount interest in the area of organic electronics, owing to the effective intermolecular charge transfer (ICT). Among D–π–A type ambipolar B-N macrocycles, the systems in which donor and acceptor sites are separated in two blocks are based on DFT calculations expected to have much lower HOMO-LUMO gaps than those with alternating donors and acceptors (**Table 4-11** and **Figure 4-29**). For example, the HOMO-LUMO gap of **MC-*b*-B3N3** (2.59 eV) is lowered by 0.73 eV in comparison with the *alternating* macrocycle **MC-B3N3** (3.32 eV). Moreover, fine-tuning of the HOMO-LUMO gaps can be achieved through modification of D/A ratio in the *block* macrocycles (**Table 4-11**).

Table 4-11. Comparison of the Calculated Orbital Energies for Cycles (DFT, B3LYP, 6-31G*)

Compound	HOMO (eV)	LUMO (eV)	HOMO-LUMO gap (eV)
MC-*b*-B3N3	–4.63	–2.04	2.59
MC-*b*-B2N4	–4.49	–1.82	2.67
MC-*b*-BN5	–4.41	–1.47	2.94
MC-B3N3	–5.01	–1.69	3.32

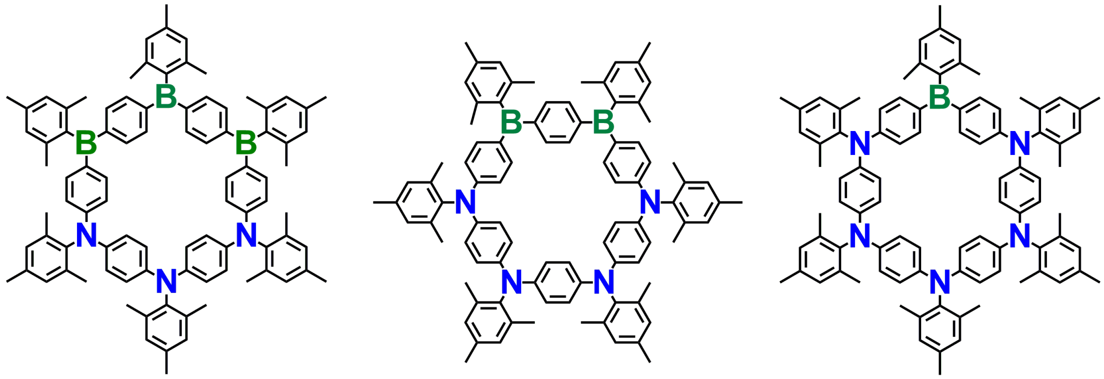

MC-*b*-B3N3 MC-*b*-B2N4 MC-*b*-BN5

Figure 4-28. Molecular structures for the proposed *block* B-N macrocycles.

4.10 Experimental Section

Materials and General Methods. *n*-BuLi (1.6 M in hexanes), BBr_3, tetrabutylammonium cyanide (TBACN), ${}^tBu_3P$ and KO^tBu were purchased from Aldrich, Me_3SiCl and carbazole from Acros, Me_3SnCl from Strem chemicals, $Pd_2(dba)_3$ from Oakwood products, propylene carbonate (PC) from Alfa Aesar, and Bio-Beads S-X Beads from Bio-Rad Laboratories (Hercules, CA, USA). Me_3SiCl was distilled under vacuum and all other commercially available chemicals were used as received without further purification. The procedures described in Chapter 2 were performed to prepare **TPA-Si2**, **TPA-Sn2**, **TPA-SiSn**, **TPA-SiB** and **O-B1N2**. **FlB2**,[47] **FlSn2**,[47] **CzSiSn**,[54] and 2,4,6-triisopropylphenyl copper[55] (TipCu) were prepared according to the previously published procedures. Tetrahydrofuran (THF) was distilled from Na/benzophenone prior to use. Hexanes and toluene were purified using a solvent purification system (Innovative Technologies; alumina/copper columns for hydrocarbon solvents). Dichloromethane

(DCM) and $CDCl_3$ were distilled from CaH_2 and degassed via several freeze-pump-thaw cycles for use with air-sensitive compounds. All reactions and manipulations involving reactive borane or organolithium species were carried out under an atmosphere of prepurified nitrogen using either Schlenk techniques or an inert-atmosphere glove box.

All 499.893 (or 600) MHz ^{1}H, 125.7 MHz ^{13}C, 160.4 MHz ^{11}B NMR, 99.25 MHz ^{29}Si NMR, and 186.455 MHz ^{119}Sn NMR spectra were recorded on a Varian INOVA spectrometer equipped with a boron-free 5 mm dual broadband gradient probe (Nalorac, Varian Inc., Martinez, CA). ^{11}B NMR spectra were acquired with boron-free quartz NMR tubes and the spectra were referenced externally to $BF_3 \cdot Et_2O$ ($\delta = 0$). ^{29}Si NMR spectra were referenced to $SiMe_4$ (δ = 0). All NMR spectra were obtained at ambient temperature.

MALDI-MS measurements were performed on an Apex-ultra 7T Hybrid FT-MS (Bruker Daltonics) in linear (+) mode. Benzo[α]pyrene (10 mg/mL) used as the matrix was mixed with the samples (10 mg/mL in toluene) in a 10:1 ratio, and then spotted on the wells of a target plate inside a glove box.

GPC analyses were performed in THF (1 mL/min) using a Waters Breeze system equipped with a 717 plus autosampler, a 1525 binary HPLC pump, a 2998 photodiode array detector, and a 2414 refractive index detector. For separation, the samples were passed through a series of styragel columns (Polymer Laboratories; two columns: Plgel 5 μm 100 Å and 500 Å), which were kept in a column heater at 35 °C. The columns were calibrated with low molecular weight polystyrene standards (Polymer Laboratories, range from 1300 to 5780 Da).

UV-visible absorption data were acquired on a Varian Cary 500 UV-Vis/NIR spectrophotometer. The fluorescence data and quantum yields were measured on a Varian Cary Eclipse fluorescence spectrophotometer with the same solutions as those used in the UV-visible measurements. The quantum yields (Φ) in DCM were calculated using 9, 10-diphenylanthracene as a standard (Φ = 0.92 in DCM).[56] Sample solutions were prepared using a microbalance (± 0.1 mg) and volumetric flasks. For titration experiments, cyanide ion solutions were prepared by dissolving the desired amount of TBACN solid in toluene; stock solutions of the samples were prepared in toluene in the glove box. Cyanide was added to the sample solution through a microsyringe (± 0.1 μL), minimizing exposure to air.

Cyclic voltammetry (CV) and square wave voltammetry (SWV) experiments were carried out on a BAS CV-50W analyzer. The three-electrode system consisted of an Au disk as working electrode, a Pt wire as secondary electrode and a Ag wire as a pseudo reference electrode. The voltammograms were recorded with ca. 10^{-3} to 10^{-4} M sample solution in THF with $Bu_4N[PF_6]$ (0.1 M) as the supporting electrolyte for the reduction and in DCM with $Bu_4N[PF_6]$ (0.1 M) for the oxidation scans. The scans were referenced after the addition of a small amount of ferrocene as an internal standard. The potentials are reported relative to the ferrocene/ferrocenium couple.

DFT calculations (gas phase) were performed using the Gaussian03 program. Geometries and electronic properties are calculated by means of the hybrid density functional B3LYP with the basis set of 6-31G(d). The input files and orbital representations were generated with Gaussview 3.07 (scaling radii of 75%, isovalue of 0.02) and C_3, D_3, D_{3d}, C_{2V} or C_2 symmetry was imposed. A true minimum was confirmed by the absence of imaginary frequencies. Excitation data were calculated using TD-DFT methods (B3LYP, 6-31G(d)). GIAO calculations were performed at the GIAO-B3LYP/6-311G*//B3LYP/6-31G* level of theory.

Single crystal X-ray diffraction intensities on **MC-B3N3** were collected on a Smart Apex2 CCD diffractometer at 100 K using Cu Kα (1.54178 Å) radiation and details of the X-ray diffraction experiment and crystal structure refinement are given in the Appendix. Since the crystals lost solvent almost immediately, they were placed in Paratone-N oil and put at 100 K as quickly as possible. Despite these precautions and the use of higher boiling dichloroethane in place of dichloromethane, the crystal did not diffract well beyond 0.84 Å resolution, where most of the "missing" data lie. The structure was solved by direct methods and refined by full-matrix least squares based on F^2 with all reflections (SHELXTL V5.10; G. Sheldrick, Siemens XRD, Madison, WI). Non-hydrogen atoms were refined with anisotropic displacement coefficients, and hydrogen atoms were treated as idealized contribution. SADABS (Sheldrick, G.M.; SADABS, 2008, University of Göttingen) absorption correction was applied. Generally, the structure solution was straightforward, and two independent dichloroethane solvent molecules were found and refined (36 molecules of dichloroethane per unit cell). However, other dichloroethane molecules in the structure (located in channels along the crystallographic *c* axis) were highly disordered and removed using the Squeeze routine in the Platon program (Spek, A. L. *J. Appl. Crystallogr.* **2003**, *36*, 7-13). The total electron density corresponds to 12 additional dichloroethane molecules (50 electrons) per unit cell (615 e^- in a total of 1689 $Å^3$ void space). The large size of the cell, facile loss of solvent from positions in channels and layers, and the disorder of solvent contribute to the relatively high R factors. Crystallographic data for the structure of **3** have been deposited with the Cambridge Crystallographic Data Center as supplementary publication CCDC-882152. Copies of the data can be obtained free of charge on application to CCDC, 12 Union Road, Cambridge CB2 IEZ, UK (fax:(+44) 1223-336-033; email: deposit@ccdc.cam.ac.uk).

Synthesis of MC-B3N3. To BBr_3 (50 mg, 200 μmol) in 5 mL of toluene was added a solution of **O-B1N2** (75 mg, 79 μmol) in 15 mL of toluene with stirring. The reaction mixture was kept stirring overnight, and then all volatile components were removed under high vacuum. The crude product was purified by recrystallization from hexanes/toluene mixture at –35 °C to give a yellow solid (70 mg, 77%). Solutions of the borylated product (70 mg, 60 μmol) in 50 mL of toluene and **TPA-Sn2** (38 mg, 60 μmol) in 50 mL of toluene were simultaneously added through two different addition funnels to a three-necked round bottom flask containing 400 mL of toluene under N_2 over a period of 12 h with stirring. After stirring for 2 days at RT, the reaction mixture was evaporated to dryness, leaving behind a yellow solid. The solid was redissolved in toluene and treated with TipCu (32 mg, 120 μmol) in 15 mL of toluene. The reaction mixture was refluxed at 120 °C under N_2 for 2 d. A solid precipitate (CuBr) was removed by filtration through a fritted glass disk. All volatile components were then removed under high vacuum and the crude product was purified by preparative size-exclusion chromatography on Bio-Beads™ using THF as the eluent. A solution of the purified product in a 5/1 hexanes/toluene mixture was kept at –35 °C to give a microcrystalline pale yellow solid (46 mg, 49%). ^{1}H NMR (499.893 MHz, $CDCl_3$): δ 1.00 (d, J = 6.5 Hz, 36H), 1.28 (d, J = 7.0 Hz, 18H), 1.30 (s, 27H), 2.58 (septet, J = 7.0 Hz, 6H), 2.88 (septet, J = 7.0 Hz, 3H), 6.95 (s, 6H), 7.14 (d, J = 8.5 Hz, 6H), 7.24 (d, J = 8.5 Hz, 12 H), 7.31 (d, J = 8.5 Hz, 6H), 7.61 (d, J = 8.5 Hz, 12H). ^{13}C NMR (150.0 MHz, $CDCl_3$): δ 24.38, 24.52, 31.59, 34.49, 34.70, 35.57, 120.08, 121.08, 126.67, 126.80, 138.08 (B-C), 138.69, 143.21, 148.22, 148.43, 148.80, 149.68. ^{11}B NMR (160.4 MHz, $CDCl_3$): δ 72 ($w_{1/2}$ = 5200 Hz). MALDI-MS (pos.) m/z: calcd. for $C_{111}H_{132}B_3N_3$ $[M]^+$ 1540.0706 found 1540.0705.

Synthesis of Me_3Si-Cz-B-Fl-B-Cz-$SiMe_3$ (O-CFC). To a solution of compound **FlB2** (0.29 g, 0.55 mmol) in 20 mL of CH_2Cl_2 was added a solution of **CzSiSn** (0.50 g, 1.10 mmol) in 10 mL of CH_2Cl_2 and the mixture was kept stirring overnight. All volatile components were removed under vacuum, leaving behind a yellowish solid. Without further purification the crude product was dissolved in 10 mL of toluene and then treated with TipCu (0.29 g, 1.10 mmol) in 10 mL of toluene. The reaction mixture was refluxed at 120 °C under N_2 for 2 d. A solid precipitate (CuBr) was removed by filtration through a fritted glass disk. All volatile components were removed under high vacuum. The crude product was purified by column chromatography on silica gel using hexanes as the eluent, and then precipitated from hexanes at –35 °C to give **O-CFC** as a white powdery solid (0.47 g, 71%). ^{1}H NMR (499.893 MHz, $CDCl_3$): δ 0.33 (s, 18H, TMS), 1.01 (m, 30H, Tip+Bu_Me), 1.38 (d, J = 7.0 Hz, 12H, Tip), 1.50 (sextet, J = 7.5 Hz, 4H, Bu), 1.55 (s, 6H, Fl), 1.90 (quint, J = 7.0 Hz, 4H, Bu), 2.61 (septet, J = 7.0 Hz, 4H, Tip), 3.00 (septet, J = 7.0 Hz, 2H, Tip), 4.34 (t, J = 7.5 Hz, 4H, Bu), 7.07 (s, 4H, Tip), 7.44 (d, J = 8.0 Hz, 2H, Cz), 7.47 (d, J = 8.0 Hz, 2H, Cz), 7.64 (d, J = 8.0 Hz, 2H, Cz), 7.88 (d, J = 8.0 Hz, 4H, Fl), 7.93 (d, J = 7.5 Hz, 2H, Cz), 7.96 (s, 2H, Fl), 8.26 (s, 2H, Cz), 8.74 (s, 2H, Cz). ^{13}C NMR (125.7 MHz, $CDCl_3$): –0.43, 14.10, 20.81, 24.41, 24.44, 27.11, 29.93, 31.40, 34.46, 35.58, 43.20, 47.08, 108.15, 108.84, 119,98, 120.19, 122.76, 123.64, 125.77, 128.45, 129.27, 130.10, 130.85, 131.38, 132.14, 133.53 (B-C), 137.04, 137.29, 141.57, 141.78 (B-C), 141.97, 143.23, 143.82 (B-C), 148.35, 149.24, 153.78. ^{11}B NMR (160.4 MHz, $CDCl_3$): δ 66 ($w_{1/2}$ = 1,400 Hz). ^{29}Si NMR (99.25 MHz, $CDCl_3$): δ –3.87. High res. MALDI-MS (pos.) m/z: calcd. for $C_{83}H_{106}B_2N_2Si_2$ [M^+] 1208.8111, found 1208.8160.

Synthesis of MC-B4N2. To BBr_3 (0.08 g, 0.30 mmol) in 5 mL of toluene was added a solution of **O-CFC** (0.14 g, 0.12 mmol) in 10 mL of toluene with stirring. The reaction mixture was kept stirring overnight, and then all volatile components were removed under high vacuum. The crude product was purified by recrystallization from hexanes/toluene mixture at –35 °C to give a light yellow solid (0.10 g, 61%). ^{1}H NMR (499.893 MHz, $CDCl_3$): δ 1.02 (m, 30H, Tip+Bu_Me), 1.38 (d, J = 7.0 Hz, 12H, Tip), 1.46 (sextet, J = 7.5 Hz, 4H, Bu), 1.55 (s, 6H, Fl), 1.93 (quint, J = 7.5 Hz, 4H, Bu), 2.59

(septet, J = 6.5 Hz, 4H, Tip), 3.01 (septet, J = 7.0 Hz, 2H, Tip), 4.38 (t, J = 8.0 Hz, 4H, Bu), 7.07 (s, 4H, Tip), 7.47 (d, J = 8.5 Hz, 2H), 7.51 (d, J = 8.5 Hz, 2H), 7.89 (d, J = 8.0 Hz, 2H), 7.95 (m, 6H), 8.34 (d, J = 8.5 Hz, 2H), 8.78 (s, 2H, Cz), 8.96 (s, 2H, Cz). ^{11}B NMR (160.4 MHz, $CDCl_3$): δ 68 ($w_{1/2}$ = 2,300 Hz). Solutions of the borylated product (100 mg, 71 μmol) in 50 mL of toluene and **FlSn2** (37 mg, 71 μmol) in 50 mL of toluene were simultaneously added through two different addition funnels to a three-necked round bottom flask containing 300 mL of toluene under N_2 over a period of 12 h with stirring. After stirring for 2 days at RT, the reaction mixture was evaporated to dryness, leaving behind a light yellow solid. The solid was redissolved in toluene and treated with TipCu (38 mg, 142 μmol) in 15 mL of toluene. The reaction mixture was refluxed at 120 °C under N_2 for 2 d. A solid precipitate (CuBr) was removed by filtration through a fritted glass disk. All volatile components were then removed under high vacuum and the crude product was purified by preparative size-exclusion chromatography on Bio-Beads™ using THF as the eluent. A solution of the purified product in hexanes was precipitated at –35 °C to give a white powdery material (40 mg, 33%). ^{1}H NMR (499.893 MHz, $CDCl_3$): δ 0.99 (m, 54H, Tip+Bu_Me), 1.34 (s, 12H, Fl), 1.37 (d, J = 7.0 Hz, 24H, Tip), 1.46 (sextet, J = 7.5 Hz, 4H, Bu), 1.93 (quint, J = 7.5 Hz, 4H, Bu), 2.59 (septet, J = 7.0 Hz, 8H, Tip), 2.99 (septet, J = 7.0 Hz, 4H, Tip), 4,36 (t, J = 7.0 Hz, 4H, Bu), 7.04 (s, 8H, Tip), 7.44 (d, J = 8.5 Hz, 4H, Fl), 7.68 (s, 4H, Fl), 7.79 (d, J = 8.5 Hz, 4H, Fl), 8.05 (d, J = 7.5 Hz, 4H, Cz), 8.17 (d, J = 8.0 Hz, 4H, Cz), 8.88 (s, 4H, Cz). ^{13}C NMR (150.0 MHz, $CDCl_3$): 14.07, 20.80, 24.36, 24.40, 24.48, 27.01, 31.38, 34.46, 35.50, 43.37, 46.88, 108.48, 119.85, 120.12, 123.52, 131.33, 132.40, 134.17 (B-C), 136.64, 137.69, 141.67 (B-C), 142.11, 143.52, 148.33, 149.20, 153.88. ^{11}B NMR (160.4 MHz, $CDCl_3$): 77 ($w_{1/2}$ = 2,600 Hz). High res. MALDI-MS (pos.) m/z: calcd. for $C_{122}H_{146}B_4N_2$ [M^+] 1683.1919 found 1683.1936.

Synthesis of 3,6-bis(trimethylstannyl)-9-*n*-butylcarbazole (CzSn2). A solution of *n*-BuLi (1.6 M in hexanes, 16 mL, 25 mmol) was added dropwise over a period of 1 h to a solution of 3,6-dibromo-9-*n*-butylcarbazole (3.81 g, 10 mmol) in dry diethyl ether (250 mL) at −78 °C. The mixture was stirred for 1 h and then allowed to slowly warm up to R. T. After cooling the reaction mixture back down to −78 °C, a solution of Me_3SnCl (4.98 g, 25 mmol) in ether (15 mL) was added via syringe. The mixture was stirred at −78 °C for 4 h and then for an additional 12 h at ambient temperature. After standard workup the crude material was purified by recrystallization from ethanol to give colorless crystals (4.0 g, 73%). ^{1}H NMR (600 MHz, $CDCl_3$): δ 0.37 (s, $J(^{117/119}Sn, H)$ = 54 Hz, 18H), 0.94 (t, J = 7.8 Hz, 3H), 1.40 (sextet, 2H), 1.85 (quintet, 2H), 4.30 (t, J = 7.2 Hz, 2H), 7.42 (d, J = 7.8 Hz, 2H), 7.56 (d, J = 8.4 Hz, 2H), 8.25 (s, $J(^{117/119}Sn, H)$ = 48.0 Hz, 2H). ^{119}Sn NMR (186.455 MHz, $CDCl_3$): δ –23.6. MALDI-MS (pos.) m/z: calcd. for $C_{22}H_{33}NSn_2$ [M^+] 549.0654 found 549.0633.

Synthesis of 2-bromo-7-trimethylstannyl-9,9-dimethylfluorene (FlSnBr). A solution of *n*-BuLi (1.6 M in hexanes, 23 mL. 36.8 mmol) was added dropwise over a period of 1 h to a solution of 2,7-dibromo-9,9-dimethylfluorene (12.95 g, 36.8 mmol) in dry THF (350 mL) at −78 °C. The mixture was stirred for 1 h and then allowed to slowly warm up to R. T. After cooling the reaction mixture back down to –78 °C, a solution of Me_3SnCl (8.00 g, 25.3 mmol) in THF (20 mL) was added via syringe. The mixture was stirred at –78 °C for 4 h and then for an additional 12 h at ambient temperature. After standard workup the crude material was purified by recrystallization from ethanol to give a colorless powdery material (11.8 g, 74%). ^{1}H NMR (499.893 MHz, $CDCl_3$): δ 0.34 (s, J($^{117/119}$Sn, H) = 54 Hz, 9H), 1.50 (s, 6H), 7.48 (m, J($^{117/119}$Sn, H) = 43.5 Hz, 2H), 7.55 (d, J = 7.0 Hz, 2H), 7.59 (d, J = 7.5 Hz, 1H), 7.68 (d, J = 7.5 Hz, 1H). ^{119}Sn NMR (186.455 MHz, $CDCl_3$): δ –24.3. GC-MS: m/z 436 (100%) [M^+], 274 (5%) [M^+ – $SnMe_3$].

Synthesis of Fl2BTip. To a solution of compound **FlSnBr** (200 mg, 459 μmol) in 15 mL of CH_2Cl_2 was added a solution of **BBr_3** (70 mg, 280 μmol) in 5 mL of CH_2Cl_2 and the mixture was kept stirring overnight. All volatile components were removed under vacuum, leaving behind a yellowish solid. Without further purification the crude product was dissolved in 10 mL of toluene and then treated with TipCu (120 mg, 459 μmol) in 10 mL of toluene. The reaction mixture was refluxed at 120 °C under N_2 for 2 d. A solid precipitate (CuBr) was removed by filtration through a fritted glass disk. All volatile components were removed under high vacuum. The crude product was purified by column chromatography on silica gel using hexanes as the eluent, and then precipitated from hexanes at –35 °C to give **Fl2BTip** as a white powdery solid (190 mg, 55%). ^{1}H NMR (499.893 MHz, $CDCl_3$): δ 0.99 (d, J = 7.0 Hz, 12H), 1.36 (d, J = 7.0 Hz, 6H), 1.49 (s, 12H), 2.47 (septet, J = 7.0 Hz, 2H), 2.98 (septet, J = 7.0 Hz, 1H), 7.03 (s, 2H), 7.51 (d, J = 8.0 Hz, 2H), 7.60 (s, 2H), 7.67 (d, J = 8.0 Hz, 2H), 7.79 (m, 4H), 7.84 (s, 2H). ^{13}C

NMR (125.7 MHz, $CDCl_3$): 24.33, 24.37, 27.14, 34.48, 35.71, 47.36, 119.47, 120.29, 122.21, 122.28, 126.56, 130.47, 132.03, 137.71, 138.12, 140.88 (B-C), 141.68, 142.79 (B-C), 148.75, 149.10, 152.51, 156.89. ^{11}B NMR (160.4 MHz, $CDCl_3$): δ 70 ($w_{1/2}$ = 3,500 Hz).

Synthesis of MC-B2N2. To a three-necked round bottom flask containing 250 mL of toluene was added KO^{t}Bu (43.0 mg, 380 μmol) under N_2, followed by addition of $Pd_2(dba)_3$ (6.0 mg, 6.3 μmol) in 20 mL of toluene and of ^{t}Bu$_3$P (1.3 mg, 6.3 μmol) in 5 mL of toluene through syringe. Solutions of **Fl2BTip** (96.0 mg, 126 μmol) in 50 mL of toluene and **CzSn2** (69.0 mg, 126 μmol) in 50 mL of toluene were simultaneously added through two different addition funnels. The reaction mixture was refluxed with stirring for 3 days, and then it was condensed to 20 mL under high vacuum, which was further washed with water to remove the salts left over. The resulting solution was flushed through a silica gel chromatography column using toluene as the eluent to remove the Pd catalyst. The crude product was further purified by preparative size-exclusion chromatography on Bio-Beads™ using THF as the eluent.

4.11 References

(1) Campbell, P. G.; Marwitz, A. J. V.; Liu, S. Y. *Angew. Chem. Int. Ed.* **2012**, *51*, 6074.

(2) Chopra, N. G.; Luyken, R. J.; Cherrey, K.; Crespi, V. H.; Cohen, M. L.; Louie, S. G.; Zettl, A. *Science* **1995**, *269*, 966.

(3) Golberg, D.; Bando, Y.; Tang, C.; Zhi, C. *Adv. Mater.* **2007**, *19*, 2413.

(4) Stock, E. P. A. *Ber. Dtsch. Chem. Ges.* **1926**, *59*, 2210.

(5) Schleyer, P. v. R.; Jiao, H.; Eikema Hommes, N. J. R. V.; Malkin, V. G.;

Malkina, O. L. *J. Am. Chem. Soc.* **1997**, *119*, 12669.
(6) Ma, K.; Scheibitz, M.; Scholz, S.; Wagner, M. *J. Organomet. Chem.* **2002**, *652*, 11.
(7) Liu, Z. Q.; Marder, T. B. *Angew. Chem. Int. Ed.* **2008**, *47*, 242.
(8) Bosdet, M. J. D.; Piers, W. E. *Can. J. Chem.* **2009**, *87*, 8.
(9) Marder, T. B. *Angew. Chem. Int. Ed.* **2007**, *46*, 8116.
(10) Abbey, E. R.; Zakharov, L. N.; Liu, S. Y. *J. Am. Chem. Soc.* **2011**, *133*, 11508.
(11) Lamm, A. N.; Garner, E. B.; Dixon, D. A.; Liu, S. Y. *Angew. Chem. Int. Ed.* **2010**, *50*, 8157.
(12) Campbell, P. G.; Zakharov, L. N.; Grant, D. J.; Dixon, D. A.; Liu, S. Y. *J. Am. Chem. Soc.* **2010**, *132*, 3289.
(13) Jaska, C. A.; Emslie, D. J. H.; Bosdet, M. J. D.; Piers, W. E.; Sorensen, T. S.; Parvez, M. *J. Am. Chem. Soc.* **2006**, *128*, 10885.
(14) Bosdet, M. J. D.; Piers, W. E.; Sorensen, T. S.; Parvez, M. *Angew. Chem. Int. Ed.* **2007**, *46*, 4940.
(15) Abbey, E. R.; Zakharov, L. N.; Liu, S. Y. *J. Am. Chem. Soc.* **2010**, *132*, 16340.
(16) Wakamiya, A.; Ide, T.; Yamaguchi, S. *J. Am. Chem. Soc.* **2005**, *127*, 14859.
(17) Hatakeyama, T.; Hashimoto, S.; Seki, S.; Nakamura, M. *J. Am. Chem. Soc.* **2011**, *133*, 18614.
(18) Yuan, Z.; Collings, J. C.; Taylor, N. J.; Marder, T. B.; Jardin, C.; Halet, J. F. *J. Sol. St. Chem.* **2000**, *154*, 5.
(19) Entwistle, C. D.; Marder, T. B. *Chem. Mater.* **2004**, *16*, 4574.
(20) Shirota, Y. *J. Mater. Chem.* **2005**, *15*, 75.
(21) Liu, X. Y.; Bai, D. R.; Wang, S. N. *Angew. Chem. Int. Ed.* **2006**, *45*, 5475.
(22) Li, F.; Jia, W.; Wang, S.; Zhao, Y.; Lu, Z. H. *J. Appl. Phys.* **2008**, *103*, 034509/1.
(23) Collings, J. C.; Poon, S. Y.; Le Droumaguet, C.; Charlot, M.; Katan, C.; Palsson, L. O.; Beeby, A.; Mosely, J. A.; Kaiser, H. M.; Kaufmann, D.; Wong, W. Y.; Blanchard-Desce, M.; Marder, T. B. *Chem. Eur. J.* **2009**, *15*, 198.
(24) Stahl, R.; Lambert, C.; Kaiser, C.; Wortmann, R.; Jakober, R. *Chem. Eur. J.* **2006**, *12*, 2358.
(25) Pron, A.; Baumgarten, M.; Müllen, K. *Org. Lett.* **2010**, *12*, 4236.
(26) Weber, L.; Eickhoff, D.; Marder, T. B.; Fox, M. A.; Low, P. J.; Dwyer, A. D.; Tozer, D. J.; Schwedler, S.; Brockhinke, A.; Stammler, H.;G.; Neumann, B. *Chem. Eur. J.* **2012**, *18*, 1369.
(27) Schmidt, H. C.; Reuter, L. G.; Hamacek, J.; Wenger, O. S. *J. Org. Chem.* **2011**, *76*, 9081.
(28) Iyoda, M. *Pure Appl. Chem.* **2010**, *82*, 831.
(29) Mishra, A.; Ma, C. Q.; Bäuerle, P. *Chem. Rev.* **2009**, *109*, 1141.
(30) Zhang, W.; Moore, J. S. *Angew. Chem., Int. Ed.* **2006**, *45*, 4416.
(31) Höger, S. *Chem. Eur. J.* **2004**, *10*, 1320.
(32) Grave, C.; Schlüter, A. D. *Eur. J. Org. Chem.* **2002**, 3075.

(33) Zang, L.; Che, Y.; Moore, J. S. *Acc. Chem. Res.* **2008**, *41*, 1596.

(34) Hartley, C. S.; Moore, J. S. *J. Am. Chem. Soc.* **2007**, *129*, 11682.

(35) Ito, A.; Yokoyama, Y.; Aihara, R.; Fukui, K.; Eguchi, S.; Shizu, K.; Sato, T.; Tanaka, K. *Angew. Chem. Int. Ed.* **2010**, *49*, 8205.

(36) Jutzi, P.; Lenze, N.; Neumann, B.; Stammler, H.-G. *Angew. Chem. Int. Ed.* **2001**, *40*, 1423.

(37) Wedge, T. J.; Hawthorne, M. F. *Coord. Chem. Rev.* **2003**, *240*, 111.

(38) Fox, M. A.; Howard, J. A. K.; MacBride, J. A. H.; Mackinnon, A.; Wade, K. *J. Organomet. Chem.* **2003**, *680*, 155.

(39) Scheibitz, M.; Winter, R. F.; Bolte, M.; Lerner, H. W.; Wagner, M. *Angew. Chem. Int. Ed.* **2003**, *42*, 924.

(40) Gong, H.-Y.; Zhang, X.-H.; Wang, D.-X.; Ma, H.-W.; Zheng, Q.-Y.; Wang, M.-X. *Chem. Eur. J.* **2006**, *12*, 9262.

(41) Venkatasubbaiah, K.; Pakkirisamy, T.; Lalancette, R. A.; Jäkle, F. *Dalton Trans.* **2008**, 4507.

(42) Zhang, E.-X.; Wang, D.-X.; Zheng, Q.-Y.; Wang, M.-X. *Org. Lett.* **2008**, *10*, 2565.

(43) Herbert, D. E.; Gilroy, J. B.; Chan, W. Y.; Chabanne, L.; Staubitz, A.; Lough, A. J.; Manners, I. *J. Am. Chem. Soc.* **2009**, *131*, 14958.

(44) Gabbaï, F. P. *Angew. Chem. Int. Ed.* **2003**, *42*, 2218.

(45) Chen, P.; Jäkle, F. *J. Am. Chem. Soc.* **2011**, *133*, 20142.

(46) Qin, Y.; Kiburu, I.; Shah, S.; Jäkle, F. *Macromolecules* **2006**, *39*, 9041.

(47) Chen, P.; Lalancette, R. A.; Jäkle, F. *J. Am. Chem. Soc.* **2011**, *133*, 8802.

(48) Wade, C. R.; Broomsgrove, A. E. J.; Aldridge, S.; Gabbai, F. P. *Chem. Rev.* **2010**, *110*, 3958.

(49) Hudson, Z. M.; Wang, S. *Acc. Chem. Res.* **2009**, *42*, 1584.

(50) Sundararaman, K.; Venkatasubbaiah, A.; Victor, M.; Zakharov, L. N.; Rheingold, A. L.; Jäkle, F. *J. Am. Chem. Soc.* **2006**, *128*, 16554.

(51) Li, H.; Jäkle, F. *Macromol. Rap. Commun.* **2010**, *31*, 915.

(52) Zhao, S.-B.; Wucher, P.; Hudson, Z. M.; McCormick, T. M.; Liu, X.-Y.; Wang, S.; Feng, X.-D.; Lu, Z.-H. *Organometallics* **2008**, *27*, 6446.

(53) Zhao, G.; Baumgarten, M.; Müllen, K. *J. Am. Chem. Soc.* **2008**, *130*, 12477.

(54) Parab, K.; Doshi, A.; Cheng, F.; Jäkle, F. *Macromolecules* **2011**, *44*, 5961.

(55) Sasaki, S.; Sutoh, K.; Murakami, F.; Yoshifuji, M. *J. Am. Chem. Soc.* **2002**, *124*, 14830.

(56) Murov, S. L.; Carmichael, I.; Hug, G. L. *Handbook of Photochemistry*, 2nd ed., Marcel Dekker: New York, **1993**.

(57) Chen, P.; Lalancette, R. A.; Jäkle, F. *Angew. Chem. Int. Ed.* **2012**, *51*, 7994.

Appendix

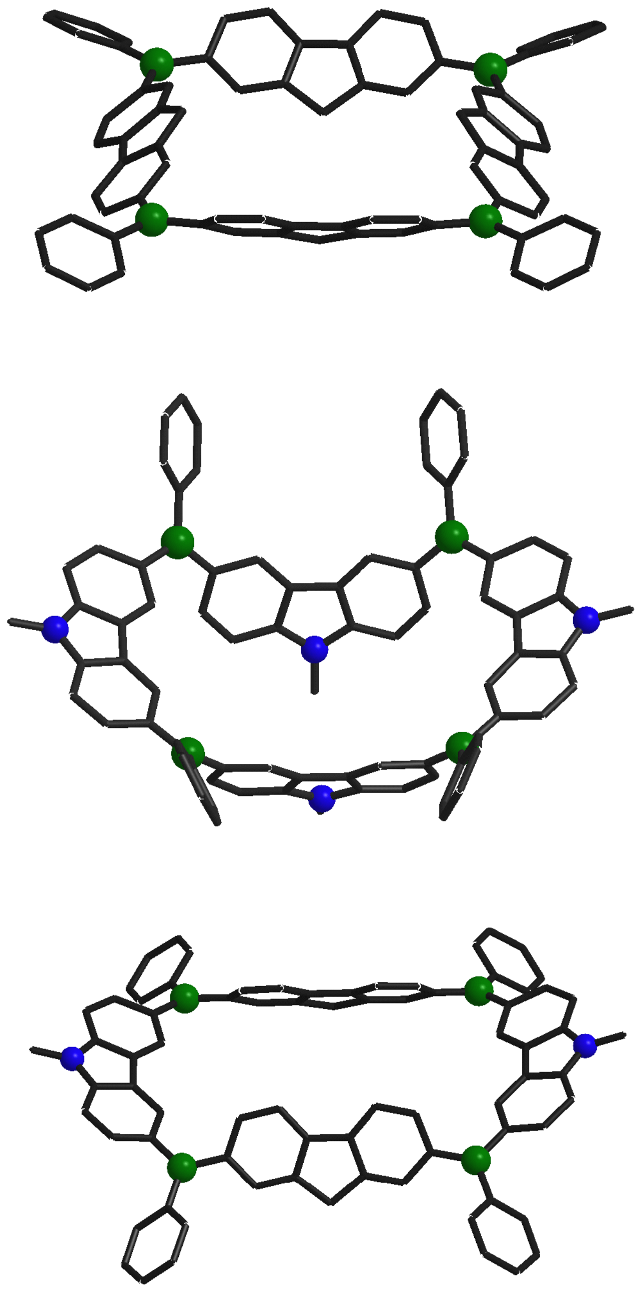

Figure 1. Optimized macrocycle structures showing endocyclic bond angles around B centers with different π systems: (top) fluorene (118.1°); (middle) carbazole (119.0°); (bottom) hybrid (120.9°).

Table 1. Crystal Data and Structure Refinement for Macrocycle **MC-B3N3**

Empirical formula	$C_{111}H_{132}B_3N_3$, 6 $C_2H_4Cl_2$
Mr	2134.34
T (K)	100(2)
λ (Å)	1.54178
Cryst system	rhombohedral
Space group	R $\bar{3}$
a (Å)	21.3886(11)
b (Å)	21.3886(11)
c (Å)	46.765(3)
α (°)	90
β (°)	90
γ (°)	120
V (Å^3)	18527.5(18)
Z	6
F(000)	6804
Cryst size (mm^3)	0.51 × 0.47 × 0.17
θ (°)	2.57 – 71.80
Index range	-26<=h<=13, 0<=k<=26, 0<=l<=56
ρ_{calcd} (g/cm^3)	1.148
μ(CuKα,mm^{-1})	2.807
Data/restraints/parameters	7563 / 0 / 433
Absorption correction	SADABS
GOF on F^2	1.460
Final R indices (I>2σ(I))[a]	R_1 = 0.1160, wR_2 = 0.348
R indices (all data)[a]	R_1 = 0.133, wR_2 = 0.360
Peak and hole (e Å^{-3})	1.32, –0.86

[a] $R_1 = \Sigma||F_o|-|F_c||/|F_o|$, $wR_2 = [\Sigma w(F_o^2-F_c^2)^2/\Sigma w(F_o^2)^2]^{1/2}$

Table 2. Selected Bond Distances (Å) and Angles (°) for **MC-B3N3** from X-ray Analysis

MC-B3N3			
N1-C4	1.427(5)	N1-C7	1.414(5)
N1-C13	1.427(5)	B1-C1	1.560(6)
B1-C10	1.546(6)	B1-C23	1.571(6)
C7-N1-C4	121.5(3)	C7-N1-C13	119.2(3)
C13-N1-C4	119.2(3)	C3-C4-N1	120.9(4)
C5-C4-N1	120.2(4)	C8-C7-N1	121.6(3)
C12-C7-N1	120.1(3)	C1-B1-C10	119.7(3)
C1-B1-C23	121.1(3)	C10-B1-C23	118.9(3)
C2-C1-B1	121.8(4)	C6-C1-B1	123.3(4)
C28-C23-B1	118.5(4)	C24-C23-B1	122.5(4)
C9-C10-B1	122.5(3)	C11-C10-B1	122.2(3)

Table 3. Selected Calculated Bond Distances (Å) and Angles (°) for simplified **MC-B3N3**, **MC-N6** and **MC-B6** (DFT, B3LYP/6-31G(d))

MC-B3N3			
Bond Distances (Å)		Bond Angles (°)	
B-C (exocyclic)	1.571	C-B-C (exocyclic)	120.2
B-C (endocyclic)	1.564	C-B-C (endocyclic)	119.6
N-C (exocyclic)	1.429	C-N-C (exocyclic)	119.3
N-C (endocyclic)	1.417	C-N-C (endocyclic)	121.4
MC-N6			
Bond Distances (Å)		Bond Angles (°)	
N-C (exocyclic)	1.421	C-N-C (exocyclic)	120.0
N-C(endocyclic)	1.421	C-N-C (endocyclic)	120.0
MC-B6			
Bond Distances (Å)		Bond Angles (°)	
B-C (exocyclic)	1.568	C-B-C (exocyclic)	120.1
B-C (endocyclic)	1.571	C-B-C (endocyclic)	119.8

Table 4. Coordinates (Å) for the Optimized Structure of **MC-B3N3** (R=Ph, phenylene π-system)

atom	x	y	z	atom	x	y	z
C	-2.351710	5.632000	0.673050	C	6.263336	-3.616139	0.000000
C	-1.235303	5.110302	-0.005578	C	7.262032	-3.302612	-0.933021
C	-1.381280	3.893370	-0.695775	C	6.491162	-4.637798	0.933021
C	-2.591052	3.211052	-0.666882	C	8.471213	-3.996156	-0.924347
C	-3.732647	3.716307	-0.004304	H	7.083805	-2.515637	-1.659204
C	-3.567569	4.958651	0.647924	C	7.696380	-5.338208	0.924347
H	-2.257713	6.565026	1.219125	H	5.720508	-4.876937	1.659204
H	-0.540492	3.486402	-1.247673	C	8.693480	-5.019183	0.000000
H	-2.664663	2.267853	-1.201446	H	9.236937	-3.743401	-1.652909
H	-4.410125	5.393177	1.179368	H	7.860348	-6.127722	1.652909
N	0.000000	5.803530	0.000000	H	9.634249	-5.562336	0.000000
B	-5.090166	2.938809	0.000000	C	0.000000	-7.448323	0.000000
C	-5.084739	1.374414	0.004304	C	1.019682	-8.187844	0.638418
C	-6.078102	0.610280	-0.647924	C	-1.019682	-8.187844	-0.638418
C	-4.076378	0.638391	0.666882	C	1.016846	-9.582170	0.651831
C	-6.053310	-0.779359	-0.673050	H	1.820591	-7.655034	1.144143
H	-6.875690	1.122692	-1.179368	C	-1.016846	-9.582170	-0.651831
C	-4.062397	-0.750462	0.695775	H	-1.820591	-7.655034	-1.144143
H	-3.296350	1.173739	1.201446	C	0.000000	-10.283545	0.000000
C	-5.043303	-1.485347	0.005578	H	1.808168	-10.122731	1.165407
H	-6.814335	-1.327276	-1.219125	H	-1.808168	-10.122731	-1.165407
H	-3.289558	-1.275121	1.247673	H	0.000000	-11.370834	0.000000
C	-6.450437	3.724162	0.000000	C	-6.263336	-3.616139	0.000000
C	-6.581040	4.976993	-0.638418	C	-7.262032	-3.302612	0.933021
C	-7.600722	3.210851	0.638418	C	-6.491162	-4.637798	-0.933021
C	-7.789979	5.671699	-0.651831	C	-8.471213	-3.996156	0.924347
H	-5.719159	5.404195	-1.144143	H	-7.083805	-2.515637	1.659204
C	-8.806825	3.910470	0.651831	C	-7.696380	-5.338208	-0.924347
H	-7.539750	2.250839	1.144143	H	-5.720508	-4.876937	-1.659204
C	-8.905811	5.141773	0.000000	C	-8.693480	-5.019183	0.000000
H	-7.862458	6.627285	-1.165407	H	-9.236937	-3.743401	1.652909
H	-9.670626	3.495446	1.165407	H	-7.860348	-6.127722	-1.652909
H	-9.847431	5.685417	0.000000	H	-9.634249	-5.562336	0.000000
N	-5.026004	-2.901765	0.000000	C	1.235303	5.110302	0.005578
C	5.084739	1.374414	-0.004304	C	2.351710	5.632000	-0.673050

C	6.078102	0.610280	0.647924	C	1.381280	3.893370	0.695775
C	4.076378	0.638391	-0.666882	C	3.567569	4.958651	-0.647924
C	6.053310	-0.779359	0.673050	H	2.257713	6.565026	-1.219125
H	6.875690	1.122692	1.179368	C	2.591052	3.211052	0.666882
C	4.062397	-0.750462	-0.695775	H	0.540492	3.486402	1.247673
H	3.296350	1.173739	-1.201446	C	3.732647	3.716307	0.004304
C	5.043303	-1.485347	-0.005578	H	4.410125	5.393177	-1.179368
H	6.814335	-1.327276	1.219125	H	2.664663	2.267853	1.201446
H	3.289558	-1.275121	-1.247673	B	5.090166	2.938809	0.000000
C	-3.807999	-3.624955	-0.005578	C	0.000000	7.232278	0.000000
C	-2.681118	-3.142908	-0.695775	C	0.770870	7.940410	0.933021
C	-3.701600	-4.852640	0.673050	C	-0.770870	7.940410	-0.933021
C	-1.485327	-3.849442	-0.666882	C	0.774834	9.334364	0.924347
H	-2.749066	-2.211281	-1.247673	H	1.363297	7.392574	1.659204
C	-2.510533	-5.568931	0.647924	C	-0.774834	9.334364	-0.924347
H	-4.556622	-5.237750	1.219125	H	-1.363297	7.392574	-1.659204
C	-1.352092	-5.090721	-0.004304	C	0.000000	10.038366	0.000000
H	-0.631687	-3.441593	-1.201446	H	1.376588	9.871122	1.652909
H	-2.465565	-6.515869	1.179368	H	-1.376588	9.871122	-1.652909
N	5.026004	-2.901765	0.000000	H	0.000000	11.124673	0.000000
C	3.807999	-3.624955	0.005578	C	6.450437	3.724162	0.000000
C	2.681118	-3.142908	0.695775	C	7.600722	3.210851	-0.638418
C	3.701600	-4.852640	-0.673050	C	6.581040	4.976993	0.638418
C	1.485327	-3.849442	0.666882	C	8.806825	3.910470	-0.651831
H	2.749066	-2.211281	1.247673	H	7.539750	2.250839	-1.144143
C	2.510533	-5.568931	-0.647924	C	7.789979	5.671699	0.651831
H	4.556622	-5.237750	-1.219125	H	5.719159	5.404195	1.144143
C	1.352092	-5.090721	0.004304	C	8.905811	5.141773	0.000000
H	0.631687	-3.441593	1.201446	H	9.670626	3.495446	-1.165407
H	2.465565	-6.515869	-1.179368	H	7.862458	6.627285	1.165407
B	0.000000	-5.877617	0.000000	H	9.847431	5.685417	0.000000

Table 5. Coordinates (Å) for the GIAO Calculations (NICS) of **MC-B3N3 (**phenylene π-system)

atom	x	y	z	atom	x	y	z
C	-3.7016	-4.85264	0.67305	C	0	7.23228	0
C	-3.808	-3.62495	-0.00558	C	-0.77087	7.94041	-0.93302

C	-2.68112	-3.14291	-0.69578	C	0.77087	7.94041	0.93302
C	-1.48533	-3.84944	-0.66688	C	-0.77483	9.33436	-0.92435
C	-1.35209	-5.09072	-0.0043	H	-1.3633	7.39257	-1.6592
C	-2.51053	-5.56893	0.64792	C	0.77483	9.33436	0.92435
H	-4.55662	-5.23775	1.21913	H	1.3633	7.39257	1.6592
H	-2.74907	-2.21128	-1.24767	C	0	10.03837	0
H	-0.63169	-3.44159	-1.20145	H	-1.37659	9.87112	-1.65291
H	-2.46557	-6.51587	1.17937	H	1.37659	9.87112	1.65291
N	-5.026	-2.90176	0	H	0	11.12467	0
B	0	-5.87762	0	C	6.45044	3.72416	0
C	1.35209	-5.09072	0.0043	C	6.58104	4.97699	0.63842
C	2.51053	-5.56893	-0.64792	C	7.60072	3.21085	-0.63842
C	1.48533	-3.84944	0.66688	C	7.78998	5.6717	0.65183
C	3.7016	-4.85264	-0.67305	H	5.71916	5.4042	1.14414
H	2.46557	-6.51587	-1.17937	C	8.80682	3.91047	-0.65183
C	2.68112	-3.14291	0.69578	H	7.53975	2.25084	-1.14414
H	0.63169	-3.44159	1.20145	C	8.90581	5.14177	0
C	3.808	-3.62495	0.00558	H	7.86246	6.62729	1.16541
H	4.55662	-5.23775	-1.21913	H	9.67063	3.49545	-1.16541
H	2.74907	-2.21128	1.24767	H	9.84743	5.68542	0.
C	0	-7.44832		C	6.26334	-3.61614	0
C	-1.01968	-8.18784	-0.63842	C	6.49116	-4.6378	0.93302
C	1.01968	-8.18784	0.63842	C	7.26203	-3.30261	-0.93302
C	-1.01685	-9.58217	-0.65183	C	7.69638	-5.33821	0.92435
H	-1.82059	-7.65503	-1.14414	H	5.72051	-4.87694	1.6592
C	1.01685	-9.58217	0.65183	C	8.47121	-3.99616	-0.92435
H	1.82059	-7.65503	1.14414	H	7.0838	-2.51564	-1.6592
C	0	-10.28355	0	C	8.69348	-5.01918	0
H	-1.80817	-10.12273	-1.16541	H	7.86035	-6.12772	1.65291
H	1.80817	-10.12273	1.16541	H	9.23694	-3.7434	-1.65291
H	0	-11.37083	0	H	9.63425	-5.56234	0
N	5.026	-2.90176	0	C	-5.0433	-1.48535	0.00558
C	-3.73265	3.71631	-0.0043	C	-6.05331	-0.77936	-0.67305
C	3.56757	4.95865	0.64792	C	-4.0624	-0.75046	0.69578
C	-2.59105	3.21105	-0.66688	C	-6.0781	0.61028	-0.64792
C	-2.35171	5.632	0.67305	H	-6.81434	-1.32728	-1.21913
H	-4.41012	5.39318	1.17937	C	-4.07638	0.63839	0.66688

C	-1.38128	3.89337	-0.69578	H	-3.28956	-1.27512	1.24767
H	-2.66466	2.26785	-1.20145	C	-5.08474	1.37441	0.0043
C	-1.2353	5.1103	-0.00558	H	-6.87569	1.12269	-1.17937
H	-2.25771	6.56503	1.21913	H	-3.29635	1.17374	1.20145
H	-0.54049	3.4864	-1.24767	B	-5.09017	2.93881	0
C	5.0433	-1.48535	-0.00558	C	-6.26334	-3.61614	0
C	4.0624	-0.75046	-0.69578	C	-7.26203	-3.30261	0.93302
C	6.05331	-0.77936	0.67305	C	-6.49116	-4.6378	-0.93302
C	4.07638	0.63839	-0.66688	C	-8.47121	-3.99616	0.92435
H	3.28956	-1.27512	-1.24767	H	-7.0838	-2.51564	1.6592
C	6.0781	0.61028	0.64792	C	-7.69638	-5.33821	-0.92435
H	6.81434	-1.32728	1.21913	H	-5.72051	-4.87694	-1.6592
C	5.08474	1.37441	-0.0043	C	-8.69348	-5.01918	0.
H	3.29635	1.17374	-1.20145	H	-9.23694	-3.7434	1.65291
H	6.87569	1.12269	1.17937	H	-7.86035	-6.12772	-1.65291
N	0	5.80353	0	H	-9.63425	-5.56234	0
C	1.2353	5.1103	0.00558	C	-6.45044	3.72416	0
C	1.38128	3.89337	0.69578	C	-6.58104	4.97699	-0.63842
C	2.35171	5.632	-0.67305	C	-7.60072	3.21085	0.63842
C	2.59105	3.21105	0.66688	C	-7.78998	5.6717	-0.65183
H	0.54049	3.4864	1.24767	H	-5.71916	5.4042	-1.14414
C	3.56757	4.95865	-0.64792	C	-8.80682	3.91047	0.65183
H	2.25771	6.56503	-1.21913	H	-7.53975	2.25084	1.14414
C	3.73265	3.71631	0.0043	C	-8.90581	5.14177	0
H	2.66466	2.26785	1.20145	H	-7.86246	6.62729	-1.16541
H	4.41012	5.39318	-1.17937	H	-9.67063	3.49545	1.16541
B	5.09017	2.93881	0	H	-9.84743	5.68542	0
				Bq	0	0	0

Table 6. Coordinates (Å) for the Optimized Structure of **MC-N6 (**R**=**Ph, phenylene π-system)

atom	x	y	z	atom	x	y	z
C	0.695217	5.801288	0.813360	C	4.962021	-1.230212	-0.000727
C	1.415615	4.912342	-0.00072	C	5.371671	-2.298569	0.813360
C	0.695519	4.021151	-0.812130	C	3.830178	-1.408238	-0.812130
C	-0.695519	4.021151	-0.812130	C	4.676454	-3.502720	0.813360
C	-1.415615	4.912342	-0.000727	H	6.235395	-2.176206	1.459232

C	-0.695217	5.801288	0.813360	C	3.134659	-2.612913	-0.812130
H	1.233048	6.488113	1.459232	H	3.503686	-0.598905	-1.457624
H	1.233176	3.333734	-1.457624	C	3.546405	-3.682130	-0.000727
H	-1.233176	3.333734	-1.457624	H	5.002347	-4.311907	1.459232
H	-1.233048	6.488113	1.459232	H	2.270510	-2.734829	-1.457624
N	2.836856	4.913579	0.000000	C	-4.962021	-1.230212	-0.000727
C	-3.546405	3.682130	0.000727	C	-3.830178	-1.408238	-0.812130
C	-4.676454	3.502720	-0.813360	C	-5.371671	-2.298569	0.813360
C	-3.134659	2.612913	0.812130	C	-3.134659	-2.612913	-0.812130
C	-5.371671	2.298569	-0.813360	H	-3.503686	-0.598905	-1.457624
H	-5.002347	4.311907	-1.459232	C	-4.676454	-3.502720	0.813360
C	-3.830178	1.408238	0.812130	H	-6.235395	-2.176206	1.459232
H	-2.270510	2.734829	1.457624	C	-3.546405	-3.682130	-0.000727
C	-4.962021	1.230212	0.000727	H	-2.270510	-2.734829	-1.457624
H	-6.235395	2.176206	-1.459232	H	-5.002347	-4.311907	1.459232
H	-3.503686	0.598905	1.457624	N	2.836856	-4.913579	0.000000
C	-3.547091	6.143742	0.000000	C	1.415615	-4.912342	0.000727
C	-3.110169	7.221326	-0.788605	C	0.695519	-4.021151	0.812130
C	-4.698767	6.304148	0.788605	C	0.695217	-5.801288	-0.813360
C	-3.805475	8.428775	-0.778439	C	-0.695519	-4.021151	0.812130
H	-2.225617	7.104647	-1.406617	H	1.233176	-3.333734	1.457624
C	-5.396796	7.510026	0.778439	C	-0.695217	-5.801288	-0.813360
H	-5.039997	5.479765	1.406617	H	1.233048	-6.488113	-1.459232
C	-4.954798	8.581962	0.000000	C	-1.415615	-4.912342	0.000727
H	-3.452032	9.250507	-1.396071	H	-1.233176	-3.333734	1.457624
H	-6.285158	7.614800	1.396071	H	-1.233048	-6.488113	-1.459232
C	-5.497913	9.522665	0.000000	C	3.547091	-6.143742	0.000000
N	-5.673712	0.000000	0.000000	C	4.698767	-6.304148	-0.788605
C	3.110169	-7.221326	0.788605	C	3.134659	2.612913	0.812130
C	5.396796	-7.510026	-0.778439	C	5.371671	2.298569	-0.81336
H	5.039997	-5.479765	-1.406617	H	5.002347	4.311907	-1.459232
C	3.805475	-8.428775	0.778439	C	3.830178	1.408238	0.812130
H	2.225617	-7.104647	1.406617	H	2.270510	2.734829	1.457624
C	4.954798	-8.581962	0.000000	C	4.962021	1.230212	0.000727
H	6.285158	-7.614800	-1.396071	H	6.235395	2.176206	-1.459232
H	3.452032	-9.250507	1.396071	H	3.503686	0.598905	1.457624
H	5.497913	-9.522665	0.000000	C	3.547091	6.143742	0.000000

C	-3.547091	-6.143742	0.000000	C	4.698767	6.304148	0.788605
C	-3.110169	-7.221326	0.788605	C	3.110169	7.221326	-0.788605
C	-4.698767	-6.304148	-0.788605	C	5.396796	7.510026	0.778439
C	-3.805475	-8.428775	0.778439	H	5.039997	5.479765	1.406617
H	-2.225617	-7.104647	1.406617	C	3.805475	8.428775	-0.778439
C	-5.396796	-7.510026	-0.778439	H	2.225617	7.104647	-1.406617
H	-5.039997	-5.479765	-1.406617	C	4.954798	8.581962	0.000000
C	-4.954798	-8.581962	0.000000	H	6.285158	7.614800	1.396071
H	-3.452032	-9.250507	1.396071	H	3.452032	9.250507	-1.396071
H	-6.285158	-7.614800	-1.396071	H	5.497913	9.522665	0.000000
H	-5.497913	-9.522665	0.000000	C	7.094183	0.000000	0.000000
C	-7.094183	0.000000	0.000000	C	7.808936	-0.917178	-0.788605
C	-7.808936	0.917178	0.788605	C	7.808936	0.917178	0.788605
C	-7.808936	-0.917178	-0.788605	C	9.202271	-0.918750	-0.778439
C	-9.202271	0.918750	0.778439	H	7.265614	-1.624883	-1.406617
H	-7.265614	1.624883	1.406617	C	9.202271	0.918750	0.778439
C	-9.202271	-0.918750	-0.778439	H	7.265614	1.624883	1.406617
H	-7.265614	-1.624883	-1.406617	C	9.909596	0.000000	0.000000
C	-9.909596	0.000000	0.000000	H	9.737190	-1.635706	-1.396071
H	-9.737190	1.635706	1.396071	H	9.737190	1.635706	1.396071
H	-9.737190	-1.635706	-1.396071	H	10.995826	0.000000	0.000000
H	-10.995826	0.000000	0.000000	N	-2.836856	-4.913579	0.000000
C	3.546405	3.682130	0.000727	N	5.673712	0.000000	0.000000
C	4.676454	3.502720	-0.813360	N	-2.836856	4.913579	0.000000

Table 7. Coordinates (Å) for the Optimized Structure of **MC-B6 (**R **=** Ph, phenylene π-system)

atom	x	y	z	atom	x	y	z
C	0.696166	6.205516	0.673485	C	3.992071	-1.500922	-0.662163
C	1.437783	5.208018	0.003571	C	5.026052	-3.705655	0.673485
C	0.696199	4.207696	-0.662163	H	6.666114	-2.434528	1.208423
C	-0.696199	4.207696	-0.662163	C	3.295872	-2.706774	-0.662163
C	-1.437783	5.208018	0.003571	H	3.575162	-0.649236	-1.193470
C	-0.696166	6.205516	0.673485	C	3.791384	-3.849166	0.003571
H	1.224694	6.990288	1.208423	H	5.441420	-4.555760	1.208423
H	1.225326	3.420799	-1.193470	H	2.349836	-2.771563	-1.193470

H	-1.225326	3.420799	-1.193470	C	-5.229167	-1.358852	0.003571
H	-1.224694	6.990288	1.208423	C	-3.992071	-1.500922	-0.662163
C	-3.791384	3.849166	-0.003571	C	-5.722218	-2.499861	0.673485
C	-5.026052	3.705655	-0.673485	C	-3.295872	-2.706774	-0.662163
C	-3.295872	2.706774	0.662163	H	-3.575162	-0.649236	-1.193470
C	-5.722218	2.499861	-0.673485	C	-5.026052	-3.705655	0.673485
H	-5.441420	4.555760	-1.208423	H	-6.666114	-2.434528	1.208423
C	-3.992071	1.500922	0.662163	C	-3.791384	-3.849166	0.003571
H	-2.349836	2.771563	1.193470	H	-2.349836	-2.771563	-1.193470
C	-5.229167	1.358852	-0.003571	H	-5.441420	-4.555760	1.208423
H	-6.666114	2.434528	-1.208423	C	1.437783	-5.208018	-0.003571
H	-3.575162	0.649236	1.193470	C	0.696199	-4.207696	0.662163
C	-3.792179	6.568246	0.000000	C	0.696166	-6.205516	-0.673485
C	-3.271547	7.721822	-0.627242	C	-0.696199	-4.207696	0.662163
C	-5.051521	6.694154	0.627242	H	1.225326	-3.420799	1.193470
C	-3.971901	8.927064	-0.641855	C	-0.696166	-6.205516	-0.673485
H	-2.306320	7.664244	-1.122782	H	1.224694	-6.990288	-1.208423
C	-5.745114	7.903299	0.641855	C	-1.437783	-5.208018	-0.003571
H	-5.484270	5.829454	1.122782	H	-1.225326	-3.420799	1.193470
C	-5.208827	9.021953	0.000000	H	-1.224694	-6.990288	-1.208423
H	-3.552866	9.793519	-1.147303	C	3.792179	-6.568246	0.000000
H	-6.705004	7.973631	1.147303	C	5.051521	-6.694154	-0.627242
H	-5.752440	9.963519	0.000000	C	3.271547	-7.721822	0.627242
C	5.229167	-1.358852	0.003571	C	5.745114	-7.903299	-0.641855
C	5.722218	-2.499861	0.673485	H	5.484270	-5.829454	-1.122782
C	3.971901	-8.927064	0.641855	C	3.992071	1.500922	0.662163
H	2.306320	-7.664244	1.122782	H	2.349836	2.771563	1.193470
C	5.208827	-9.021953	0.000000	C	5.229167	1.358852	-0.003571
H	6.705004	-7.973631	-1.147303	H	6.666114	2.434528	-1.208423
H	3.552866	-9.793519	1.147303	H	3.575162	0.649236	1.193470
H	5.752440	-9.963519	0.000000	C	3.792179	6.568246	0.000000
C	-3.792179	-6.568246	0.000000	C	5.051521	6.694154	0.627242
C	-3.271547	-7.721822	0.627242	C	3.271547	7.721822	-0.627242
C	-5.051521	-6.694154	-0.627242	C	5.745114	7.903299	0.641855
C	-3.971901	-8.927064	0.641855	H	5.484270	5.829454	1.122782
H	-2.306320	-7.664244	1.122782	C	3.971901	8.927064	-0.641855
C	-5.745114	-7.903299	-0.641855	H	2.306320	7.664244	-1.122782

H	-5.484270	-5.829454	-1.122782	C	5.208827	9.021953	0.000000
C	-5.208827	-9.021953	0.000000	H	6.705004	7.973631	1.147303
H	-3.552866	-9.793519	1.147303	H	3.552866	9.793519	-1.147303
H	-6.705004	-7.973631	-1.147303	H	5.752440	9.963519	0.000000
H	-5.752440	-9.963519	0.000000	C	7.584358	0.000000	0.000000
C	-7.584358	0.000000	0.000000	C	8.323068	-1.027669	-0.627242
C	-8.323068	1.027669	0.627242	C	8.323068	1.027669	0.627242
C	-8.323068	-1.027669	-0.627242	C	9.717015	-1.023765	-0.641855
C	-9.717015	1.023765	0.641855	H	7.790590	-1.834790	-1.122782
H	-7.790590	1.834790	1.122782	C	9.717015	1.023765	0.641855
C	-9.717015	-1.023765	-0.641855	H	7.790590	1.834790	1.122782
H	-7.790590	-1.834790	-1.122782	C	10.417654	0.000000	0.000000
C	-10.417654	0.000000	0.000000	H	10.257869	-1.819888	-1.147303
H	-10.257869	1.819888	1.147303	H	10.257869	1.819888	1.147303
H	-10.257869	-1.819888	-1.147303	H	11.504881	0.000000	0.000000
H	-11.504881	0.000000	0.000000	B	3.008382	5.210670	0.000000
C	3.791384	3.849166	-0.003571	B	-3.008382	5.210670	0.000000
C	5.026052	3.705655	-0.673485	B	-6.016764	0.000000	0.000000
C	3.295872	2.706774	0.662163	B	-3.008382	-5.210670	0.000000
C	5.722218	2.499861	-0.673485	B	3.008382	-5.210670	0.000000
H	5.441420	4.555760	-1.208423	B	6.016764	0.000000	0.000000

Table 8. Coordinates (Å) for the Optimized Structure of **MC-B4N2**

atom	x	y	z	atom	x	y	z
C	3.935779	3.499771	-0.169482	H	2.682872	-3.731695	-1.913362
C	0.000000	-10.144539	-1.719016	H	-4.472629	-7.645397	-0.834919
C	3.145333	3.015486	-1.239961	H	5.144886	-2.879195	1.516928
C	2.961725	1.654571	-1.476704	H	-2.792979	-9.329232	-1.459511
C	3.559372	0.732908	-0.612372	H	-1.392972	-4.772593	0.073488
C	4.336156	1.184050	0.476718	H	2.792979	-9.329232	-1.459511
C	4.531351	2.541108	0.685426	H	4.472629	-7.645397	-0.834919
C	2.961725	-1.654571	-1.476704	H	1.392972	-4.772593	0.073488
C	3.559372	-0.732908	-0.612372	C	-3.935779	-3.499771	-0.169482
C	3.145333	-3.015486	-1.239961	C	-4.531351	-2.541108	0.685426
C	3.935779	-3.499771	-0.169482	C	-3.145333	-3.015486	-1.239961

C	4.531351	-2.541108	0.685426	C	-4.336156	-1.184050	0.476718
C	4.336156	-1.184050	0.476718	H	-5.144886	-2.879195	1.516928
B	-4.173087	-5.035855	0.043860	C	-2.961725	-1.654571	-1.476704
B	4.173087	-5.035855	0.043860	H	-2.682872	-3.731695	-1.913362
C	-3.070426	-6.077957	-0.330816	C	-3.559372	-0.732908	-0.612372
C	-3.420245	-7.388069	-0.759521	C	-3.559372	0.732908	-0.612372
C	-2.479733	-8.350001	-1.109349	C	-2.961725	1.654571	-1.476704
C	-1.128781	-8.008770	-0.992671	C	-4.336156	1.184050	0.476718
C	-0.726370	-6.715710	-0.562412	C	-3.145333	3.015486	-1.239961
C	-1.696916	-5.764111	-0.251080	C	-4.531351	2.541108	0.685426
N	0.000000	-8.779456	-1.235873	C	-3.935779	3.499771	-0.169482
C	1.128781	-8.008770	-0.992671	H	-2.682872	3.731695	-1.913362
C	0.726370	-6.715710	-0.562412	H	-5.144886	2.879195	1.516928
C	2.479733	-8.350001	-1.109349	B	-4.173087	5.035855	0.043860
C	3.420245	-7.388069	-0.759521	B	4.173087	5.035855	0.043860
C	3.070426	-6.077957	-0.330816	C	-3.070426	6.077957	-0.330816
C	1.696916	-5.764111	-0.251080	C	-3.420245	7.388069	-0.759521
H	0.000000	-10.193206	-2.815719	C	-1.696916	5.764111	-0.251080
H	-0.884058	-10.665797	-1.343172	C	-2.479733	8.350001	-1.109349
H	0.884058	-10.665797	-1.343172	H	-4.472629	7.645397	-0.834919
H	2.682872	3.731695	-1.913362	C	-0.726370	6.715710	-0.562412
H	5.144886	2.879195	1.516928	H	-1.392972	4.772593	0.073488
H	6.748510	-4.028403	-0.345803	C	-1.128781	8.008770	-0.992671
C	8.013357	-6.412409	1.715796	H	-2.792979	9.329232	-1.459511
H	6.844637	-7.906662	2.742857	C	0.726370	6.715710	-0.562412
H	8.901093	-4.817067	0.566807	C	1.128781	8.008770	-0.992671
H	8.960141	-6.751294	2.129305	C	1.696916	5.764111	-0.251080
C	5.544492	5.527851	0.638370	C	2.479733	8.350001	-1.109349
C	6.760929	4.883570	0.324865	C	3.070426	6.077957	-0.330816
C	5.615210	6.633122	1.513965	H	1.392972	4.772593	0.073488
C	7.979300	5.324486	0.840724	C	3.420245	7.388069	-0.759521
H	6.748510	4.028403	-0.345803	H	2.792979	9.329232	-1.459511
C	6.825581	7.062716	2.057567	H	4.472629	7.645397	-0.834919
H	4.699905	7.154824	1.781070	N	0.000000	8.779456	-1.235873
C	8.013357	6.412409	1.715796	C	0.000000	10.144539	-1.719016
H	8.901093	4.817067	0.566807	H	0.000000	10.193206	-2.815719
H	6.844637	7.906662	2.742857	H	-0.884058	10.665797	-1.343172

H	8.960141	6.751294	2.129305	H	0.884058	10.665797	-1.343172
C	-5.544492	5.527851	0.638370	C	-5.544492	-5.527851	0.638370
C	-5.615210	6.633122	1.513965	C	-5.615210	-6.633122	1.513965
C	-6.760929	4.883570	0.324865	C	-6.760929	-4.883570	0.324865
C	-6.825581	7.062716	2.057567	C	-6.825581	-7.062716	2.057567
H	-4.699905	7.154824	1.781070	H	-4.699905	-7.154824	1.781070
C	-7.979300	5.324486	0.840724	C	-7.979300	-5.324486	0.840724
H	-6.748510	4.028403	-0.345803	H	-6.748510	-4.028403	-0.345803
C	-8.013357	6.412409	1.715796	C	-8.013357	-6.412409	1.715796
C	-4.868899	0.000000	1.259622	H	-6.844637	-7.906662	2.742857
C	4.868899	0.000000	1.259622	H	-8.901093	-4.817067	0.566807
H	-6.844637	7.906662	2.742857	H	-8.960141	-6.751294	2.129305
H	-8.901093	4.817067	0.566807	C	5.544492	-5.527851	0.638370
H	-8.960141	6.751294	2.129305	C	5.615210	-6.633122	1.513965
H	2.365410	1.320294	-2.322218	C	6.760929	-4.883570	0.324865
H	2.365410	-1.320294	-2.322218	C	6.825581	-7.062716	2.057567
H	-2.365410	1.320294	-2.322218	H	4.699905	-7.154824	1.781070
H	-2.365410	-1.320294	-2.322218	C	7.979300	-5.324486	0.840724
H	-4.508235	0.000000	2.297889	H	5.966258	0.000000	1.314989
H	-5.966258	0.000000	1.314989	H	4.508235	0.000000	2.297889

Table 9. Coordinates (Å) for the Optimized Structure of **MC-B2N2**

atom	x	y	z	atom	x	y	z
C	7.910840	-3.021073	-0.472872	H	3.448970	-5.165228	1.737216
C	9.278015	-3.384523	-0.513817	C	2.810296	-6.409906	0.063956
C	10.301663	-2.453861	-0.375417	H	2.685954	-4.262308	0.435287
C	9.948946	-1.114584	-0.191029	C	3.739193	-6.946561	-0.853839
C	8.587181	-0.716718	-0.128620	C	1.615732	-7.066959	0.319146
C	7.579976	-1.672932	-0.275594	C	3.467009	-8.153890	-1.503048
H	9.538059	-4.432626	-0.627058	C	1.322848	-8.305128	-0.303327
H	11.339128	-2.773924	-0.393920	H	0.900753	-6.643462	1.020775
H	6.536795	-1.369327	-0.262150	C	2.280392	-8.821804	-1.209121
C	9.948984	1.117004	0.136959	H	4.171807	-8.574847	-2.216058
C	10.301632	2.452204	0.348413	H	2.076760	-9.769327	-1.700138
C	9.278015	3.381764	0.494235	C	6.857533	4.052031	0.612260

C	7.910837	3.019642	0.444442	C	5.657644	3.989998	-0.124508
C	7.579976	1.673372	0.234494	C	7.040112	5.124278	1.509543
C	8.587167	0.718314	0.080302	C	4.691276	4.973077	0.034850
H	11.339424	2.768521	0.394081	H	5.509960	3.185238	-0.840482
H	9.538516	4.427281	0.628267	C	6.078055	6.118297	1.668987
H	6.536866	1.369466	0.221974	H	7.946029	5.163193	2.107527
N	10.759847	0.004133	-0.046888	C	3.348005	5.123796	-0.653406
C	12.205960	-0.002368	-0.003766	C	4.897579	6.047104	0.925886
H	12.589746	-0.148498	1.014827	H	6.248095	6.931624	2.370007
H	12.587789	-0.803827	-0.641697	H	3.450461	5.186778	-1.745657
H	12.588816	0.945544	-0.391162	C	2.809492	6.412159	-0.059209
C	6.857787	-4.055428	-0.629701	H	2.686719	4.268703	-0.454810
C	5.657104	-3.985710	0.105047	C	3.737453	6.939266	0.865053
C	7.041885	-5.137558	-1.514701	C	1.614698	7.071238	-0.307977
C	4.691347	-4.970917	-0.044470	C	3.464246	8.139393	1.527068
H	5.508292	-3.173186	0.811949	C	1.320780	8.302436	0.327689
C	6.080371	-6.133644	-1.664309	H	0.900258	6.654982	-1.014470
H	7.948709	-5.182682	-2.110897	C	2.277524	8.809869	1.239517
C	3.347559	-5.114698	0.644233	H	4.168353	8.552970	2.245063
C	4.899004	-6.054629	-0.923402	H	2.073125	9.751967	1.740560
H	6.251529	-6.954666	-2.356028	B	0.001209	-9.083691	0.016301
B	-0.001209	9.083691	0.016301	C	-7.910837	-3.019642	0.444442
C	-1.322848	8.305128	-0.303327	C	-9.278015	-3.381764	0.494235
C	-2.280392	8.821804	-1.209121	C	-7.579976	-1.673372	0.234494
C	-1.615732	7.066959	0.319146	C	-10.301632	-2.452204	0.348413
C	-3.467009	8.153890	-1.503048	H	-9.538516	-4.427281	0.628267
H	-2.076760	9.769327	-1.700138	C	-8.587167	-0.718314	0.080302
C	-2.810296	6.409906	0.063956	H	-6.536866	-1.369466	0.221974
H	-0.900753	6.643462	1.020775	C	-9.948984	-1.117004	0.136959
C	-3.739193	6.946561	-0.853839	H	-11.339424	-2.768521	0.394081
C	-6.080371	6.133644	-1.664309	C	-8.587181	0.716718	-0.128620
C	-4.899004	6.054629	-0.923402	C	-9.948946	1.114584	-0.191029
C	-7.041885	5.137558	-1.514701	C	-7.579976	1.672932	-0.275594
C	-4.691347	4.970917	-0.044470	C	-10.301663	2.453861	-0.375417
C	-6.857787	4.055428	-0.629701	C	-7.910840	3.021073	-0.472872
H	-7.948709	5.182682	-2.110897	H	-6.536795	1.369327	-0.262150
C	-5.657104	3.985710	0.105047	C	-9.278015	3.384523	-0.513817

H	-5.508292	3.173186	0.811949	H	-11.339128	2.773924	-0.393920
C	-1.320780	-8.302436	0.327689	H	-9.538059	4.432626	-0.627058
C	-2.277524	-8.809869	1.239517	N	-10.759847	-0.004133	-0.046888
C	-1.614698	-7.071238	-0.307977	C	-12.205960	0.002368	-0.003766
C	-3.464246	-8.139393	1.527068	H	-12.588816	-0.945544	-0.391162
H	-2.073125	-9.751967	1.740560	H	-12.589746	0.148498	1.014827
C	-2.809492	-6.412159	-0.059209	H	-12.587789	0.803827	-0.641697
H	-0.900258	-6.654982	-1.014470	C	-0.001459	10.655178	0.024064
C	-3.737453	-6.939266	0.865053	C	1.132262	11.396691	-0.374995
C	-6.078055	-6.118297	1.668987	C	-1.135348	11.392388	0.430531
C	-4.897579	-6.047104	0.925886	C	1.131670	12.791039	-0.382720
C	-7.040112	-5.124278	1.509543	H	2.024454	10.866246	-0.696722
C	-4.691276	-4.973077	0.034850	C	-1.135030	12.786593	0.452302
C	-6.857533	-4.052031	0.612260	H	-2.027435	10.858549	0.746896
H	-7.946029	-5.163193	2.107527	C	-0.001756	13.490160	0.038323
C	-5.657644	-3.989998	-0.124508	H	2.015059	13.333151	-0.711123
H	-5.509960	-3.185238	-0.840482	H	-2.018529	13.325189	0.786150
H	-0.001874	14.577451	0.043796	H	2.018529	-13.325189	0.786150
C	0.001459	-10.655178	0.024064	H	0.001874	-14.577451	0.043796
C	-1.132262	-11.396691	-0.374995	H	-4.168353	-8.552970	2.245063
C	1.135348	-11.392388	0.430531	H	-6.248095	-6.931624	2.370007
C	-1.131670	-12.791039	-0.382720	H	-4.171807	8.574847	-2.216058
H	-2.024454	-10.866246	-0.696722	H	-6.251529	6.954666	-2.356028
C	1.135030	-12.786593	0.452302	C	-3.348005	-5.123796	-0.653406
H	2.027435	-10.858549	0.746896	C	-3.347559	5.114698	0.644233
C	0.001756	-13.490160	0.038323	H	-2.685954	4.262308	0.435287
H	-2.015059	-13.333151	-0.711123	H	-3.448970	5.165228	1.737216
H	-2.686719	-4.268703	-0.454810	H	-3.450461	-5.186778	-1.745657

List of Publications

Publications on PhD work:

1. π–Expanded Borazines: An Ambipolar Conjugated B–π–N Macrocyle, Pangkuan Chen, Roger A. Lalancette, and Frieder Jäkle, *Angew. Chem. Int. Ed.* **2012**, *51*, 7994.
   - Selected as a VIP paper;
   - HIGHLIGHT as "Building a Bigger Borazine ", *C&E News*, **2012,** *90*, 29.

2. Highly Luminescent Electron-Deficient Bora-cyclophanes, Pangkuan Chen, and Frieder Jäkle, *JACS* **2011**, *133*, 20142.
   - HIGHLIGHT as "Glowing Ring Could Find Use In Electronics ", *C&E News*, **2011,** *49*, 35;
   - SPOTLIGHT on Recent JACS Publications, *JACS* **2012,** *134*, 745;
   - FEATURED IN JACS EDITORIAL"Advances at the Frontiers of Photochemical Sciences", *JACS* **2012**, *134*, 8289;
   - HIGHLIGHT as "Lewis-Acidic Cyclophanes", *Angew. Chem. Int. Ed.* **2012**, *51*, 6316.

3. Applying the Oligomer Approach to Luminescent Conjugated Organoboranes, Pangkuan Chen, Roger A. Lalancette, and Frieder Jäkle, *JACS* **2011**, *133*, 8802.

Selected publications before PhD study:

4. Network topology and property studies for two binodal self- penetrated coordination polymers, Pangkuan Chen, Yan Qi, Yun-Xia Che, and Ji-Min Zheng, *CrystEngComm*. **2010**, *12*, 720.

5. Three new polycatenation networks based on 4,4'-oxybis(benzoate) and Bis(imidazole)Ligands:Synthesis, structure and photoluminescence, Yun Xu, Pangkuan Chen, Yun-Xia Che, Ji-Min Zheng, *Eur. J. Inorg. Chem*. **2010**, *34*, 5478.

6. Two 3-D cluster-based frameworks: Highly eight-connected molecular topology and magnetism, Pangkuan Chen, Stuart R.Batten, Yan Qi, and Ji-min Zheng. *Cryst. Growth & Des*. **2009**, *9*, 2756.

7. Heteronuclear Metamagnet Showing Spin Canting and Single-Crystal to Single-Crystal Phase Transformation, Pangkuan Chen, Yun-Xia Che, Ji-Min Zheng, and Stuart R. Batten,

Chem. Mater. **2007**, *19*, 2162.

8. Novel $(4^2 \cdot 8^4)(4^3 \cdot 6^3)_2(4^6 \cdot 6^3 \cdot 8^6)_2$ topology network built up from the highly connective pyridine-2,4,6-tricarboxylate ligand, Peng Ren, Pangkuan Chen *****, Gong-Feng Xu, Zhi Chen, *Inorg. Chem. Commun*. **2007**, 10, 836.

9. An inclined interpenetrating heteropolynuclear polymer with unusual propagation of metal carboxylate secondary building units by both carboxylate and pyridyl bridging ligands, Pangkuan Chen, Yun-Xia Che, Stuart R. Batten, and Ji-Min Zheng, *Inorg. Chem. Commun*. **2007**,10, 415.

10. Unusual T4(1) Water Chain Stabilized in the One-Dimensional Chains of Copper (II) Coordination Polymer, Yi Jin, Yunxia Che, Stuart R. Batten, Pangkuan Chen, Jimin Zheng, *Eur. J. Inorg. Chem*. **2007**, 1925.

11. Two 2-Fold Interpenetrated Frameworks Showing Different Topologies Based on the Isomerous Benzenedicarboxylate Mixed with a Flexible N, N'-Type Ligand, Pangkuan Chen, Lin Xue, Ji-Min Zheng, *Cryst. Growth & Des*. **2006**, *6*, 2517.

12. System-pH-Dependent Supramolecular Isomers of Puckered Three-Dimensional Layered Hydrogen-Bonded Networks: Syntheses, Characterization and Fluorescent Properties, Pangkuan Chen, Yun-xia Che, Yu-mei Li, Ji-Min Zheng, et al, *J. Solid State Chem.* **2006**, *179*, 2656.

13. A 3D heteropolynuclear network with 4,6–connected $(4^4 \cdot 6^2)(4^8 \cdot 6^6 \cdot 8)$ topology: synthesis, structure, thermal and magnetic properties, Pangkuan Chen, Yun-Xia Che, Ji-Min Zheng, *Inorg. Chem. Commun*. **2006**, *10*, 187.

Curriculum Vitae

Education and Teaching

2007 – 2012	Ph.D study, Polymer Chemistry, Rutgers University, USA. Advisor: Prof. Frieder Jäkle Thesis: Synthesis and Characterization of Luminescent Conjugated Organoboron Oligomers and Macrocycles
2007	M.S. received, Inorganic Chemistry, Nankai University, China. Projects: Self-Assembled 3D Entanglements for Topology and Magnetism Studies
2001 – 2004	Teaching high school, Hubei province, China
2001	B.S. received, Chemistry, Three Gorges University, China
2001–2004	Teaching high school students, Hubei province, China

Honors and Awards

2012	Selected to Participate in "*Excellence in Graduate Polymer Research Symposium*", 243rd ACS National Meeting, San Diego, USA
2007	Best thesis of Master students, Nankai University, China